THE GEOCHEMISTRY, KINEMATICS AND GEODYNAMICS OF THE GANNAKOURIEP DYKE SWARM

Ian G.D. Ransome
Department of Geochemistry, University of Cape Town

Submitted in fulfillment of the requirements for the degree Master of Science

THE GEOCHEMISTRY, KINEMATICS AND GEODYNAMICS OF THE GANNAKOURIEP DYKE SWARM.

Ian G.D. Ransome
Department of Geochemistry, University of Cape Town, South Africa.

ABSTRACT

The Gannakouriep dyke swarm comprises a linear swarm of north to northeast striking mafic dykes emplaced during late Proterozoic rifting in the Gariep belt. The swarm has a strike length of over 300 km crossing terrane boundaries of the Gordonia sub-province, Richtersveld igneous sub-province and Bushmanland sub-province of the Namaqua Mobile Province. The main axis of dyke intrusion is centred within the 2.0 Ga Richtersveld igneous sub-province where the density of dyking increases westwards across strike towards the Gariep belt, prior to disappearing within the sediment/basement contact of the para-autochthonous Port Nolloth Assemblage. An internal Rb-Sr mineral isochron, together with pyroxene K-Ar plateau and whole rock model T_{CHUR} ages, indicate that the dyke swarm was intruded around 720 Ma.

The majority of the dykes comprise subophitic relict gabbros and dolerites of alkali affinities replaced by metamorphic minerals of both greenschist and amphibolite facies. The greenstones are encountered within the NE striking eastern sector of the dyke swarm which records the original tensile stress field, whilst amphibolites are encountered in the northerly striking western sector of the swarm which has been rotated 26° anticlockwise during Pan-African (500-550 Ma) deformation in the Gariep belt. The latter age of regional metamorphism and deformation is supported by available K-Ar age data on whole rock samples and amphibole mineral separates.

Integrated field relationships, continuum mechanics modelling and geochemical studies suggest that the swarm was initiated as a series of low level crustal magma chambers which subsequently gave rise to a series of dyke complexes that comprise the Gannakouriep dyke swarm. The geochemical variability between individual dyke complexes across the entire swarm is negligible; only slight differences being recorded by their high-field-strength element concentrations. The latter suggests that all dykes are genetically linked to a single mantle diapir, with only slight source characteristic heterogeneities. All dykes are ferro-tholeiites with no primitive (picritic) member being present. Geochemical trends recorded by the swarm are easily reconcilable in terms of fractionation of the phenocryst assemblage olivine, plagioclase, clinopyroxene, (ilmenite and Ti-magnetite). However an earlier phase of fractionation of essentially olivine and plagioclase at the base of the crust is suggested since constraints on the degree of partial melting (3-6%) imposed by REE patterns would derive an alkali basalt parental melt.

The geodynamic relationship between the Gannakouriep dyke swarm and rifting in the Gariep belt is accounted for by a lithospheric plate model containing non-coincidental crustal and mantle weaknesses represented by late Namaquan D4n extensional faults and a mantle weakness possibly resulting from crustal thickening within the Richtersveld igneous sub-province during Namaquan tectonics.

TABLE OF CONTENTS

1 Introduction 4
- *1.1 Overview* 4
- *1.2 Scope of this thesis* 6
- *1.3 Acknowledgements* 6

2 Description of dykes within sectors 6
- *2.1 Introduction* 6
- *2.2 Sector I dykes* 7
  - *2.2.1 Basement lithologies* 7
  - *2.2.2 Structural characteristics* 8
  - *2.2.3 Lithologies* 9
  - *2.2.4 Xenoliths* 9
  - *2.2.5 Metamorphism and rheomorphism* 10
  - *2.2.6 Post Gannakouriep deformation* 10
- *2.3 Sector II dykes* 12
  - *2.3.1 Basement lithologies and anisotropy* 12
  - *2.3.2 Structural characteristics* 12
  - *2.3.3 Lithology* 12
  - *2.3.4 Xenoliths* 13
- *2.4 Sector III dykes* 13
  - *2.4.1 Basement lithologies and anisotropy* 13
  - *2.4.2 Structural characteristics* 13
  - *2.4.3 Lithologies* 17
  - *2.4.4 Crustal assimilation* 17
  - *2.4.5 Sills in the Stinkfontein Sequence* 17
  - *2.4.6 Post Gannakouriep deformation* 20
- *2.5 Discussion* 21
  - *2.5.1 Relationship of swarm to inferred rift axis* 21

3 Petrography and mineralogy 21
- *3.1 Introduction* 21
- *3.2 Petrography* 21
  - *3.2.1 Metadolerites* 23
  - *3.2.2 Metagabbros* 23
    - *3.2.2.1 Subophitic Gabbros* 24
    - *3.2.2.2 Layered Gabbros* 26
- *3.3 Mineralogy* 27
  - *3.3.1 Olivine* 27
  - *3.3.2 Pyroxene* 27
  - *3.3.3 Feldspar* 27
  - *3.3.4 Fe Opaques* 27
  - *3.3.5 Miscellaneous phases* 28
- *3.4 Metamorphism* 28
- *3.5 Geothermometry* 29
- *3.6 Petrological considerations* 29

4 Intrusion Mechanics 30
- *4.1 Introduction* 30
- *4.2 Outcrop configuration of dykes* 30
- *4.3 Dyke geometries* 33
- *4.4 Remote stress orientation and dilation vectors* 35
- *4.5 Flow lineations* 37
- *4.6 Inelastic deformation* 39
- *4.7 Lateral versus vertical propagation* 43
- *4.8 Generation of xenoliths* 46
- *4.9 The Main Dyke Complex* 49
- *4.10 Summary* 50

5 Geochronology 50
- *5.1 Introduction* 50
- *5.2 Rb-Sr Isotopic System* 51
  - *5.2.1 Introduction* 51
  - *5.2.2 Results* 51
- *5.3 Nd/Sm Isotopes* 53
  - *5.3.1 Introduction* 53
  - *5.3.2 Results* 53

5.4. K-Ar and Ar/Ar Isotopes 54
5.4.1 Introduction 54
5.4.2 K-Ar data on amphibole separates 54
5.4.3 Pyroxene separates 57
5.4.4 Whole rock samples 59
5.4.5 Discussion 59
6 Intradyke geochemical variations recorded by the Gannakouriep dyke swarm 61
6.1 Introduction 61
6.2 Field relationships 61
6.3 Petrography 61
6.4 Mineral chemistry 62
6.5 Geochemical variations 63
6.6 Alteration 66
6.7 Bulk compositions 71
6.8 Origin of chemical variation within individual intrusions 71
6.8.1 Profile GD-I 71
6.8.2 Profile GD-II 73
6.9 Isotopic variations 74
6.9.1 Introduction 74
6.9.2 Results 74
6.9.3 Discussion 74
6.10 Summary 77
7 Geochemistry of the Gannakouriep dyke swarm 79
7.1 Introduction 79
7.2 Geochemical Variations 80
7.2.1 Introduction 80
7.2.2 Major Elements 80
7.2.3 Trace Element characterisation 80
7.2.3.1 High Field Strength elements 80
7.2.3.2 Other Incompatible and base trace elements 86
7.2.3.3 Compatible ferromagnesian trace elements 86
7.2.3.4 Rare Earth Elements 86
7.3 Normalised trace element abundances 86
7.4 Assessment of crustal contamination 90
7.5 Petrogenesis 93
7.6 Discussion 93
7.7 Summary 96
8 Synthesis 97
8.1 Introduction 97
8.2 Discussion 97
8.2.1 Crustal kinematics 97
8.2.2 Mantle lithosphere/crustal lithosphere interface kinematics 100
8.2.3 Geodynamics 102
8.3 Conclusion 105
References 106

Appendices 111

List of Abreviations used in this thesis

A: area under consideration of a flaw ellipsoid tip
B: angle measured between the stress direction and the X_2 axis of a flaw ellipsoid
c: specific heat capacity of rock
CIA: $[Al_2O_3/Al_2O_3 + CaO^* + Na_2O + K_2O] \times 100$; CaO^* = CaO in silicate fraction
CL: continental lithosphere
$d^{18}O$: $(({}^{18}O/{}^{16}O_{(rock/mineral)} - {}^{18}O/{}^{16}O_{SMOW})/SMOW)*10^3$
D_b: density of basalt
D^h: density of host rock
D_n: Namaquan deformational episode
E_0: boundary ellipsoid
E,n: orthogonal co-ordinates
E_{Nd}: epsilon Neodynium
E_{Sr}: epsilon Strontium
g: acceleration due to gravity
G: shear modulus
G_{xy}: displacement vector
h: height of rock column
I: Airy stress function
Im: imaginary complex number
k: thermal diffusivity
K: stress intensity factor
kb: kilobars
km: kilometres
Kz: permeability
l: length of dyke
L: latent heat of fusion of a magma
LS: lineation/foliation fabric
Ma: million years
ML: mantle lithosphere
P: magma pressure
p: rock density
P_{eb}: effective magma pressure at the base of a magmatic column
P_{et}: effective magma pressure at the top of a magmatic column
P_m: magma pressure acting normal to a joint wall after dilation
P_p: pore pressure
R: stress intensity ratio
Re: real complex number
Rf: ratio of a process zone
R,θ: polar co-ordinates
S: structural fabric of a rock
SMOW: standard mean ocean water
t: thickness of a dyke
T: tensile strength of a rock
T_m: temperature of the intruding magma
To: temperature of country rock prior to emplacement of a dyke
U: viscosity of a rock
u: Poissons ratio
u,v: displacement vectors acting positively in the directions -
y_r-x in a cartesian co-ordinate system
x: height of a rock column
x_1: short axis of an ellipsoid
x_2: long axis of an ellipsoid
α: angle between short axis and σ3 of a potential joint
σ^1: maximum stress axis
σ^2: intermediate stress axis
σ^3: minimum stress axis
σ_{3r}: remote minimal stress axis
σ^{a3}:local minimal stress axis at a dyke tip
σ_{ij}: elastic stress components of an area under consideration in the K-dominant region of a dyke tip.
σ_{xx}, σ_{yy}, σ_{xy}: the normal and shear components of stress
σ_{11}, σ_{11r}: local and remote stress axes in a process zone
σ_{ys}: yield strength in uniaxial extension
ρ: radius of curvature at a dyke tip

1 INTRODUCTION

1.1 Overview

The Gannakouriep dyke swarm is essentially composed of northeast trending dykes emplaced into simple dilational fractures in a basement complex, comprising the weakly metamorphosed 2.0 Ga Richtersveld igneous subprovince and the high grade gneisses of the Gordonia and Bushmanland subprovinces of the Namaqua Metamorphic Province (Figure 1.1) (Hartnady et. al, 1985). The swarm is considered to comprise an integral part of late Proterozoic rifting during the development of the seaborne arm of the Damaran orogen (Porada, 1989) during which the sediments of the Port Nolloth Assemblage were deposited (Figure 1.2). The latter are considered to constitute a passive continental margin sequence (Von Veh, 1988) which overlie the basement complexes along an angular unconformity, and are intruded in their lowermost succession by the Gannakouriep dyke swarm (Kroner, 1972).

The lateral extent of the swarm is bounded along its western margin by the Port Nolloth Assemblage whilst intensity of dyke injection decreases eastwards over a distance of 150km prior to disappearing under later cover sequences in southern Namaland. The northeastern and southeastern segments of the swarm reflect a primary extensional trend being relatively unmodified. The western segment of the swarm is deformed by steeply dipping north-south striking sinistral brittle-ductile shear zones (Booth, 1988) and has been rotated by late Proterozoic - early Cambrian orogenesis anticlockwise by 26° (Von Veh, 1988).

LITHOLOGY AND STRATIGRAPHY IN THE GARIEP BELT

Superficial sand, gravel, calcrete, silcrete, soil			Cenozoic units	POST-GARIEPIAN
Granite, syenite, quartz-syenite		Kuboos-Swartbank plutons	Cape Granite Suite ?	
Metagreywacke, phyllite, schist, greenstone			Oranjemund Complex	MARMORA TERRANE
Schistose melange, ultramafics, amphibolite, metagabbro, metabasalt			Chameis Complex	
Dolomite, brecciated dolomite		Gais Formation	Schakalsberge Complex	
Bostonite		Rooilepel Suite		
Greenstone, chlorite schist, pyroclastic breccia, amphibolite, ultramafics		Grootderm Suite		
Greywacke, quartzite, arkose, limestone		Sanddrif Formation	Holgat Sequence (Nama Group ?)	PORT NOLLOTH ZONE
Dolomite		Bloeddrif Formation		
Diamictite, quartzite, shale		Sendelingsdrif Formation	Numees Sequence	
Banded ironstone, ferruginous quartzite, diamictite		Jakkalsberg Formation		
Dolomite, marble, limestone (part brecciated)		Dabie River Formation	Hilda Sequence	
Conglomerate, grit, quartzite, schist, phyllite, minor limestone		Wallekraal Formation		
Limestone, dolomite, calcarenite		Pickelhaube Formation		
Diamictite, conglomerate, grit, subgreywacke, phyllite			Kaigas Formation	
Mafic dyke swarm			Gannakouriep Suite	
Namibia / *Western Richtersveld*				
Felsites, arkose, phyllite	Rosh Pinah Fm	*Feldspathic quartzite, arkose, volcanics*	Vredefontein Formation	Stinkfontein Sequence
Grits, arkose, calcarenite	Gumchavib Fm	*Orthoquartzite, conglomerate*	Lekkersing Formation	
Granite, quartz-porphyry, quartz-syenite			Richtersveld Suite	NAMAQUA PROVINCE
Granodiorite, granite, gneiss			Vioolsdrif Suite	
Metavolcanics, metasediments			Orange River Group	

Figure 1.2. *Schematic stratigraphy and lithology in the Gariep Belt, after Von Veh, (1988).*

Figure 1.1. *Geological outcrop map of the Gannakouriep dyke swarm shown in black, with basement terrane provinces after Hartnady et al., (1985). Dyke distribution based on mapping by Ritter, (1980); Blignault, (1977); De Villers and Söhnge, (1959); McMillan, (1968); and the author. Abbreviations of localities mentioned in the text: V = Vioosdrif; S = Steinkopf; KK = Klein Karas; FR = Lower Fish River; RP = Rosh Pinah; DR = Doring River.*

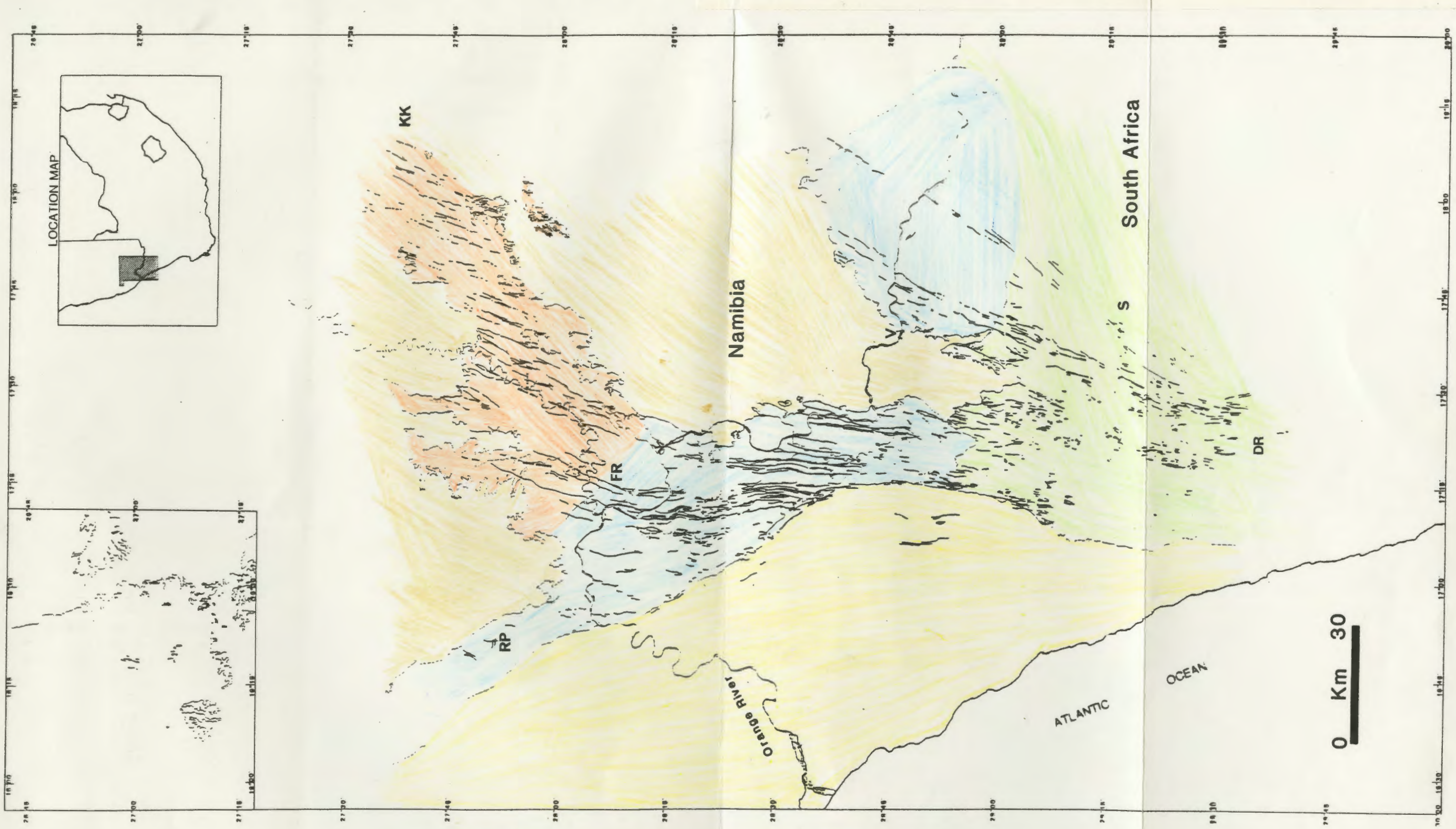

1.2 Scope of this thesis

The present study was stimulated by the current International Geological Correlation Program 257, entitled "Precambrian Mafic Dyke swarms".

The main aims of this study are:

(i) To describe and establish the mechanics of intrusion of the Gannakouriep dyke swarm.

(ii) To establish the geochronology recorded by the Gannakouriep Dyke swarm.

(iii) To establish and characterise the extent of intradyke geochemical variations and to assess the effects of alteration and metamorphism.

(iv) To characterise regional geochemical variations within the dyke swarm, and constrain the mode of their petrogenesis.

(v) To use all available data in order to assess the geodynamic significance of the Gannakouriep Dyke Swarm.

The emphasis in this study has been placed on an integrated approach to understanding the geodynamics, kinematics and anatomy of the Gannakouriep dyke swarm. The geochemical data recorded from the swarm have been used to constrain processes occurring during generation and emplacement of the dykes rather than provide a window on mantle petrogenetic problems.

1.3 Acknowledgements

Dr Dave Reid and Professor A.J. Erlank are acknowledged for their supervisory capacities, whilst a receipt of a bursary from the FRD is also acknowledged. Further finacial support through a UCT Jagger scholarship and from the Department of Geochemistry was also gratefully received. Additional XRF whole rock data were provided courtesy of Dave Reid. Many thanks to Ron Watkins, Anton le Roex, Mike Watkeys, Chris Hartnady, John Moore, Rich Armstrong, Chandra Mehl, Chris Harris (for $d^{18}O$ analyses) and Craig Smith are in order. Special thanks to Maarten de Wit for keeping body and soul together in the latter months, and for more than a few enlightening discussions. Kim Lord and Russell Herbert are accordingly thanked for the bruises and computer wizardry. Logistic support in the field was supplied by the Precambrian Research Unit, Department of Geology, University of Cape Town. U2 and Bob Marley are thanked for retaining some of my sanity during severn months of alone under a desert sky.

2 DESCRIPTION OF DYKES WITHIN SECTORS

2.1 Introduction

On the basis of the degree of deformation and geographical extent, the Gannakouriep dyke swarm is divided into three sectors (Figure 2.1). Sectors I and II both comprise NE striking dykes metamorphosed in the greenschist facies, yet are not structural continuations of each other and thus regarded as separate segments of the dyke swarm. Sector III dykes comprise a southerly continuation of sector II, and border sector I dykes on their southeastern margin. They are distinct from the latter two sectors by consisting of northerly striking dykes metamorphosed in the amphibolite facies.

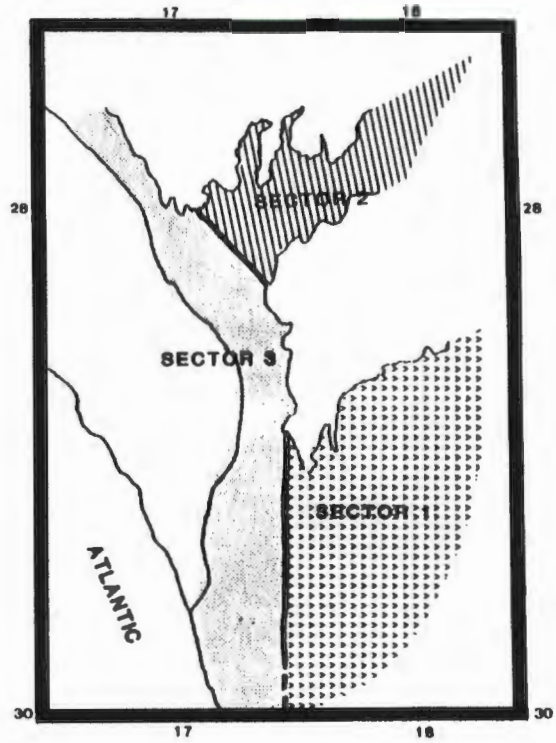

Figure 2.1. *Subdivision of the Gannakouriep dyke swarm into three sectors. Sectors I and II are relatively undeformed by subsequent deformation (550 - 500 Ma), and now represented by greenstones, whilst sector III dykes are pervasively sheared and re-orientated, predominantly comprising low grade amphibolites.*

2.2 Sector I dykes

2.2.1 Basement Lithologies and Anisotropy

Dykes ascribed to sector I have been studied in the area immediately southeast of Vioolsdrif extending down to Steinkopf (Figure 2.1). In the north of the area the local basement comprises folded and sheared supracrustal sequences of interbedded rhyolite, porphyritic andesites, trachyitic lavas,agglomerates and volcaniclastics of the Haib sub group (Blignault, 1977). The latter are in part intruded by and partly in sheared contact with underlying adamellite, granodiorite, tonalite and leucogranite of the Vioolsdrif Intrusive Suite (Reid, 1979), which comprises most of the basement to the south.

Towards the southern end of sector I the granitoids of the Vioolsdrif suite are superseded by another basement complex locally comprising poly-deformed quartzites, amphibolites, biotite gneisses and migmatites of the Bushmanland sub-province. The two basement complexes are juxtaposed along the ENE striking Groothoek thrust (Hartnady et al., 1985).

Namaquan tectonogenesis has imparted a discontinuous penetrative foliation and lineation in the Vioolsdrif granitoids. On approaching the Groothoek thrust to the south, development of the LS fabric intensifies whilst the associated stretching lineation becomes rotated into the horizontal towards the transport direction (Figure 2.2).

Basement anisotropy in the northern and central areas of sector I mainly comprise a series of northwest striking right lateral shear zones which contain a northerly dip slip component (Van der Merwe and Botha, 1988). WNW striking discordant pegmatites of the Namaqua Pegmatite swarm are discontinuously emplaced over the entire basement (Van der Merwe and Botha, op. cit.).

2.2.2 Structural Characteristics

The dykes are intruded along tensile fractures striking N031°E (Figure 2.3) and generally dip subvertically to vertically. Locally they attain widths and strike lengths of up to 52 metres and 32 km respectively, though more commonly dykes are in the order 20 metres wide. Multiple dykes are rare, only one example being recorded northwest of Swartkop.

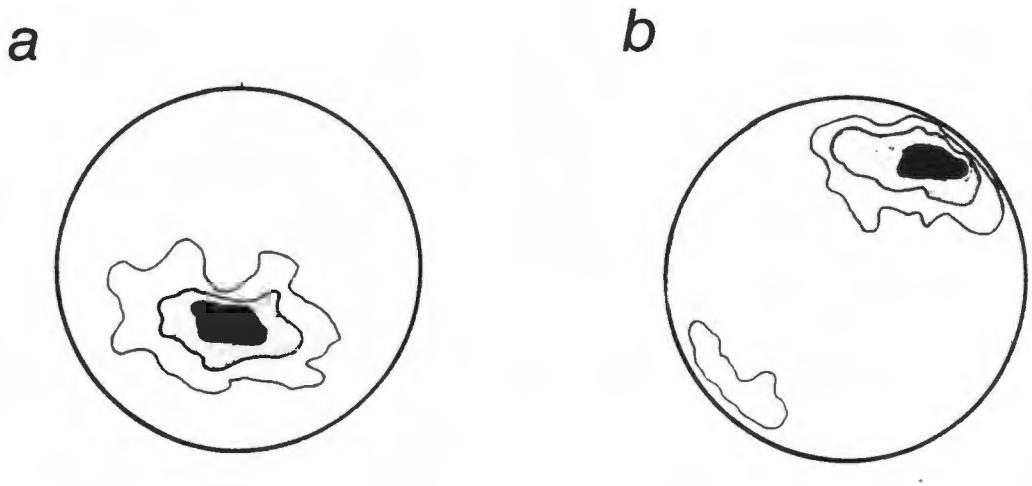

Figure 2.2. *Lambert equal area nets of basement fabrics prior to the intrusion of the Gannakouriep dyke swarm in Sector 1. A: S fabrics n = 287; B: Lineations n = 216. Contouring interval at 2%.*

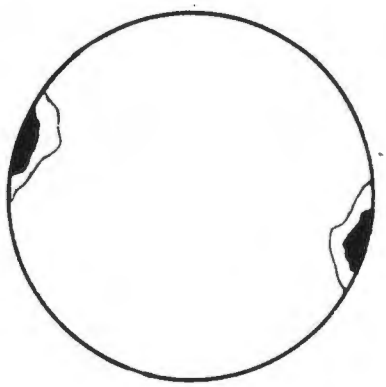

Figure 2.3. *Lambert equal area net of poles to dyke dip and strike in Sector 1. n = 311, contouring interval at 2%.*

Basement anisotropy is cut almost perpendicularly by the dykes, effectively responding to emplacement in a homogeneous manner, although some minor deflection is encountered along northwest trending Namaquan shears and faults. Deformation of the basement by the dykes is essentially discontinuous, intrusions tending to be

concentrated in structurally related complexes confined to zones of high strain, whilst the intermediate basement remains relatively unaffected. The latter observation makes calculation of total crustal extension due to dilation of the dykes difficult, but total extension in the sector is estimated to comprise 3 %. Locally, intradyke complex extension may reach 23%.

2.2.3 Lithologies

The dykes mainly comprise phanerocrystalline alkali gabbros which are subophitic in their cores, but approximately 5 % are sparsely porphyritic containing large (5 cm) zoned phenocrysts of plagioclase. Chilled margin facies are normally aphyric often containing sparse microphenocrysts of plagioclase. The typical dyke rock is formed of plagioclase (An63-24), clinopyroxene +/- olivine, apatite, ilmenite, titanomagnetite and late secondary pyrite. Lateral intradyke lithological heterogeneity is evident amongst these dykes suggesting complex fractionation and magma crystallisation processes during intrusion and subsequent consolidation. Whilst the majority of dykes exhibit cores that are more leucocratic than their corresponding marginal facies, intradyke interiors can vary from mesogabbros to porphyritic anorthositic cores within a kilometre along strike.

Much of the primary mineralogy has subsequently been replaced during low grade metamorphism in the chlorite-epidote-albite-quartz zone of the greenschist facies (Winkler, 1967). Evidence for gross alteration and fluid rock interaction with the dykes is frequently manifest by epidote veins "intruding" the gabbros.

2.2.4 Xenoliths

The dykes occasionally contain xenoliths of local basement and Namaqua pegmatites. The xenoliths occur in three basic categories;

(i) as enclaves of basement,
(ii) xenocrysts of alkali feldspar and quartz, and
(iii) thin selvages and dismembered bridges of country rock left in the intervening spaces of anastomosing dykes (Figure 2.4).

Figure 2.4. *Selvages of Vioolsdrif granite within dykes of the Gannakouriep suite. The former are interpreted as representing broken bridges and screens separating anastomosing dykes during the initiation and propagation stages of emplacement. Sample locality S028°53'00''E017°44'05''.*

Most xenolith enclaves are only partially corroded and frequently exhibit partial quench textures of subophitic dolerite surrounding them. The latter observation suggests that they have undergone limited transport and assimilation. Where enclaves do exhibit extensive assimilation and disintegration, biotite and other hydrous phases within the xenoliths appear to have been completely extracted in a melt phase leaving a residue of quartz and feldspar. Xenocrysts of alkali feldspar and quartz are normally confined to the cores of larger (> 30 m wide) dykes where at first glance they often mimic plagioclase phenocrysts. They contrast from the latter by typically exhibiting corroded 'amoeboidal' morphs.

2.2.5 Metamorphism and Rheomorphism

The degree of contact metamorphism inflicted upon the country rock is dependant on the width of the intruding dyke (or complex). Larger dykes tend to impart a greater degree of contact metamorphism which, in the field, is apparent by ridges of metamorphosed basement straddling either side of dykes along strike. Metamorphic aureoles associated with the dykes have not been studied in detail in this thesis, however a dyke of the order of 30 metres in width will commonly produce an aureole in excess of 100 metres.

Samples of metamorphosed Vioolsdrif adamellite collected from the contacts of, and 5 metres either side of two dykes 45 metres wide have been examined in thin section. At the dyke wall contacts partial anatexis has occurred, producing pseudo-buchites with relict maculoses of amoeboidal quartz (Figure 2.5) frequently surrounded by coronas of chlorite. Textures are characterised by myrmekitic intergrowths of alkali feldspar and quartz, and perthitic exsolution in feldspars. Index minerals of prograde metamorphism of the country rock by the dykes are obliterated by retrograde chlorite, though pseudomorphs after amphibole are inferred to have occurred in the upper part of the PTt loop.

At five metres from the dyke contacts metamorphism is characterised by a combination of dynamic and thermal metamorphism. Small fracture zones 0.5 cm wide contain undulose mosaic quartz, some of which has been polygonised, associated with chlorite (Figure 2.6). The latter comprise zones of cataclasites which may serve as sites of melt generation.

The degree of partial anatexis occurring along strike of a dyke is heterogeneous. Though variability in composition of the country can comprise a major factor, high degrees of anatectic melting are probably only achieved locally where conditions of high pH_20 sufficiently depress the eutectic melting point of the country rock.

2.2.6 Post Gannakouriep Deformation

The Gannakouriep dykes are essentially undeformed in sector I bar three phases of minor brittle faulting. These comprise;

(i) Northwest striking normal faults dipping subvertically to the northeast. The latter displace the Gannakouriep dykes prior to the development of the Nama erosional unconformity.

(ii) A series of northerly striking faults comprising normal dip slip faults down thrown to the east. These faults may have been initiated during the the earlier phase of extension described in (i). Displacement on these faults can be constrained where they cut the Nama sediments. Net throw along these faults is usually of the order of 15 metres, although some faults may comprise over 100 metre of movement.

(iii) A set of northwesterly striking faults that similarly displace the Nama sediments and give an apparent conjugate fault pattern with the northerly striking faults. However the latter are displaced by these faults which comprise variably dipping normal dip slip faults with crustal blocks either downthrown to the northeast or southwest. Where they displace the Nama sediments on the Neint Nababeep plateau the apparent throw is of the order of 30 metres, however there is also an apparent sinistral component associated with these faults, suggesting that they comprise scissor faults.

Figure 2.5. *Photomicrograph of partially assimilated Vioolsdrif adamellite taken from the country rock/chill contact of a 38 metre wide dyke in Sector I. Specimen is 12 cm long. Within the assimilated adamellite a fabric parallel to the dyke is developed accompanied by the disappearance of hydrous mineral phases from the country rock. Sample locality: S028°53'07''E017°44'02''.*

Figure 2.6. *Photomicrograph of dynamic metamorphism affecting the country rock (Vioolsdrif adamellite) during dyke intrusion. The sample is taken 3 metres away from the contact with a 42 metre wide dyke. Note the development of dyke parallel fracture which appear to serve as sites for anatectic melt segregation, and fluid migration. Sample is 5 cm in length. Sample locality: S028°54'48''E017°42'12''.*

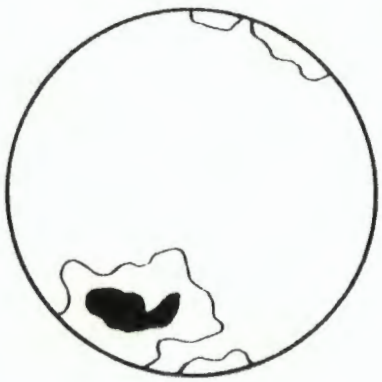

Figure 2.7. *Lambert equal area net of pre-existing S fabrics from the Lower Fish River region of Sector 2. n = 241, contouring interval at 2 %.*

2.3 Sector II Dykes

Sector II dykes are exposed along a major basement window extending from Klein Karas to the lower the Fish River in Namibia (Figure 2.1). The dykes in this region have only been studied in the Ai Ais and the lower Fish River areas due to the inaccessability of this terrain.

2.3.1 Basement Lithologies and Anisotropy

A window though the Nama sediments exposes the northern part of the basement which comprises granitic gneisses of the Namaqua Metamorphic Province. Further to the south these include quarzites, granitic gneisses and amphibolites of the Ai Ais Complex and Paragneiss Unit (Blignault, 1977). At the mouth of the Fish River, basement comprising granodiorites, adamellite and (quartz) feldspar porphyry of the Vioolsdrif Igneous Suite and De Hoop subgroup respectively is juxtapositioned against gneisses of the Namaqua Metamorphic Province along a northwesterly striking high strain tectonic discontinuity (Blignault, op. cit.).

The predominant basement anisotropy developed in the Namaqua Metamorphic Province and Richtersveld Igneous Sub Province was imparted during the main phase of Namaquan deformation (Dn2). In the southern area of the sector the dominant fabric is a northwesterly striking penetrative LS fabric developed in the Vioolsdrif granitoids and marginal rocks of the Namaqua Metamorphic Complex (Figure 2.7). The structural fabric to the northeast in the central zone (Blignaut, op. cit.) is more complex due to five deformational episodes predating dyke emplacement, however it still comprises a predominant northwesterly striking discontinuity.

2.3.2 Structural Characteristics

The dykes incise the basement fabric almost perpendicularly, striking on average N028°E dipping vertically to subvertically (Figure 2.8). They share many of the structural characteristics of dykes comprising sector I, occupying tensile fractures associated in structurally related complexes and thus are considered to have been emplaced in the same structural and crustal domain as the latter. Extension due to emplacement of the dyke is calculated in the order of 2 %.

On approaching the Orange River in the southern part of the sector the dykes veer from their northeasterly strike to a more northerly course. The latter are rotated in northwesterly striking left lateral shear zones (Blignaut 1977) which demark the northeastern most boundary of late Proterozoic - early Cambrian basement deformation. The lower Fish River area thus describes a transition zone between dykes comprising sector II and sector III. Although much of the intervening exposure between sector I and the southeastern part of sector II is obscured by later sediments, the continuity of strike between dykes of these two sectors suggest they may comprise a continuation of each other. Aeromagnetic correlation between these two sectors has been attempted, but in part due to the low natural remnant magnetisation preserved in the dykes (Onstott et al., 1986), and the low resolution of the aeromagnetic survey, correlation proved fruitless.

2.3.3 Lithology

The dykes comprise subophitic gabbros with well developed dolerite marginal facies, although some dykes are clearly porphyritic with plagioclase forming a prominent phenocryst phase. The typical dyke rock comprises clinopyroxene, plagioclase, apatite, titanomagnetite and ilmenite. Olivine is (apparently) lacking in thin section, although the presence of only clinopyroxene would indicate they maybe olivine normative. The mineral assemblage differs from dykes comprising sector I by titanomagnetite comprising the dominant oxide phase as opposed to ilmenite. The latter may reflect decreased oxygen fugacity (Haggerty, 1976) in the northern part of the swarm.

Metamorphism of the dykes is evident in the field by their green colouration associated with incipient chloritisation. Metamorphism is typically low grade, within the epidote -chlorite - albite - quartz zone of the greenschist facies (Winkler, 1967).

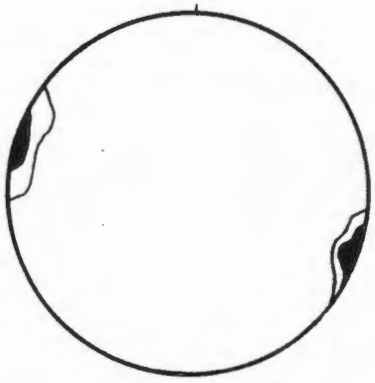

Figure 2.8. *Lambert equal area net of poles to dyke dip and strike in Sector 2. n = 168, contouring interval at 2%.*

Figure 2.9. *Lambert equal area net of poles to dyke dip and strike in Sector 3. n = 292, contouring interval at 2%.*

2.3.4 Xenoliths

Xenolith enclaves comprising granitic gneisses of the Namaqua Metamorphic Province are occasionally observed within the dykes. More commonly xenocrysts of alkali feldspar and occasionally quartz are detectible in thin section, often exhibiting partially corroded amoeboidal morphs.

2.4 Sector III Dykes

Dykes comprising sector III describe an area extending from Rosh Pinah in the north to south of the Doring River (Figure 2.1). The northeastern boundary of the sector is juxtaposed with sector II along northwest striking shears in the lower Fish River (Blignaut, 1977), whilst the southeastern margin is delineated west of the sector I by a series of northerly striking late Proterozoic - early Cambrian left lateral shears (Joubert, 1971; Booth, 1988). The boundary encompassing sector III can be partially approximated by the present course of the Orange River.

2.4.1 Basement Lithologies and Anisotropy

In the northeastern Richtersveld, the dykes are emplaced into a basement complex comprising granodiorites, granite and leucogranites of the Vioolsdrif Intrusive Suite and intercalated tuffs and lavas of the De Hoop subgroup (Ritter, 1980; Reid, 1977). They strike southerly across the moderately to steeply dipping west to northwesterly striking metasediments of the Rosyntjieberg Formation before re-entering granitoids and volcanics of the Vioolsdrif Intrusive Suite and De Hoop subgroup, thrust juxtapositioned along the westerly striking Mount Erebus fault. In the southern Richtersveld they also intrude, and thus post-date granitoids of the Richtersveld Igneous Complex which locally invade the basement.

Deflection of the dykes due to basement anisotropies is a common feature in this sector. The dykes are frequently diverted from their apparent northerly course along northwest striking late Namaquan brittle-ductile shear zones (Shimron and Von Veh, 1987) and minor basement faults. Sinistral refraction of dyke propagation direction across steeply dipping northwest striking foliation in the De Hoop subgroup is common, which upon exiting, the dykes resume their normal course.

Basement anisotropies are strongly encountered within bedding planes of the Rosyntjieberg Formation quartzites which are folded in a southerly plunging anticlinorium (Ritter, 1980). Due to the high degree of basement anisotropies and lithological heterogeneity, the host rocks in sector III appear not to have responded as an isotropic homogeneous medium during emplacement of the Gannakouriep dyke swarm.

2.4.2 Structural Characteristics

Apart from local deviations caused by basement anisotropies the dykes occupy tensile fractures striking in an apparent northerly direction dipping steeply subvertically to vertically (Figure 2.9). Multiple intrusions are rare, except in the case of the Main Dyke Complex situated in the Gannakouriep valley.

Basement deformation due to intrusion of the dykes is discontinuous within this sector. Four main sub-swarms comprising zones of relatively high strain during intrusion are discernible;

(i) The Swartpoot subswarm,
(ii) The Gannakouriep Valley subswarm,
(iii) The Mount Terror subswarm, and
(iv) The Mount Stewart subswarm.

The Gannakouriep valley subswarm contains the Main Dyke Complex comprising a teardrop dyke in excess of 1500 metres in width at its maximum extent (Figures 2.10 and 2.11). Examination of the Main Dyke Complex

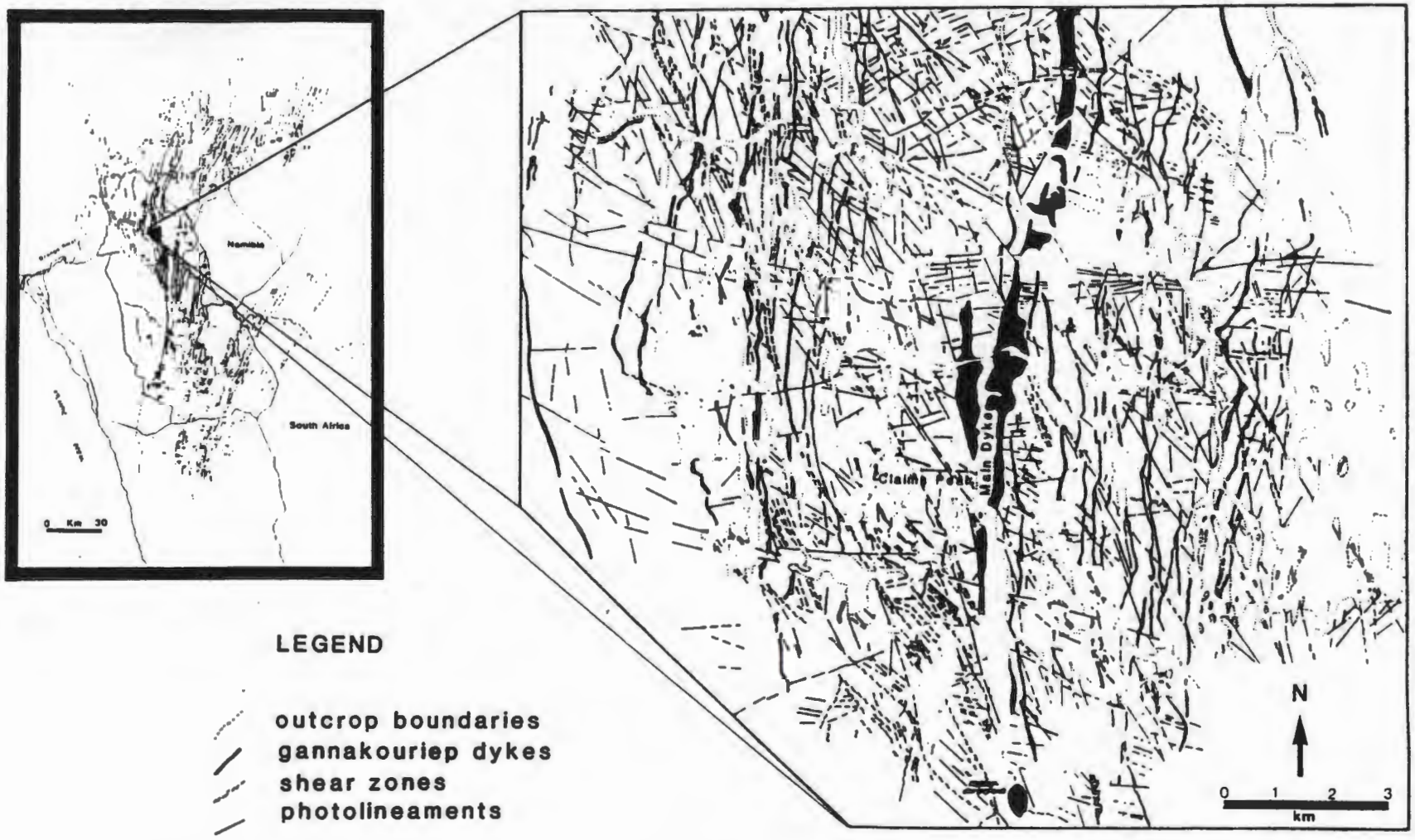

Figure 2.10. *Geological outcrop map of part of the Main Dyke Complex in Sector 3, which occupies the Gannakouriep Valley. After Ritter, (1980).*

Figure 2.11. *Photograph of the Gannakouriep Valley viewed from the Rosyntjieberg Mountains looking north. The Main Dyke occupies the entire valley floor , and is now partially obscured by later alluvium deposits. View is to the North.*

Figure 2.12. *Photograph of multiple intrusions in the Main Dyke. This shows evidence of partial solidification of the Main Dyke during emplacement, suggesting prolonged igneous activity, since some partial solidification of the magma must have occurred to permit brittle / brittle-ductile intrusion mechanics. Hammer is aligned NW-SE.*

in the Gannakouriep valley shows that the dyke comprises a series of multiple intrusions (Figure 2.12) and an array of anastomosing relict dykes (Figure 2.13).

Both De Villiers and Söhnge (1959) and Ritter (1980) regard the Main Dyke Complex as intruding metasediments of the Rosyntjieberg Formation in the southern end of the Gannakouriep valley. The latter observation is not borne out by this study. At the southern end of the Gannakouriep valley gabbros comprising the Main Dyke Complex are replaced by partially remobilised pendant granites and tuffs that form a lineament on areal photographs, which intrude the lowermost unit of the Rosyntjieberg Formation. The photolineament often used to infer the continuation of the Main Dyke Complex southwards through the Rosyntjieberg Formation comprises a later (late Proterozoic - early Cambrian?) high angle reverse fault steeply dipping to the west.

Dykes intruding the Rosyntjieberg Formation in the Twasies and Paradysberg mountains frequently are observed silling out along strike of the bedding, where the latter forms an acute angle with the dyke propagation direction. Further to the east around Devils Tooth and Mount Terror the bedding of the Rosyntjieberg formation is almost perpendicular to the strike of the dykes which are uninterrupted by the basement anisotropy.

2.4.3 Lithologies

The majority of sector III dykes comprise relict subophitic gabbros, though variations from melanocratic to leucocratic varieties are more pronounced than in the previous two sectors. Metamorphism of the dykes has rendered them amphibolites, schistosity only being developed in the marginal facies of the dykes.

The largest petrographic variation occurs within the Main Dyke Complex. Layered gabbroic complexes comprising alternative layers of plagioclase / olivine cumulate and olivine / pyroxene cumulate are common in the southern end of the Gannakouriep valley (Figure 2.14). Cumulitic pockets comprising labradorite and minor amounts of clinopyroxene, ilmenite and quartz frequently outcrop in plug and dyke like exposures within the gabbros near Claims Peak (Figure 2.15). Quartz bearing 'anorthositic' rocks have also been observed comprising a segregated transitional unit at the top of the Main Dyke Complex south of the Rosyntjieberg mountains.

2.4.4 Crustal Assimilation

Field evidence for crustal assimilation in the majority of the dykes is lacking however wholescale assimilation of country rock by the Main Dyke Complex in the Gannakouriep valley is clearly evident. The mechanism of assimilation is not directly attributable to stoping, but is a function of the intrusion mechanics of the Main Dyke Complex (Figure 2.16). Frequently granitic selvages are observed in the Main Dyke Complex bounded by relict dykes on either side. The dissection of the basement by the syn-intrusion of a complex array of closely spaced (>1 metre) dykes appears to be responsible for the formation of these xenoliths. The latter are frequently partially or totally assimilated by the enveloping gabbroic magma, such that distinction between leucogabbro and gabbro / granite mixing is no longer possible in the field. In the Main Dyke Complex it is probable that large quantities of country rock has been assimilated in this manner around Claims Peak.

2.4.5 Sills in the Stinkfontein Sequence

The relationship between the Stinkfontein Sequence and the Gannakouriep dykes has been briefly studied in the Cornellesberg above the preserved Port Nolloth Assemblage / basement unconformity (De Villiers and Söhnge, 1959). Within 0.5 km of entering the basal conglomerates, the dykes transgress into sills along bedding planes. They form a series of transgressive sills emplaced under brittle fracture which comprise multiply and compositely intruded medium grained dolerites. Many of the sills are developed along pre-existing volcanic horizons which were contact metamorphosed by the dolerites to amphibolites. No hyaloclastics or pepperites are associated with intrusion. Subsequent parallel bedding thrusting in the Stinkfontein Sequence has transformed many of the sills to greenschists.

Sills in the Stinkfontein Sequence have also been reported from southeast of Gelykwerf, north of Biesiesfontein,

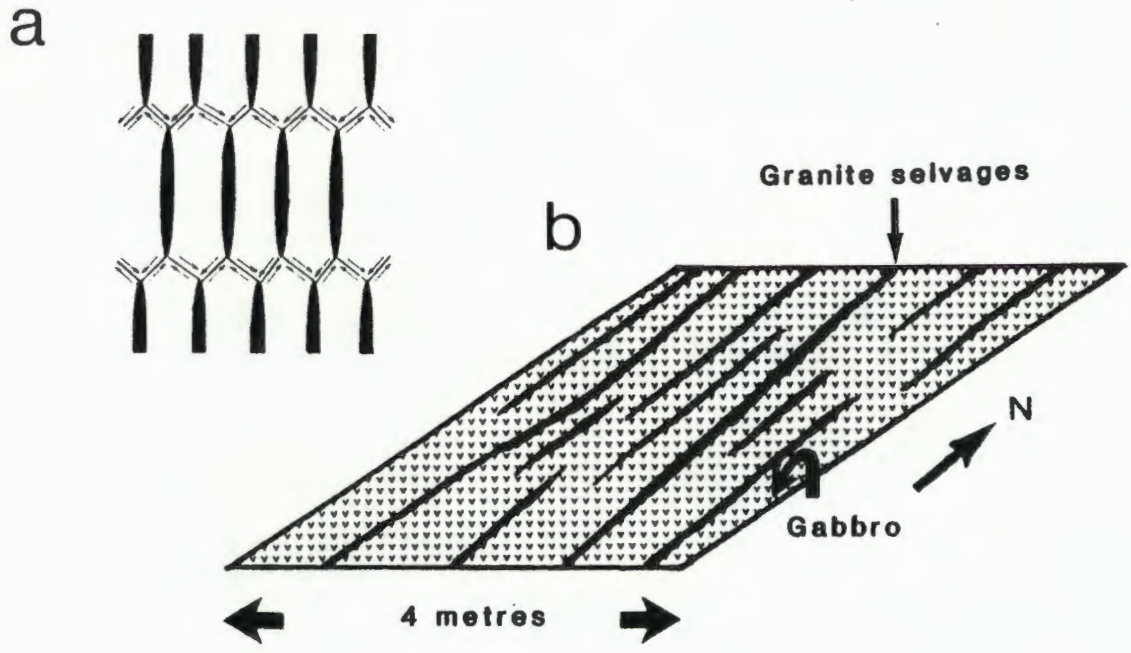

Figure 2.13. *Field sketch of relict granitic selvages in the western limb of the Main Dyke Complex near Claims Peak. The selvages of granite are interpreted as comprising relict anastomosing dykes which were emplaced as a series of dyke segments (**a**), subsequently converging in a network of shear fractures during continued dilation (**b**).*

Figure 2.14. *Photograph of banded cumulate facies in the Main Dyke. The mineral assemblages comprise Cpx + Ol + Ti-mag + (Plag) (dark bands), and Plag + (Cpx) + (Ti-mag) (light bands). Section shown is vertical, lens cap for scale.*

Figure 2.15. *Photograph of cumulate 'plugs' in the Main Dyke near Claims Peak (light coloured). The mineral assemblages comprise Plag + K-felds + (Ti-mag) + (Biotite) + (Cpx).*

Figure 2.16. *Photographic evidence of whole scale removal of granitic selvages separating dykes within the Main Dyke Complex by assimilation. View of photograph is to the north. The gabbro (dark coloured) is assimulating granite (light coloured) in the centre and left side of the photograph.*

south of the Duns Mountain trigonometric station, and in the Wildeperderand west of Noufontein (De Villiers and Söhnge, op. cit.).

2.4.6 Post Gannakouriep Deformation

Late Proterozoic - early Cambrian collisional orogenesis within the Gariep Arc resulted in sinistral rotation of the adjacent basement comprising sector III by 26° (Von Veh, 1988). In the southern part of sector III basement rotation has been accommodated by transpressive movement along a series of north striking shear zones. The latter comprise the Steenbok, Riethoek, Witbankensberg, Tierkloof and Kromnek shears which separate rotated crustal blocks in the order of 5-10 Km wide (Booth, 1988). Calculated net vertical thrust component associated with some of these shears is estimated circa 7 km to the west (Booth, op. cit.), suggesting that some of the dykes comprising sector III represent deeper levels of crustal exposure than the other two sectors.

Within the northeastern Richtersveld rotation is accommodated within a series of discrete anastomosing left lateral shear zones. The latter displace the Rosyntjieberg Formation in the vicinity of Mount Terror striking northwesterly through the Noms River, and may continue northwesterly across the Orange River along the domain boundary separating westerly and easterly verging folds in the Rosh Pinah area (McMillan, 1968; Hartnady, pers. comm.).

Within these rotated blocks the dykes are frequently sinistrally sheared along their margins, responding in a similar manner to reactivated faults. The confinement of deformation to the marginal facies of the dykes may reflect a competency contrast between dolerites and leucogabbros comprising their cores. Evidence for this is manifest by the occurrence of small multiple dykes intruding a coarse-grained leucogabbro dyke near Rosyntjieswater (Figure 2.17). The later dykes comprising dolerites are sheared against the gabbroic host dyke.

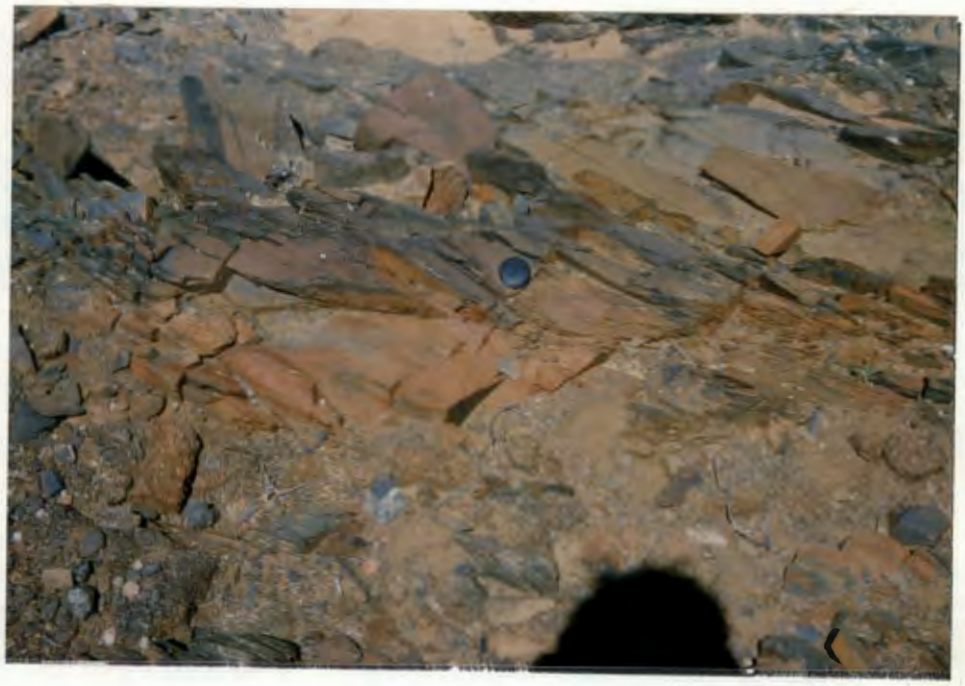

Figure 2.17. *Deformation of the Gannakouriep dykes in Sector III during Gariepian orogenesis (550 - 500 Ma) often results in shearing of dykes preferentially along their margins, in a similar manner to re-activated faults. In this example, south of Rosyntjiewater, a multiple dyke in which dolerite dykes have intruded the core of a leucocratic gabbro dyke exhibit preferential s fabric development in comparison to the host dyke. The latter provides strong field evidence that the loci of stress accommodation during subsequent activation of the dykes is in part petrographically controlled.*

2.5 Discussion

2.5.1 Relationships of Swarm to Inferred Rift Axis

A pseudo-palinspastic reconstruction of the dyke swarm prior to late Proterozoic - early Cambrian deformation removing angular shear strain in the dykes is presented in Figure 2.18. The extent of sediment deposition of the Port Nolloth Group eastwards of present day outcrops is poorly constrained. However the erosional unconformity associated with Nama deposition in the Hunsberge and Nababiepberge may constrain an eastern limit which has clearly had a different uplift history to the Gariep Arc (Kroner, 1977).

The swarm therefore appears to be injected close to an axis of differential uplift. However as Figure 2.18 suggests, the swarm was essentially emplaced east of the site of inferred rifting and basin development. The Gannakouriep dyke swarm bears a similar tectonic resemblance to off-rift dykes observed on the eastern flanks of the Red Sea (Coleman and McGuire, 1988).

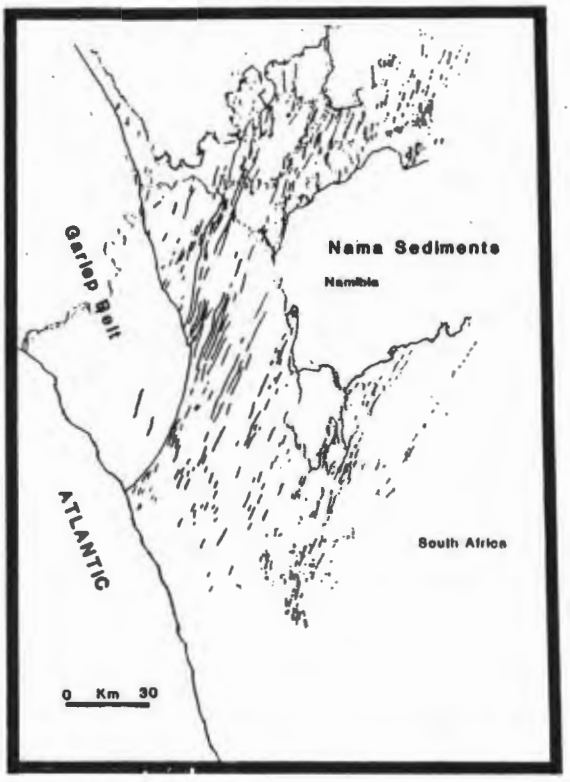

Figure 2.18. *A pseudo-palinspastic reconstruction of the Gannakouriep dyke swarm, prior to late Precambrian deformation.*

3 PETROGRAPHY AND MINERALOGY

3.1 Introduction

The majority of the dykes are in excess of 5 metres in width and thus tend to grade from doleritic chilled margins to coarse grained gabbroic interiors. Most of the lithologies lie either side of the critical plane of silica

saturation in the system Di-Fo-Ne-Qtz (Yoder and Tilley, 1962) and thus are normatively transitional between alkali olivine basalts and tholeiitic basalts. This is borne out by a total alkalis versus silica plot (Figure 3.1). The distinction between olivine normative and quartz normative gabbros in thin section is a tenuous one. The presence of primary quartz in thin section is difficult to establish in most dykes due to greenschist facies metamorphism producing quartz in the mineral paragenesis.

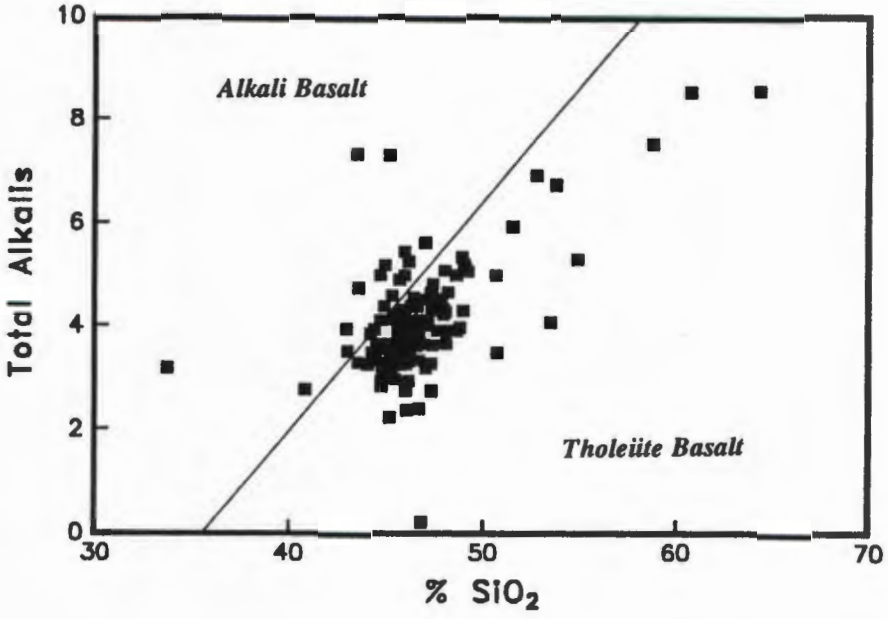

Figure 3.1. *Total alkalis ($Na_2O + K_2O$)n versus SiO_2 of the Gannakouriep suite, indicating their transitional nature between alkali and tholeiite basalts. Field boundaries from Macdonald and Katsura, (1964).*

The petrography of the Gannakouriep Dyke Swarm has been previously described by Middlemost (1964) who termed them hornblende diorites. His observations were restricted to samples collected from the central Richtersveld (sector III) where the dykes have undergone shearing and higher grades of metamorphism than encountered in other parts of the swarm. Thus the classification utilised by Middlemost (op. cit.) essentially refers to their metamorphic assemblage rather than their primary mineralogy.

Despite pervasive alteration and incipient metamorphism that characterises the petrography of the Gannakouriep dyke swarm, description of the lithologies adopted here is based on estimated modal composition of primary phases. In certain circumstances modal estimates can only at best be regarded as approximate due to the large degree of overprinting by secondary mineral assemblages.

3.2 Petrography

Mineralogical descriptions and analyses presented below were determined both optically using techniques outlined by Deer et al.,(1966), and by electron microprobe using the techniques described in Appendix 1.

3.2.1 Metadolerites

The metadolerites are restricted in occurrence to dykes less than 5 metres in width and chilled margin facies of larger dykes. They are typically aphyric with sparse euhedral microphenocrysts of plagioclase, although both aphanitic and less commonly porphyritic varieties are encountered.

The aphyric variety often display sub-trachytic textures in close proximity to chilled margins, with the alignment of microphenocrysts of plagioclase laths set in a hypocrystalline groundmass comprising dominantly of pyroxene and Fe-Ti opaques (Figure 3.2). Incipient metamorphism and devitrification of these dolerites frequently renders both pyroxene and plagioclase to a pale green mass of chlorite and carbonate. Aphanitic metadolerites are characterised by a hypocrystalline mass of cryptocrystalline mafic phases now altered to chlorite. Xenocrysts of unresorbed alkali feldspar (+/- plagioclase) and quartz are only observed in the aphantic dolerites where they intrude along cataclasite zones in dyke walls produced by thermal cracking.

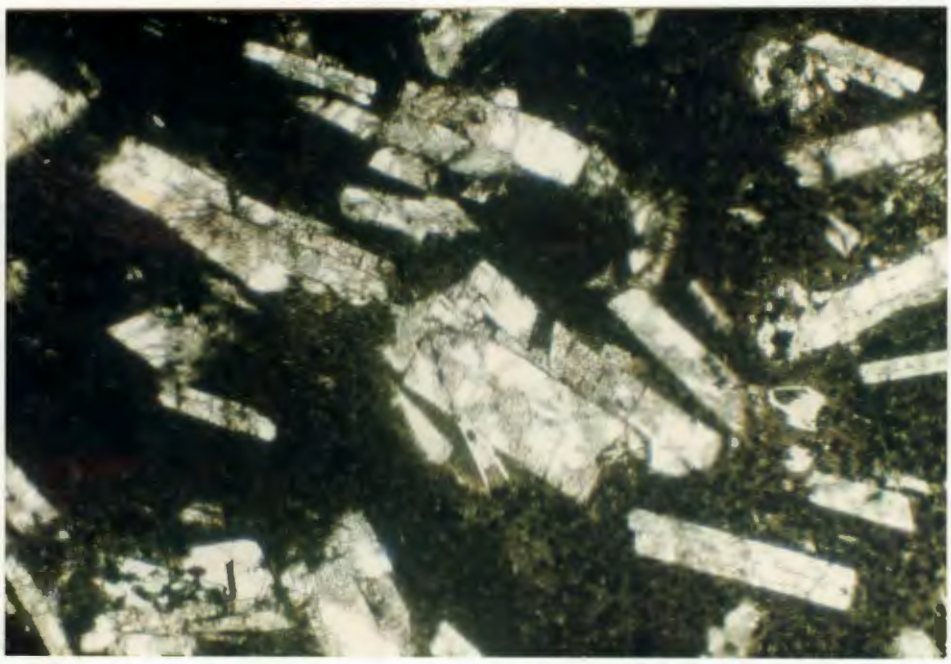

Figure 3.2. *Photomicrograph of a dolerite, with flow aligned plagioclase laths. Field of view is 23 mm, plane polarised light. Sample GKR-153 from Sector I.*

Porphyritic dolerites are very rare; only one occurrence of this variety was recorded in the southeastern Richtersveld. This example comprised medium grained trachytic textured labradorite plagioclase set in a holocrystalline fine grained hypidiomorphic groundmass constituting of ilmenite, biotite, plagioclase, pyroxene and apatite. The latter constituents with the exception of ilmenite are altered to chlorite, quartz, epidote and calcite. The labradorite phenocrysts exhibit slight zoning from core to rim with a decrease in anorthite content, though incipient albitisation and alteration to sericite and calcite may be partially responsible for this.

In all dolerites studied olivine is totally psuedomorphed by carbonate and chlorite or amphibole.

3.2.2 Metagabbros

The metagabbros are distinct from the dolerites in three ways;

(i) orthopyroxene is observed in some samples,

(ii) the gabbros exhibit a much wider modal composition varying from melanogabbros (px50-pg40; px = pyroxene, pg = plagioclse) to leucogabbros (px20-pg70), and

(iii) The gabbros display a much wider textural variation, including rhythmic layering and cumulate varieties.

3.2.3 Subophitic Gabbros

The gabbros are invariably coarsely phanerocrystalline. The main constituent phases consist of +/- olivine, clinopyroxene, plagioclase, and ilmenite, whilst minor and accessory phases comprise +/- alkali feldspar, apatite, biotite and magnetite. Modal olivine (or pseudomorphs there of) is minor, typically less than 5 % situated in intergranular spaces between plagioclase laths, or subophitically enclosed in prisms of clinopyroxene. The absence of essential olivine in some samples collected from the interior of large dykes (in excess of 30 metres in width) may indicate fractionation and cumulate settling either during intrusion or consolidation of these dykes. Clinopyroxene forms the dominant ferro-magnesian phase and almost invariably subophitically encloses plagioclase laths of labradorite and euhedral acicular prims of apatite (Figure 3.3). Partially developed coronas of brown hornblende are occasionally developed along the faces of clinopyroxene in intergranular spaces. These are typically zoned from brown hornblende through actinolite to tremolite towards the outer edges of the coronas and are considered products of down temperature deuteric alteration (Figure 3.4).

Fe-Ti opaque phases comprise ilmenite and subordinate magnetite occupying intergranular spaces between plagioclase laths, and minor inclusions in both pyroxene and olivine. Ilmenite is often present in the form of exsolution trellises (Figure 3.5) commonly associated with the alteration products sphene and rutile, and mantled by brown biotite.

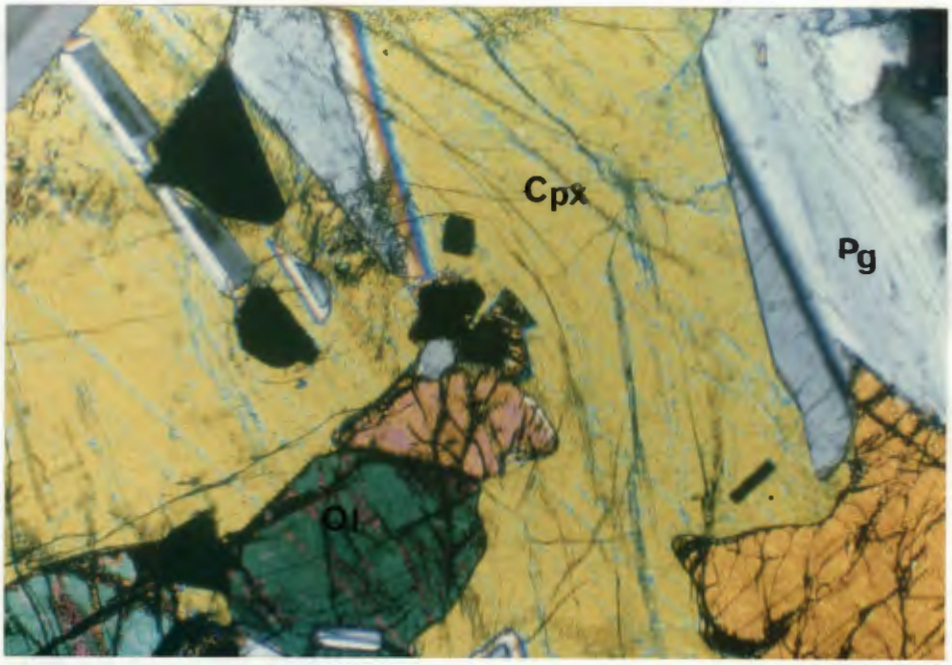

Figure 3.3. *Textural relationships between clinopyroxene and plagioclase is typically subophitic within relict gabbros of the Gannakouriep suite. Sample DRD-151, field of view 23 mm, crossed polars. Pg= Plagioclase; Cpx= Clinopyroxene; Ol= Olivine.*

Alkali feldspar only becomes modally important in the more leucocratic members of the gabbros, and even then it usually constitutes less than 10 % of the total mineralogy. It typically occupies two habits. In melano- to mesocratic gabbros, alkali feldspar is only present as partially developed coronas surrounding plagioclase,

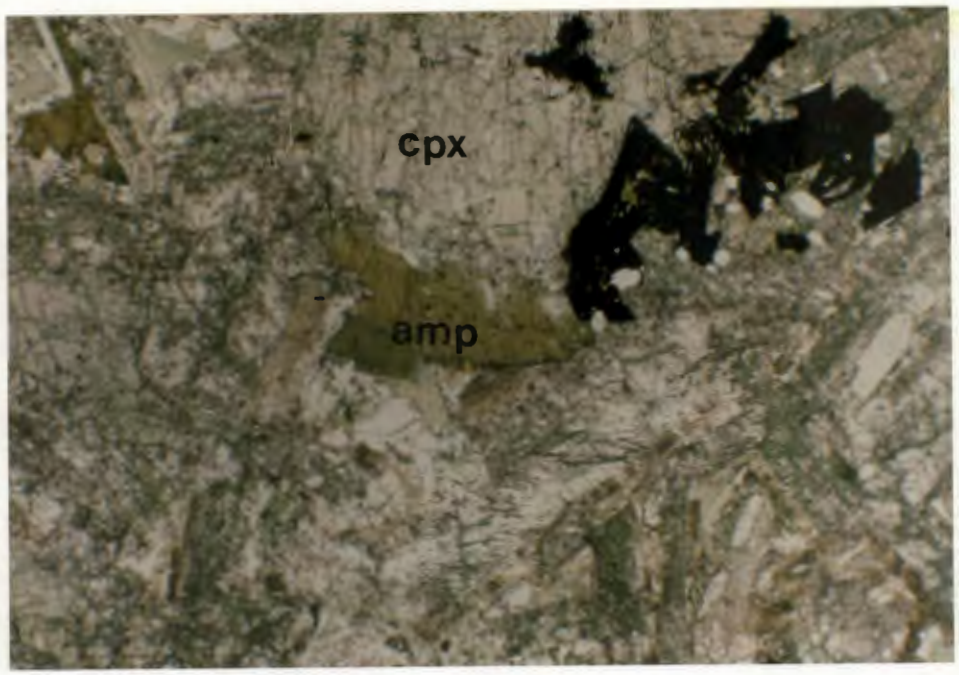

Figure 3.4. *Partially developed coronas of amphibole rimming clinopyroxene. The former are zoned from brown closest to the core to green and colourless, probably as a result of subsolidus deuteric alteration. Sample DRD-57, field of view is 23 mm, plane polarised light. Cpx= Clinopyroxene; Amp= Amphibole.*

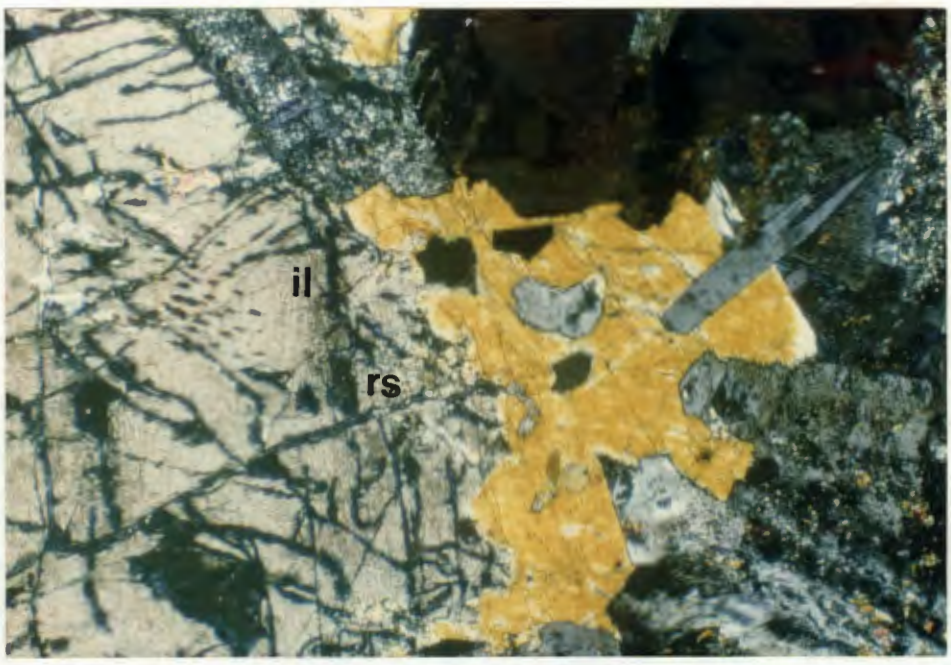

Figure 3.5. *Oxy-exsolution trellises of ilmenite exsolved from Ti-magnetite, now altered to a groundmass of rutile and sphene. Sample DRD-60, field of view is 23 mm, plane polarised light. Il= Ilmenite; RS= altered groundmass of rutile and sphene.*

whereas leucogabbros contain subhedral alkali feldspar in intergranular sites between plagioclase laths. Orthopyroxene has only been observed in a few samples. In these gabbros, it is only nominally important in the mode, usually comprising less than 15 % of the total pyroxene phases. Quartz is detected in intergranular spaces only in the most leucocratic tholeiites.

3.2.4 Layered and Differentiated Gabbros

The cumulus assemblages from the most primitive and the most differentiated gabbros are virtually all confined to the Main Dyke Complex, and are tabulated in Table 3.1. Plagioclase cumulus assemblages have also been recorded in a dyke from Sector I, which are thought to comprise Gannakouriep allochtholiths from the mid to lower crust transported to upper crustal levels during dyke propagation.

Ti-magnetite is now represented by complex intergrowths of exsolved magnetite and ilmenite. Olivine is psuedomorphed by carbonate whilst clinopyroxene (augite) has been replaced by brown amphibole. Biotite is present in most facies of the Main Dyke Complex, although absent in syenitic cumulates from sector I. Typically it occurs as fringes around opaques or in interstitial areas, grown either from intercumulus magma or as a deuteric alteration product.

Plagioclase invariably forms large tabular laths, which in the most basic cumulates is typically An63. In the lower temperature cumulates plagioclase is replaced at about An23 by alkali feldspar, which is usually cryptoperthitic. The latter mineral often occurs as coronas surrounding normally zoned plagioclase or as primocrysts in the more 'syenitic' cumulates. The original alkali feldspar are thought to represent the high temperature series anorthoclase - sanidine, but are currently present as perthites.

Table 3.1 *Summary of cumulate phases in the layered gabbros.*

	Assemblages
(1)	*Olivine + Clinopyroxene + Ti-magnetite + (Plagioclase)*
(2)	*Plagiocalse + Clinopyroxene + (alkali feldspar) + (apatite)*
(3)	*Plagioclase + alkali feldspar + (Ti-magnetite) + (Clinopyroxene) + (apatite)*
(4)	*Plagioclase + alkali feldspar + (Ti-magnetite) + (apatite) + (quartz) + (biotite)*

* *Minerals listed in order of importance, brackets denotes minor phases.*

3.3 Mineralogy

3.3.1 Olivine

Fresh olivine has only been observed in thin section in one sample (DRD-151) although the presence of olivine is often inferred by pseudomorphs comprising carbonate cores surrounded by coronas of pale green chlorite. A selected analysis is presented in Table 3.2. These depict a range in olivine composition of Fo 50 - 58. No zonation is recorded in any of the olivines. It should be noted that the olivines in this sample are not in equilibrium with the whole rock composition. Using an Fe^{3+}/Fe^{2+} of 0.15 for the whole rock compositon, the latter yields a magnesium number of 49 which, using Roeder and Emslies (1970) K_d =0.3, should crystallise olivines of the composition Fo 83. Since this particular sample comes from the main dyke complex, the disparity in respective magnesium numbers may reflect gravitational settling of olivines crystallising in a more Fe rich part of the magma chamber.

3.3.2 Pyroxene

Clinopyroxene is by far the dominant species of the two pyroxenes. The slight lilac pleochroism in thin section suggest that it is titaniferous augite, which is borne out by electron microprobe analysis (Table 3.2). No difference in clinopyroxene composition is detected between the two gabbroic suites; both exhibit a limited range in composition from Wo43Fs16En40 - Wo41Fs17En40. No zonation between cores and rim is observed, however simple twinning along the 100 plane is quite common.

The orthopyroxenes, when they comprise part of the mineral assembledge, are typically colourless when viewed under plane polarised light in thin section. Selected orthopyroxene analyses are given in Appendix 1 and show a limited compositional range Wo03Fs57En40 classifying them as hypersthene. Incipient recrystallisation of pyroxene of both species to chlorite +/-epidote or amphibole + biotite is widespread, often resulting in complete pseudomorphs poikilitically enclosing relict cores of pyroxene.

3.3.3 Feldspar

Plagioclase is by far the most abundant mineral phase, normally constituting about 60 % of the modal composition. Broad albite twin lamellae are characteristic combined in many cases with carlsbad and/or periclinal twins. Normally the plagioclases are of platy habit flattened parallel to the side pinacoid {010}, thus typically show alignment in layered gabbros. The range in plagioclase composition varies between An63 - An23. A selected electron microprobe analysis is given in Table 3.2.

Zonation is only encountered in phenocrystic plagioclase, which typically exhibit normal zonation from cores to rim (An56 - An26). Occasionally small subhedral crystals of ore are included along successive zonation boundaries.

Alkali feldspars occur in two principal habits, either as subhedral prisms occupying intergranular spaces, or as coronas to plagioclase laths. The varieties of alkali feldspar are all low temperature members of the solid solution series, comprising albite, microcline and abundant perthites. The perthites occur as both coarse and microperthites which display flame, braided and compound textures. The advanced degree of alteration affecting the alkali feldspars make it difficult to elucidate perthitic textures developed during magmatic crystallisation from those derived from subsolidus exsolution.

3.3.4 Fe Opaques

Both ilmenite and magnetite occur in the groundmass of most specimens. The former often is present as exsolution lamellae situated in a groundmass comprising sphene and/or biotite. When associated with this paragenesis, these latter two mineral phases are thought to represent deuteric alteration and incipient recrystallisation of Ti-magnetite from which the ilmenite was exsolved. Whether the exsolution of these lamellae

Table 3.2 *Representative phenocryst chemical compositions.*

	(1)	(2)	(3)	(4)	(5)
SiO_2	32.87	50.23	56.37	ND	ND
TiO_2	.03	1.09	ND	9.58	47.03
Al_2O_3	.03	2.42	28.55	4.79	ND
FeO	40.93	11.61	.26	79.54	51.71
MnO	.64	.35	ND	.24	.63
MgO	25.28	13.68	ND	1.18	.61
CaO	.08	19.88	11.93	ND	ND
Na_2O	-	.37	4.40	ND	ND
K_2O	-	ND	.44	ND	ND
Cr_2O_3	.02	ND	ND	.73	ND
NiO	.04	ND	ND	ND	ND
Total	99.92	99.63	100.00	96.06	99.98

ND = not determined: - = not detected.

(1) Olivine: (2) Clinopyroxene: (3) Plagioclase: (4) Ti-magnetite: (5) Ilmenite. All Fe expressed as FeO.

occurred during primary magmatic crystallisation (oxygen fugacity of around 10^{-6} atmospheres) (Haggerty, 1976) is difficult to ascertain unequivocally. However petrographic examination of samples obtained across strike from large dykes display an increasing ilmenite to magnetite (or pseudomorphs thereof) ratio towards the centre of these dykes. The latter observation may be a result of delayed cooling away from the margins of the dyke, permitting exsolution during magmatic cooling. Selected electron microprobe analyses of ilmenite and magnetite are given in Table 3.2. Both ilmenites and magnetites exhibit a restricted ranges with up to 1.5 % substitution of MgO for FeO.

Pyrite is the only other Fe phase present, occurring as irregular blebs. The pyrite content increases notably towards the dyke centres.

3.3.5 Miscellaneous Phases

Apatite is commonly observed as an accessory phase in the gabbros. Typically it occurs as euhedral acicular prisms which are subophitically enclosed in pyroxene. It obtains a modal maximum of ca 1 %, the dominant species being determined optically as hydroxy-apatite.

Biotite occurs in the groundmass in three forms, either as metamorphic, deuteric or primary biotite. Deuteric biotite is distinguishable from primary magmatic biotite since the former is almost invariably associated with alteration products from Fe opaques, whilst metamorphic biotite is always observed as part of the amphibolite mineral paragenesis.

3.4 Metamorphism

In nearly all the dykes primary textural relationships have been overprinted to varying degrees by partial metamorphic recrystallisation. Disequilibrium textures are characteristic of the very low grade of metamorphism attained. Metamorphism of the dykes has not been studied in detail, however two distinct facies have been ascertained.

(i) Greenschist Facies

The lowest grade of metamorphism is confined to dykes occurring in sectors I and II, characterised by the mineral paragenesis chlorite +/- epidote +/- albite +/ quartz +/- calcite. Chlorite is invariably associated with the recrystallisation of pyroxene and olivine, the latter typically being totally psuedomorphed. Epidote is commonly found associated with the recrystallisation of pyroxene and plagioclase, forming aggregate masses. The variety present is Fe rich and is stable through most grades of low temperature metamorphism, thus is unsuitable for determining reaction isograds (Winkler, 1967).

(ii) Amphibolite Facies

Slightly higher grades of metamorphism are indicated in sector III by the mineral paragenesis hornblende + biotite +/- chlorite +/- albite.

Metamorphic recrystallisation is more advanced than in the other two sectors, original textures often being obliterated by the growth of secondary minerals. Amphibole and biotite often form intergrown textures sub-poikioblastically enclosing relicts of pyroxene. Original grain boundaries are not always preserved. Metamorphic biotite is distinguishable from deuteric biotite, since the latter forms relatively large crystals encompassing Fe opaques, whilst metamorphic biotite associated with amphibole is partially derived by the recrystallisation of pyroxene.

3.5 Geothermometry

Various geothermometers have been devised to elucidate temperatures of crystallisation for a wide variety of rock types. The method employed here is an extension of the two pyroxene thermometry pioneered by Davis and Boyd (1966) and developed further by Lindsley (1983). The method utilises corrected Ca partitioning between clino and orthopyroxenes. Estimated temperatures of crystallisation using the graphical technique of Lindsley (op. cit.) yield values around 1020° C at 1 Kb.

3.6 Petrological Considerations

On the basis of textural relationships the deduced crystallisation sequence is ilmenite/magnetite - olivine - plagioclase - pyroxene. The crystallisation of plagioclase prior to pyroxene suggests that the liquid was enriched in normative anorthite prior to the emplacement of the dykes. Furthermore the development of subophitic textures is often interpreted as being due to saturation of the liquid with plagioclase with respect to pyroxene at the time of intrusion (Cox et al., 1979).

When considered in the system CaO-MgO-Al_2O_3–SiO_2 the petrological sequence could only result in low pressure fractionation (ca- 1kb) (Figure 3.6). At higher pressures the anorthite and fosterite fields contract, whilst those of diopside and spinel expand causing pyroxene to replace anorthite on the liquidus (Presnall et al., 1978).

However, low-pressure fractionation cannot account for the formation of thoeliitic gabrros from an alkali basalt parent. Yoder and Tilley (1962) demonstrated that the thermal divide between alkalic and tholeiite basalts is broken at pressures above 20 kb due to appearance of garnet and jadeitic pyroxene in the assemblage. This estimate was subsequently revised by O'Hara (1965, 1968) who suggested that the thermal divide disappears at about 8 kb. More recently Presnall et al. (1978) have suggested that tholeiitic basalts could be produced by fractional crystallisation from an alkalic basalt parent between pressures of 4-12 kb.

Thus, subsequent to the generation of the parental Gannakouriep magmas, at least two fractionation events have affected the composition of these magmas, one at intermediate pressures, and the other at low pressures.

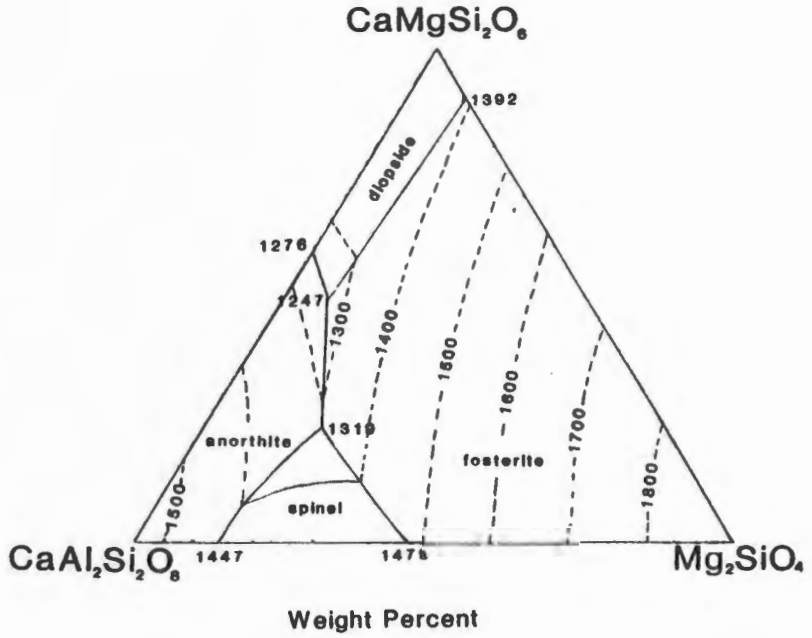

Figure 3.6. *Phase relationships in the system CaO-MgO-Al_2O_3-SiO_2 at 1 Kb, after Presnall et. al., (1978).*

4 INTRUSION MECHANICS

4.1 Introduction

Emphasis on mafic dykes occupying fractures and the principle of continuum fracture mechanics has been used to determine the emplacement processes of the Gannakouriep dyke swarm. A historical perspective of continuum fracture mechanics has been given by Pollard (1987). Most modern analyses of dyke intrusions are based on the criteria defined by Griffiths (1924), which consider a dyke to comprise a pressurised ellipsoidal flaw (flaw ellipsoid) contained within a homogeneous elastic medium (Figure 4.1). An important addition to the model of Griffiths (op.cit.) has been the recognition of a region of inelastic deformation encompassing the tips of propagating fractures (Figure 4.2) (Irwin, 1957).

The intrusion mechanics of the swarm has been studied in sector I where the dykes are relatively undeformed. The dykes are idealised as mode I elastic cracks in which basement response is regarded as approximately homogeneous and continuous on a regional scale. The latter assumption is validated by the observed lack of basement anisotropies affecting dyke propagation, and the similarity in rheological properties of the host rock within the sector.

4.2 Outcrop Configuration of the Dykes

The outcrop configuration of the dykes in the study area are shown in Figure 4.3. The latter defines four dyke complexes (GDC-1 to 4) which constitute zones of relatively high strain by comparison with the intervening country rock. Within each complex the dykes are emplaced as a series of segments whose trends are broadly parallel to the dyke complex as a whole. Typically they are in the order of 5 to 10 km in length attaining thicknesses up to 50 metres, and plunge vertically to subvertically. Local interaction between dyke segments during intrusion of the complex is evident by the development of bridge structures (Pollard et al., 1982) and

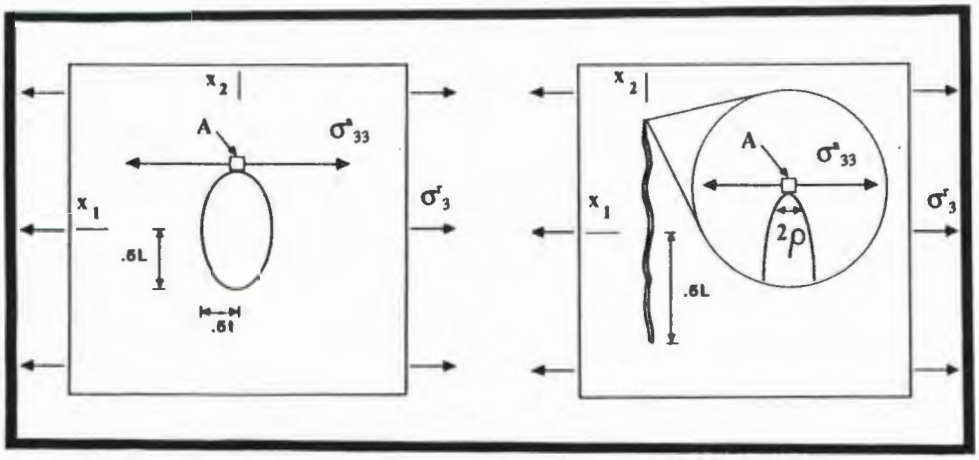

Figure 4.1. *The flaw ellipsoid is envisaged as a perfectly elliptical crack within an infinite elastic medium, with principal geometric axes X_1 and X_2 and dimensions L and t. Remote principal tensile stress is denoted as σ^3, whilst local tensile stress at the crack tip (A) is denoted by σ^a_{33}. The radius of curvature at the crack tip is denoted by θ. After Pollard, (1987).*

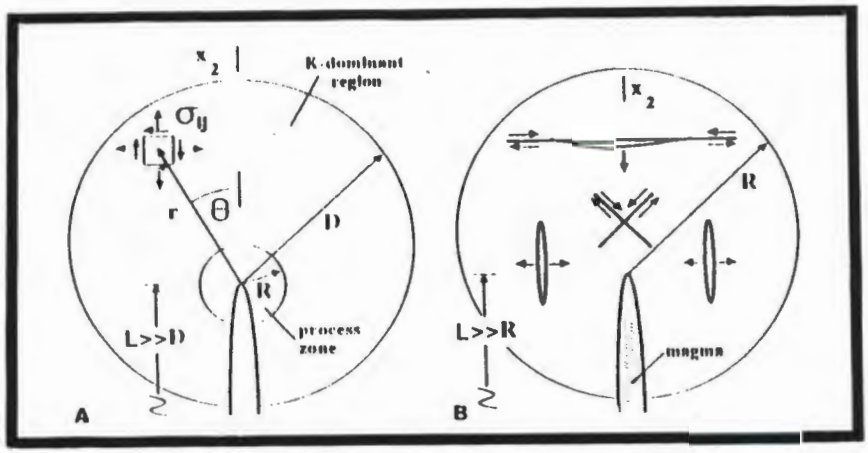

Figure 4.2. *The near tip region of a crack with the length L. (A) polar coordinates centred at the tip are r and θ. The region between R,r,D is referred to the K-dominant region for which the elastic stress component is denoted by σ_{ij}, being proportional to the stress intensity factor, K. The inelastic process zone is within a radial distance R of the crack tip. (B) propagation within the process zone, bounded by the radial distance R. Processes occurring within this zone include dyke-parallel jointing, conjugate faulting, and the opening and sliding of planes of weaknesses such as bedding planes and grain boundaries. Modified after Pollard, (1987).*

17'45

28'45

NAMIBIA

Vioolsdrif

Orange River

SOUTH AFRICA

Neint Nababiep Plateau

32

29'00

LEGEND

- Drift
- Dwyka tillite
- Nama sediments
- Gannakouriep dykes
- Bostonite dykes
- Pegmatites
- Amphibolite dykes

RICHTERSVELD SUB-PROVINCE	BUSHMANLAND SUB-PROVINCE
Ultramafic xenoliths	Porphyroblastic schist
Ademellite, granite	Biotite gneiss
Porphyroblastic gneiss	Amphibolite
Hornblende gneiss	Metaquartzite
Haib volcanics	

Structural and Geographic notation

- Jointing
- Dip and strike of bedding
- Foliation
- Shear foliation
- Plunge of lineation
- Shear foliation with lineation
- Fault
- Shear zone
- Thrust
- Plunge of fold axis
- Dry water course
- Road
- Track
- Mine prospect

Grootnoek Thrust

Kilometres

0 1 2 3 4 5

Figure 4.3 Geological map of sector I

shear fractures adjoining different dyke segments.

4.3 Dyke Geometries

The geometries of the dykes have been studied in dyke Complex GDC-4 by measuring the dyke thicknesses and their respective strike lengths. Dyke segment GD-17 (Figure 4.4) was selected for detailed study since it is continuously exposed, whilst data for all other dyke segments are combined to characterise dyke geometries present in complex GDC-4. The results from both studies are shown in Figures 4.5 and 4.6 respectively. Dyke

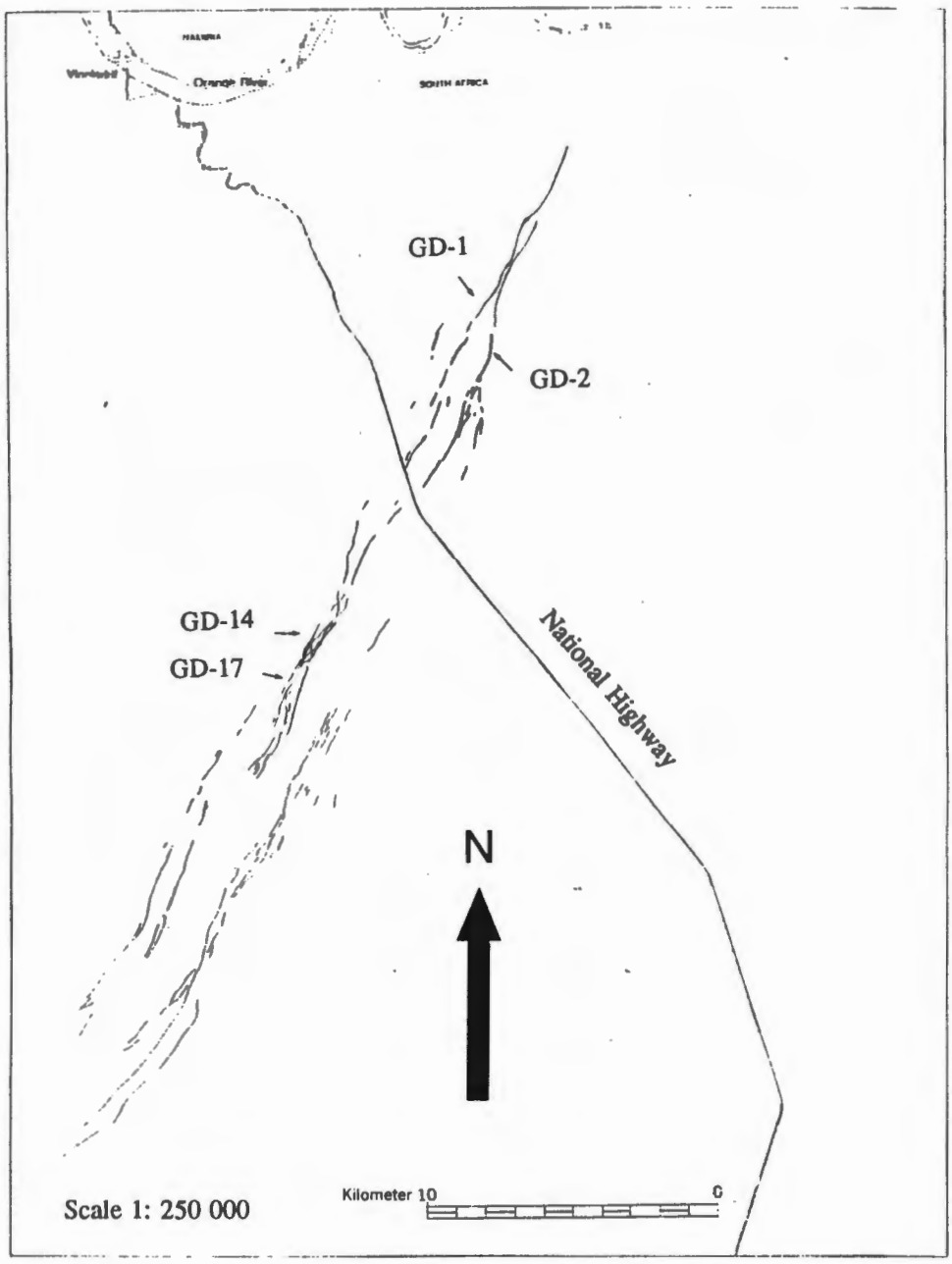

Figure 4.4. *Geological outcrop map of dyke complex GDC-4.*

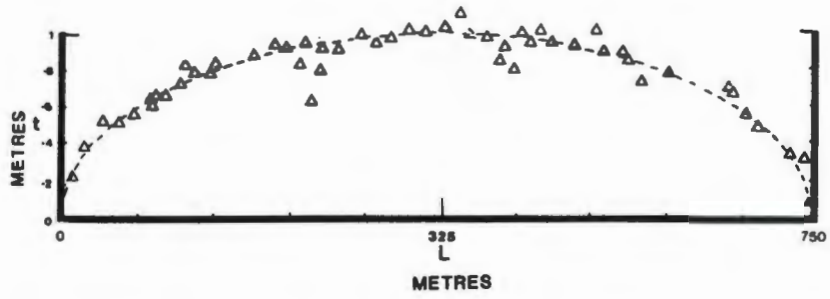

Figure 4.5. *Half widths of dyke Gd-17 plotted against total dyke length, with best fit ellipsoid superimposed (dashed line), n = 83.*

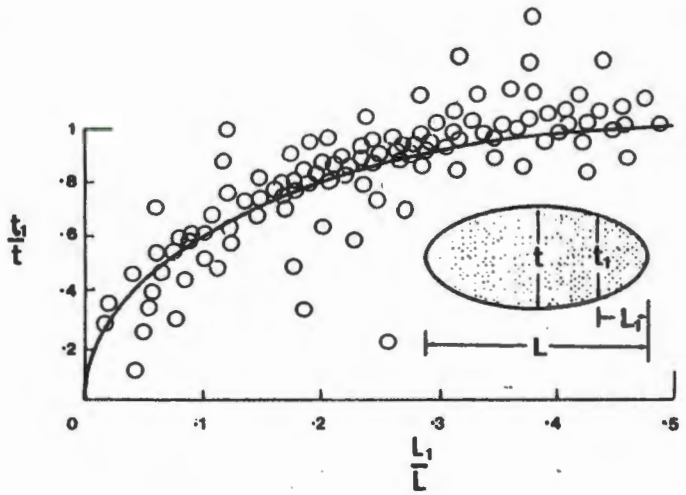

Figure 4.6. *All half width and length data for dykes studied in Sector 1 plotted on width (t) and length (L) normalised plot. Idealised ellipsoid curve shown in solid line.*

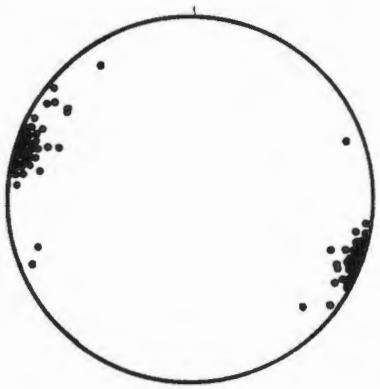

Figure 4.7. *Wulf stereonet of dilation vectors for dyke complex GDC-4. n = 85.*

segment GD-17 attains a maximum half width of 1.15 metres (from field measurements) with a total length of 1.03 km, which approximates to the best fit ellipsoid (Figure 4.5). Similarly the data acquired from all dykes exhibit good contact ellipiticity (Figure 4.6). The data points fall close to the curve defining ellipsoids, suggesting all dykes comprising complex GDC-4 can be approximated as flaw ellipsoids for continuum mechanics modelling. The apparent lack of tear-drop dyke geometries further suggests that remote stress fields during emplacement of the complex was uniformly distributed throughout the basement granitoids (Pollard and Muller, 1976), and the latter effectively acted as a homogeneous medium with a constant Young's modulus. Discrepancies away from the elliptical curve in Figure 4.6 by several data points are also evident. The latter may comprise zones of buds and cusps within the dykes, and are interpreted as zones of nucleation and preferential magma flow and dilation during intrusion.

4.4 Remote Stress Orientation and Dilation Vectors

That dykes are often perpendicular to the minimum regional stress axis is a well known principle (Anderson, 1938). However three dimensional displacement, and the incorporation of shear displacement by tensile fractures can often lead to erroneous interpretation of stress axes configuration during emplacement. A study of dilation vectors in dyke complex GDC-4 has been undertaken using a method similar to that described by Bussell (1989). Both displacements of pre-existing basement structures (especially apllite veins) in the basement host rock as well as displaced offsets (Currie and Ferguson, 1980) have been used. Although Bussell (1989) notes caution in using pre-existing structures to determine dilation vectors, the latter have been used here since the dykes appear to occupy tensile fractures generated during intrusion as opposed to exploiting fractures which may have had a prior kinematic movement history.

In Figure 4.7 the lenght/width geometries for all data points from the complex are shown. Most dykes tend to comprise pure horizontal extension fractures, indicating a mean $\sigma 3$ stress field orientated N121° E. However closer inspection of the data shows that vertical and shear slip components are present in some of the dykes. This is especially prominent in dykes GD-14 to GD-20 (Figure 4.4) where extensional conjugate cross fractures have linked different dyke segments during intrusion.

The local stress fields developed within the surrounding host rocks during intrusion and dilation of the dykes may cause variation in the orientation of stress axis in adjacent dykes. Such interactions of stress fields developed between neighbouring dykes has been used to determine the kinematics of bridge formation during the emplacement of en echelon dyke segments (Nicholson and Pollard, 1985). The extent of interaction of stress fields between neighbouring dykes has been investigated for a part of dyke complex GDC-4 using Anderson's (1938) model regarding dykes as a pressured elliptical hole in an elastic medium. The dykes are idealistic as mode I elastic cracks which are modelled with a constant magma pressure during intrusion and propagation of the dyke complex. In two dimensions an elastic solution for the stresses around a dyke can be resolved by calculating the appropriate Airy stress function, I, which satisfy the boundary conditions for any particular dyke.

The Airy stress function can be expressed as:

$$I = \mathrm{Re}\,(wq(w) + X(w)) \qquad (1)$$

Where $w = x+iy$, $w = x-iy$ and $q(w)$, $X(w)$ are complex potentials. The stresses σ and displacement u and V acting in the x and y directions are related to the complex potential (Pollard, 1973) by:

$$\sigma_{xx} = \mathrm{Re}[2q'(w)-wq''(w)-X'(w)] \qquad (2)$$

$$\sigma_{yy} = \mathrm{Re}[2q(w)+wq''(w)+X''(w)] \qquad (3)$$

$$\sigma_{xy} = \sigma_{yx} = \mathrm{Im}[wq(w)+X''(w)] \qquad (4)$$

$$2Gv = Re[(3-4v)q(w)-wq'(w)-X'(w)] \quad (5)$$

and

$$2Gv = Im\ [(3-4v)Y(w)-wY'(w)-X'(w)] \quad (6)$$

The double scripts refer to the direction normal to the plane on which the stress acts, and direction in which it acts (Figure 4.8). Compressive stresses are regarded as positive, whilst displacement is positive when acting in the negative direction of the x and y axis. G and v are the shear modulus and Poissons ratio of the host rock while Re and Im refer to real and imaginary parts of the complex functions. Prime denotes differentiation with respect to w. All functions here are written for plane strain. The complex potentials are related to stress as displacements on curvilinear co-ordinate directions (ε,n) by equations given by Timoshenko and Goodier (1951).

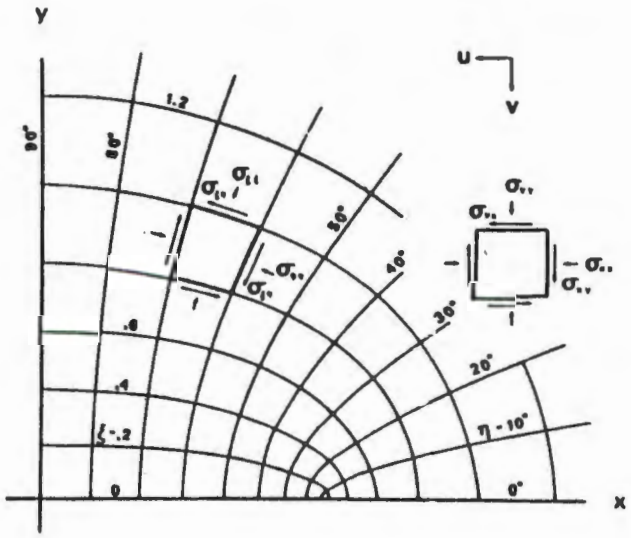

Figure 4.8. *Relationship between cartesian (x,y) and elliptical (ξ,η) orthogonal coordinates. The stresses state at any point is defined by σ_{xx}, σ_{xy}, σ_{yy} and the displacement at any point are u, v. Stresses are positive when they act in the vectors shown. Diagram from Pollard, (1973b).*

A mathematical study of the interactive local stress fields developed between adjacent dykes has been undertaken to qualify the control that they might exert on the remote stress orientation vectors. For the purpose of modelling interactive stress fields of adjacent dykes,the host rock of sector I is regarded as isotropic, homogeneous and elastic. The latter assumptions appear validated by the dyke geometry data. Contact between the magma and host rock is represented by the boundary ellipse $(x/l)^2 + (y/t)^2 = 0.25$, i.e. $\varepsilon = \varepsilon_0$ centred at the origin. Length to thickness ratios of the dykes as taken from field data $l/t = {}^1/_{\tanh \varepsilon_0}$, whilst magma pressure is considered to act normally to the dyke walls. Remote principal stresses, σ1 and σ3 act at infinity on the dyke with angle B and B+ pi/2 respectively from the x-axis which, from the dilation vector data, a value of β=0 has been assumed.

Boundary conditions for each individual dyke are satisfied by two different stress solutions (Pollard, 1973a):

(i) Uniaxial stress σ = σ1-p acting at infinity as an angle β to the x-axis.

(ii) A uniaxial stress σ = σ3-p acting at infinity at an angle β+pi/2 to the x-axis.

(iii) A hydrostatic stress p acting over the entire x-y plane of the host rock.

Stress and displacements for solution 1 and 2 are found by calculating the appropriate complex potentials q(w) and X(w) for $\sigma=\sigma 3-p$, β and $\sigma=\sigma 1-p$, $\beta+pi/2$, whilst solution 3 is derived by substituting the complex potential for hydrostatic stress (q(w)-pw/2, X(w)=0) (Pollard, op. cit.). The solution for these three criteria are subsequently summed, and shear stresses calculated from ε_{xx} and G_{xy} by constructing the appropriate Mohr envelope.

A computer program has been written to calculate individual stress fields for each particular dyke, and consequently summed with the stress field generated by adjacent dykes in Complex GDC-4. The results of shear stress calculations as presented in Figure 4.9, using v=0.25, G=0.5, $\sigma 1=p$ and $\sigma 3=0.5p$.

The interaction of stress fields between neighbouring dykes has been modelled on two scenarios;

(a) when two dykes are parallel and oppositely opposed to each other,

(b) where two dykes are parallel offset intrusions (Figure 4.9).

In both cases the stress fields between adjacent dykes is a partial function of the interdyke spacing normal to their strike lengths (i.e. the closer the interdyke spacing, the greater the net interference stress fields). In the first case the calculated interference stress field results in a higher shear stress field outboard from the two propagating dyke tips. The latter results in a local opposed rotation of the principle stress fields at the dyke tips, tending for divergent propagation. By contrast offset dykes generate a net stress field which is greatest inboard between the two propagating dyke tips. Rotation of the remote stress vectors sympathetically about a common pole will tend to converge the propagating dykes. Dykes intruded along the same line of strike are enhanced in their lateral propagation towards each other.

A study of the outcrop pattern of dyke complex GDC-4 indicates two master dykes (GD-1, and GD-2) in the northeastern part of the complex. Flow lineation data (section 4.5) suggests that these two dykes acted as feeders to laterally propagating dykes in the southwestern part of the complex. A likely sequence of dyke emplacement can be qualified using relative interaction of their stress fields to account for deviations away from common remote stress vectors. The outcrop pattern by dyke complex GDC-4 exhibits divergence between two master dykes (GD-1 and GD-2) in the northern part of the complex (Figure 4.4). Continuum mechanics modelling would suggest that these two dykes were initiated simultaneously parallel to each other (case a), consequently generating a net local interacting stress field causing divergent lateral propagation southwestwards. However the two master dykes appear to have differed in their initial emplacement mechanics. Whereas the master dyke GD-2 appears to occupy a single tensile fracture (or a series of fractures in the same strike), dyke GD-1 appears to have been initiated as at least two major offsets, that converged to form a broken bridge structure (case b).

4.5 Flow Lineations

Flow structures within the Gannakouriep dykes are relatively rare since they predominantly comprise even-grained gabbros. However close inspections of the dykes yields three criteria by which the flow kinematics of the dyke can be recorded. These comprise;

(i) Phenocryst alignment
(ii) Xenolith alignment
(iii) Deflection by previous basement anisotropies.

Large phenocrysts of plagioclase feldspar are rare in most dykes,however there are more commonly found in the southern area of Sector I. Typically they occur as laths up to 3 cm in length with aspect ratios exceeding 10:1 aligned in the plane of the dyke. Close inspection of dolerite chilled margin facies of the dykes often reveal

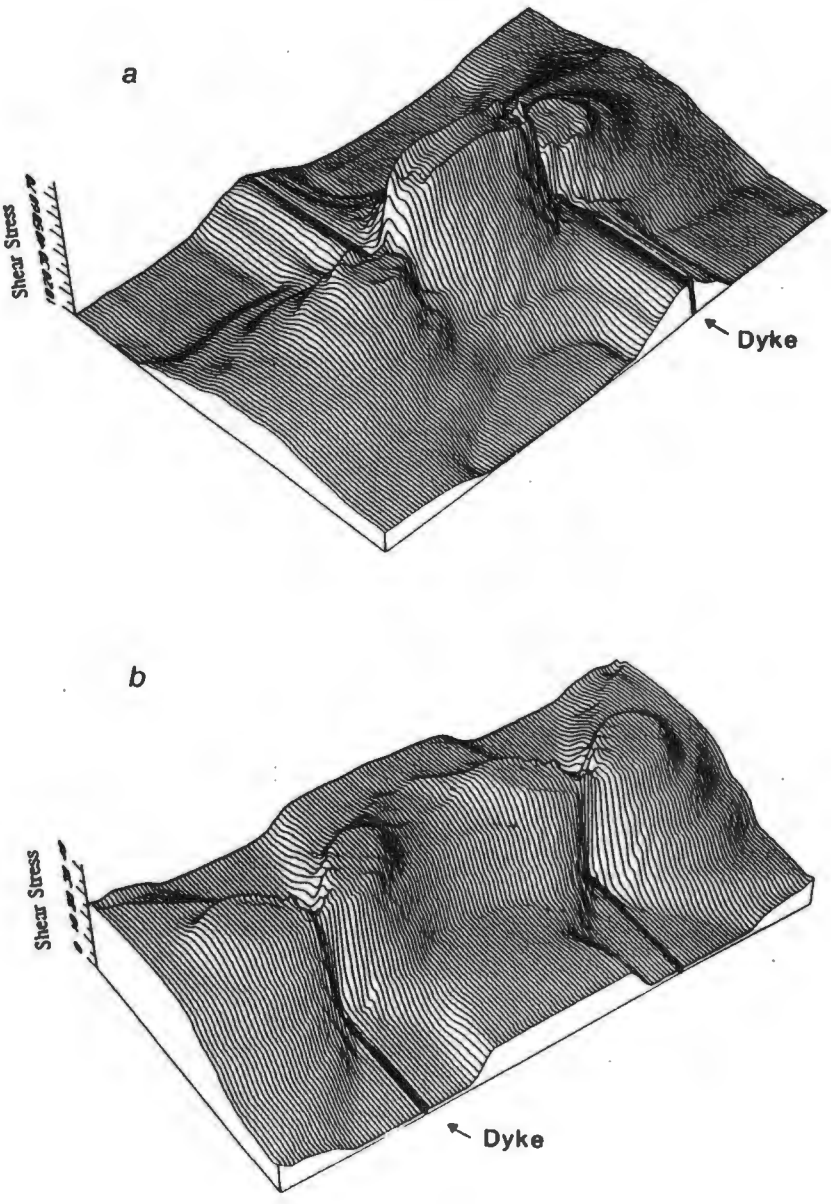

Figure 4.9. *Calculated integrated shear stress fields for synchronously emplaced dykes. (A) Two en echelon dykes propagating towards each other. Note the highest resolved shear stress occurs in the region between the two dykes, resulting in their propagation towards each other. (B) Two dykes propagating parallel to each other. The greatest resolved shear stresses lie in the region outboard of the dyke tips, resulting in their divergence during subsequent propagation. Note the highest shear stresses which occur at the dyke tips have been omitted for clarity. Shear stresses (Z axis) are reported in terms of* $((\sigma 1-\sigma 2)/2)\sin 2\theta)*100$, *where* θ=*the angle of the plane from the* $\sigma 1$ *axis that will undergo shear.*

microphenocrysts of plagioclase frozen in a devitrified mesostasis. These are almost invariably aligned in the plane of the dyke and display good directional textures.

Xenolith alignment occurs in the two forms. The more common variety comprises xenocrysts derived from the host rock aligned during magma flow. The most useful of these are xenocrysts of alkali feldspar which are often up to 2 cm in length with aspect ratios of around 3:1. Xenocrysts of other phases tend to be less useful due to their low aspect ratios. The second variety of xenolith lineaments comprises small clasts of country rock which demonstrably exhibit anatexsis and disintegration during magma flow. The latter often results in quartz-feldspathic xenocrysts strewn from the disintegrating clasts in lines orientated in the direction of flow.

Propagation and flow characteristics of the dykes can also be demonstrated by their deflection due to basement anisotropies. The latter is not quantitive but qualitive only, since a dyke deflected by a basement discontinuity towards the tip of the dyke must have propagated laterally into the anisotropy. Such structures are rare in Sector I dykes, only occurring where previous structures are suitably orientated for dilation.

The results obtained from flow analysis of dyke complex GDC-4 are depicted in Figure 4.10. Despite some variability recorded by the data, the majority of dykes indicate both lateral and vertical transport of magma during dyke initiation and dilation. The matter is best resolved when considering the data in terms of the criteria used to distinguish flow alignment. The majority of data recorded by alignment of microphenocrysts in dolerite chilled margins indicate a predominance of vertical magma transport, where as the occurrence of large plagioclase phenocrysts and xenoliths recorded from the gabbroic interiors of the dykes indicate lateral transport, notably plunging northeasterly. The disparity between the two groups of kinematic flow indicators is best resolved by initiation of fractures and initial dilation under predominantly vertical magma transport which is rapidly superseded by lateral magma transport during dilation and continued propagation. The data further define a predominant northeast to southwest propagation of the dykes.

Figure 4.10. *Wulf stereonet of flow lineations within dyke complex GDC-4. Open triangles = plagioclase microphenocrysts, dots = xenoliths, xenocrysts, and phenocrysts. n = 76.*

4.6 Inelastic Deformation

Inelastic deformation by the Gannakouriep dykes has been recorded both across strike and at the tips of dykes in complex GDC-4. Inelastic deformation within the Gannakouriep dykes is generally confined to the formation of systematic dyke parallel joints generated within the process zone during dyke propagation (Figure 4.2). The relative frequency of dyke parallel joints measured normal to dyke strike for two sections comprising a central

dyke section and a dyke tip are shown in Figures 4.11 and 4.12. The latter display a systematic initial rise in the frequency of jointing prior to decreasing away from the dyke margins.

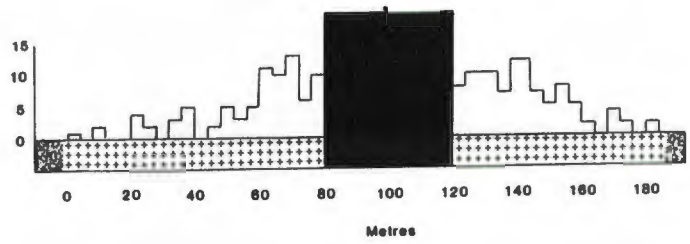

Figure 4.11. *Histogram of the frequency of dyke parallel joints adjacent to a 41 metre wide dyke in Sector I. The dyke is represented by the black bar, whilst the extent of the granite country rock is denoted by the area shaded in small crosses. The 'rubble' shading denotes the boundary between the granite and drift. These dyke parallel joints are regarded as syntectonic features rather than cooling joints, since microscopic examination shows that inpart they acted as channels for melt segregation of the country rock during emplacement of the dykes.*

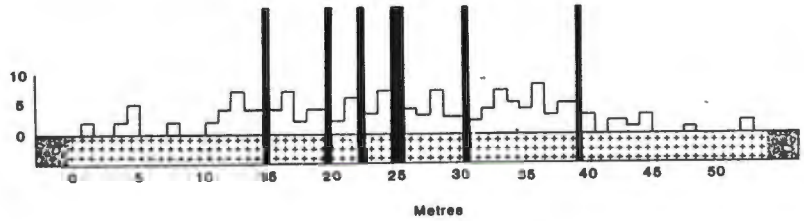

Figure 4.12. *Histogram of the frequency of dyke parallel joints occurring within the process zone near the tip of a 17 metre wide dyke in Sector I. The black bars represent dykelets dilating dyke parallel joints. The notation used is the same as that for Figure 4.11.*

The distance over which jointing patterns occur appear proportional to the dyke geometries, such that larger dykes comprise zones of greater inelastic deformation. The similarity between development of dyke parallel joints and the accompaniment of master dykes by daughter dykes, suggest stress field development similar for both processes (Figure 4.13). Initiation of joints within the process zone of dykes may therefore lead to their subsequent dilation by the advancing magma, and thus may provide a mechanism for brittle fracture branching of dykes within the upper 5 km of the crust.

Interpretation of dilation and formation of jointing patterns developed within the process zone of dykes can be constrained mathematically using techniques developed by Delaney et al. (1986) where they consider the stress intensity ratio (R) of any particular point occurring within the process zone of the dyke. The stress intensity ratio R is defined as

$$R = \frac{(P_m-\sigma_H) + (P_m-\sigma_h)}{\sigma_H-\sigma_h} > -\cos 2(\alpha) \qquad (7)$$

Where P_m = joint wall magma pressure after dilation which is equal to the $-\sigma_{11}$ stress axis across the joint under consideration, assuming σ_{12} across the joint = 0 due to negligible pressure gradient during magma flow. σ_H and

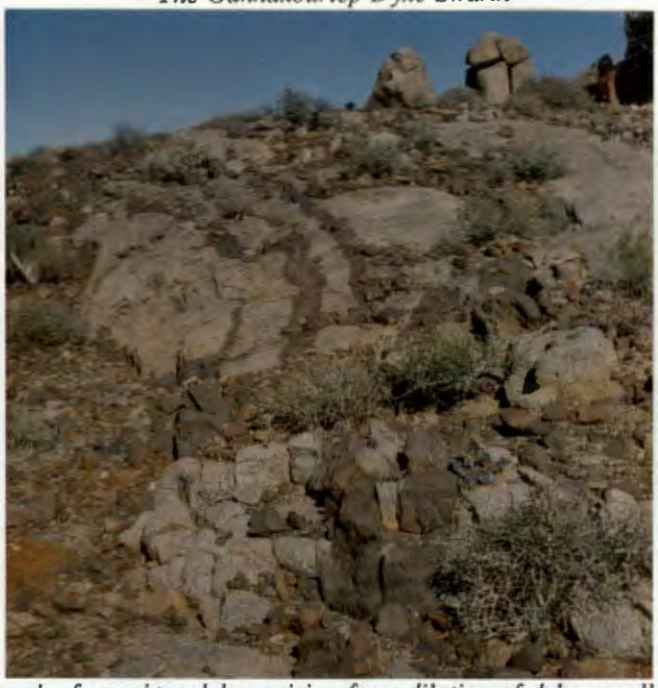

Figure 4.13. *Photograph of daughter dykes arising from dilation of dyke parallel joints formed within the inelastic process zone of a parent dyke at depth. View is to the southeast, dykes are approximately 10cm wide. Location S028°56'03''E017°40'11''.*

σ_h are the principal horizontal stress axis in two dimensions, and α is the angle between the minimum regional stress axis and σ_h is the short axis of any potential joint (Figure 4.14). For R<-1 the magma pressure is effectively less than the minimum compressive regional stress, therefore incapable of dilating joints of any orientation. Conversely when R>1 the magma pressure exceeds the maximum regional compressive stress ($\sigma 1$) thus capable of dilating joints of any orientation. The stress intensity ratio versus the angle a between joints occurring within a process zone derived by Delaney et al. (op.cit.) is shown in Figure 4.14. The critical field defined by R as a function of the angle a between a vertical joint plane and the direction of the least principle stress lies between the values -1 and 1, which is the field occupied by all dykes. Clearly in the case of dyke belonging to dyke complex GDC-4 initiation of dyke parallel joints in the process zone, and the lack of deviation by dykes from their propagation paths by local basement anisotropies indicate very low stress intensity ratios during intrusion. A calculated stress intensity ratio for these dykes around R= -0.8 suggests that the occurrence of dyke parallel joints are controlled by regional stress patterns in the process zone, rather than pre-existing basement discontinuities.

Conversely it has been previously noted that dykes occurring in sector III are frequently affected by basement structure with angular deviations upto 35° from propagation direction. The latter suggests that the stress intensity ratio for Sector III dykes is higher, R = -0.1, indicating higher magma pressures within dykes comprising Sector III.

The generation of joints in the process zone ahead of a propagating dyke tip has been considered in terms of changes in horizontal stresses relative to perpendicular distance from a dyke tip by Delaney et al. (op cit) using the equation derived by Broek (1978).

$$\frac{\sigma_{ij} - \sigma_{ijr}}{P_m - \sigma_h} = \frac{C g_{xy}(\Theta)}{(2r/a)^{1/2}} \quad r/a \ll 1 \qquad (8)$$

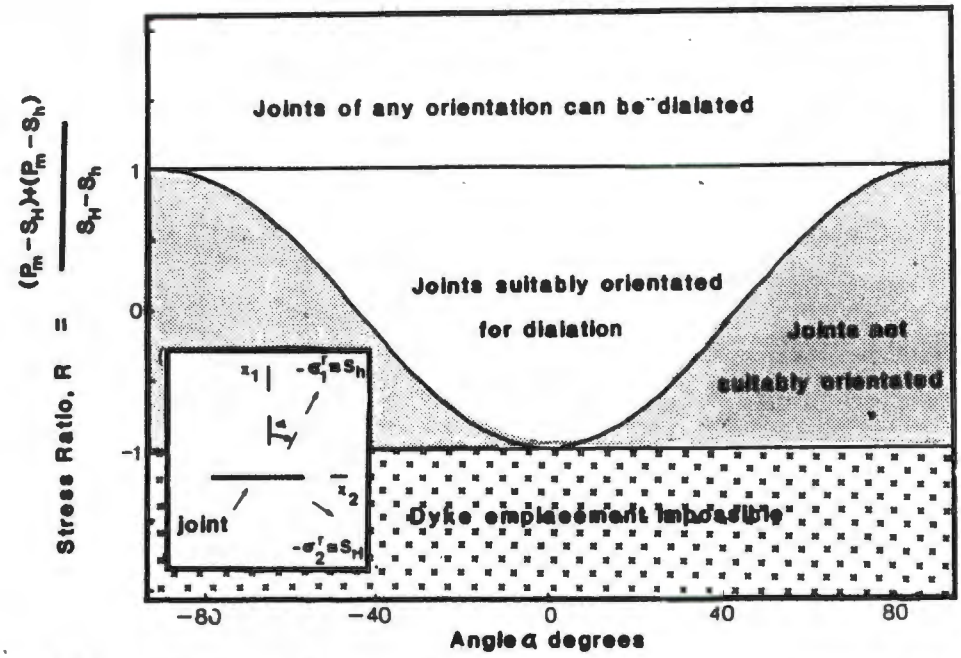

Figure 4.14. *Stress ratio R as a function of angle α between vertical joint plane and direction of least principal stress. Inset shows a horizontal plan with conventions for coordinates and stresses. After Delaney et al., (1986).*

Where the diverging force for intrusion is P_m-σ_h, stress changes at any point is σ_{ij}-σ_{ijr} of a dyke with a half length along strike a, whilst the position of any point under consideration is expressed in terms of polar co-ordinates r and Θ centred at the dyke tip. It is a factor of the order of unity and g_{ij} is a trigometric function given by Lawn and Wilshaw (1975) which acting in a σ_{11} direction normal to the dyke plane is

$$g_{ij}(\Theta) = \cos(\Theta/2) \times (1/2)\sin(\Theta)\sin(3\Theta/2) \qquad (9)$$

The results from the solution of this equation have been given by Delaney et al. (1986) versus distance perpendicular to dyke length (Figure 4.15). The successive profiles can be regarded as representative of digital modelled stress tensors during the encroachment of a propagating dyke tip towards a plane viewed in one dimension. During propagation of the process zone horizontal stresses are focused to a maximum bimodally distributed either side of the dyke tip.

The distribution of dyke parallel joints at both dyke margins and tip (Figures 4.11, 4.12) and the calculated stress profiles are remarkably similar, suggesting the formation of jointing and the subsequent development of daughter dykes are directly attributable to deformational process within the inelastic deformation zone during dyke propagation. Expansion of the concept to attempt to explain the outcrop pattern of dyke complex of dyke complex GDC-4 as a megaprocess zone derived by vertical propagation of a magma sheet can be qualified by calculating the ratios of the process zone (Rf).

The latter can be defined by

$$Rf/a <= 1/2\ [(P_m - \sigma_h) / (T+\sigma_H)]^2 \qquad (10)$$

(Delaney et al., 1986)

When g_{11} Θ =1, C=1 and T is the tensile strength of the host rock.

Consider a dyke with ellipsoidal geometry propagating vertically through the continental crust such that a=25

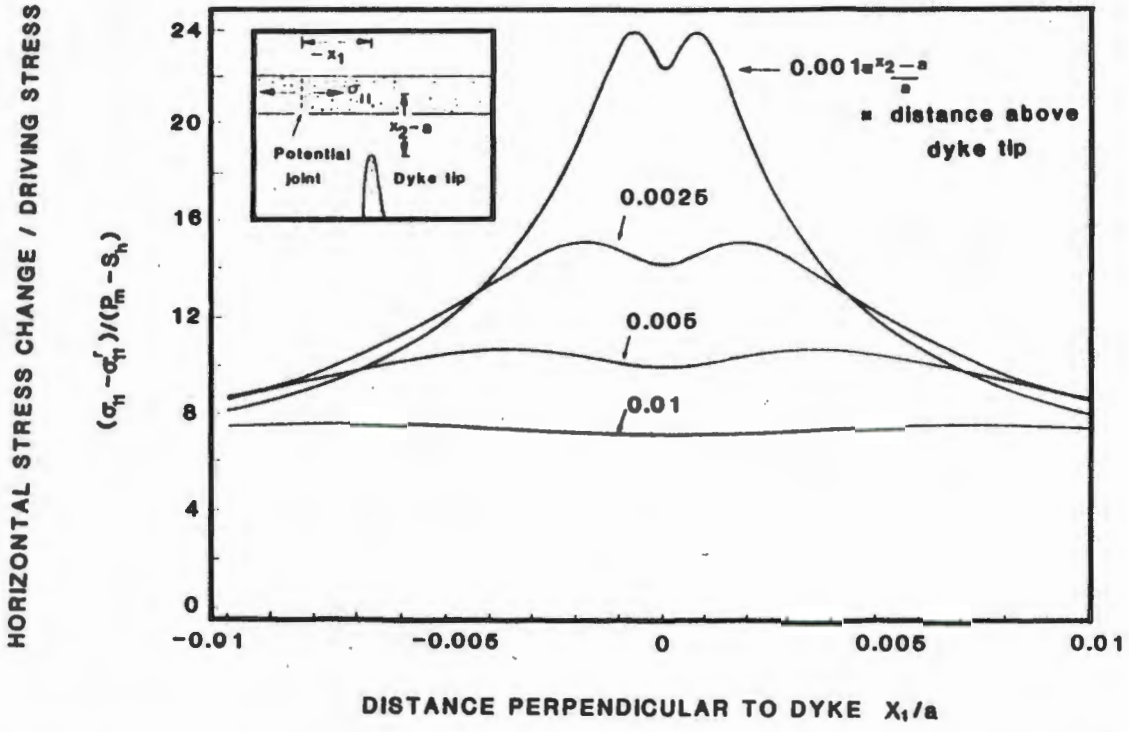

Figure 4.15. *Horizontal normal stress change near the tip of a vertical dyke as a function of distance perpendicular to the dyke plane. After Delaney et al., (1986).*

km, σ_H=24 Mpa and T=1Mpa and σ_m-σ_h=10 Mpa. The ratios of the process zone would be in the order of 2 km, an interesting result if a dyke is regarded to comprise a penny shaped crack propagating vertically. The 2 km radius encompasses almost the entire width of dyke complex GDC-4. However the plausibility of such a mechanism for the generation of parallel dyke segments dilating from joint patterns formed by the process zone of an intruding mega-dyke stock is probably too simplistic in reality since;

(i) clearly dyke parallel joints are also derived by lateral propagation (a dyke 10 km long can comprise a process zone several hundred metres wide),

(ii) shear fracturing during ductile brittle transition in the crust is also likely to occur, causing some splay branching of dykes.

4.7 Lateral versus Vertical Propagation

In considering the dominance of lateral propagation over vertical propagation or vice versa during intrusion of the Gannakouriep dykes, the rheology and style of deformation in the crust has to be considered as well as variation in effective lithostatic and magma driving pressures during intrusion. At high levels of intrusion in the upper crust (<5 km) brittle deformation and extensional fractures are the predominant deformational mode (Figure 4.16) (Jaeger and Cooke, 1969), whereas below 5 km (at mid crustal levels) brittle-ductile deformation of the crust is characterised by shear failure along surfaces deviating 30° from the regional σ1 axis, containing elements of σ2 (Robson and Barr, 1964). At greater depths ductile failure along shear planes orientated 45° to σ1 occurs.

For brittle deformation Pollard (1973b) derived the criteria

$$\sigma1-\sigma3-p+P_p\ (p-\sigma3)2l/t = T \qquad (11)$$

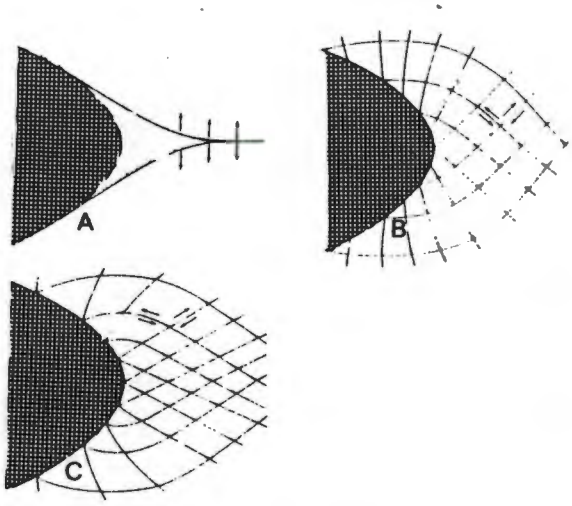

Figure 4.16. *Styles of predominant deformation occurring at a propagating dyke tip within different crustal regimes. (A) pure tensile fracturing in the brittle regime; (B) conjugate shear failure at 30° in the brittle-ductile regime; (C) conjugate shear failure at 45° in the ductile regime. After Pollard, (1973a)*

for dyke propagation where T= tensile strength of the rock, P_p= pore pressure of the host rock, p= magma pressure, l and t refer to dyke length and thickness respectively. The dominant term in this equation is 2l/t, which suggests only very small values of p are required for dyke propagation, almost to the point where dykes are mechanically unstable and will continue propagating.

At deeper crustal levels where ductile deformation is dominant, the yield criteria for propagation can be described by the Von Mises criterion

$$(\sigma 1 - \sigma 3)^2 + (\sigma 3 - \sigma 1)^2 + (\sigma 1 - \sigma 2)^2 = 2\sigma_{ys} \quad (12)$$

where σ_{ys} = the yield strength in uniaxial extension.

For the special condition $\sigma 1 = \sigma 3$ = lithostatic pressure Pollard (1973a) rearranged equation (12) so that

$$\sigma_{ys} = \sqrt{3}\,(\sigma 1-\sigma 3)/2 + (P-\sigma 3)l/t \quad (13)$$

Whilst still containing the term l/t, it is important to note that yield stresses at deeper crustal levels are greater than that of the brittle failure regime. Furthermore ellipsoids undergoing ductile propagation tend to increase their termination radius of curvature at the dyke tip prior to propagating only when the composite yield strength of the rock is met (Wang, 1953). In other words ductile propagating ellipsoids tend to undergo a inflate - deflate propagating pattern in lower levels of the crust where true Young's modulus is greater than for brittle regimes. The latter arguments suggest that lateral propagation is predominant in upper crustal levels by comparison to deeper levels of the crust.

A further point in consideration that must be taken into account is the vertical differences in magma pressure due to the action of gravity. In the case of the Gannakouriep dykes the latter comprise ferro-tholeiites of alkaline parentage which are dense in comparison to their host rock granitoids. Consider the simplest case that a dyke comprises a blade shaped intrusion (Figure 4.17), intruded at an initial pressure P acting vertically, the effective magma pressure at the base of the dyke can be regarded in its simplest form as

$P_{eb} = P - xd_hg$ (14)

whilst at the top of the dyke the effective vertical magma pressure is

$P_{et} = P - (hd_hg + (x-h)d_bg)$ (15)

Where P_{eb} and P_{et} refer to effective vertical magma pressures at the base and top of the dyke respectively, d_h and d_b are the respective densities for the host rock and Gannakouriep magmas; g= acceleration due to gravity; x= the height of the overlying lithospheric column under consideration; and h= the vertical height of the intruding magma column.

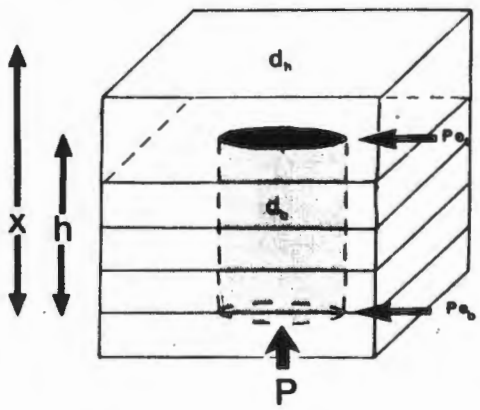

Figure 4.17. *Idealised model of a blade shaped dyke analogous to a manometer. X = thickness of the crust considered; h = vertical height of the dyke; P = initial magma driving pressure; d_b = density of the basaltic magma; d_h = density of the country rock; Pe_b = effective magma pressure at the base of the dyke; Pe_t = effective magma pressure at the top of the dyke.*

Clearly the greater the density contrast between magma and host rock, the greater the decline in effective pressure at the top of the dyke during propagation (i.e. analogous to a manometer). Consequently a dyke propagating vertically where $d_b > d_h$, the effective remote confining pressure ($\sigma 2$) increases during dyke ascent.

Accounting for these factors it is possible that dykes comprising complex GDC-4 may have been nucleated within relatively small ellipsoidal flaws at the base of the crust (or upper mantle), where vertical propagation predominated over lateral propagation. Consequently upon reacting higher crustal levels, under declining effective vertical magma pressures the host rock preceeding the dykes undergo brittle-ductile shear failure, permitting lateral propagation and segmentation of the intruding stock. Vertical propagation although constantly waning still continued with the formation of inelastic deformation in the brittle upper crustal regimes allowing jointing and subsequent dilation within the process zones derived both by lateral and vertical propagation, causing further segmentation of the dykes into master and daughter dykes.

Lateral propagation of individual dykes in upper crustal regimes would also tend to be enhanced by their vertical segmentation into fingers (Figure 4.18). The latter may theoretically occur either as individual dyke of kilometres in length or as individual nucleation points on the centimetre scale.

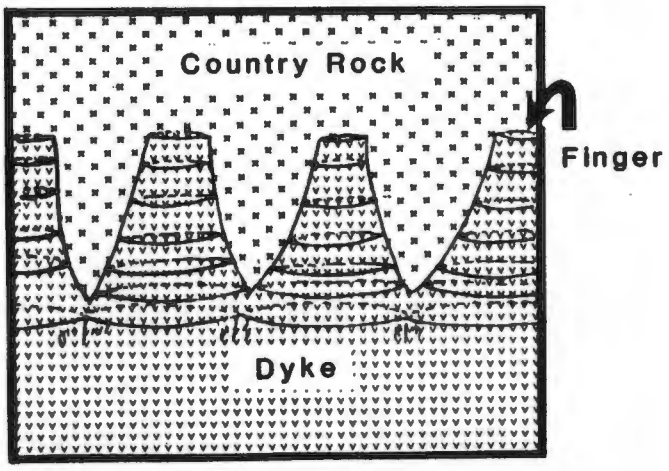

Figure 4.18. *Schematic illustration of dyke fingers nucleating at the leading vertical edge of an intruding magma sheet.*

Several dykes in complex GDC-4 display characteristics that could be regarded as being fingers that represent a continuation of the same dyke at depth. That these fingers represent mode I and III cracks (Figure 4.19) is discounted, since field evidence indicates that shear components associated with initiation and dilation are essentially lacking in the majority of the dykes. Alternative explanations may be explained along two avenues of thought. The break up of the leading edge of a vertically propagating magma shear into preferential zones of advance may be caused by local basement discontinuities or variations in tensile strength. However a continuum mechanics model could be based on the poorly constrained Heleshaw effect (Figure 4.20). The latter is a viscoplastic problem whereby instabilities exist at the interface between two fluids of contrasting viscosities that can be described if

$$\frac{(U_2 - U_1)}{Kz_2}\, w + \frac{(P_2-P_1)g}{Kz_1} < 0 \qquad (16)$$

(Elder, 1975).

Where U,P,Kz refer to viscosity, density and permeability of the rock matrix, and the suffixes refer to these properties of the two different rock types under consideration.

The problem is essentially a fluid/fluid problem, and thus the applicability to a fluid/solid is debatable, although in ductile mantle and crustal regimes the Heleshaw effect may contribute to the segmentation of dykes. Lateral propagation is enhanced over vertical propagation once these fingers are established since from Figure 4.9 they will preferentially propagate laterally towards each other by virtue of their interfering stress fields. The morphological aspects of fingered dyke segments mapped from successive rock slabs cut from dykelets are shown in Figure 4.21.

4.8 Generation of Xenoliths

The presence of crustal xenoliths within the Gannakouriep dykes has been cited as evidence that the dykes were emplaced over a long period of time, with stoping comprising the main mechanism of intrusion (De Villiers and

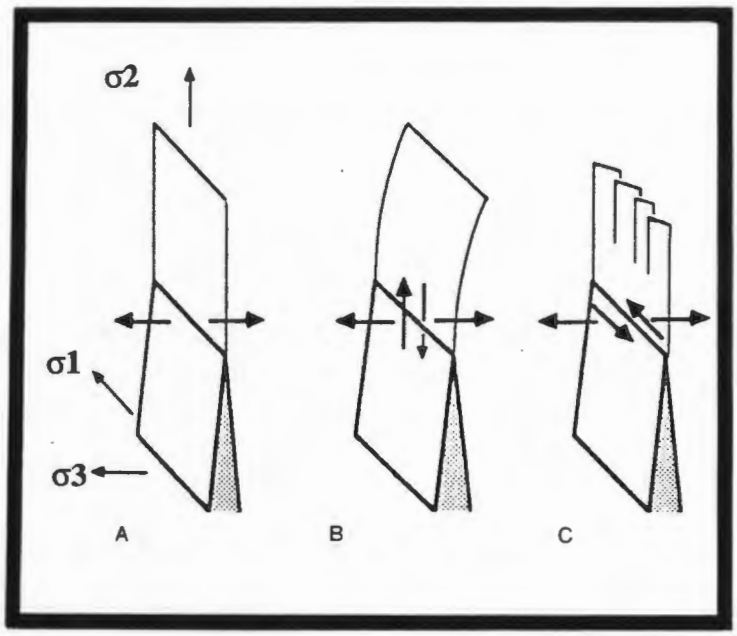

Figure 4.19. *Differing types of cracks in response to local and or remote stress configurations. (A) Mode 1 crack, (B) mode 1 and 2 crack, (C) mode 1 and 3 crack. After Pollard, (1987).*

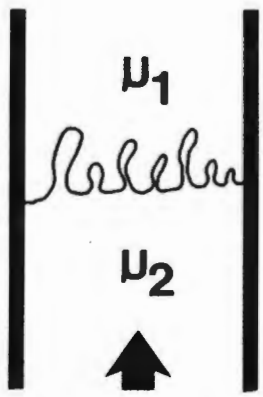

Figure 4.20. *The Heleshaw effect demonstrated by Pollard, (1986). In this experiment air with a viscosity u_2 is forced along a tube containing gelatine with a viscosity u_1. At the interface between the two contrasting viscosities instabilities occur resulting in fingering of one medium into another.*

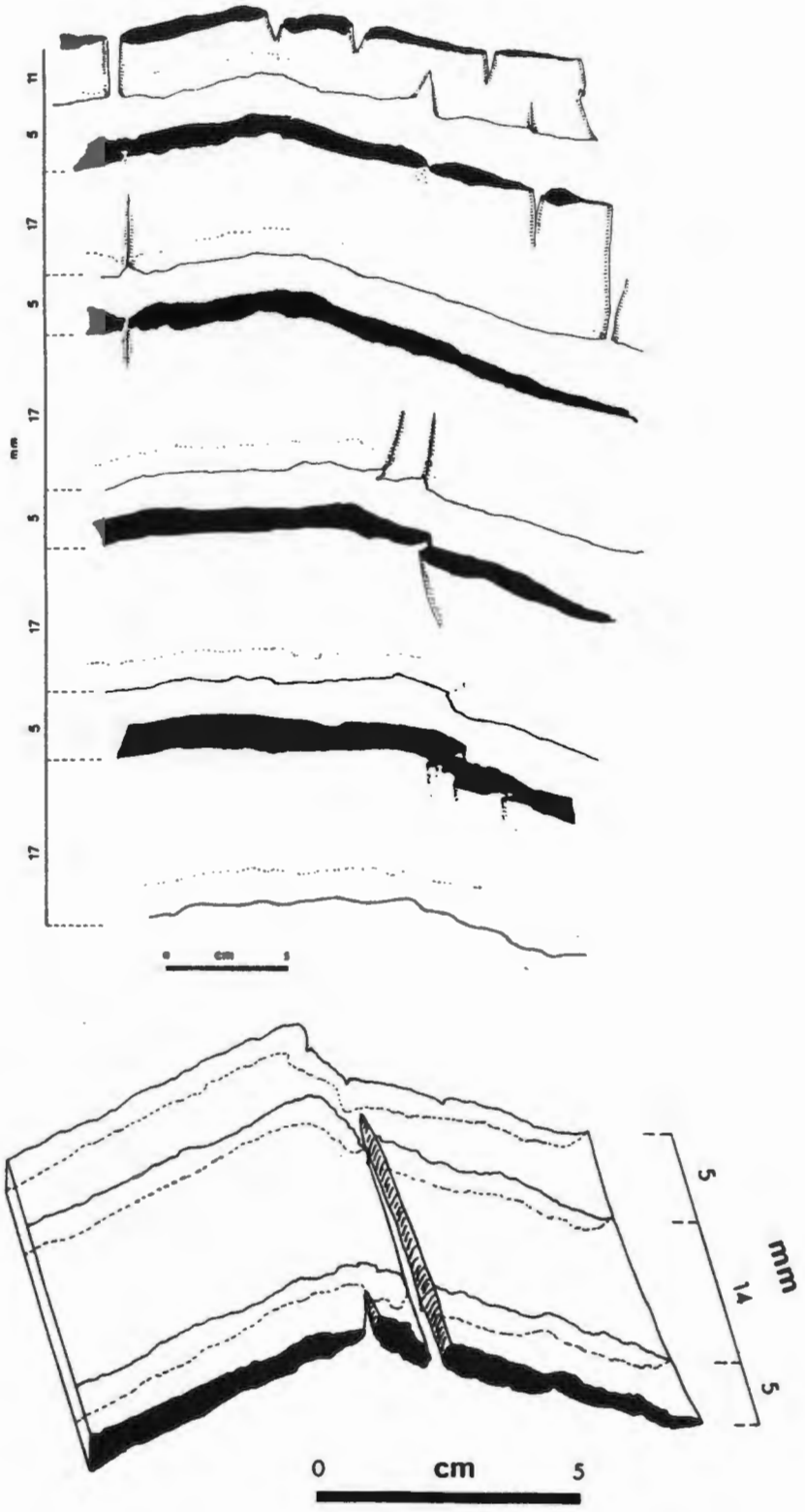

Figure 4.21. *Three dimensional reconstruction of dykelets from the Gannakouriep dyke swarm. The models have been constructed by successively mapping slab faces cut perpendicular to the dykelets. Both samples are from sector I, and were originally vertical in the field.*

Söhnge, 1959). Field investigations in this study tend to mitigate against such a conclusion.

The initial rate of heat transfer (h j/s) during intrusion of the dyke can be expressed in a simplified form as

$h = (sta) / c$ (17)

where s is the specific heat capacity of the rock; t is the difference in temperature between the country rock and intruding magma in degree C; a is the area of wall rock magma interface, and c is the thermal conductivity of the rocks expressed in joules per square metre per second.

Where dykes branch into a subset of dykes (Figure 4.22) the rate of heat transferal into selvages of country rock in the intervening spaces increase linearly (equation 17) since the surface area of magma - wall rock interface is increased. The net effect can produce thermal cracking, anatexis and assimilation of the wall rock selvages.

Thus the presence of crustal xenoliths within the Gannakouriep dykes need not imply stoping as a mechanism of emplacement. On the contrary they may reflect the modus operandi of fracture mechanics in the process zone (Pollard, 1987) at the leading edge of an intruding magma sheet.

Figure 4.22. *Photograph of vertical branching and assimilation within the Gannakouriep dykes of sector I. View is to the northeast, lens cap for scale.*

4.9 The Main Dyke Complex

Pollard (1972) suggested that teardrop dykes may reflect differences in either

(i) the Young's modulus of the basement being intruded, or

(ii) differential $\sigma 3$ strain applied perpendicularly along strike of the dyke during intrusion and subsequent dilation.

Neither of these two criteria appear applicable in the case of the Main Dyke Complex since:

(i) Basement comprising granitoids of the Vioolsdrif Igneous Suite form the local country rock to the Main Dyke Complex. The basement can be approximated locally as being homogeneous, and the elastic moduli is therefore not considered to be significantly different along strike of the dyke.

(ii) Differential $\sigma 3$ strain along strike of the dyke during emplacement would seem unlikely since other dykes associated with the Main Dyke Complex exhibit no tendencies to develop teardrop geometries.

Although the resolution of existing Areomagnetic surveys is poor, aeromagnetic modelling of the dyke infers the presence of an intrusive plug shaped intrusion near Claims Peak. Evans (1987) has highlighted the problems of interpreting aeromagnetic anomalies associated with mafic dykes. However the intensity of dyke arrays in this area of the Main Dyke Complex also suggests the presence of a large plutonic body at shallow depth. The large amount of crustal assimilation observed within this area suggests that dilation of the Main Dyke Complex has been partially accommodated by the wholesale removal of intervening country rock selvages.

4.10 Summary

Thus in summation, structural studies of the Gannakouriep dyke swarm indicate the following:

(i) The dyke swarm was initiated as a series of low aspect ratio nucleation points within the upper mantle/lower crust from a diapiric source during extensional tectonics.

(ii) Subsequently magma propagated predominantly vertically through the lower to mid crustal levels from these nucleation points in regimes of containing a ductile component. They comprise the stocks of individual dyke complexes.

(iii) Dyke branching of dyke complexes in mid to upper crustal levels may have been the result of a Heleshaw type effect and/or inelastic deformation encountered at higher crustal levels in more brittle crustal regimes.

(iv) At upper crustal levels, lateral dyke popagation predominated over vertical magma transport.

(v) Xenolith generated by dyke emplacement are reflective of subsequent dilation of the inelastic process zone during dyke intrusion.

5 GEOCHRONOLOGY

5.1 Introduction

The Gannakouriep dyke swarm is often cited as being co-genetic with the outset of late Proterozoic rifting within the Gariep Arc (eg Ritter, 1980; Von Veh, 1988). Thus the swarm offers the only real geochronological constraint on rifting purported to have occurred along the so called seaborne arm of the Damaran triple junction during the formation of the Adamaster Ocean (Porada, 1989; Hartnady et al., 1985).
The swarm intrudes both granitoids of the Richtersveld Intrusive Complex and sediments of the basal Stinkfontein sequence (Ritter, 1980; Von Veh, 1988; Middlemost 1964). Thus the maximum age constraint for the emplacement of the Gannakouriep dykes is regarded as 920 +/- 10 Ma (Allsopp et al., 1979). The only unequivocal minimum age constraint that can be placed on the relative timing of dyke emplacement comprises the post orogenic Kuboos-Bremen line of granitoids (525 +/- 60 Ma; Allsopp et al., op. cit) which intrude dykes of the Gannakouriep Suite (De Villiers and Söhnge, 1959).

The absence of dykes in the Lekkersing Granite (780 +/- 10 Ma; Allsopp et al., 1979) or the lack of dykes intruding the upper Stinkfontein Sequence (Kroner, 1977) cannot be used to provide chronostratigraphic controls since;

(i) Deformation of the basement by the dyke swarm is discontinuous; the Lekkersing Granite constitutes a geographically small exposure away from the main site of dyke injection.

(ii) The dykes form sills along bedding planes in the lower Stinkfontein sequence under a brittle fracture regime with no hyaloclastites or pepperites. These criteria suggest that Stinkfontein Sequence was well consolidated at the time of intrusion. The dykes therefore bear a strong resemblance to dolerite dykes of Jurassic age intruding sediments of Ordovician age in the Cape Peninsula (Walker, 1957).

Circumstantial evidence may indicate an older minimum age for the emplacement of the dykes. These lines of evidence are controversial, however they comprise;

(i) The late Proterozoic / early Cambrian Nama Sequence overlies the Gannakouriep dyke swarm along an erosional unconformity. These sediments contain detrital muscovites derived from the Damaran orogenic front to the north (Horstman, 1987) yielding ages ranging from 670 - 570 Ma. They also contain Ediacaran fauna of possible late Vendian age (750 - 570 Ma) (Germs, 1972; 1983; Germs et al., 1986). Sediments of the Nama sequence exposed on the Neint Nababieb Plateau do not contain a Pan African (Kennedy, 1964) metamorphic imprint in their argon release spectra (Hartnady, pers.comm.) which is present in the underlying Gannakouriep dykes (Piper, 1975; Onstott et al., 1986).

(ii) Clasts of the Gannakouriep suite are present in the Numees diamictite, correlated with the global Varangian glacial episode (680 Ma) (Von Veh, 1988; Harland, 1983).

(iii) Late Proterozoic - early Cambrian D1 left lateral shearing deforming dykes of the Gannakouriep suite is thought to be responsible for the late Vendian Nomtsas unconformity (-570 Ma) in the Nama basin (Germs, 1983).

In this chapter new Rb/Sr and Sm/Nd data are presented to constrain the age of intrusion of the Gannakouriep dyke swarm. Subsequently previous K-Ar and Ar-Ar data obtained from the swarm is reviewed and interpreted in the light of these new data. Relevant analytical techniques and data used are given in Appendix 2.

5.2 Rb-Sr Isotopic System

5.2.1 Introduction

Initial attempts to obtain a Rb-Sr isochron from whole rock samples in Sector I of the swarm yielded a scatter plot on a conventional Rb/Sr isochron diagram (Figure 5.1). The latter suggests that both dykes had been subjected to variable degrees of crustal contamination and or secondary alteration. To alleviate these problems gabbro sample DRD-151 from the Main Dyke Complex in Sector III was used to attempt to construct an internal mineral isochron. In thin section the sample appears unmetamorphosed, with subhedral augite and minor hypersthene subophitically enclosing olivine and plagioclase laths. Deep red-brown biotite is confined to the groundmass, and often exhibits a psuedohexagonal tabular habit. Negligible amounts of secondary sericite in plagioclase and incipient chloritisation of pyroxene along fracture surfaces is evident in thin sections.

5.2.2 Results

To obtain a reasonable spread in Rb/Sr, biotite, pyroxene and plagioclase together with two whole rock fractions were analysed. The results obtained from all mineral separates and whole rock analysis are given in Table 5.1. Since the spread in Rb/Sr ratios of the mineral separates and whole rock samples are negligible in comparison to biotite the latter effectively controls the slope of the internal isochron. Inclusion of all data points on a conventional Rb/Sr diagram yields an errorchron age of 672 +/- 47 Ma with a MSUM of 157. The large error is primarily contributable to Mica separate A, which has both low Rb/Sr and $^{87}Sr/^{86}Sr$ in comparison with the other two biotite separates (Figure 5.2). The latter observation suggests that mica separate A is anomalous, possible since it was the only mica separate sorted and picked in alcohol. Exclusion of this datum point yields

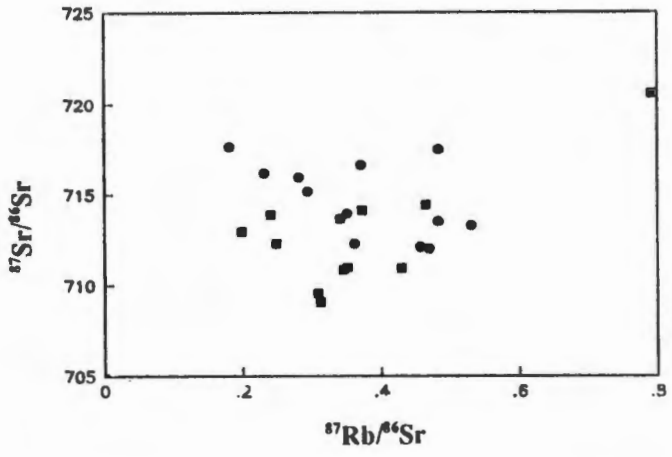

Figure 5.1. *Whole rock Rb/Sr isochron plot of two dykes from Sector 1. Both dykes provide a complete scatter. The data is listed is Appendix 2.*

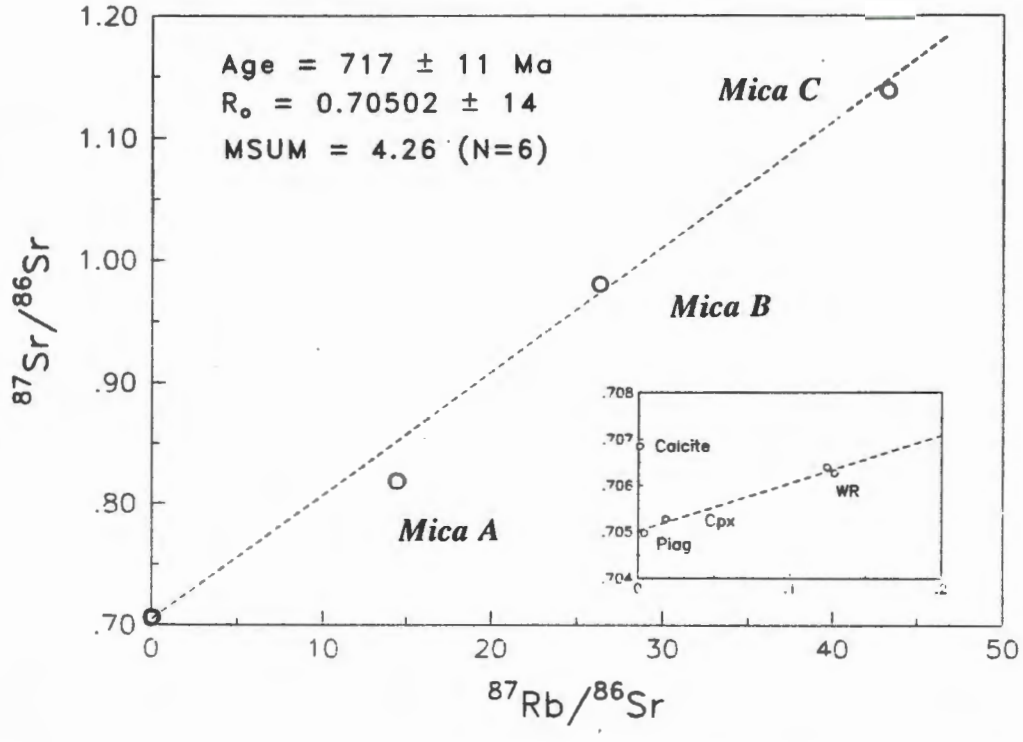

Figure 5.2. *Rb/Sr internal mineral isochron plot from sample DRD-151, taken from the Main Dyke in Sector 3.*

Table 5.1. *Rb/Sr data from Gannakouriep Sample DRD-151.*

Name	Rb	Sr	$^{87}Rb/^{86}Sr$	$^{87}Sr/^{86}Sr$
WRa	20.9	485.5	.124	.706387 +/- 18
WRb	21.4	479	.129	.706265 +/- 39
Plag	1.17	826.9	.004	.704965 +/- 20
Cpx	0.31	49.95	.018	.705265 +/- 62
Mica A	283.7	58.76	14.12	.819432 +/- 36
Mica B	300.2	33.84	26.35	.980363 +/- 66
Mica C	355.6	24.77	43.28	1.138344 +/- 52

a more precise age of 717 +/- 11 Ma with a MSUM of 4.26. The initial Sr ratio associated with this age is 0.70502 +/- 14, corresponding to an E_{Sr} of 4.2.

5.3 Sm/Nd Isotopes

5.3.1 Introduction

The Sm/Nd systematics of the Gannakouriep dyke swarm have only been briefly investigated. Sample DRD-53 was selected for whole rock analysis from sector I. This sample now comprises relict sub-ophitic gabbros which is metamorphosed in the lower greenschist facies. Although relict augite and plagioclase are discernable in thin section, the bulk of the rock currently comprises chlorite, epidote, calcite and quartz. Apatite needles, subophitically enclosed within clinopyroxene prisms have remained unaltered.

The sample had been previously analysed for whole rock Rb/Sr data (Figure 5.1). Although clearly being derived from a dyke in which the whole rock Rb/Sr systematics have been affected, the Rb/Sr data for DRD-53 yields an initial Sr ratio of 0.705 calculated at 717 Ma, close to the initial Sr ratio determined from the internal Rb/Sr mineral isochron (Figure 5.2)

Table 5.2. *Nd/Sm Isotope data from sample DRD-53.*

Sample	Sm(ppm)	Nd(ppm)	$^{143}Nd/^{144}Nd$	$^{147}Nd/^{144}Nd$
DRD-53	6.633	30.42	0.512342 +/- 38	0.1317

THCUR age = 696 Ma

5.3.2 Results

The results for whole rock analysis of sample DRD-53 are given in table 5.2. The derived model TCHUR age is 696 Ma +/- 90 Ma, which is very close to the Rb-Sr internal mineral isochron age notwithstanding the applicability of a CHUR source. Calculation of E_{Nd} at 717 Ma, the inferred age of intrusion from the preferred Rb/Sr errorchron, yields an E_{Nd} +0.17.

5.4.0 K-Ar and Ar/Ar Isotopes

5.4.1 *Introduction*

Several K-Ar and $^{40}Ar/^{39}Ar$ studies have been carried out, although only that of Onstott et al. (1986) has been published. Whole rock and mineral separates have been analysed by a number of workers (Adams, unpublished; Charton, unpublished; Snelling, unpublished; Onstott et al., 1986). Integrated $^{40}Ar/^{39}Ar$ dates obtained from step heating analyses of whole rock samples have yielded ages ranging from 179 +/- 2 Ma to 1326 +/- 141 Ma (Charlton, unpublished). However the majority of whole rock samples contain a circa 500 Ma metamorphic imprint on their ^{40}Ar release spectra (Onstott et al., 1986).

All available data together with details of sample locations have been collated. They are presented in Table 5.3 and Figure 5.3 respectively.

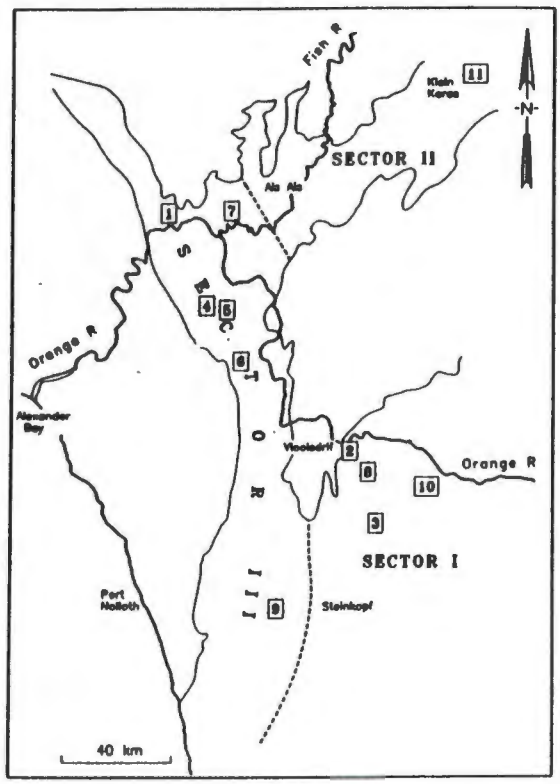

Figure 5.3. *Location map of K-Ar sample sites.*

5.4.2 K-Ar data on Amphibole Separates

Amphibole from several Gannakouriep dykes in sector III (Figure 5.3) has been dated by Adams (unpublished) using the conventional K-Ar technique (Table 5.3). The data obtained by Adams (op.cit.) are presented here on a ^{40}K-^{40}Ar isochron plot (Harper, 1970; Shafquillah and Damon, 1974) (Figure 5.4). The isochron yields an apparent age of amphibole closure to ^{40}Ar loss at 514 +/- 17 Ma with a negative ^{40}Ar intercept of 1.68 +/- 0.14 nl/gm.

The amphiboles in sector III dykes are a product of amphibolite metamorphism (M1) associated with late

Table 5.3. *K-Ar data collated from previous workers.*

Sampling localities within the Gannakouriep Dyke swarm.

Point	Locality	Coordinates	Description
1	Boom River	28° 0'S 17° 3'E	Two adjacent dykes
2	Koubank River	28°53' 17°44'	Five dykes along a 10 km stretch of highway
3	Aribes River	29° 3' 17°51'	Highway cutting
4	Abiekwas River	28°18' 17° 7'	Next to main track through NE Richtersveld
5	Gannakouriep River	28°20' 17°10'	Main dyke at its widest point
6	Bak River	28°32' 17°15'	
7	Fish River	28° 5' 17°12'	
8	Vioolsdrif area	28° 50' 17°45'	
9	Rietkloof	29°15' 17°33'	Quarry next to highway to Port Nolloth
10	Noujaseb River	28°54' 17°56'	
11	Klein Karas	27°34' 18° 5'	Highway cutting

Summary of $^{40}Ar/^{39}Ar$ data from the unpublished study of Charlton (1975).

Run	Sample	Total Fusion Age (Ma)		Isochron Age (Ma)	Step Heating Age (Ma)	
		Outgassed	Recombined		Steps	Age
SC061	A1/2	-	217 ± 10	212	5	209 ± 31
SC068	B1/2	196 ± 6	189 ± 10	179	5	179 ± 2
SC069	B2/3	210 ± 10	222 ± 15	210	5	217 ± 10
SC070	A1/1	-	178 ± 10	210	7	181 ± 35
SC081	NAS5/A	-	1328 ± 10	1300	6	1326 ± 141

Outgassed Age: Integrated Age excluding first three low temperature heating steps.
Isochron Age: Regression of $^{39}Ar/^{36}Ar$ versus $^{40}Ar/^{36}Ar$.

Coventional K-Ar age data for Gannakouriep dykes (mainly from Sector III), including Hornblende separates (Hb) and whole rock (TR) samples.

Run	Sample	K %	$^{40}Ar_{rad}$ (nl/gm)	$\%^{40}Ar_{rad}$	Age Ma
Locality 1					
GC27TR	RAD6	.196	8.729	75	887 ± 41
GC28TR	RAD7	.486	12.181	78	551 ± 15
Locality 3					
	42TR	0.94	16.809	95	410 ± 16
Locality 4					
R3202Hb	K580	.645	11.98	91	423 ± 3
R3203Hb	K581	.372	7.25	92	442 ± 3
R3203Hb	K581	.372	7.30	93	444 ± 3
Locality 5					
R3204Hb	K582	1.158	25.87	97	498 ± 3
R3204TR	K582	.763	15.83	95	466 ± 4
R3204TR	K582	.763	15.94	89	469 ± 4
R3205Hb	K588	.550	5.90	80	256 ± 2
Locality 6					
R3206Hb	K589	1.038	23.29	96	500 ± 4
R3206TR	K589	.902	18.21	93	455 ± 3
R3207Hb	K590	1.026	22.69	97	494 ± 4
Locality 7					
R3743Hb	B847	.528	10.67	94	456 ± 3
R3744Hb	B848	.394	6.99	87	406 ± 3

Locality 1: Analyst N J Snelling, I.G.S., Oxford, 1968
Locality 3: Analyst D C Rex, Leeds, 1973
Localities 4-7: Analyst C J Adams, 1975

Table 5.3 Continued. *K-Ar data collated from previous workers.*

$^{40}Ar/^{39}Ar$ step heating data for Gannakouriep pyroxene separates. Analyst: T C Onstott, 1987

Sample: DRD-12 (Locality 10)

T(°C)	f1	f2	Atm (%)	$^{40}Ar^{*}$ ($x10^{-6}$ cc STP)	Cum f(39)	$^{37}Ar_{Ca}/^{39}Ar_{K}$	Date(Ma)*
550	-0.00234	0.02056	19.1	0.197	0.047	3.597	412.3±5.6
800	-0.00128	0.03128	7.4	2.012	0.470	1.961	457.8±1.4
850	-0.00075	0.39008	0.2	0.409	0.554	1.152	468.2±2.4
900	-0.00097	0.40397	0.3	0.357	0.632	1.485	444.0±2.4
950	-0.00095	0.28244	0.5	0.193	0.732	1.462	451.8±6.2
975	-0.00106	0.25629	0.6	0.155	0.763	1.628	490.5±5.2
1000	-0.00110	0.23543	0.7	0.178	0.797	1.692	493.3±4.0
1025	-0.00112	0.24587	0.7	0.185	0.836	1.716	456.3±5.8
1050	-0.00142	0.27803	0.7	0.184	0.873	2.184	475.5±5.4
1075	-0.00268	0.14695	2.7	0.182	0.907	4.111	511.3±7.1
1100	-0.00651	0.11276	7.0	0.169	0.933	9.995	591.8±7.2
1125	-0.01508	0.13014	11.2	0.176	0.958	23.159	649.2±10.0
1150	-0.03572	0.23431	11.5	0.149	0.977	54.869	695.9±3.8
1175	-0.06719	0.41039	8.7	0.113	0.990	103.22	764.0±11.8
1200	-0.11554	0.49065	9.2	0.092	1.000	177.48	825.1±11.8

Mass 0.500 gm

Average Standard J-Value = 0.005256±0.000019*

Integrated Age = 480.9±1.8 Ma

Plateau Age (800 - 1050°C) = ~450 Ma

Sample: DRD-55 (Locality 9)

T(°C)	f1	f2	Atm (%)	$^{40}Ar^{*}$ ($x10^{-6}$ cc STP)	Cum f(39)	$^{37}Ar_{Ca}/^{39}Ar_{K}$	Date(Ma)*
550	-0.00215	0.02180	22.5	0.321	0.055	3.304	303.1±10.4
800	-0.00105	0.03873	8.3	1.772	0.380	1.611	282.7±0.7
850	-0.00078	0.20041	1.1	0.610	0.487	1.204	294.4±1.4
900	-0.00235	0.32837	1.6	0.638	0.596	3.615	301.3±2.1
925	-0.00245	0.69772	0.4	0.384	0.663	3.762	297.7±2.1
950	-0.00131	0.51367	0.4	0.342	0.722	2.017	299.1±1.8
975	-0.00104	0.40415	0.5	0.304	0.769	1.604	329.2±2.7
1000	-0.00109	0.30630	0.7	0.205	0.801	1.671	334.1±5.3
1025	-0.00149	0.18630	1.6	0.302	0.841	2.287	379.2±1.5
1050	-0.00227	0.08763	5.0	0.371	0.885	3.481	423.3±2.0
1075	-0.00444	0.59241	0.7	0.217	0.910	6.823	429.3±4.2
1100	-0.00730	0.17259	6.6	0.323	0.944	11.209	459.1±7.8
1125	-0.01562	0.18112	10.5	0.252	0.968	24.001	520.5±6.1
1150	-0.04829	0.31765	12.5	0.193	0.984	74.177	584.4±5.4
1175	-0.09959	0.57089	7.6	0.066	0.988	152.98	696.5±23.4
1200	-0.10404	0.46918	11.6	0.173	1.000	159.81	666.2±6.7

Mass = 0.500 gm

Average Standard J-Value = 0.005252±0.000019*

Integrated Age = 331.3±1.3 Ma

Plateau Age (800-1050°C) = ~306 Ma

Sample: GD-2

T(°C)	f1	f2	Atm (%)	$^{40}Ar^{*}$ ($x10^{-6}$ cc STP)	Cum f(39)	$^{37}Ar_{Ca}/^{39}Ar_{K}$	Date(Ma)*
550	-0.00157	0.00549	27.8	0.205	0.072	2.413	543.1±8.0
800	-0.00083	0.00574	21.0	0.816	0.428	1.268	453.2±3.4
850	-0.00062	0.21675	0.5	0.178	0.508	0.956	440.9±4.8
900	-0.00144	0.38165	0.5	0.202	0.601	2.211	432.1±4.9
925	-0.00149	0.34716	0.6	0.136	0.664	2.289	426.4±3.8
950	-0.00124	0.24193	0.8	0.147	0.724	1.910	479.7±3.8
975	-0.00095	0.14811	1.3	0.084	0.765	1.461	410.1±5.3
1000	-0.00116	0.17644	1.3	0.082	0.807	1.786	394.6±9.3
1025	-0.00157	0.19764	1.5	0.067	0.840	2.419	404.7±17.4
1050	-0.00214	0.20400	1.9	0.067	0.873	3.284	409.9±4.6
1075	-0.00277	0.35900	1.0	0.080	0.907	4.248	459.7±9.1
1100	-0.00585	0.09698	9.4	0.071	0.937	8.991	475.0±15.0
1125	-0.01127	0.08365	15.9	0.072	0.963	17.316	540.9±10.7
1150	-0.02566	0.12064	17.7	0.077	0.984	39.419	651.8±12.6
1175	-0.08476	0.20374	18.2	0.053	0.995	130.20	890.7±21.5
1200	-0.27745	0.27484	15.3	0.050	1.000	426.19	1439

Mass = 0.500 gm

Average Standard J-Value = 0.005256±0.000019*

Integrated Age = 469.3±2.4

Plateau Age (800 - 1100°C) = ~483 Ma

Sample: DRD-104

T(°C)	f1	f2	Atm (%)	$^{40}Ar^{*}$ ($x10^{-6}$ cc STP)	Cum f(39)	$^{37}Ar_{Ca}/^{39}Ar_{K}$	Date(Ma)*
550	-0.00133	0.00332	20.7	0.847	0.097	2.046	917.7±12.1
650	-0.00212	0.00297	16.6	1.129	0.165	3.253	1472
750	-0.00138	0.01391	10.7	0.595	0.266	2.122	669.1±5.4
800	-0.00146	0.06046	3.5	0.382	0.346	2.244	562.2±2.7
850	-0.00253	0.03457	8.5	0.588	0.450	3.879	644.0±2.9
900	-0.00462	0.05914	8.1	0.779	0.577	7.100	693.3±1.4
975	-0.00380	0.03741	9.5	0.423	0.775	5.845	746.1±4.2
1000	-0.00391	0.03504	10.3	0.249	0.812	6.006	741.6±5.2
1025	-0.00561	0.02960	14.4	0.180	0.837	8.624	798.1±6.5
1050	-0.00806	0.03345	15.0	0.201	0.861	12.380	895.0±7.6
1075	-0.01110	0.03006	14.7	0.249	0.881	17.051	1178.8±9.0
1100	-0.01312	0.02276	17.4	0.227	0.898	20.151	1275.6±16.8
1150	-0.03099	0.02528	14.6	1.136	0.944	47.601	1917.1±7.5
1200	-0.10546	-0.01769	15.1	3.080	1.000	162.00	2963.6±5.5

Mass = 0.3939 gm

Average Standard J-Value = 0.005252±0.000019*

Integrated Date = 1094.3±3.3

Plateau Age = (750 - 1000°C) = ~702 Ma

Proterozoic - early Cambrian D1 deformation of the Gariep Belt (Von Veh, 1988; Booth, 1990). That the amphibole separated by Adams (unpublished) constitutes post orogenic contact metamorphic aureoles associated with the intrusion of the Kuboos - Bremen line is discounted, since the samples are regionally dispersed within the sector away from main intrusion sites of the granitoids. Thus the 505 +/- 17 Ma age would appear to date the crystallisation age of the amphiboles. The negative ^{40}Ar intercept produced by the ^{40}K - ^{40}Ar isochron may reflect the amount of ^{40}Ar loss by the amphiboles whilst above their blocking temperature during the peak of M1 metamorphism. ^{40}Ar loss may have been accommodated by equilibration with a lower Ar partial pressure present in the host rock (Vioolsdrif Igneous Suite) at the time of metamorphism.

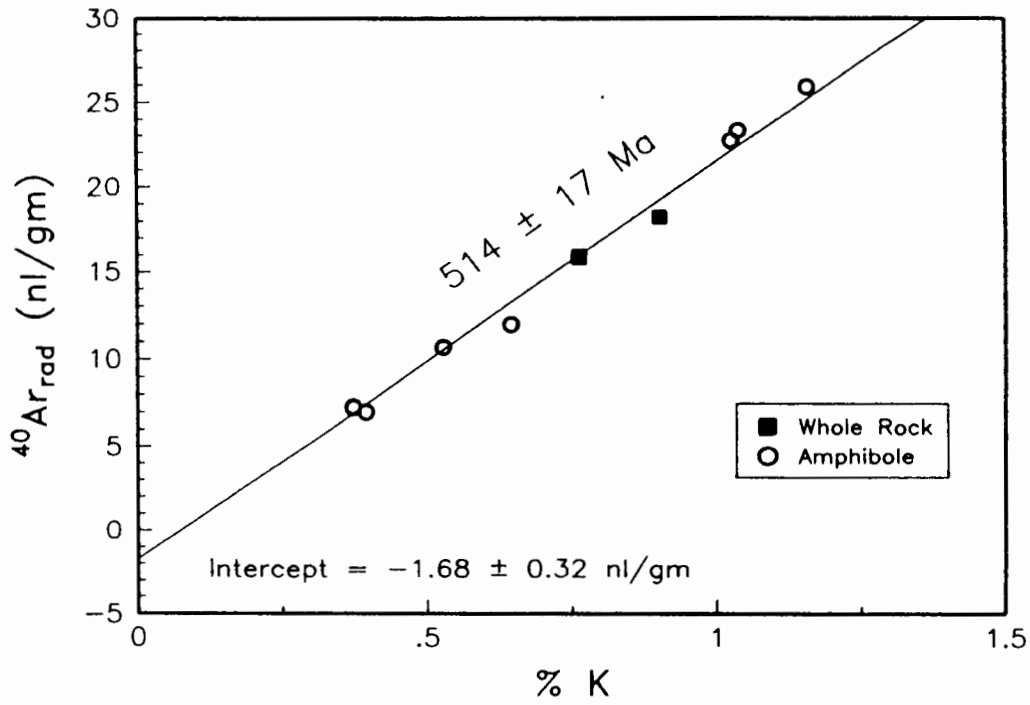

Figure 5.4. *K-Ar plot isochron plot of amphibole separates taken from Sector III dykes. Adams, unpublished data.*

5.4.3 Pyroxene Separates

Pyroxene separates have been investigated using the ^{40}Ar-^{39}Ar step heating technique in an attempt to obtain a primary Ar release spectra from the Gannakouriep dyke swarm (Onstott et al., 1986). Four samples comprising augite of similar major element composition were prepared from dykes sectors I, II and III (Figure 5.3).

Augite from sectors I and II, which have experienced a similar low grade greenschist metamorphic history exhibit staircase Ar release spectras (Figure 5.5) yielding integrated ages varying from 331 Ma - 481 Ma (Table 5.3). The progressive increase in apparent ages at high temperatures appears typical of pyroxenes with excess ^{40}Ar in Ca lattice sites, (Lanphere and Dalrymple, 1977; Harrison and McDougall, 1981).

By contrast, the augite separate (DRD-104) obtained from relict gabbro in the Main Dyke Complex in sector III displays a saddle shaped ^{40}Ar release spectrum (Figure 5.5), suggestive of excess ^{40}Ar. It also yields a saddle age close to 700 Ma.

$^{37}Ar^{Ca}/^{39}Ar^{K}$ isotopic ratio for the respective pyroxene separates is shown in Figure 5.6. The latter Ar isotope ratio obtained during step heating is proportional to the Ca/K ratio of the pyroxenes. The low apparent Ca/K ratios observed for the three augites from sectors I and II suggest that Ar release spectra are dominated by high

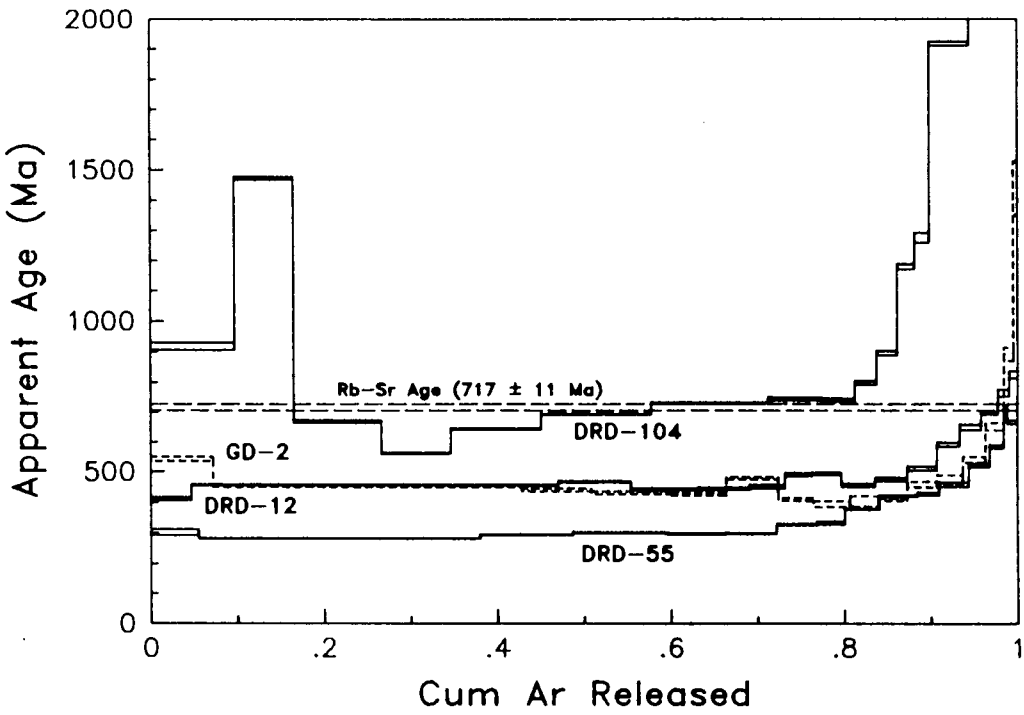

Figure 5.5. *Ar release spectra of pyroxene mineral separates from sectors I, II, and III. Data from Onstott et al., (1986), Table 5.3.*

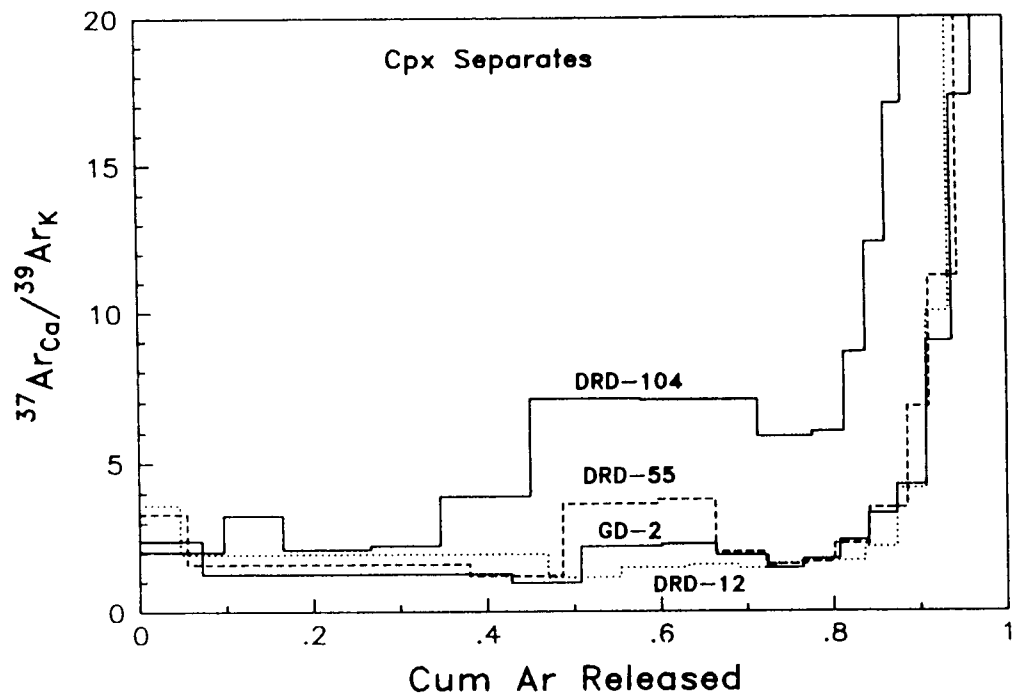

Figure 5.6. *$^{37}Ar_{Ca}$ / $^{39}Ar_K$ release spectra of clinopyroxene mineral separates of dykes from sectors I, II, and III shown in Table 5.3.*

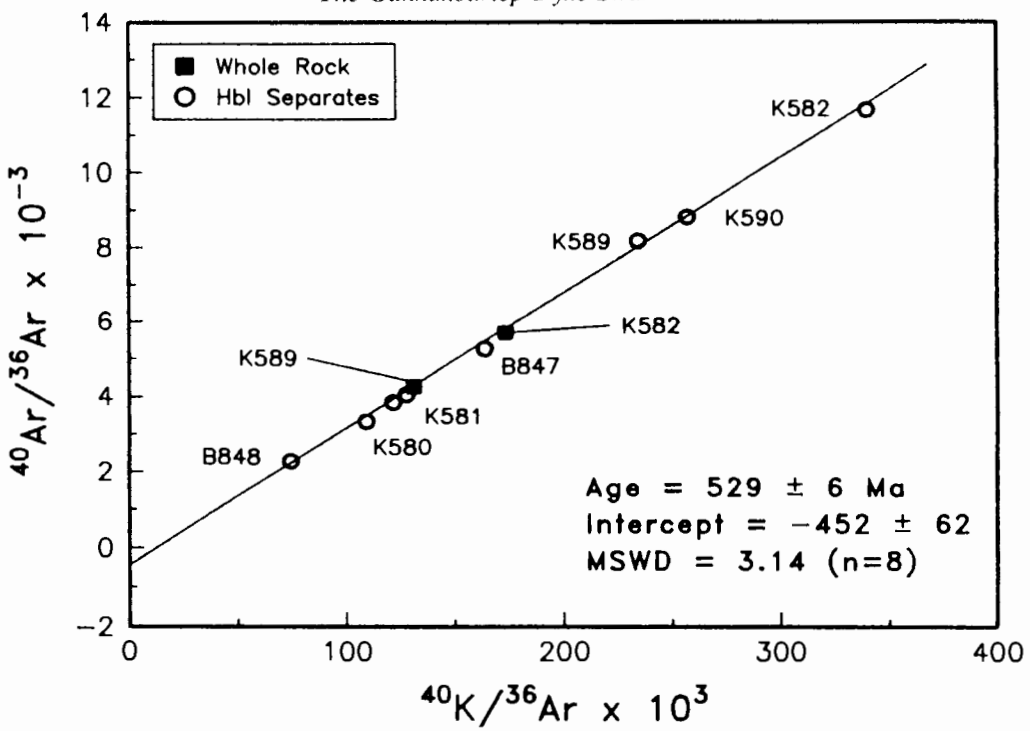

Figure 5.7. *$^{40}Ar/^{36}Ar$ versus $^{40}K/^{36}Ar$ isochron plot of whole rock and amphibole mineral separates from sector III dykes. Data from Adams, (unpublished), Table 5.3.*

K alteration sites. In contrast, augite separate DRD-104 from sector III exhibits a much higher apparent Ca/K ratio more appropriate to the pyroxene, suggesting a lower degree of secondary alteration. Thus the saddle shaped Ar release spectra observed for DRD-104 (Figure 5.5), which is similar to than found by many other workers (Lanphere and Dalrymple, 1976), may reflect 40Ar release from primary K sites located within the pyroxene lattice.

5.4.4 Whole Rock Samples

Whole rock samples obtained from the Gannakouriep dykes in Sectors I and III have also been analysed for K-Ar isotopes. Samples collected from dykes comprising Sector III (Figure 5.3, Table 5.3) yield whole rock K-Ar and integrated $^{40}Ar/^{39}Ar$ ages of 543 +/- 15 Ma, 848 Ma (Snelling, unpublished), and 542 +/- 4 Ma (Onstott et al., 1986).

Whole rock samples obtained from dykes comprising Sector I tend to yield anomalously low K-Ar ages by comparison to Sector III dykes. Integrated ages ranging from 179 Ma to 500 Ma have been recorded by Charlton (unpublished) and Onstott et al. (1986). However an conventional K-Ar date of 843 Ma has been obtained obtain from a sector III dyke Snelling (unpublished).

5.4.5 Discussion

The internal mineral Rb/Sr isochron age is close to the model mica ages of separates B and C (Table 5.4). The E_{Sr} for the mantle underlying the Richtersveld igneous sub-province 2.0 Ga ago yielded a value of 10 (Reid, 1977). Providing no change in the E_{Sr} of the underlying mantle had occurred since then, and prior to the intrusion of the Gannakouriep dyke swarm, the model mica ages may approximate to primary crystallisation ages. The 717 +/- 11 Ma age defined by the preferred internal mineral errochron is consequently regarded as representing the age of intrusion of the Gannakouriep dykes. Furthermore the age derived is much more in keeping with regional geological break-up of Gondwana during the late Proterozoic (eg the Damaran Belt, 750 Ma - 650 Ma, Breitkopf, 1989), and sediment deposition in the Gariep belt. If the Numess dimictite is correctly calculated with

Table 5.4. *Model Mica Rb/Sr ages from sample DRD-151, assuming different initial ratios (R_0).*

	R_0			
	Bulk Earth	.705	.710	.715
Mica A	-	568	544	445
Mica B	735	732	719	666
Mica C	703	702	694	661

the Vangalarian Glacial episode (680 Ma, Harland, 1983), older ages (848 Ma, Kroner, 1977) ascribed to the Gannakouriep dyke swarm would necessitate the deposition of the Stinkfontein and Hilda sequences over an unlikely geological time span of 160 - 190 Ma.

The K-Ar and Ar-Ar systematics of the dyke swarm recorded a variety of events. In Figure 5.7 the corresponding whole rock samples from which the amphibole separates were obtained by Adams (unpublished) plot close to the $^{40}Ar/^{36}Ar$ $^{40}K/^{36}Ar$ isochron defined by the latter, and yield similar integrated ages (Table 5.3). This suggests that amphibole comprises the main ^{40}Ar reservoir and is controlling the ^{40}Ar release spectra of the whole rock samples. Since amphibole is ubiquitous in Sector III dykes, comprising part of the Gariepian M1 mineral paragenesis, the Pan African (Kennedy, 1964) ages derived from the whole rock samples in Sector III may predominantly reflect the age of amphibole growth (and closure to further ^{40}Ar loss).

By contrast, the dykes in sector I and II have only experienced lower greenschist facies metamorphism, and consequently lack amphibole as a retentive ^{40}Ar reservoir. In other words, the greenschist mineral paragenesis in these dykes imparts a significantly lower blocking temperature to ^{40}Ar loss. The younger K-Ar and $^{40}Ar/^{39}Ar$ plateau ages of sector I and II dykes may reflect continuation of Ar loss after the M1 late Proterozoic - early Cambrian deformation and/or subsequent thermal resetting during younger geological episodes (eg. the Karoo igneous episode).

The pyroxene separates analysed by Onstott et al. (1986) yield anomalous $^{40}Ar/^{39}Ar$ ages probably because of secondary alteration. The possible exception comprises augite separate DRD-104 which yields a saddle age of 700 ma, close to both the internal mineral Rb/Sr isochron and model TCHUR Sm/Nd age. Consequently the K-Ar and Ar-Ar systematics appear to record both a primary age of dyke intrusion (and hence associated extension in the Gariep belt), and deformation of the dyke swarm during D1/M1 (514 +/- 17 Ma).

Thus the alleged Adamaster ocean would appear to have been initiated along the southern limb of the Damaran triple junction around 750 Ma (Miller, 1983), allowing for the development of the Gariep basin and deposition of the Stinkfontein sediments. Consequently close of the ocean with deformation and uplift of the adjacent basement in the Gariep belt is thought to have occurred between 514 +/- 17 Ma and 542 Ma (Adams, unpublished; Onstott et al., 1986). Thus the ocean inferred by Hartnady et al. (1985) appears to have had a maximum life of around 200 Ma.

6 INTRADYKE GEOCHEMICAL VARIATIONS RECORDED BY THE GANNAKOURIEP DYKE SWARM

6.1 Introduction

Quantitive modelling of geochemical variations across dykes and sills have been well documented (eg. le Roex and Reid, 1978; Richardson, 1979; 1984). However these studies have generally been confined to unaltered rocks in which a single stage precess has been inferred to account for the observed geochemical variability. By contrast to the Karoo dolerite sills investigated by Richardson (1979), lateral heterogeneity along strike of the Gannakouriep dykes is very evident in field outcrop. The chemical variation across strike of dykes of the Gannakouriep suite are investigated in this chapter to characterise geochemical processes occurring within these dykes.

Whole rock samples have been analysed for major and some trace elements by XRF, whilst mineral composition have been determined by electron microprobe. Rare earth elements have been determined by INAA, and Sr and O isotopes by mass spectrometry. Relevant analytical techniques , data and element precision are reported in Appendix 3.

6.2 Field Relationships

Two dykes both 45 metres in width from dyke Complex GDC-4 in sector I were extensively sampled across their strike. Dyke GD-II (Figure 6.1) was selected since structural studies indicated that it comprised one of the master feeder dykes during the emplacement of complex GDC-4. No internal contracts are visible within the dyke although a melanocratic core is evident in field outcrop. By contrast the daughter dyke GD-I 7 km southwest along strike from the sample location of dyke GD-II, exhibits a leucocratic core in comparison to dyke GD-II and its chilled margins. Lateral petrographic variations in both dykes is marked. 1 kilometre southeast from sample location point of dyke GD-I, the dyke contains a porphyritic feldspar cumulate. Both dykes intrude basement comprising Vioolsdrif Igneous Suite granitoids.

Whilst the country rock at both dyke localities shows evidence of limited partial melting, no evidence for magma mixing or rheomorphism at the dyke contacts is present. However partially digested xenoliths of granite country rock in both dykes is indicated by field studies. Small epidosite veins are observed in dyke GD-II 1 kilometre northeast of the present sampling site.

6.3 Petrography

Both dykes contain dolerite forming the chilled margin extending inwards for 10 cm from the dyke contracts with the Vioolsdrif granitoids. These subsequently grade into fine/medium grained dolerites over a distance of 3 metres inwards towards the dyke centre and comprise the dykes' marginal dolerite facies. The bulk of both dykes occupying their cores are composed of relict coarse grained gabbros. Both dykes are currently represented by greenstones, the original primary igneous mineralogy being extensively retrogressed to the current greenschist mineral assemblage chlorite-epidote-quartz-albite-calcite. The petrography for both dykes is similar, and a general description is given below.

The dyke chilled margins are aphyric with microphenocrysts of rounded olivine and glomeroporphyritic plagioclase laths with subhedral clinopyroxene (augite), and sub equant Fe-Ti oxides. Olivine is totally psuedomorphed by carbonate encapsulated by coronas of green fibrous chlorite. Plagioclase occurs both glomeroporphytically with clinopyroxene and as individual microlites, but is always altered to sericite and carbonate. Clinopyroxene is almost totally replaced by green chlorite. Phenocryst phases make up approximately 10 % of the chill contacts. The groundmass comprises an aphanitic mesostasis of intergrown plagioclase microlite, irregular clinopyroxene and Fe-Ti oxides. Alteration of the groundmass to chlorite, epidote and carbonate is widespread. The groundmass coarsens rapidly away from the chilled margins and passes into

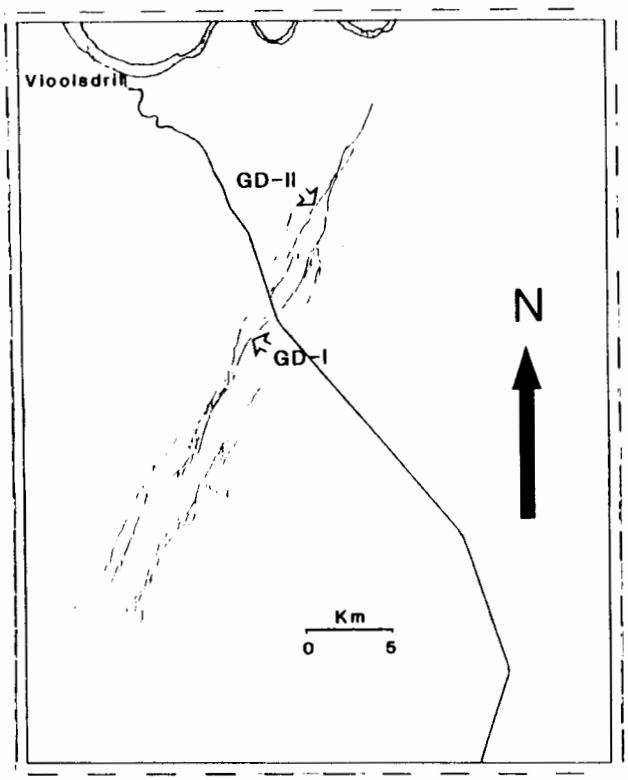

Figure 6.1. *Outcrop map of dyke complex GDC-4 showing dyke profile location sites GD-I and GD-II.*

subophitic dolerite 10 cm from the contact prior to grading into coarse (5-7 mm) subophitic gabbro in the centre of the dyke.

The major portion of the dykes comprise subophitic intergrowths of pyroxene and plagioclase enclosing stubby euhedral prisms of apatite, whilst Fe-Ti oxides, alkali feldspar, biotite and apatite occupy interstitial areas. Augite is the only pyroxene phase present occurring as large euhedral prisms exhibiting simple twinning and a faint lilac pleochroism under plane polarised light. The augites are partially rimmed by amphibole developed along crystal faces adjoining interstitial areas. Subsolidus deuteric zonation of amphibole coronas is indicated since they grade from hornblende to green actinolite with an outer zone of tremolite. Plagioclase laths frequently exhibit epitaxial coronas of alkali feldspar, both mineral phases being highly sausseritised to an aggregate of sericite, carbonate and epidote. Fe-Ti oxides are best developed in the centre of the dyke, comprising ilmenite and very rare relicts of titanomagnetite. Ilmenite is always in the form of exsolution trellises (R7-R8; Haggerty, 1976) which are associated with an alteration groundmass of rutile and sphene, and often mantled by brown biotite. The latter is now completely chloritised and contains stringers of carbonate along cleavage fractures. Olivine is rare in the centre of both dykes, being psuedomorphed in a similar fashion to the chilled margins. The high degree of alteration in both dykes preclude modal analysis, however the degree of secondary alteration in dyke GD-II is markedly higher than for dyke GD-1.

6.4 Mineral Chemistry

The mineral chemistry for both dyke profiles is similar and a general description is given below.

Representative composition of microphenocryst phase comprising the chilled margins were unobtainable from either dyke due to their extensive alteration. However EMP analyses of two of the four phenocryst phases were obtainable from the centre of the dykes (Table 6.1). Augite phenocryst are uniform in composition Wo31En46Fs23. Mineral chemistry data for both olivine and plagioclase were unobtainable due to their total alteration, however an optical study suggest that plagioclases are normally zoned in the range An53 - An26.

Table 6.1 *Selected electron microprobe analyses of clinopyroxene and ilmenite from dyke profiles GD-I and GD-II.*

Oxides	Clinopyroxene	Ilmenite
SiO_2	51.17	Nd
TiO_2	00.70	53.59
Al_2O_3	01.67	Nd
FeO	11.66	44.82
MnO	00.35	00.65
MgO	14.11	01.33
CaO	20.65	Nd
Na_2O	00.36	Nd
K_2O	Nd	Nd
P_2O_5	Nd	Nd
Cr_2O_3	Nd	Nd
NiO	Nd	Nd
Total	100.67	100.39

* *All Fe expressed as FeO. Nd = Not determined, - below detection limits.*

6.5 Geochemical Variations

Geochemical variations of 10 major elements, 12 trace elements and the volatiles CO_2, H_2O+ plotted against dyke width are shown through profile of dykes GD-I and GD-II in Figure 6.2. Major element composition have been normalised to 100 % volatile free, and all Fe expressed as FeO (designated FeO*). REE data for both dyke profiles are shown in Figure 6.3.

Both dyke profiles appear to have similar initial composition reflected by the chilled margins, and contain geochemically incoherent zones extending inwards from the dyke chills over a few metres, characterised by large and rapid fluctuations in element concentrations. The existence of lateral chemical heterogeneity between the centres of the dykes is immediately apparent by their divergent chemical trends. The dyke profiles are thus treated separately in the ensuing discussion.

Small but systematic trends are observable in dyke profile GD-I. These trends are roughly symmetrical around the centre of the dyke which is enriched in SiO_2, Al_2O_3, MnO, K_2O and P_2O_5 relative to the chilled margins. Of these elements K_2O shows the greatest apparent increase of 167 % whilst P_2O_5 is enriched in the core by 25 %. Conversely TiO_2, FeO*, MgO and CaO are depleted in the dyke centre, whilst MgO exhibits the largest random variation at 30 % relative to the dyke contrast.

The best defined trace element trends are those for Ni, Co, Cr and V, which all display a relative decrease from the margins towards the centre of the dyke. Conversely Rb shows an increase of 193 % from the margins to the dyke centre, displaying a rough correlation with K_2O and Ba. Perhaps the most interesting systematic trends

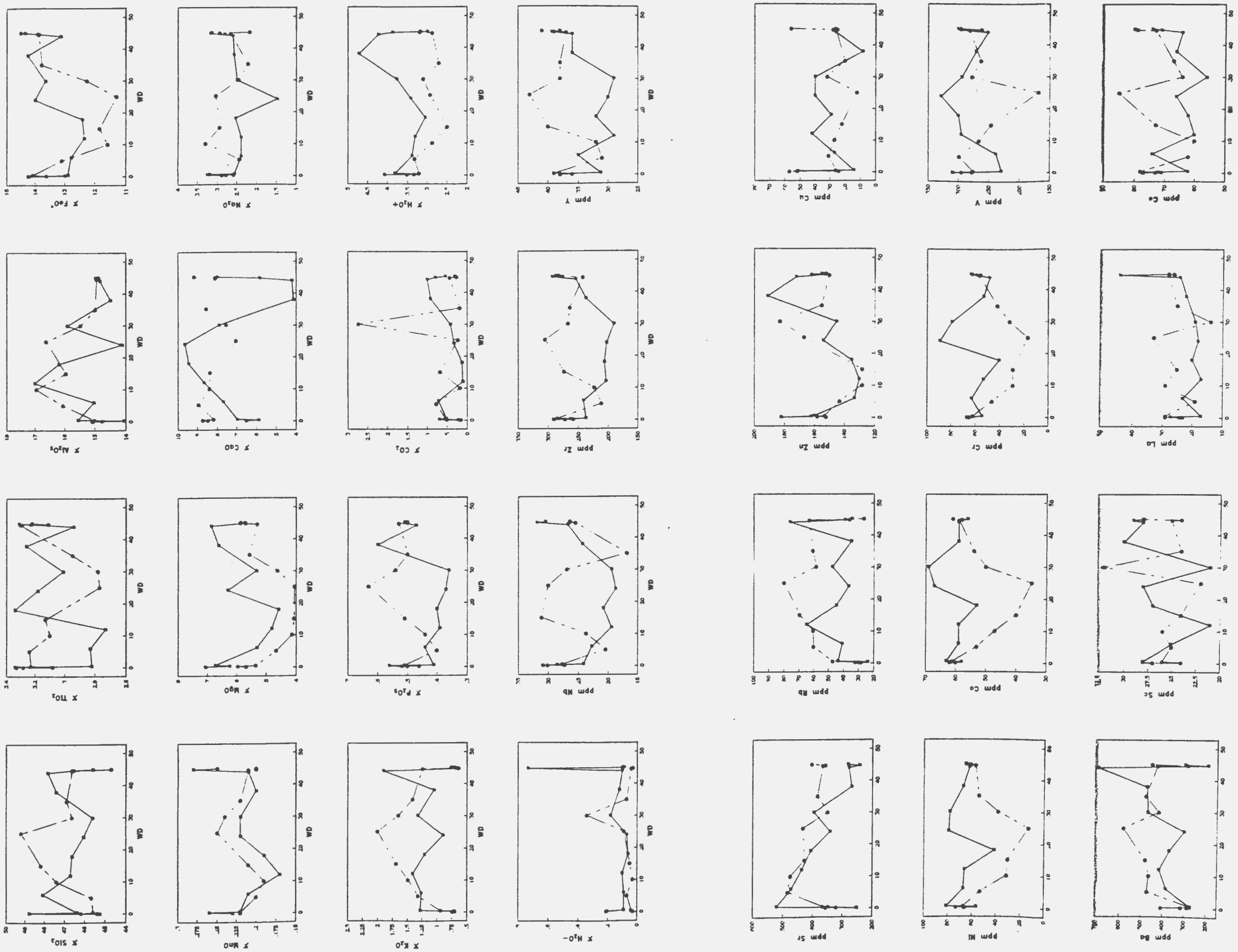

Figure 6.2. *Major and trace element concentration variations across dyke widths (WD) of dyke profiles GD-I and II. Profile Gd-I broken line with circles, Gd-II solid line with squares.*

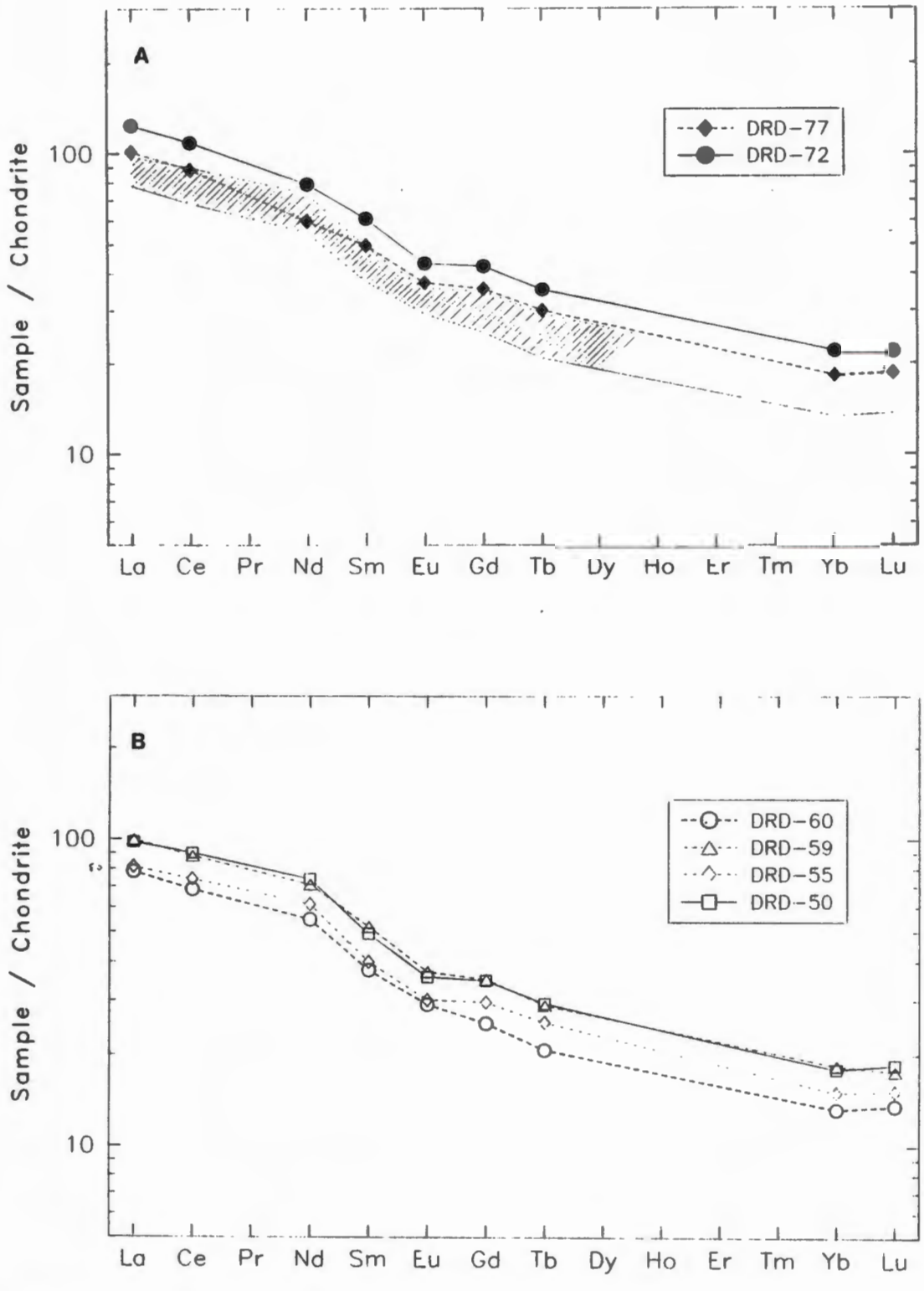

Figure 6.3. *(A) Chondrite normalised REE profiles from dyke profile Gd-I. Sample DRD-72 from dyke centre, sample DRD-77 from east chill margin. Also shown REE field from dyke profile Gd-II in hachured. (B) Chondrite normalised REE profiles from dyke profile Gd-II. Samples DRD-50 and DRD-59 west and east chilled margins respectively, samples DRD-54 and DRD-55 24 and 30 metres respectively.*

are displayed by the high field strength elements Zr, Nb and Y which behave coherently as a group. The latter elements exhibit an initial decrease in concentration within the first 10 m away from either chilled margin, prior to increasing systematically to a maximum in the centre of the dyke. The chondrite normalised profiles of the REE display identical LREE enriched patterns and are quantitatively increased as a group in the dyke centre.

The chemical trends for dyke profile GD-II are more complex and less systematic or symmetrical about the dyke centre than for GD-I. SiO_2 and Al_2O_3 both display a general increase in concentration away from the chilled margins, prior to decreasing rapidly in the central portion of the dyke. Conversely TiO_2, FeO* and MgO display depletion relative to the margins prior to decreasing in concentration at the centre of the dyke.

CaO is asymmetrically distributed through the dyke, quantitively increasing by 34 % in the centre of the dyke from the northwestern margin, prior to being depleted by 42 % relative to the dyke chills. P_2O_5 is depleted in the centre of the dyke relative to the contracts by 27 %. No systematic correlation is observed between major element concentrations, with the exception of TiO_2 and FeO*.

The chemical trends for the trace elements are similarly less well defined than those for dyke profile GD-I. Ni, Co, Cr and V fluctuate with the incoherent geochemical zones, but exhibit a systematic decrease relative to the chills in the marginal dolerite facies, prior to increasing towards the dyke centre. The high field strength elements Nb, Zr and Y display a good interelement correlation, all three elements being sympathetically depleted in the centre of the dyke. Sr in both dyke profiles is asymmetrically distributed, attaining values around 500 ppm in the northwestern marginal dolerite facies, prior to decreasing across the dykes' widths to around 250 ppm towards the southeastern margins.

6.6 Alteration

Alteration of the dykes is evident in thin section with the development of lowgrade greenschist mineral paragenesis epidote, chlorite, carbonate and quartz. An initial comparative assessment of the degree of chemical alteration affecting both dyke profiles using the Chemical Index of Alteration (CIA) (Nesbitt and Young, 1982) plotted against H_2O+, MgO, CaO and FeO* is shown in Figure 6.4. Although in the basaltic system the CIA also serves as a fractionation index (Sweeney, 1989), the trends displayed suggest that profile GD-I has remained essentially unaltered (CIA-55) comparing well to a CIA value of 57 obtained from the freshest sample of the dyke swarm (DRD-151). Conversely profile GD-II exhibits a sympathetic increase between CIA and H_2O+, suggesting an alteration threshold around 3.5 % hydration. The major elements MgO, CaO and FeO* similarly display a rough correlation with the CIA. A sympathetic rise in both FeO* and MgO with increasing alteration depicted by an increase in the CIA is concomitant with a decrease in CaO.

Whilst the CIA may be sensitive to major chemical alteration, it only considers the elements CaO, Al_2O_3, Na_2O and K_2O. Previous studies on chemical alteration of dolerite/gabbroic dykes has mainly concentrated on quantifying differences observed between fresh and amphibolite dykes (Elliot, 1973; Field and Elliot, 1974; Zeck and Kalsbeck, 1981; Morthurst et al., 1983; Hageskov, 1987). Three basic approaches have been employed;

(i) comparison of paired chilled margin/dyke centre samples (Elliot, 1973; Field and Elliot, 1974; Morthurst et al., 1983; Hageskov, 1987),

(ii) comparison of mean composition of altered/fresh samples (Zeck and Kalsbeck, 1981; Hageskov, 1987).

(iii) comparison of individual samples to magmatic trends established from fresh rock suites (Zeck and Kalsbeck, 1981; Morthurst et al., 1984; Hageskov, 1987).

An attempt to qualify and quantify alteration in both dyke profiles has been made using a method similar to that outlined in (iii), since neither of the first two methods satisfactorily account for differences due to magmatic fractionation effects. The foregoing arguments assumes differential crustal contamination was negligable.

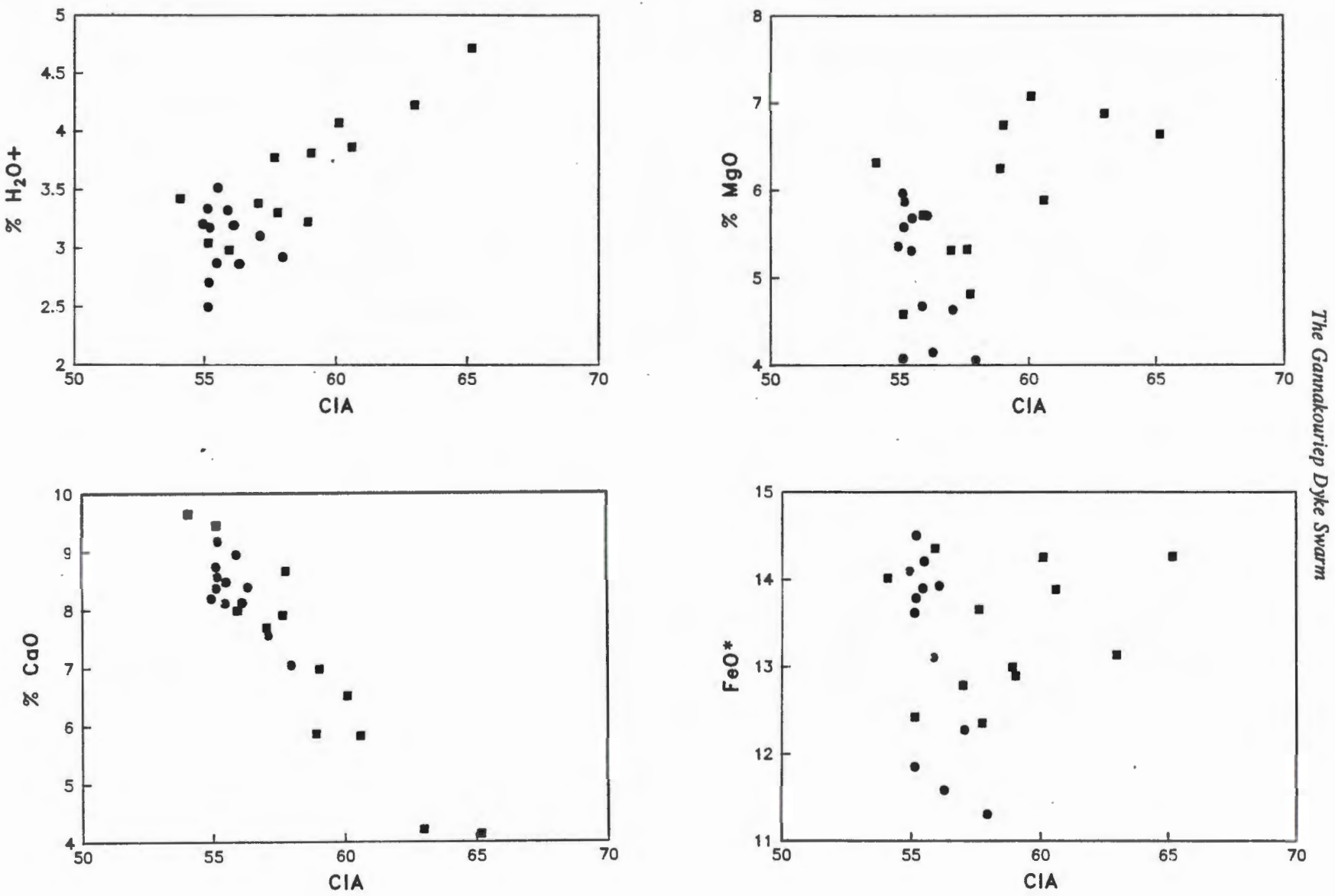

Figure 6.4. *Chemical Index of Alteration (CIA) versus H_2O+, MgO, CaO and FeO* from dyke profiles GD-I and II. Profile GD-I circles, GD-II squares. Total Fe expressed as FeO*.*

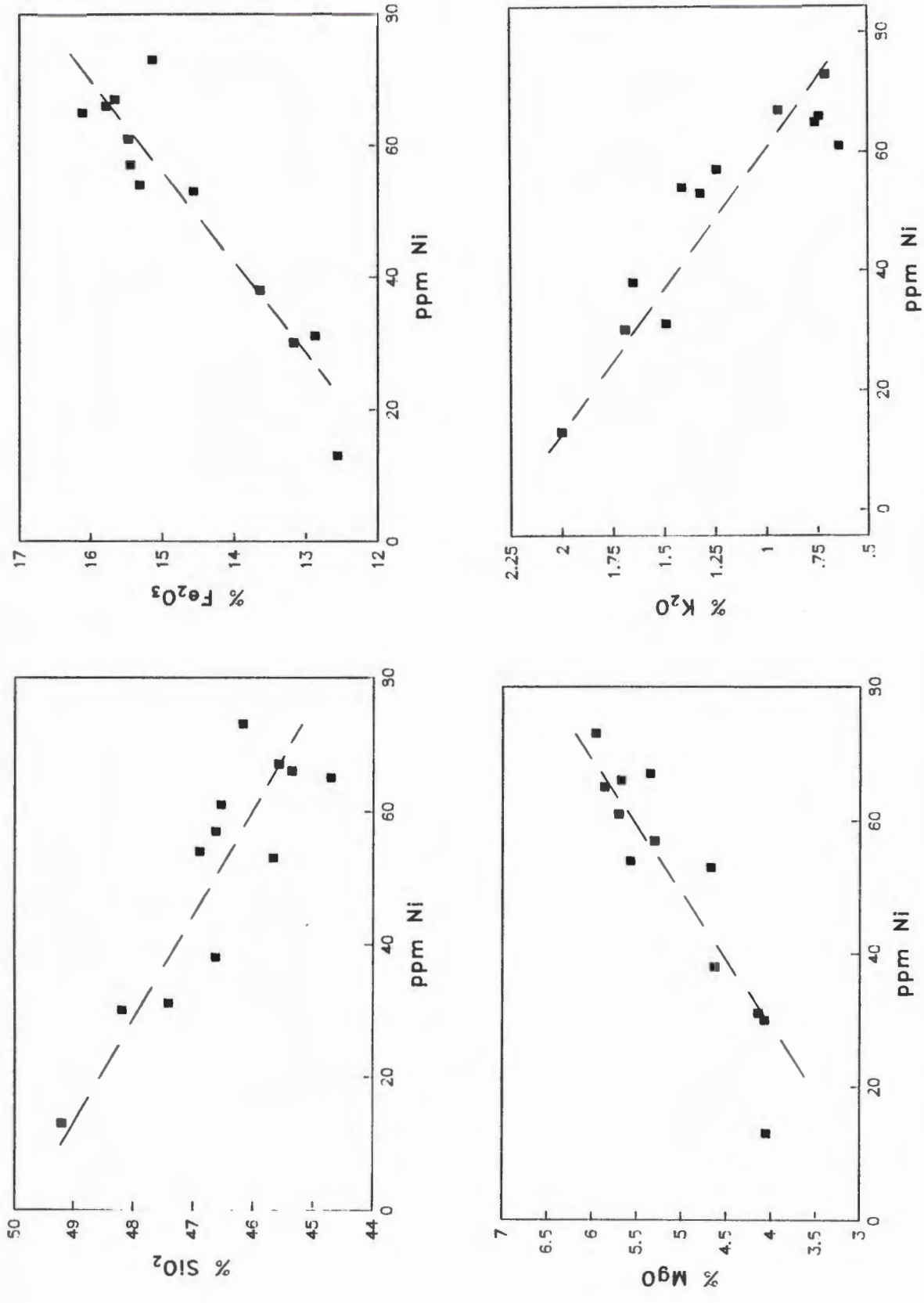

Figure 6.5. *X, Y scatter plot of Ni versus SiO_2, MgO, Fe_2O_3 and K_2O from dyke profile GD-I with approximate primary igneous trends shown in dashed lines. Although Raleigh fractionation should predict a curve using trace elements, due to the large degree of error and limited range of fractionation, a linear regression has been used for first order calculation.*

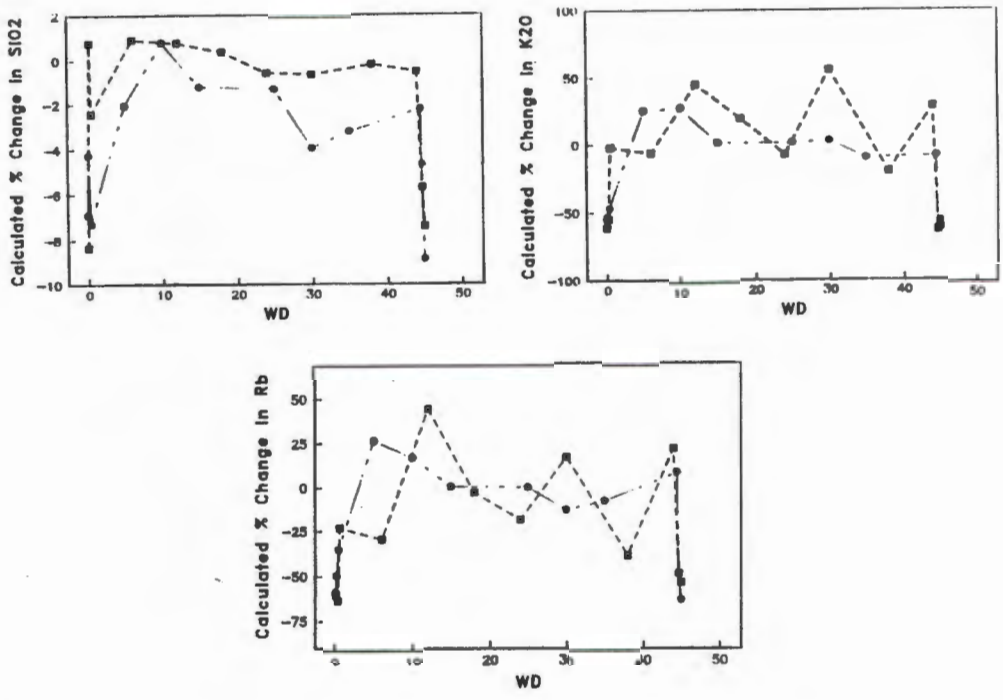

Figure 6.6. *Calculated % change of SiO_2, K_2O and Rb relative to that predicted by the Y content of samples from profiles GD-I and II. Correlation co-efficients beteween Y and these oxides and element has been calculated by regression analyses of samples DRD-72 to DRD-74. The observed Y value has then been used to produce a therortical value for these oxides and element using the derived correlation co-efficients. These theoretical values are then subtracted from the observed values for these oxides and element, and express as a % difference fromthe theoretical values. Profile GD-I circles with broken line, profile GD-II squares with dashed line.*

The geochemistry at profile GD-I produces trends that are comprehensible in terms of magmatic processes (Figure 6.5). Chemical alteration in this dyke profile has been investigated for the elements SiO_2, K_2O and Rb by comparison of chill margins to the dyke centre. The high field strength elements (Zr, Y, Nb) are essentially immobile during secondary alteration (Elliot, 1973; Field and Elliot, 1974) and have been used to calculate a regression analysis of (magmatic) trends in the dyke centre between Y and SiO_2, K_2O and Rb. Extrapolation of these regressions equations using the Y content of the marginal samples permits a theoretical value for these elements to be calculated for the dyke margins. The relative changes in element abundances are shown in Figure 6.6 as well as extrapolation of these regressions to dyke profile GD-II. Although some fluctuation is observed across both dyke profiles, the salient features of Figure 6.6 is that all dyke margins have lost SiO_2, K_2O and Rb. The latter results are compatible with observed devitrification of the chilled margins.

Whereas use of absolute abundances of immobile elements in regression analysis of magmatic trends may elucidate alteration processes by their extrapolation, relative changes in the absolute abundances of these immobile elements in the rock samples due to hydration or whole scale loss/addition of other elements is excluded from this type of modelling. In investigating the metals Ca-Fe-Mg, the TiO_2/P_2O_5 ratio of individual samples has been used in an attempt to alleviate the problem of secondary alteration. The latter elements are both considered immobile (Morthurst et al., 1983) and in the Gannakouriep suite serve as a fractionation index, since TiO_2 is compatible with the phenocryst phases Fe-Ti oxides and clinopyroxene, whilst P_2O_5 is incompatible being confined to the fractionating phase apatite.

Regression analyses of chemical trends interpreted as magmatic for the element CaO, FeO* and MgO versus TiO_2/P_2O_5 - from profile GD-I are given in Figure 6.7. Whilst most of the correlation co-efficents are above

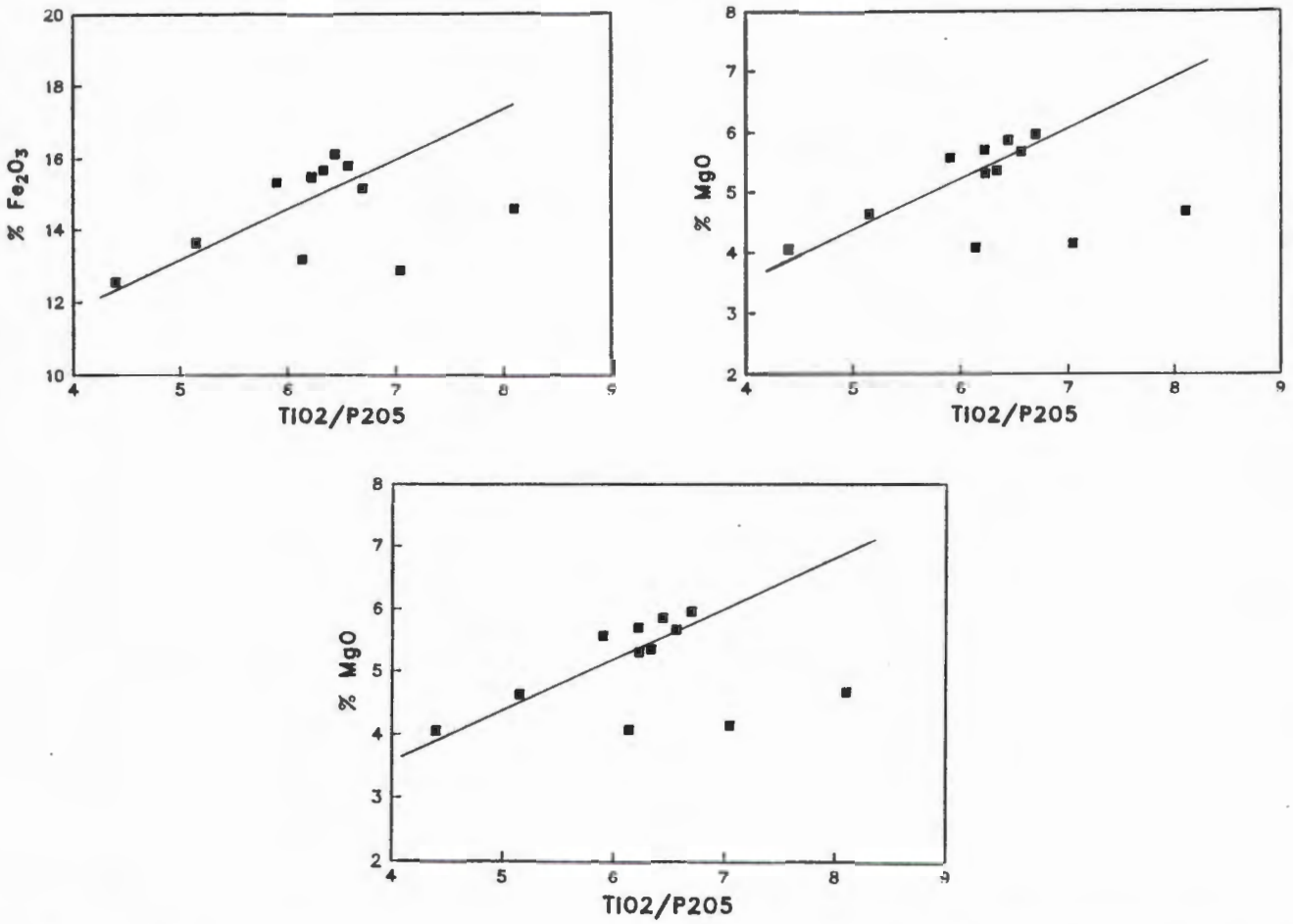

Figure 6.7. *X, Y scatter plots of Ni/Zr (Moorhurst et al., 1983) versus CaO, MgO and Fe_2O_3 from dyke profile GD-I. Regression analysis omitting the three aberrant samples DRD-69, 70 and 71 are R = 0.912, 0.897 and 0.901 respectively.*

the 90 % confidence limits, three samples, DRD-69, 70 and 71, consistently comprise aberrant points. That these samples comprise a discrete magma series intruded into the dyke is discounted since they have similar high field strength interelement ratios compatible with the rest of the dyke. Differential bulk contamination by the surrounding country rock would seem unlikely since the TiO_2/P_2O_5 ratio vector for the latter is in the opposite direction for such a mechanism to have occurred. Two other possibilities exist, either the TiO_2/P_2O_5 ratio in these samples is a primary magmatic feature, due to differential phenocryst sorting during and/or subsequent to dyke emplacement, or the TiO_2/P_2O_5 ratio in these samples has been subsequently altered. These data points have thus been omitted from the regression calculations.

The differences between present element abundances relative to that predicted by this modelling are shown in Figure 6.8 for both profiles. The relative percentage change versus H_2O+ suggests major CaO loss from the rocks with increasing hydration. The most noticeable affect is exhibited by profile GD-II where CaO losses of 46 % and 48 % are predicted in samples DRD-56 and DRD-57 respectively. Perhaps less well defined by this type of modelling is the sympathetic increase in both MgO and FeO* with H_2O+ observed in profile GD-II, where quantitive estimates for both MgO and FeO* appear consistently high. Nevertheless, it would appear that CaO loss is accompanied by a concomitant rise in both MgO and FeO* in profile GD-II. The latter observations are compatible with the observed chloritisation of augite in thin section, suggesting profile GD-II at least has undergone major calcium loss during retrogression to greenschist mineral assemblages. CaO migration in the

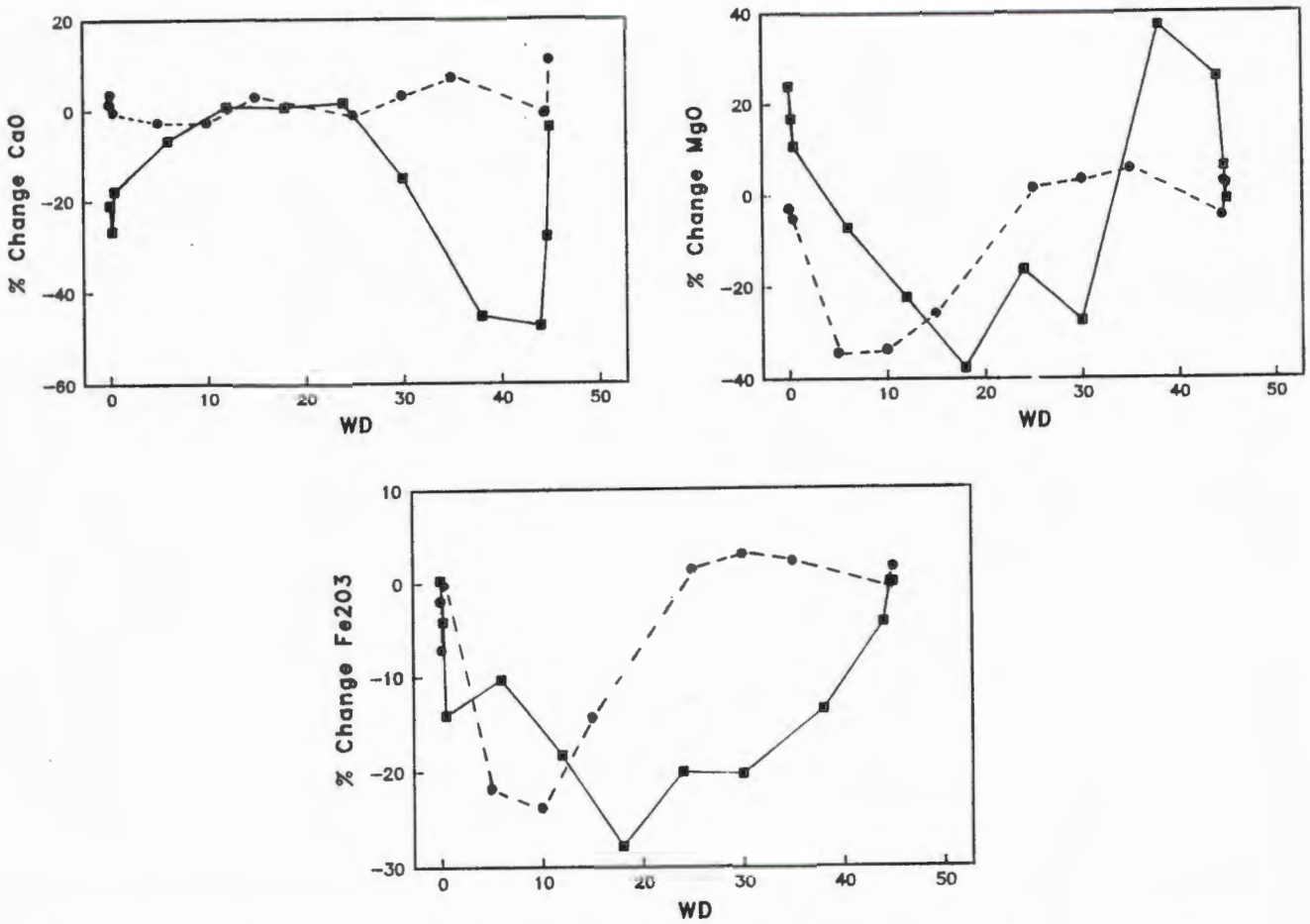

Figure 6.8. *Predicted relative % change in the major oxides CaO, MgO and total Fe expressed as Fe_2O_3 relative to their Ni/Zr from dyke profiles GD-I and II. The method of presentation is similar to that described in Figure 6.6. Profile GD-I circles with dashed line, profile GD-II squares with broken line.*

dykes is further indicated by the appearance of epidosite veins within the dykes.

6.7 Bulk Composition

The bulk composition of both dykes given in Table 6.2 have been calculated by integrating the area under each element/dyke width profile, and subsequently normalised by comparison with the dyke widths. Direct comparison between chill margin composition and the integrated bulk composition of the dykes to establish the relationship between the initial composition of the intruding magma to that which subsequently crystallised is inappropriate since both dykes profiles have been subjected to differing degrees of alteration. However a comparison between the integrated bulk composition of profiles GD-I and GD-II (Figure 6.9) demonstrates that profile GD-II is consistently depleted in incompatible elements, and enriched in compatible elements relative to profile GD-I.

6.8 Origin of Chemical Variation within Individual Intrusions

6.8.1 Profile GD-I

Single Stage Process

The rare earth element analyses for profile GD-I exhibit a 22 % enrichment in the dyke sore relative to the

Element	Profile Gd-I	Profile Gd-II
SiO_2	48.29	48.06
TiO_2	3.10	3.13
Al_2O_3	16.15	15.81
Fe_2O_3	14.29	15.14
MnO	0.22	.21
MgO	4.77	5.87
CaO	8.28	7.64
Na_2O	2.81	2.44
K_2O	1.56	1.27
P_2O_5	.53	.45
Rb	65	48
Ba	476	425
Sr	421	391
Zr	267	225
Nb	26	22
Cr	37	63
V	258	289
Sc	26	26
Ni	41	69
Co	49	63
Y	38	33

All Fe expressed as Fe_2O_3.

Table 6.3. *Integrated bulk compositions of dyke profiles GD-I and II, normalised to 100% volatile free.*

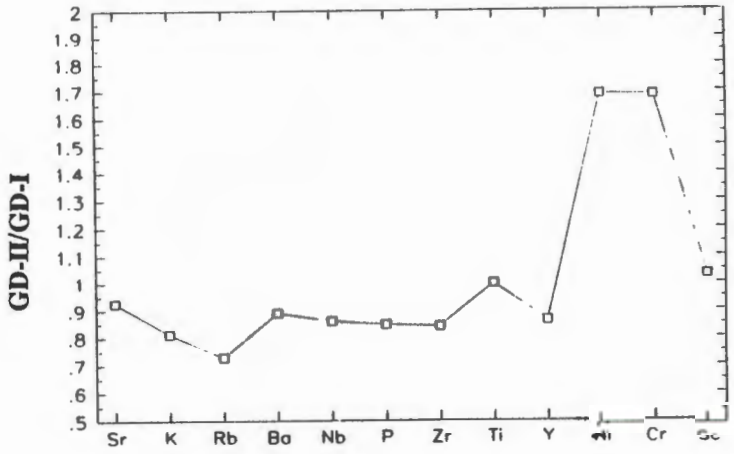

Figure 6.9. *Linear spidergram of the integrated bulk composition of dyke profile GD-II normalised by the bulk composition of profile GD-I.*

chilled margins (calculated 100 % volatile free) (Figure 6.3). Similar patterns of enrichment are also displayed by the incompatible major and trace elements P, Zr, Y and Nb. Although the trends displayed in Figure 6.5 appear compatible with a simple fractionation model of clinopyroxene, Fe-Ti oxides and olivine, the crystallisation of plagioclase must be excluded, since Al_2O_3 (regarded as an immobile element; Hageskov, 1987; Elliot, 1973; Field and Elliot, 1974; Zeck and Kalsbeck, 1981; Morthurst et al., 1983) quantitatively increases towards the dyke centre. The latter assumption that Al_2O_3 will decrease during fractionation clearly depends on the clinopyroxene/plagiocalse ratio remaining sufficently small. However petrographic data indicates that plagioclase comprises part of the phenocryst assemblage. Furthermore the development of subophitic textures recorded by the dyke is regarded as resulting from the supersaturation of plagioclase on the liquidus combined with difficulty in pyroxene nucleation (Cox et al., 1979). Thus a simple fractionation model from dyke margins to centre excluding plagioclase as a phenocryst phase is untenable.

A possible mechanism for producing dykes with more evolved cores relative to their margins could result from bulk contamination of magma in a magma chamber prior to the emplacement of the dyke. This mechanism has been investigated but discarded since bulk contamination of the dyke centre by the country rock should be accompanied by changes in inter-element ratios Y/Nb, Zr/Nb (both higher in the adamellite host rock by comparison with the dyke; Reid, 1977) which remain constant across the dyke width. This does not exclude selective contamination by easily fusible host rock components, but constraint on the latter cannot be placed by the present geochemistry of the Gannakouriep magmas.

The Two Stage Processes

Flow differentiation of early forming plagioclase phenocrysts in the centre of the dyke could account for the 10-15 % enrichment of Al_2O_3 observed in the core of the dyke. Subsequent crystallisation and fractionation of olivine, augite and Fe-Ti oxides (+/- plagioclase) at the propagating solidification fronts from the walls of the dyke would exclude incompatible elements and enrich them towards the dyke centre where late crystallising phases such as alkali feldspar are observed comprising coronas around plagioclase. Two problems exist with such a model. Firstly incompatible elements in the dyke centre may be expected to be depleted relative to the

chill margins by pure dilution due to the preferential accumulation of early forming phenocryst phase in the dyke centre. Secondly, the plausibility of any fractional crystallisation mechanism in situ during consolidation is debatable. As Gibson et al. (1987) points out the more evolved portion of the dyke must represent the residual differentiate from a significant volume of magma above or below the present level of exposure. The time it required to solidify a static dyke with a width 2b is given by

$$t = b_y/4kx^2 \quad (1)$$

Where k is the thermal diffusivity and x is given by the transcendental equation

$$\frac{L}{c(Tm-To)} = \frac{e}{(1+erf)} \quad (2)$$

(Turcotte and Schubert, 1982)

Where L is the latent heat of fusion of the magma, c is the specific heat capacity of the solidified magma and country rock, Tm is the temperature of the intruding magma and To is the temperature of the country rock prior to emplacement.

Assuming Tm-To = 1000° K, L= 320 Kj/Kg, k= 0.5 mm/s, and c= 1.2 Kj/Kg^{-1}, the time required for solidification of the dyke is in the order of 15 years. Using high pyroxene settling velocities of 0.5 m/year (Kushiro, 1980) the maximum amount of downward migration under gravitational settling for pyroxenes in the dyke centre can be constrained in the order of <7.5 metres. Furthermore depletion of compatible elements, and by inference sympathetic enrichment of incompatible elements in the dyke centre by this mechanism also would have to assume no vertical compensation by crystal settling from magma above the present level of exposure. Thus based on thermal constraints any model purporting in situ fractional crystallisation and settling of pyroxene is regarded as unlikely.

A more plausible model that could account for the observed geochemical trends involves pre-emplacement fractionation and magma segregation. The composition of this dyke suggests that the magma equilibrated at intermediate pressures and is not a primary high pressure mantle liquid (O'Hara, 1968; Kretz et al., 1985). A low to mid level crustal magma chamber would have a natural tendency to form chemical and mineral zonations due to the pressure and thermal gradients occurring in that crustal regime (Gibson et al., 1987). The chemical profiles of dyke GD-I may thus represent different fractions successively tapped by the dyke. The more evolved core, enriched with plagioclase relative to the margins may represent late tapping of plagioclase horizons from such a feeder chamber during dyke dilation. The association of plagioclase with incompatible elements required by this model is in accord with observed layered gabbro complexes observed within the Main Dyke Complex where alkali feldspar and apatite are concentrated within plagioclase cumulates. Indeed 1 km southwest along strike of the dyke from the sample location, the dyke core contains porphyritic (up to 10 cm) cumulus plagioclase associated with alkali feldspar and apatite.

6.8.2 Profile GD-II

The interpretation of primary igneous processes responsible for the observed chemical trends in dyke GD-1 are complicated by the higher degree of alteration affecting this dyke. The loss of CaO from the southeastern part of the profile is thought to have skewed the absolute concentrations of Ni, Cr, MgO and Fe_2O_3 in these samples, manifested by the total conversion of augite to chlorite. However the rare earth elements analysed exhibit a 21 % depletion in the core relative to the dyke chilled margins. Similar depletion patterns are displayed by the incompatible elements P_2O_5, Zr, Y and Nb (Figure 6.2).

The most appropriate single stage model that could be envisaged which might account for the observed geochemical trends is flow differentiation of early forming phenocryst phases, Fe-Ti oxides, olivine,

clinopyroxene and plagioclase in the dyke centre. Whilst such a model could account for the observed depletion of incompatible elements in the dyke centre, a sympathetic increase in Al_2O_3, MgO, CaO, Fe_2O_3, Ni, Cr and TiO_2 relative to the margins would be expected. Although CaO, TiO_2 and Al_2O_3 do exhibit varying degrees of enrichment towards the centre of the dyke, a sympathetic increase in MgO, Fe_2O_3, Ni and Cr is only developed in sample DRD-55 in the dyke centre. Ironically the latter sample is also lower in Al_2O_3 and TiO_2 than the surrounding dyke core samples, which would require preferential concentration of olivine and augite as opposed to Fe-Ti oxides and plagioclase in the dyke centre. Considering plagioclase to have the greatest liquid drag coefficient of all the early phenocryst phases, such a mechanism of preferential sorting during flow differentiation would be hard to envisage.

Perhaps a more credible approach is that the primary geochemical differences observed across the dyke records the differential tapping from a lower to mid crustal differentiated magma chamber during dyke dilation. The observed geochemical variations could be accounted for by successively tapping increasingly mafic magmas, initially enriched in plagioclase and clinopyroxene components relative to the chilled margins, and subsequently enriched in clinopyroxene and olivine. The latter could account for the concomitant enrichment in MgO, Fe_2O_3, Ni and Cr and relative depletion in Al_2O_3 in the centre of the dyke.

6.9 Isotopic Variations

6.9.1 Introduction

Isotopic ratios of basaltic magmas have commonly been used to infer the isotopic composition of their upper mantle source regions (Gast, 1960) or the degree of crustal contamination they have been subjected to during ascent (Cox and Hawkesworth, 1985). Isotopic heterogeneity recorded in dykes has been extensively modelled by Patchett (1979), using physical constraints to estimate likely mechanisms of crustal contamination.

Both dykes have been analysed for $^{87}Sr/^{86}Sr$ whole rock variations across their strike, as well as calcite and epidote separates obtained along strike from highly altered Gannakouriep dykes (DRD-170). In addition whole rock $^{18}O/^{16}O$ analyses have been undertaken for dyke profile GD-II. The freshest rock sample from this dyke (DRD-55) was selected for $^{18}O/^{16}O$ mineral separate analysis of augite. A quartz-chlorite mineral pair was also separated from sample DRD-170. Mineral separation was initially accomplished using a Frantz magnetic separator, and subsequently hand picked with the aid of a binocular microscope. Whilst calcite provided minimal problems in obtaining a pure sample, difficulty was experienced in obtaining a clean epidote separate. The latter contained upto 10 % relict plagioclase and minor sericite. Similarly due to incipient chloritisation of pyroxene, difficulty was also experienced in obtaining totally pure augite cores for ^{18}O analysis. Minor chloritisation (<5 %) was observed along internal mineral fractures.

6.9.2 Results

Rb-Sr data from both dykes together with a reference isochron obtained in this study defining an intrusion age at 717 Ma with an initial Sr ratio of 0.705 are shown in Figure 6.10, whilst variation in whole rock $d^{18}O$ for profile GD-II is shown in Figure 6.11. Data obtained for all samples is listed in Table 6.3.

All data points in Figure 6.10 lie significantly above the reference isochron with a range in $^{87}Sr/^{86}Sr$ ratios of 0.708 to 0.72 with a variation in Rb/Sr ratios of 0.18 to 0.79. The corresponding calculated initial Sr ratios in Figure 6.12 exhibit a similar pattern in both profiles, displaying marked apparent ^{87}Sr enrichment towards the dyke margins. By contrast the $d^{18}O$ profile for dyke GD-II is relatively flat showing near mantle values, with only a minor negative shift in $d^{18}O$ recorded at the dyke margins. The co-existing quartz-chlorite mineral pair yield a $d^{18}O$ fractionation of 6 ‰ which, using the method of Wenner and Taylor (1971), suggests they last equilibrated with a fluid phase at 210° C.

6.9.3 Discussion

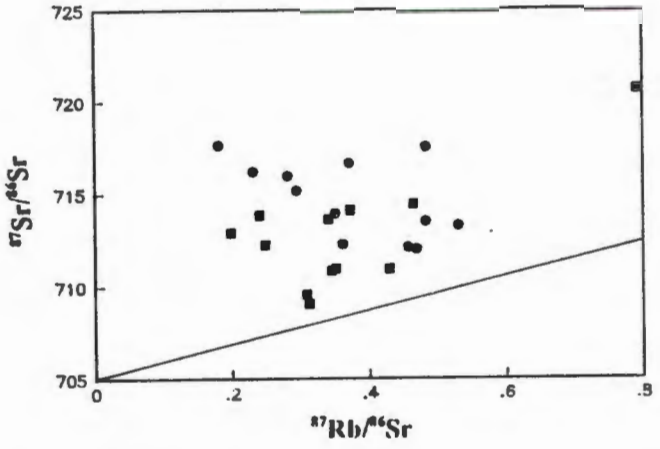

Figure 6.10. *Rb-Sr isochron plot from dyke profiles Gd-I and Gd-II, with a reference isochron of 717 Ma (initial $^{87}Sr/^{86}Sr$ = 0.705). Profile GD-I circles, GD-II squares.*

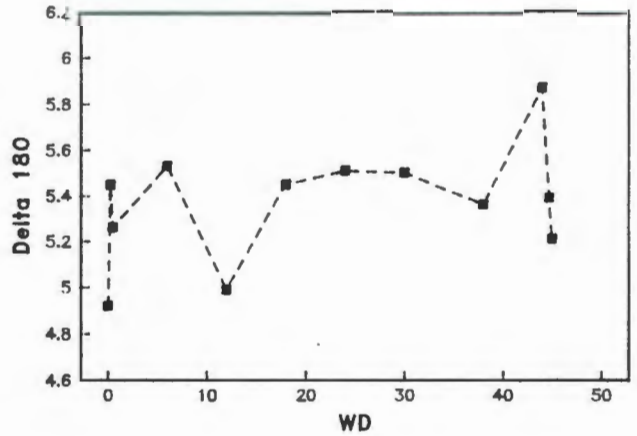

Figure 6.11. *Delta ^{18}O variation across width of dyke profile GD-II. Error limits +/- 0.3‰.*

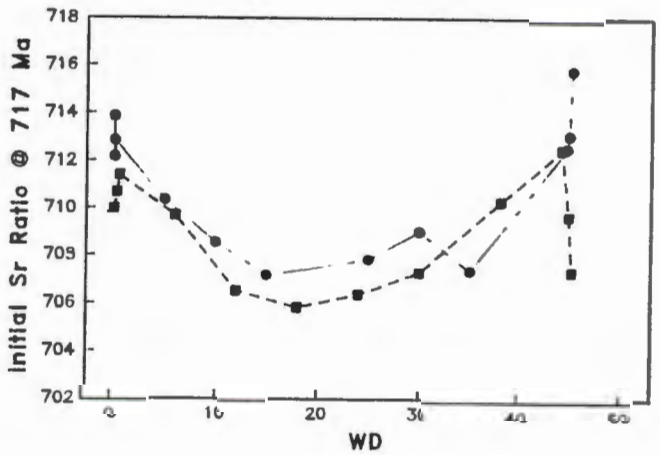

Figure 6.12. *Whole rock initial $^{87}Sr/^{86}Sr$ calculated at 717 Ma across the widths of dyke profiles GD-I and II. Profile GD-I circles with broken line, profile GD-II squares with dashed line.*

In the ensuing discussion two points are important to bear in mind;

(i) Acid leaching of the whole rock samples (Table 6.3) yield little or no change in their measured present day $^{87}Sr/^{86}Sr$ isotopic ratios. Calcite separates obtained from DRD-170 although yielding high $^{87}Sr/^{86}Sr$ ratios contain only 40ppm Sr, and thus are unlikely to serve as a major ^{87}Sr contaminant. However epidote analysed from the same sample also yields a high $^{87}Sr/^{86}Sr$ ratio (0.7170), and since it comprises a silicate phase, leaching with dilute hydrochloric acid would essentially have no effect on the whole rock $^{87}Sr/^{86}Sr$ ratios. Epidote is modally important in some samples of these rocks, reaching levels of up to 30%. Thus if the epidote contains a significant quantity of Sr, the former may constitute a major ^{87}Sr contaminant.

(ii) The observed disruption of the $^{87}Sr/^{86}Sr$ whole rock ratios in the dykes is not reflected by the surrounding country rock (initial $^{87}Sr/^{86}Sr = 0.727$ @ 717 Ma) which has been essentially undisturbed since their emplacement 1.8 Ga (Reid, 1977). Thus by implication the observed heterogeneity of Sr isotopes appears to be confined to the dykes.

That the observed ^{87}Sr enrichment trends towards the dyke margins could be derived by magma mixing and hybridisation at the top of a magma chamber would seem unlikely. Any fractionation of Sr isotopes towards a more evolved magma during magma mixing and hybridisation would also require ^{87}Sr enrichment in the centre of dyke GD-I. Similarly that the observed ^{87}Sr trends are a product of bulk contamination of the intruding magma by the incorporation and digestion of wall rock xenoliths (Figure 6.13) is also untenable since the

Table 6.3. *Strontium Isotopic Data from Dyke Profiles GD-I and GD-II*

Sample #	Rb	Sr	$^{87}Sr/^{86}Sr$	$^{87}Rb/^{86}Sr$	$^{87}Sr/^{86}Sr$ @ 717 Ma	$d^{18}O$
DRD-66	28.1	350	.716232+/-16	.232	.7138	-
DRD-67	32.0	314	.71593+/-26	.295	.7122	-
DRD-68	45.6	355	.716672+/-20	.372	.7129	-
DRD-69	57.9	478	.713958+/-20	.351	.7104	-
DRD-70	58.3	466	.712283+/-18	.362	.7086	-
DRD-71	67.4	415	.712016+/-18	.470	.7072	-
DRD-72	77.2	421	.713308+/-24	.531	.7079	-
DRD-73	56.5	339	.713549+/-20	.483	.7086	-
DRD-74	57.5	364	.712081+/-18	.457	.7074	-
DRD-75	61.5	368	.717534+/-32	.484	.7126	-
DRD-76	34.4	353	.715998+/-28	.282	.7131	-
DRD-77	26.8	404	.717669+/-38	.182	.7158	-
DRD-50	29.6	250	.713364+/-88	.341	.7095	4.91
DRD-50A	23.7	345	.71290+/-14	.199	.7106	5.47
DRD-51	43.4	520	.713871+/-36	.241	.7111	5.27
DRD-52	40.7	472	.71224+/-14	.249	.7090	5.58
DRD-53	64.8	436	.71093+/-17	.430	.7060	5.01
DRD-54	44.6	405	.709068+/-32	.313	.7054	5.45
DRD-55	36.3	339	.709569+/-46	.309	.7060	5.53
DRD-60	47.3	395	.710861+/-56	.346	.7069	5.38
DRD-56	34.5	267	.7714134+/-38	.373	.7099	5.46
DRD-57	76.0	277	.72061+/-11	.792	.7116	5.93
DRD-58	38.8	241	.71444+/-15	.465	.7091	5.38
DRD-59	34.1	280	.710966+/-14	.352	.7069	5.18
Cpx	-	-	-	-	-	5.43

Notes: - not determined

ratio of country rock to magma required to produce the calculated initial Sr ratios observed in the dyke marginal facies is at variance with trace element concentrations of the rock samples.

Two other mechanisms that could produce the observed ^{87}Sr enrichment include selective contamination, or subsolidus hydrothermal alteration. Whilst ionic diffusion of Sr across the dyke-country rock interface may have occurred, the low diffusion rates of Sr calculated by Springer et al. (1983) would tend to suggest that the effects of such a mechanism would be minor, and furthermore fail to accommodate the deep penetration of ^{87}Sr diffusion towards the dyke centres within their given age.

Given the lack of constraints on possible chemical and isotopic composition of selective contaminants involving minimum eutectic melts, the selective contamination is difficult to exclude outright. A rough correlation between MgO and initial ^{87}Sr is observed in both dyke profiles suggests conduit contamination in a similar manner envisaged by Huppert and Sparks (1985). The proposed mechanism is outlined in Figure 6.13. However such correlations must be treated with caution since;

(i) MgO has been affected by secondary alteration,

(ii) Rb has similarly been affected by secondary alteration, thus interpreting initial Sr ratios as a function of primary processes is suspect, and

(iii) Despite having a lower MgO content, dyke profile GD-I has a higher overall initial Sr ratio by comparison to dyke GD-II.

However given that both dyke profiles comprise similar ^{87}Sr and Sr trends across their width in disaccord with inferred magmatic processes, an alternative explanation may be sought involving preferential hydrothermal alteration and ^{87}Sr contamination at the dyke margins. A possible alteration vector is shown in Figure 6.14. Whilst many of the data points from both dyke profiles lie off this vector, they majority fall to the right hand side of it, suggesting subsequent wholesale leaching of Sr from these samples. The samples exhibiting the greatest inferred Sr leaching correspond to those samples which have experienced major calcium loss (45%).

Constraints placed on either fluid rock interaction or selective contamination of the dykes by the oxygen isotope data are poor. The current $d^{18}O$ of the surrounding granite country rock is around +7 ‰ (Reid, written comm.), thus oxygen isotopes are effectively insensitive to small degrees of crustal contamination (Taylor, 1968). However whole rock and mineral separate $d^{18}O$ data do suggest that dyke GD-II has been isotopically altered by +1 ‰, since plagioclase is inferred to be 1 ‰ heavier in $d^{18}O$ than the estimated whole rock $d^{18}O$ of around 6.2 ‰ (dolerite = 50 % plag, 50 % cpx). Interaction with a meteoric fluid is thus implied, though the actual $d^{18}O$ value of the hydrothermal fluid remains unconstrained. The quartz-chlorite thermometry suggests that closure to further fluid-rock interaction took place at 210° C, which may constitute either a Pan-African metamorphic closure, or closure subsequent to the generation of hydrothermal cells generated during intrusion.

Enhanced $d^{18}O$ depletion at the dyke margins suggest preferential exchange between meteoric waters and dyke chills. The latter is concomitant with ^{87}Sr depletion of the dyke contacts in profile GD-II. Dykes are known to form structural barriers to meteoric water flow (Watkins, pers. comm.). Thus the deviation of $d^{18}O$ composition of the dyke margins in comparison to the bulk of the dyke may reflect enhanced $d^{18}O$ exchange and ^{87}Sr leaching at the dyke contacts during subsequent preferential percolation of meteoric water along the granite country rock-dyke interface.

6.10 Summary

In summarising the intra-dyke geochemistry, several features pertinent to the emplacement process are distinguishable:

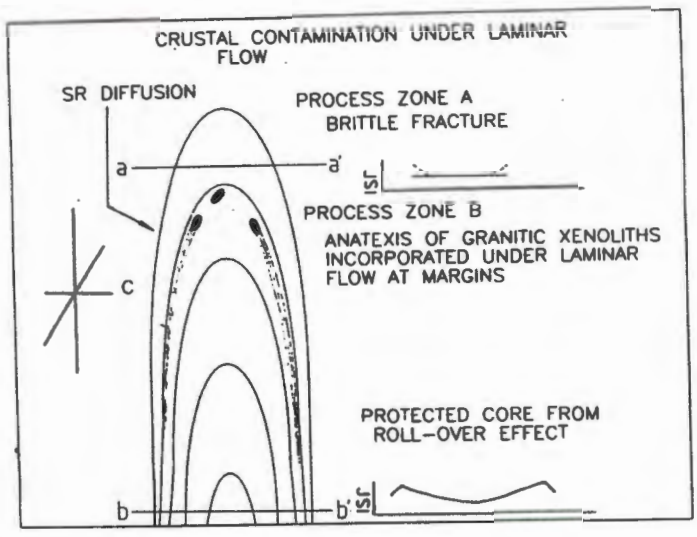

Figure 6.13. *Model scenario by which the observed variation in initial $^{87}Sr/^{86}Sr$ could be produced by conduit contamination during dilation of the dykes under laminar flow conditions. During the initiation and formation of the dyke fracture, contamination of the magma dilating the dyke is enhanced by thermal cracking of the host rock, incorporating it into the advancing magma sheet, raising the initial Sr ratio of the magma.*
From the argument eluded to in Chapter 2, this process would not immediately affect the chilled margins of the dyke, since the thermal energy released by intial solidification of the chills would not be sufficent to produce anatexsis of the country rock. The main contamination would occur once the dyke had dilated sufficently to incorporate xenolith by thermo-mechanical processes. Subsequently continued dilation of the dyke would bring magma from depth which is effectively sealed from crustal contamination with the host rock due to the presence of already solidifying magma at the dyke walls, producing a roll-over effect.

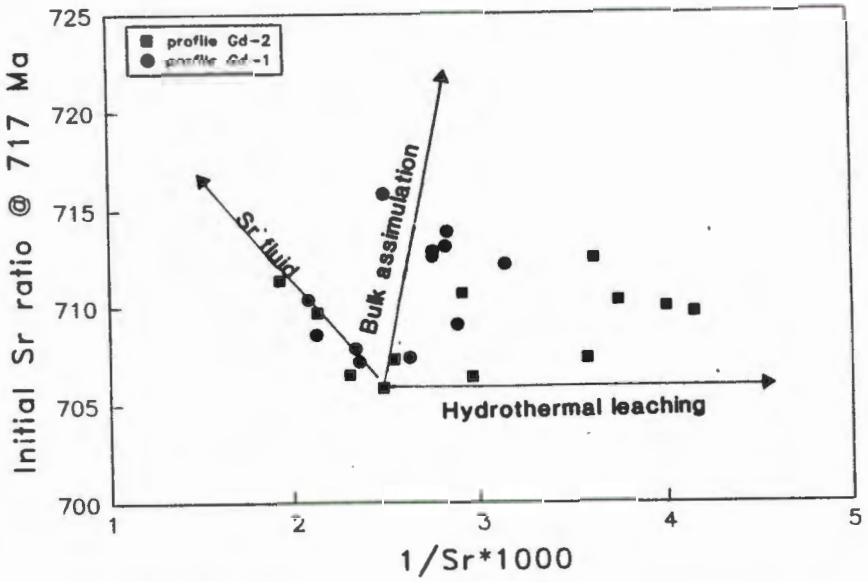

Figure 6.14. *1/Sr*1000 versus initial $^{87}Sr/^{86}Sr$ at 717 Ma. Vectors shown indicate possible hydrothermal exchange with a fluid containing a higher $^{87}Sr/^{86}Sr$ ratio than the Gannakouriep dykes, crustal contamination with Vioolsdrif adamellite, and Sr leaching. Vioolsdrif adamellite data taken from average values given in Reid, (1977). Alteration of the initial Sr ratios of the dykes may have been accomodated by a two stage process. Initial interaction with a Sr fluid may have increased the Sr isotopic ratio along the Sr fluid vector, prior to hydrothermal leaching of Sr.*

(i) The geochemical profiles constructed accross dykes GD-I and GD-II exhibit similar initial composition of the intruding magmas, yet display contrasting geochemical variations in their cores.

(ii) The degree of secondary alteration in both dykes is marked, with a higher degree of alteration being exhibited by dyke GD-I in the northern part of the dyke complex GDC-4. The concentration of the major elements (Fe, Mg and Ca) appear to have been affected by greenschist metamorphism, with the conversion of clinopyroxene to chlorite. The alkali metals (K, Rb) are inferred to have been lost from the dolerite chilled margins during devitrification.

(iii) Geochemical processes accounting for the observed intra-dyke chemistry are poorly constrained given the inferred degree of secondary alteration. However both geochemical profiles are not easily reconcilable in simple terms of in situ fractionation or flow differentiation. A more plausible explanation may be sought by regarding the geochemistry to represent successively tapped portions feed, from a mid to lower level crust fractionated magma chamber.

(iv) The Sr isotopic variations across both dykes is similar, indicating ^{87}Sr enrchment towards the chilled margins of the dykes. The variation in Sr isotopic ratios is regarded as a product of secondary open sysytem behaviour during alteration, although a component of primary isotopic heterogeneity due to conduit contamination cannot be excluded outright.

(v) The O isotopes data on whole rock samples yield a relatively flat profile across dyke GD-I, close to primary mantle values. Quartz-chorite thermometry indicates closure to further fluid rock interaction occurred at 210°C. Since the greenschist mineral assemblage is inferred to be of Pan African metamorphism (from the K-Ar data, section 5.4), the O isotopic signature recorded by the dyke probably reflects open system behaviour.

7 GEOCHEMISTRY OF THE GANNAKOURIEP DYKE SWARM

7.1 Introduction

The Gannakouriep dyke swarm intrudes a basement constituted from a variety of tectono-stratigraphic terranes (Hartnady et al, 1985). The latter observation permits comparison of chemical data obtained from different parts of the swarm to test if local heterogeneities are present in the underlying mantle/lithosphere which can be ascribed to different basement terranes. If apparent mantle heterogeneities reflected by trace element ratios of the Gannakouriep magmas are absent, the source region of the swarm may be situated in one particular mantle/lithospheric domain, subsequent to which the derived magma propagated laterally through the continental crust of juxtaposed basement terranes.

The geochemistry of the dyke swarm has been investigated on two levels,

(i) Individual dyke complexes ascribed to sector I have been intensively sampled to constrain chemical variations occurring within each complex. Subsequently they are compared to elucidate if different chemical processes occurred during the formation and intrusion of these complexes

(ii) Dykes spanning all three sectors of the swarm, which intrude differing basement terranes, were sampled to characterise inter-sector geochemical variations to elucidate any mantle/lithosphere heterogeneities that may be involved in the petrogenesis of the Gannakouriep magmas.

All samples have been analysed for a suite of trace elements by XRF, whilst a selected sub-set samples were augmented by major element analyses. REE data were obtained by ion chromatography and INAA for a suite of rock samples encompassing the entire dyke swarm. Relevant analytical techniques, data and their precision are to be found in Appendix 4, whilst sample locations are listed in Appendix 5.

7.2 Geochemical Variations

7.2.1 Introduction

The large degree of element mobility during secondary alteration processes has been broached in the previous chapter. In order to alleviate secondary alteration whilst attempting to unravel primary geochemical trends of magmas, a ratio technique of x oxide (element)/x immobile oxide (element) (where immobile elements are defined as Ti, Al, P, Zr, Y and Nb; Pearce and Cann, 1973) has been used by several workers (c.f. Zeck and Kalsbeck, 1981). However these techniques can often lead to spurious trends, and erronaneous interpretation. Major and trace element variation trends have been established using the Zr content of individual rock samples. Zr serves as a fractionation index in the Gannakouriep magamas since Zr is is almost wholly excluded from potential phenocryst phases within a basaltic system, with a bulk partition co-efficent approaching zero (Cox et al., 1979).

7.2.2 Major Elements

All samples obtained from the Gannakouriep dyke swarm are fairly evolved tholeiites exhibiting a limited range in Mg# (molecular Mg/Mg+Fe adjusted to wt % Fe_2O_3/FeO ratio of 0.15) of 52-67 and plot in a tight grouping in the tholeiite field on a conventional AFM diagram (Figure 7.1). A statistical analysis for the major element chemistry from the entire swarm is shown in Table 7.1. Two features are prominent from their whole rock major element chemistry: firstly all dykes are enriched in Fe, comprising ferro-tholeiites, no primitive samples (in regards to Mg-Fe fractionation trends) are apparent; and secondly all dykes are similarly enriched with TiO_2.

Selected normative composition of the least altered samples from the dyke swarm are plotted on the conventional expanded basalt tetrahedron (Figure 7.2) in conjunction with;

(i) one atmospheric cotectic curve,

(ii) suggested basalt cotectic curve at deep crustal levels,

(iii) a pressure sensitive MORB melting curve (Thompson, 1982; Thompson et al., 1983).

Although comprising a considerable scatter probably attributable to secondary alteration, the samples fall close to the cotectic curve for deep crustal levels suggesting that the magmas were erupted from deep crustal reservoirs rather than high level magma chambers.

Major element variation diagrams for five dyke complexes (GDC-1 to 5) from Sector I are shown in Figure 7.3, in conjunction with dykes from Sectors II and III. Major element variations across the entire dyke swarm define the same geochemical co-variations suggesting that similar magmatic processes have been operative in producing the swarm. A significant degree of scatter of data is clearly visible in these diagrams for the major oxides SiO_2, Al_2O_3, TiO_2, MgO, CaO, Fe_2O_3, Na_2O and K_2O, with primary igneous trends being difficult to discriminate. The scatter, especially that of CaO is compatible with the previously described loss of CaO from the Gannakouriep dykes during secondary alteration. The loss of CaO and deviation from inferred igneous trends is restricted to dykes comprising sectors I and II which have undergone greenschist facies metamorphism, suggesting extensive chloritisation of clinopyroxene is responsible.

However, for the oxides MgO, Al_2O_3, CaO there appears to be a negative correlation with increasing Zr. Conversely, a positive correlation with increasing Zr can be observed for the oxides TiO_2, Fe_2O_3, and P_2O_5. TiO_2 and Fe_2O_3 show a relatively good correlation (Figure 7.4).

7.2.3 Trace Element Characterisation

7.2.3.1 High Field Strength Trace Elements

	MEAN	MINIMUM	MAXIMUM	MEAN + 1 S.D.	MEAN - 1 S.D.
SIO2	46.60	33.69	64.27	49.71	43.48
TIO2	3.16	.98	5.48	3.77	2.56
AL2O3	15.18	11.14	18.42	16.23	14.14
FE2O3	14.70	9.10	18.78	16.37	13.03
FEO					
MNO	.22	.04	.71	.27	.16
MGO	5.19	.94	7.48	6.35	4.03
CAO	7.75	1.06	18.14	9.55	5.95
NA2O	2.56	.05	8.28	3.43	1.69
K2O	1.49	.13	5.73	2.31	.66
P2O5	.57	.26	2.36	.83	.31
CR2O3					
NIO					
H2O-	.14	.02	.73	.24	.05
H2O+	2.7	.4	5.1	3.6	1.8
CO2	.5	.1	3.5	1.2	
LOI	2.87	.43	11.95	4.47	1.26
TOTAL	100.39				
NO	2.3	.7	7.4	4.1	.5
NB	25	11	137	36	15
ZR	282	134	677	359	206
Y	45	20	90	55	34
SR	349	34	1771	540	157
U	2.8	1.7	11	4.4	1.2
RB	65	5.8	360	109	20
TH	4.7	2.5	15	7.5	2.0
PB	17	3.4	456	59	
ZN	145	16	335	180	110
CU	27	2.8	212	51	2.7
NI	50	3.4	277	83	16
CO	54	17	89	63	44
MN	1653.0	801.8	3464.3	2032.7	1273.3
CR	50	4.0	308	81	18
V	267	34	470	318	217
BA	474	46	1636	709	240
SC	26	8.6	38	31	22
LA	28	13	88	37	19
CE	71	35	200	89	53
ND	46	27	111	57	36

*** ALL ZERO VALUES PRINTED AS BLANKS ***

Table 7.1. *Average whole rock composition and statistical variations of XRF data from the Gannakouriep suite.*

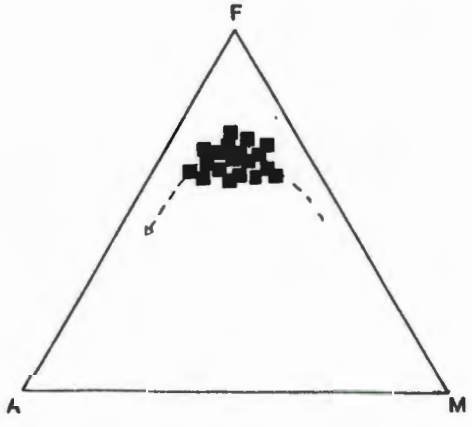

Figure 7.1. *Conventional AFM diagram of the Gannakouriep suite, with tholeiitic and basalt trend indicated.*

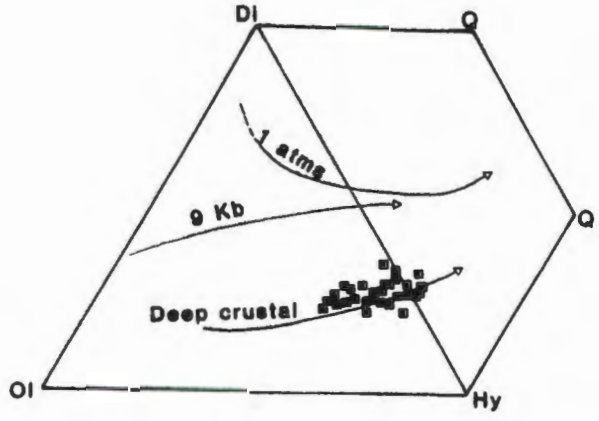

Figure 7.2. *Normative compositions of the Gannakouriep suite plotted on an expanded basalt tetrahedron. Also shown are the 1 atmosphere, 9 kb and lower crustal cotectics from Thompson, (1982); Thompson et al., (1983). Tne number of samples plotted is 27, taken from samples showing the least alteration to metamorphic assembledges.*

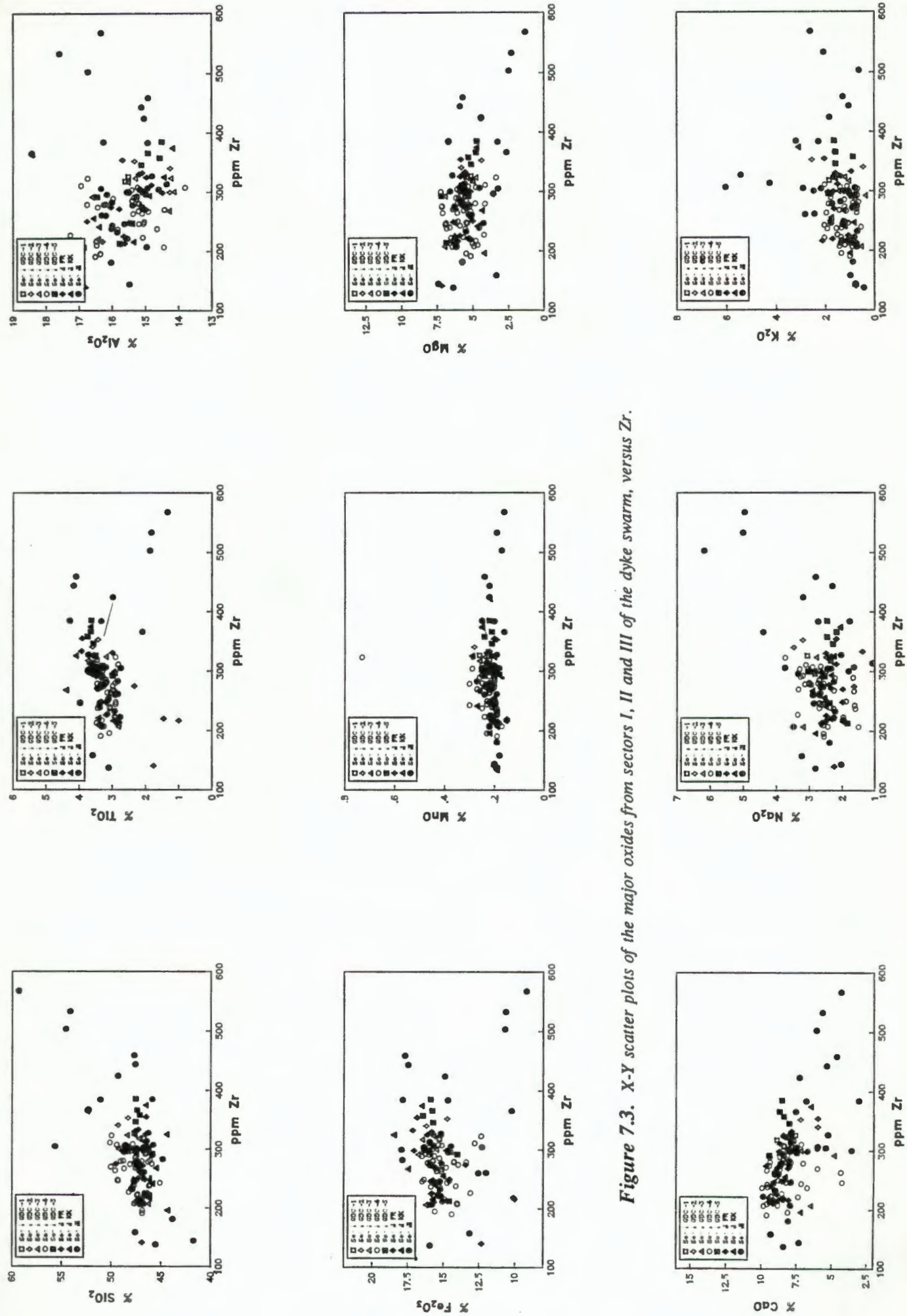

Figure 7.3. X-Y scatter plots of the major oxides from sectors I, II and III of the dyke swarm, versus Zr.

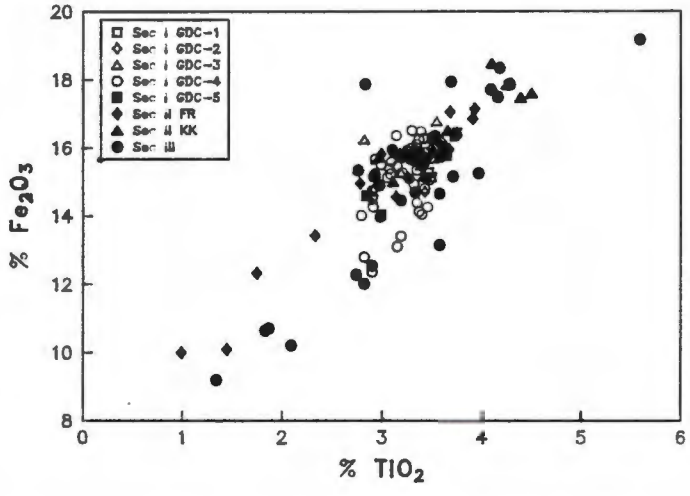

Figure 7.4. *TiO_2 versus Fe_2O_3 for the Gannakouriep dyke swarm.*

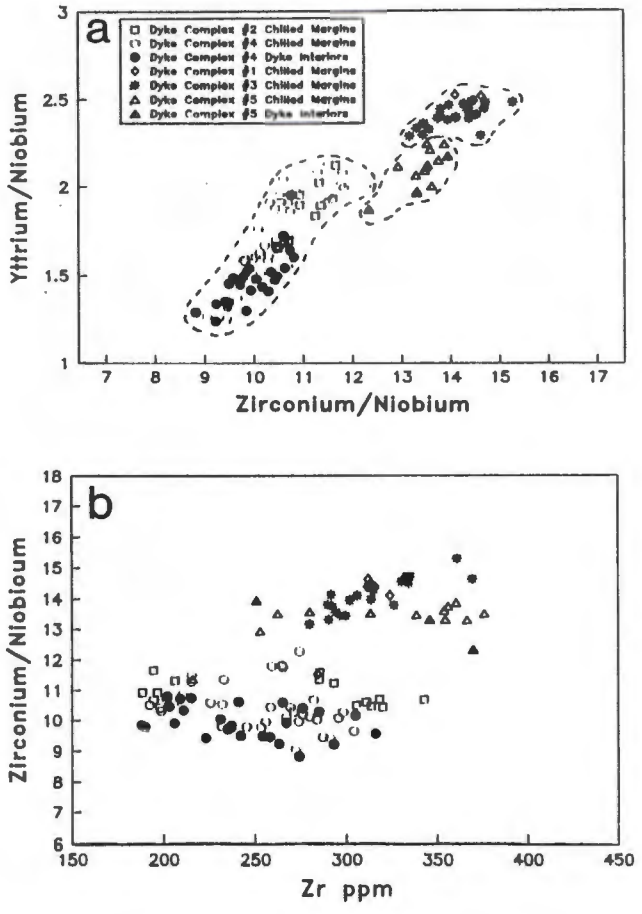

Figure 7.5. *(a) Niobium normalised Zr versus Y variations of dyke complexes GDC-1 to 5. (b) Zr/Nb versus Zr of dyke complexes GDC-1 to 5 from Sector I.*

The high field strength and incompatible elements Zr, Y and Nb are largely unaffected by secondary alteration processes (Pearce and Cann, 1973; Mueke et al., 1979) and variation in their interelement ratios have often been used to discriminate different magma types (Pearce and Norry, 1979; Reid et al., 1987). Co-variation amongst these elements for dyke complexes GDC-1 to 5 from sector I are shown in Figure 7.5. At least three magma types can be distinguished from dyke complexes GDC-1 to 5 on the basis of their niobium normalised Zr/Y ratios. The latter correspond to stratigraphic controls placed upon the dyke complexes by field mapping. Both dyke complexes GDC-1 and GDC-3 are characterised by Zr/Nb ratios spanning 13-15 and an Y/Nb ratio around 2.4, whilst dyke complex GDC-5 is defined by a Zr/Nb ratio of 13-14 and an Y/Nb ratio around 2.1. The largest variation in niobium normalised Zr/Y ratios is recorded by dyke complex GDC-4 which has a range in Zr/Nb ratios of 9-12, and Y/Nb ratios of 1.2 - 2.1. Samples taken from dyke complex GDC-2 lie on the same variation described for dyke complex GDC-4, however it exhibits a more limited range in concentrations of Zr/Nb = 10.5 - 11.8, and Y/Nb = 1.6 - 2.1. Variation in Zr/Nb ratios of these magma types versus absolute abundance of Zr indicate that dyke complexes GDC-1, 3 and 5 comprise more evolved magma series than dyke complexes GDC-2 and 4.

Niobium normalised Zr/Y ratios across the entire dyke swarm is shown in Figure 7.6. The swarm exhibits a range in niobium normalised Zr/Y ratios of 5 to 7. No geographic control is exerted on these interelement ratios, the range in ratios being attributable to dykes from all three sectors. Assignment of individual dykes to complexes which may show similar co-variations in high field strength interelement ratios to those described in Sector I is untenable in the absence of detailed field control and systematic sampling.

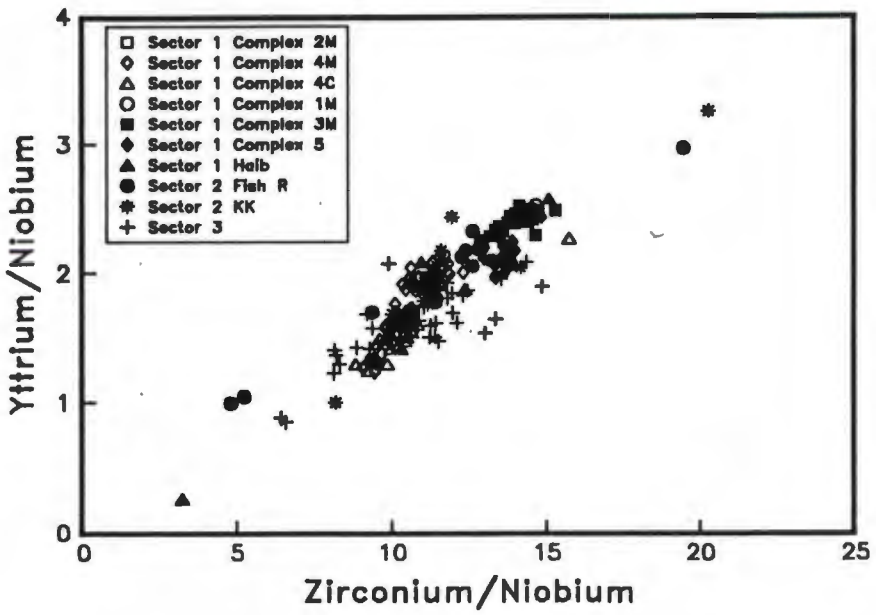

Figure 7.6. *Niobium normalised Zr versus Y variations of the entire Gannakouriep dyke swarm.*

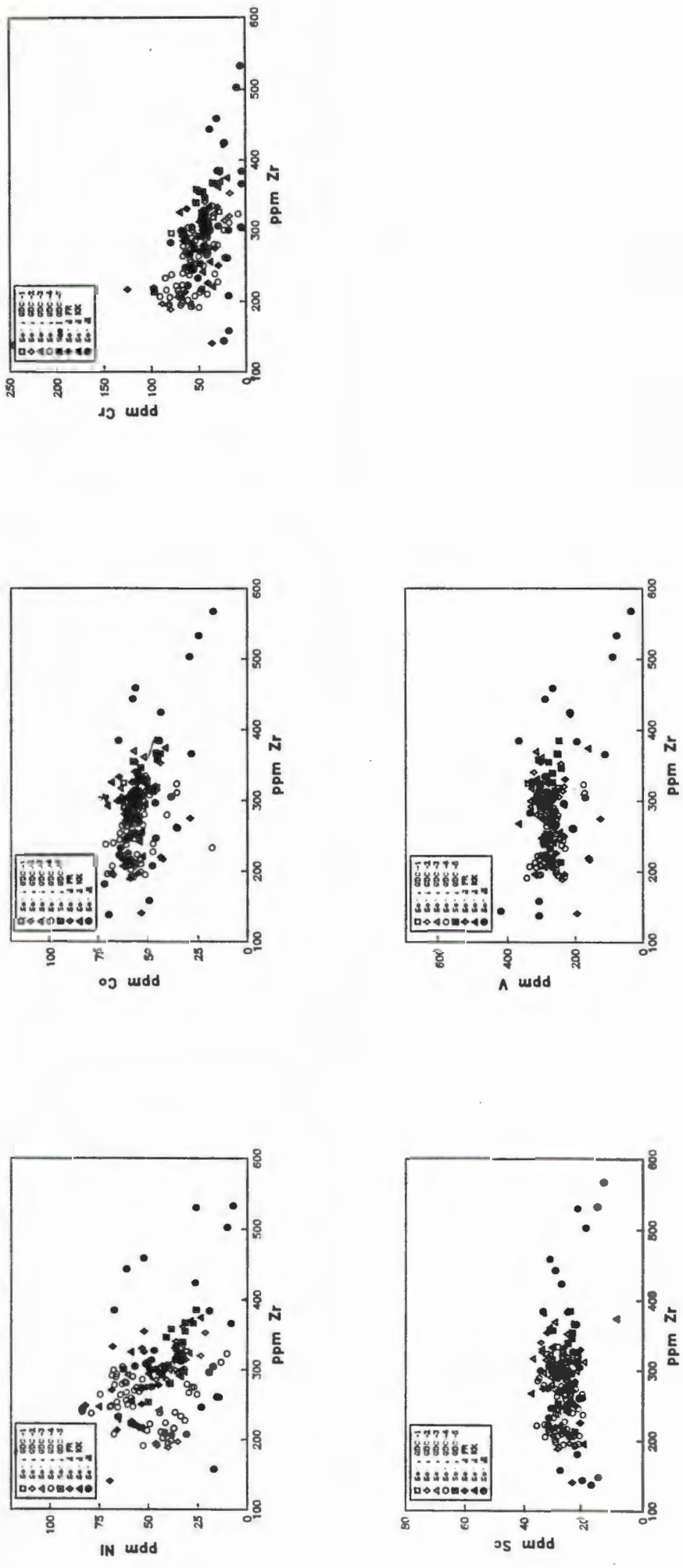

Figure 7.7. *X-Y plots of Ni, Co, Cr, Sc and V versus Zr of dyke complexes GDC-1 to 5 from Sector I, and from Sectors II and III of the Gannakouriep dyke swarm.*

7.2.3.2 Other Incompatible and Base Metal Trace Elements

The incompatible trace element Sr, Rb and Ba have been variably affected by secondary alteration thus their interelement co-variation is erratic in comparison to the immobile trace elements Zr, Y and Nb. Similarly the base metals Zn and Cu exhibit a large degree of scatter suggesting that they too have been subjected to variable secondary alteration, and consequently x-y plots for all these elements are not shown. Zn is in the order of around 150 ppm in the Gannakouriep magmas whilst Cu is more variable, around 30 ppm. Pb is consistently below XRF detection limits (5 ppm).

7.2.3.3 Compatible Ferromagnesian Trace Elements

The compatible ferromagnensian elements Ni, Cr, Co, Sc and V plotted against Zr are shown in Figure 7.7 for all dykes comprising complexes GDC-1 to 5 from Sector I. All elements exhibit a considerable scatter. The trace elements Ni and Cr exhibit the best negative correlation with increasing Zr, whilst Co, Sc and V exhibit variable trends. Despite the slight scatter which may be attributable to secondary alteration or variable mechanical accumulation of ferromagnesian phases, the salient feature to emerge from Figure 7.7 is that dyke complexes GDC-2 and 4 exhibit a markedly greater span in compositional range than complexes GDC-1, 3 and 5. Furthermore complexes GDC-1, 3 and 5 are as a whole typically more evolved them both complexes GDC-2 and 4.

Compatible ferromagnesian element variations for the entire dyke swarm are shown in Figure 7.7b, and exhibit similar geochemical co-variations to those observed in sector I dykes. The largest variation in interelement ratios is apparent in sector III dykes, compatible with the greater degree of fractionation observed within the Main Dyke Complex.

7.2.3.4 Rare Earth Elements

Chondrite-normalised REE patterns for the five dyke complexes GDC-1 to 5 (sector I) are shown in Figure 7.8. All samples exhibit similar light-REE-enriched patterns, with only slight negative europium anomalies developed in some samples. Light REE enrichment is in the range 60 to 110 x chondrite for La, whilst Yb exhibits enrichment in the order of 16 to 25 x by comparison to chondrite. No consistency in light rare earth enrichment over heavy rare earths is discernable which can be correlated with stratigraphic controls, however dyke complexes GDC-2 and 4 exhibit samples (GKR-105, GKR-84) comprising the lowest HREE content, with the least negative Eu anomaly present.

The regional pattern for REE across the extremities of the dyke swarm is similar for those of sector I, only very slight variations in light rare earth element enrichment in comparison with heavy rare earth element being discernable. The LREEs exhibit ranges from 60-160 x chondrite values for La, whilst Yb is enriched up to 30 x chondrite (Figure 7.9).

7.3 Normalised trace element abundances

Comparison and characterisation of the Gannakouriep magmas from different sections of the dyke swarm can be evaluated by using normalised elemental abundances. For direct comparison of elemental variations across the swarm the normalising value used for this purpose comprises sample GKR-104 of dyke complex GDC-4 from sector I of the swarm. Comparison with representative samples from dyke complexes GDC-1, 2, 3, 4 and 5 are shown in Figure 7.10. The normalised element patterns depicted in Figure 7.10 only change their overall abundance levels in response to fractional crystallisation, otherwise their patterns remain largely unaffected. Similarly partial melting to the degree often associated with the production of tholeiites (>10 %) (Reid et al., 1987) has little or relatively no effects on the shape of the spidergrams. Thus differences observed in the shape of normalised elemental abundances can best be attributable to source characteristic heterogeneities (caused by melting or metasomatic processes), or differential crustal contamination. Thus the relatively flat patterns

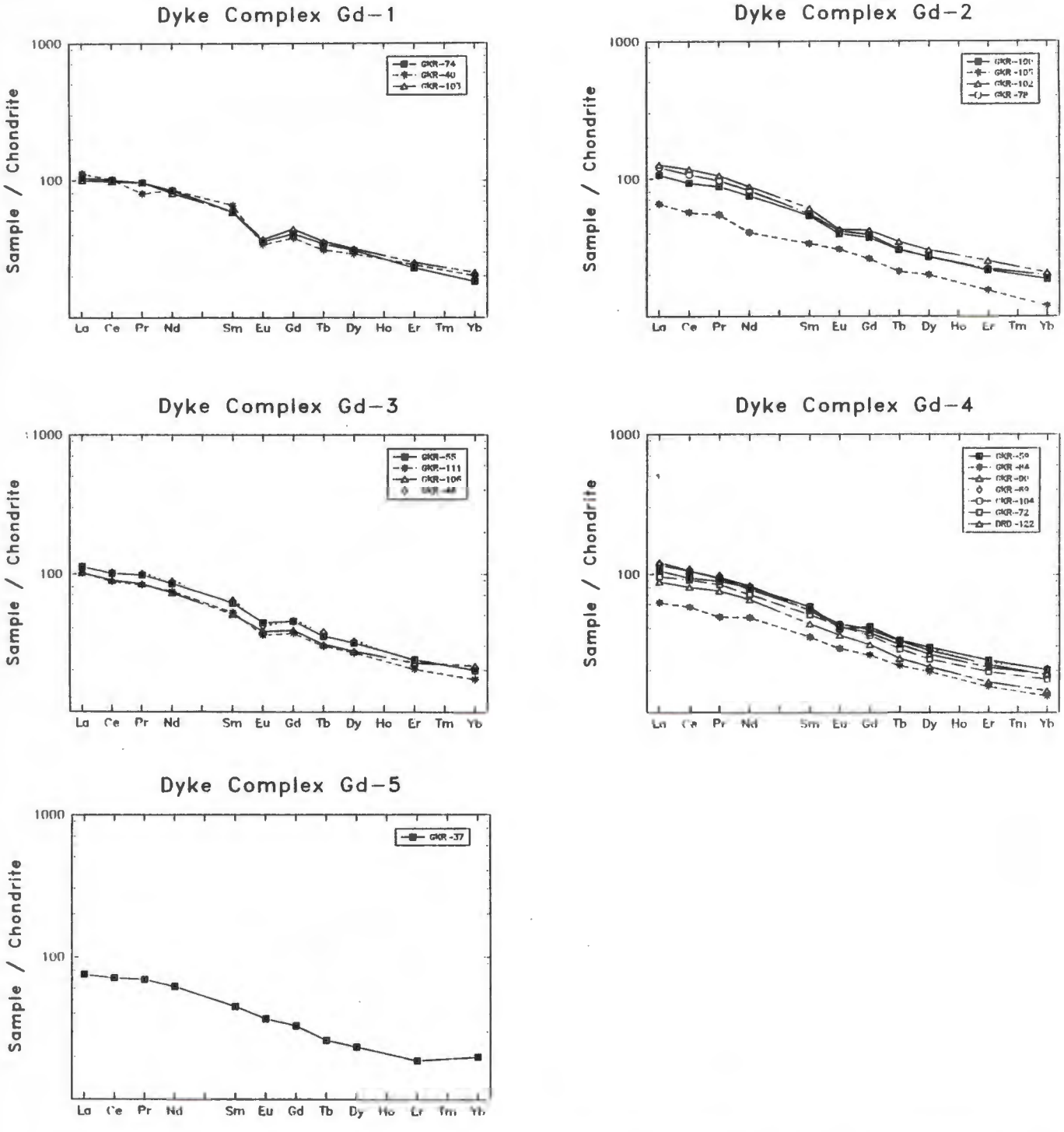

Figure 7.8. *Chondrite normalised REE patterns from dyke complexes GDC-1 to 5, Sector I. Chondrite normalising values taken from Nakamura, (1978).*

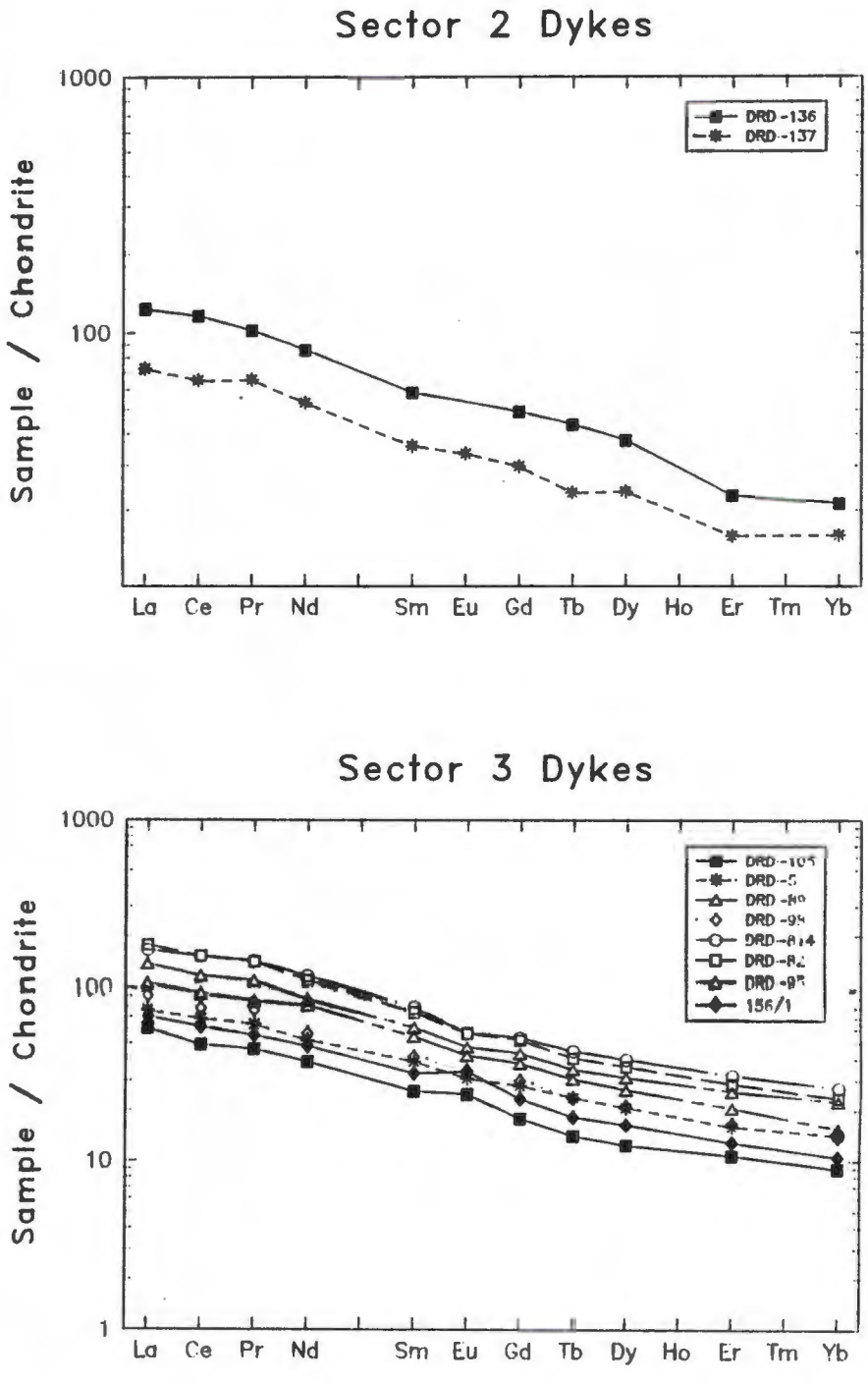

Figure 7.9. *Chondrite normalised REE patterns from Sectors II and III of the Gannakouriep dyke swarm. Chondrite normalising values are taken from Nakamura, (1978).*

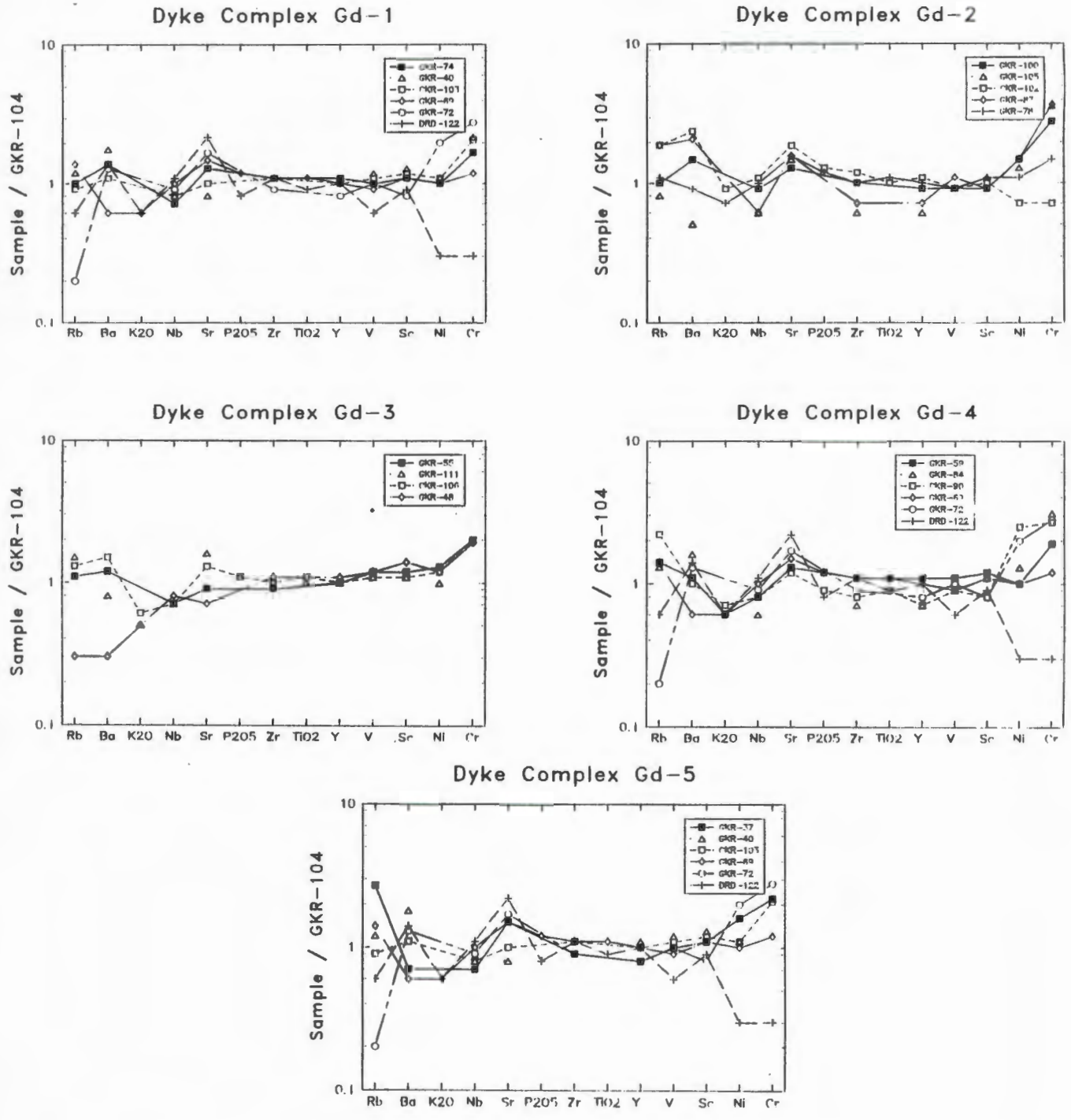

Figure 7.10. *Chemical variations between dyke complexes GDC-1 to 5 of Sector I depicted on spidergrams normalised by sample GKR-104 from complex GDC-4.*

observed in Figure 7.10 indicate similar source characteristics for dyke complexes GDC-1 to 5. The observed fluctuations in Rb, Ba, K and Sr are regarded as products of secondary alteration, while the variation in Ni and Cr are attributed to fractional crystallisation. Indeed, comparison of relative trace element abundances across the entire dyke swarm (Figure 7.11) indicate similar source characteristics and processes were responsible for the generation of the entire dyke swarm, despite the dykes crossing terrane boundaries. The latter observations indicate that the dykes were derived from a relatively homogeneous (with exception of the narrow range of high field strength inter-element ratios) mantle source.

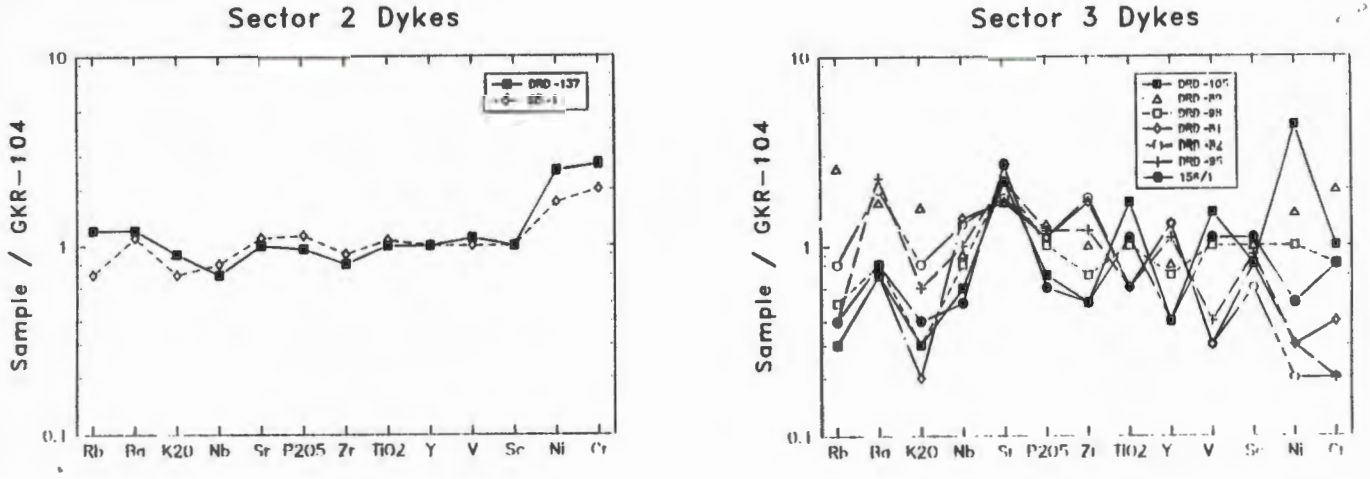

Figure 7.11. *Chemical variations of Sectors II and III of the dyke swarm depicted on spidergrams normalised by sample GKR-104 from Sector I.*

Characteristics of the mantle source for the Gannakouriep magmas relative to N -type MORB (Pearce, 1983) is shown in Figure 7.12. Also depicted in Figure 7.12 are normalised trace element abundances for the Lesotho Karoo basaltic magmas (Marsh and Eales, 1984). The Gannakouriep magmas are characterised by incompatible element enrichment relative to MORB and approximate closely to the Lesotho type Karoo magmas although the niobium anomaly, where present, is poorly developed. The erratic behaviour of the LIL elements (K, Rb, Ba) is due to secondary alteration, although these elements were probably originally enriched relative to MORB, but to what extent remains unconstrained.

7.4 Assessment of Crustal Contamination

The problem of crustal contamination in mafic dyke swarms is still the subject of continuing debate. Because average continental crust of whatever age is enriched in LIL elements (Weaver and Tarney, 1984, 1985) it is

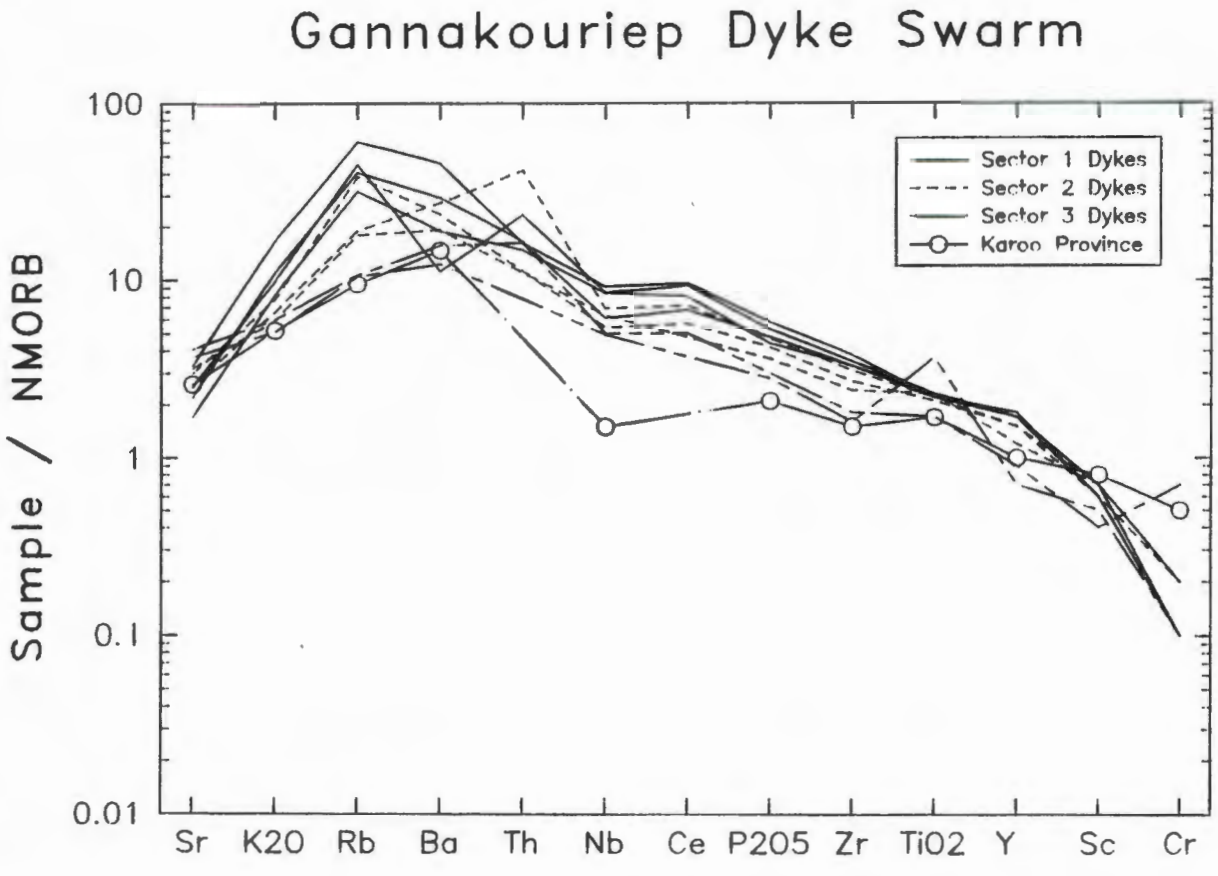

Figure 7.12. *N-MORB normalised spidergrams of Sectors I, II and III of the Gannakouriep dyke swarm. Also shown is the pattern of the Lesotho Formation, the most abundant magma type of the Karoo province.*

often difficult to distinguish the effects of crustal assimilation from primary mantle characteristics which may have been enriched in LILs relative to MORB by processes such as subduction mantle metasomatism. For the Gannakouriep magmas the problem is exacerbated by the high degree of secondary alteration. However two approaches can be used to infer that crustal contamination did not comprise a major factor in the generation of the Gannakouriep magmas.

(i) Evidence from Sr isotope data

Most of the Sr isotopic data has been analysed from sector I dykes where the host rocks comprise adamellite of the Vioolsdrif Igneous Suite (Reid, 1977). Thus in assessing the possible effects of crustal contamination on the Gannakouriep magmas, the adamellite has been chosen as a suitable candidate for modelling purposes. The values used here are taken from average values derived by Reid (1977). The composition of mid- to lower crustal rocks beneath the Richtersveld Igneous sub-province, where crustal contamination is more likely to have occurred, is unknown. Hence the parameters for assessing crustal contamination within the dykes are very poorly constrained.

The $^{87}Sr/^{86}Sr$ ratios of the Gannakouriep dykes and the adamellite contamination vector calculated at 717 Ma are shown in Figure 6.14 plotted against 1/(Sr*1000). If bulk contamination had occurred, the Gannakouriep magmas and the contaminant should lie on a straight mixing line, which clearly they do not. Nevertheless, to investigate the possibility further, sample DRD-151 which has the lowest Sr ratio (initial Sr ratio .705, 495 ppm

Sr; tables 5.1 and 6.4), and sample DRD-77 which has the highest initial Sr ratio (initial Sr ratio .716, 413 ppm Sr), have been chosen as starting and intermediate compositions in a possible bulk mixing calculation. To achieve the isotopic composition of DRD-77 from DRD-151, 10.01 % mixing is required of an adamellite with an $^{87}Sr/^{86}Sr$ ratio of 0.727 at 717Ma, and 279 ppm Sr. However, 10% bulk contamination of DRD-151 by the adamellite cannot produce the elemental composition of DRD-77. For example 10% bulk mixing of DRD-151 with the contaminant would produce an intermediate member with a composition of 0.32% P_2O_5, (contaminant 0.14% P_2O_5, DRD-151 0.36% P_2O_5), where as DRD-77 contains 0.51% P_2O_5. Thus on the basis of Sr isotopic data, bulk contamination of the dyke appears untenable.

(ii) Evidence from MORB normalised spidergrams

The problem of crustal contamination can be explored further by comparison of MORB-normalised trace element abundances of the Gannakouriep magmas with the Vioolsdrif adamellite host rock (Figure 7.13). Although enrichment in Rb, Ba, K and Sr in the Gannakouriep dyke may be attributed to crustal assimilation, the correlative degree of enrichment in Nb is absent. Therefore a model purporting simple contamination of a MORB-type source by the adamellite to produce the Gannakouriep magamas is incapable of producing the observed enrichment of elements in the Gannakouriep dyke relative to MORB. Is is therefore likely that the elemental patterns depicted in Figure 7.14 are inherited either from an athenospheric or mantle lithospheric source region.

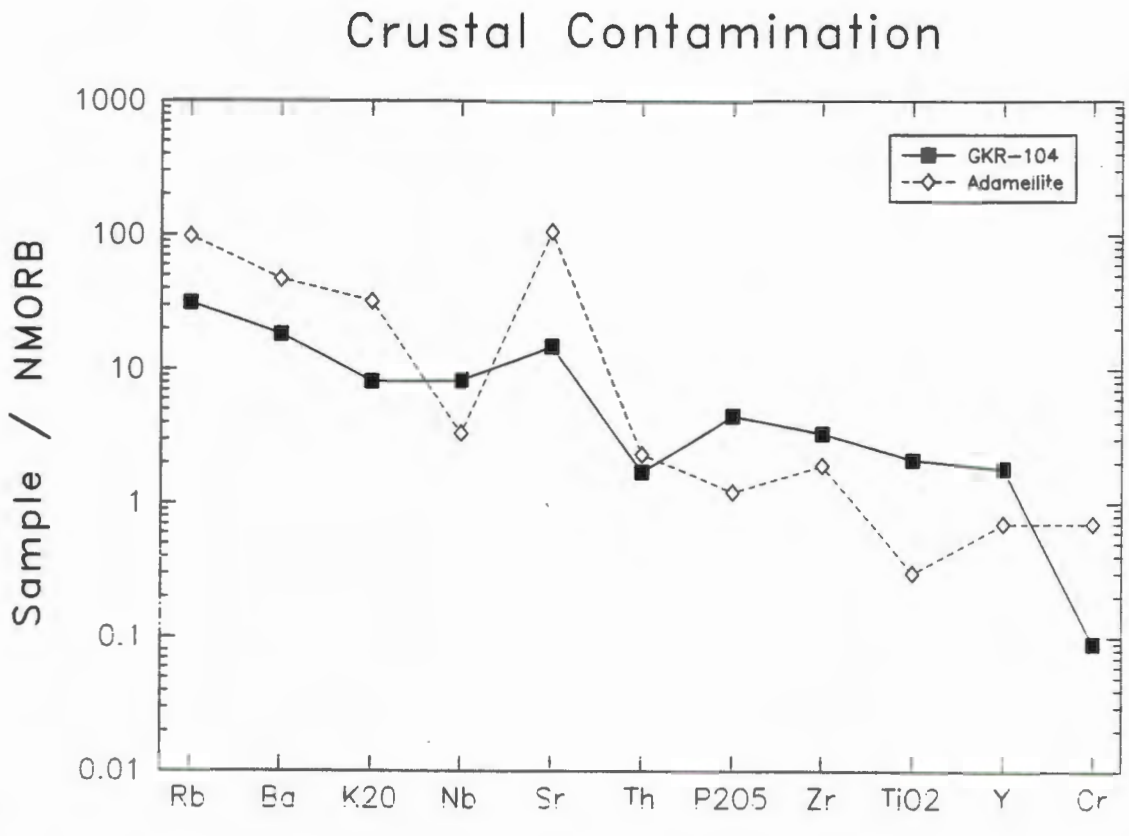

Figure 7.13. *Conventional spidergram of N-MORB normalised Vioolsdrif adamellite and sample GKR-104.*

7.5 Petrogenesis

Interpretation of the petrogenesis of the Gannakouriep dyke swarm is fraught with complications due to secondary alteration masking primary geochemical trends. Furthermore, the possibility of variable assemblages of phenocryst phases crystallising at different pressure and temperature conditions further pronounce the problems in any simple petrogenetic models. It was noted in Chapter 3 that the petrological sequence observed in many of the sample indicated the presence of spinel on the liquidus during crystallisation, comprising part of the phenocryst assemblage. It was also noted in Chapters 3 and 6, respectively, that a high pressure fractionation event at pressures between 10-12 kb occurred prior to the intrusion of the dykes, and only limited fractionation at low pressures could occur due to thermal constraints.

The geochemical trends exhibited for the major oxides and elements in Figures 7.3 and 7.7 are predominantly compatible with the crystallisation of olivine + clinopyroxene + plagioclase, removing MgO, Al_2O_3, CaO, Ni, and Cr from the melt. However Fe_2O_3 and TiO_2 appear to quatitatively increase with differentiation, suggesting that olivine and plagioclase dominated the phenocryst assemblage. The lack of spinel as a phenocryst indicates a period of high pressure fractionation for the Gannakouriep magmas, prior to their emplacement at higher levels of the crust as residual magmas. As eluded to in Chapter 6, the emplacememt of these residual magmas probably occurred from zoned magma chambers, which had undergone differential degrees of differentiation (and replenishement?). The net result would be variable compositions of the residual magma now subjected to low pressure fractionation, and hence a different phenocryst assemblage. The inclusion of spinel as a phenocryst phase and increasing importance of clinopyroxene during limited late low pressure fractionation may account for the variable trends observed within the oxides and elements Fe_2O_3, TiO_2, V, Sc, and Co shown in Figure 7.15.

The best estimate ~~to~~ the degree of fractionation occurring within the Gannakouriep magmas can be estimated from the Zr content. Zr quantitatively increases from 200 ppm Zr to 400 ppm Zr for the bulk of the dykes. Considering a bulk distribution co-efficent for Zr approaching 0 for any of the potential phenocryst phases, this yield an F= 0.5. However niobium-normalised Zr/Y ratios defining different magma types (Figures 7.5 and 7.6) associated with the dyke complexes cannot be derived by fractionation from a common parent since all three elements are essentially incompatible with the phenocryst phases, thus it is likely that homogeneity of source material is involved. In dyke complex GDC-4 the linear range in niobium-normalised Zr and Y content of the complex could be produced by magma mixing of two end members comprising niobium-normalised Zr/Y ratios of 7.5 and 5.7, but the lack of co-variations by other major and trace elements preclude qualitative modelling of such a process. The observed differences in Zr/Nb ratios do not correlate with differences in REE inter-element ratios, suggesting they are not attributable to differering degrees of partial melting.

7.6 Discussion

The magma types defined by differing high field strength interelement ratios (Figure 7.5) all show similar incompatible element enrichment with respect to MORB and comprise similar gabbroic fractionation trends, suggesting that they have undergone parallel igneous processes. The observed variation in high field strength interelement ratios are not basement terrane dependant with respect to where the dykes crop out, since dykes intruding the Richtersveld igneous subprovince span the entire range of high field strength interelement ratios recorded across the dyke swarm. Furthermore dyke complexes which have been defined as discontinuous structural entities (eg. dyke complexes GDC-1 and 3) separated by several tens of kilometres of intervening basement comprise identical magma types. Variations in high field strength interelement ratios therefore may not be ascribed to differing lithospheric/crustal domains, nor can these heterogeneities be attributed to differing geographical location of the mantle source region underlying the Richtersveld igneous sub-province.

Any model pertaining to these problems must reconcile why during different periods of magma injection into the crust, dyke complexes of similar geographical location (eg. dyke complexes GDC-3 and 4) may have different high field strength interelement ratios, yet complexes spanning the swarm may also have identical

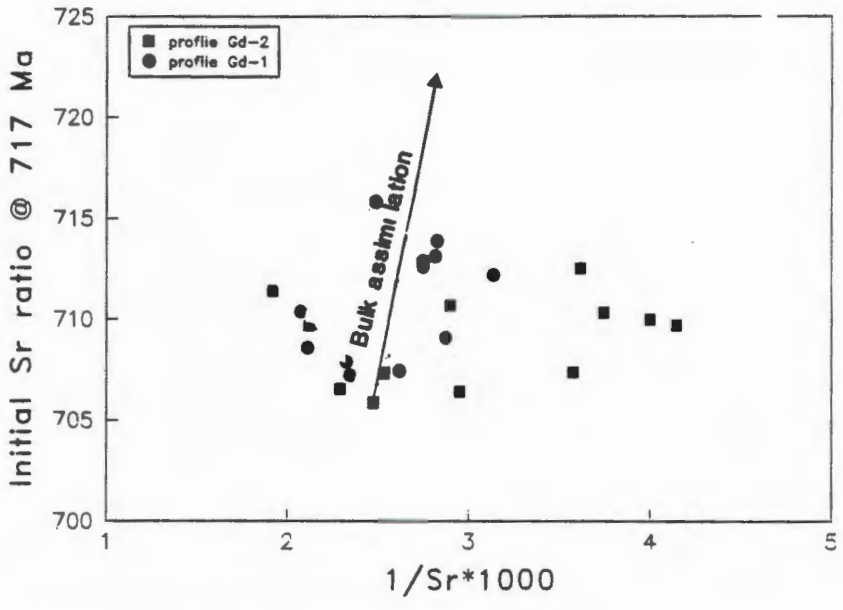

Figure 7.14. *1/Sr*1000 versus initial $^{87}Sr/^{86}Sr$ at 717 Ma for the Gannakouriep dykes. Also shown is the potential contaminant Vioolsdrif adamellite. Data taken from Reid, (1977).*

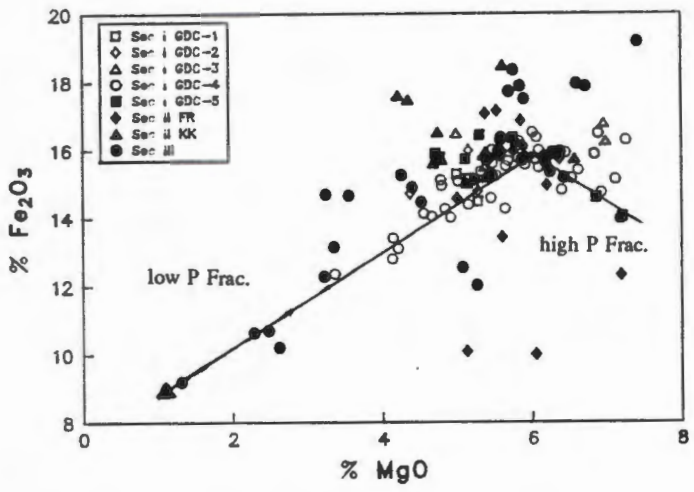

Figure 7.15. *MgO versus Fe_2O_3 for the Gannakouriep dyke swarm.*

magma characteristics. An explanation may be sought by envisaging the dynamic processes involved during the generation of the Gannakouriep magmas.

Assuming a chondrite-normalised REE pattern for the source region, since the Nd isotope data yield an E_{Nd}=0.17, constraints on the degree of batch partial melting of a hypothetical garnet peridotite can be calculated using the REE data. The source geochemistry, modal composition and likely partition co-efficients are taken from Cox et al.(1979), and are shown in Table 7.2. The Gannakouriep magmas can be produced by 4.3 - 6.2 % partial melting of this mantle composition. The amount of partial melting is small by comparison to that normally associated with the production of tholeiites (Ringwood, 1985). However is in good agreement with the amount of melt that would be extracted from a source region due to compaction (McKenzie, 1984). The observed variations in high field strength interelement ratios cannot be produced by differing degrees of partial melting, since the elements Zr, Y and Nb comprise similar bulk partition co-efficients, entering the liquid phase in a constant ratio during the degree of melting calculated.

Table 7.2 *Hypothetical Garnet Peridotite composition and solid/melt partition co-efficents used in batch melting calculations. Proportions of minerals entering the melt are the same as the mode.*

Mineral Phase	Mode	K_D Ce	K_D Yb
Olivine	60%	0.001	0.002
Orthopyroxene	25%	0.003	0.05
Clinopyroxene	10%	0.01	0.28
Garnet	5%	0.02	1.6

The lithospheric signature depicted by the MORB normalised spidergrams (Figure 7.12) may suggest some adiabatic decompressive melting and interaction with the overlying Richtersveld mantle lithosphere, which could account for the observed variations in high field strength interelement ratios. The mantle lithosphere should be depleted in light rare earth elements and LILs (Jordan, 1978) during the formation of the Richtersveld Igneous sub-province 2.0 Ga ago (Reid, 1977). Thus if enrichment of the Gannakouriep magmas in incompatible elements with respect to MORB is due to interaction with the lithosphere, the latter must have been enriched in these elements prior to the generation of the Gannakouriep magmas by some process such as mantle metasomatism including subduction related metasomatism (Erlank et al., 1987).

However correlative variation in LILs with different dyke complexes describing differing high field strength element magama types (Figure 7.10) are not apparent. This may inpart be due to the effects of secondary alteration. Furthermore, although the degree of lithospheric interaction remains unconstrained, an E_{Sr} of 4.17 derived from the internal mineral errorchron of sample DRD-151 suggests that it may have well been limited. Thus variations in the high field strength interelement ratios probably reflect slight but differing melting domains within an underlying mantle (asthenospheric) source.

Extensive gabbroic fractionation within the lithospheric/crustal domain is indicated however since to derive ferro-tholeiites plagioclase and olivine must be on the liquidus (Yoder and Tilley, 1962) suggesting fractionation at around 10-12 kb depth. The latter is also within the pressure realm where the thermal divide between alkali

basalts and tholeiites breaks down, permitting tholeiites to be derived from an alkali parent. Only after extensive fractionation can the dyke complexes be nucleated within the crustal regime, since no primitive (ie. high Mg#) members are recorded. The residence time of these dyke complex nucleation points (ie. low level crustal magma chambers) is regarded as limited, since crustal contamination is also regarded as negligible.

The differences recorded by the high field strength interelement ratios indicate that the sub-crustal magma reservoir at the base of the crust may have been initially homogeneous with respects to high field strength interelement ratios during various phases of magma injection into the crustal domain, but was periodically altered prior to subsequent dyke complex nucleation. Such a process could be envisaged as being similar to that proposed by O'Hara (1977) whereby the subcrustal magma chamber is periodically replenished by uprising partial melts, prior to continual fractionation (RTF) and subsequent initiation of new crustal dyke complexes. Indeed periodic replenishment of the sub-crustal magma reservoir may initiate instabilities along the magma reservoir situated at a mantle/crustal lithosphere interface causing dyke complex initiation within the crust. It is notable that the major dyke complexes (eg. GDC-4) exhibit the largest range in their high field strength interelement ratios (Figure 7.6), and comprise the most basic members of the Gannakouriep Suite.

7.7 Summary

The regional geochemistry of the Gannakouriep dyke swarm can be summarised as follows:

(i) All dykes of the Gannakouriep suite comprise ferro-tholeiites; no primitive (picritic) compositions are present.

(ii) The Gannakouriep magmas fall close to the basalt cotectic curve for deep crustal levels defined by Thompson, (1982), Thompson et al., (1983) when plotted on a conventional expanded basalt tetrahedron (Figure 7.3).

(iii) All dykes across the swarm exhibit similar LREE enriched chondrite normalised patterns.

(iv) All dykes have similar N-MORB normalised trace and major element patterns, which are enriched in Sr, K, Rb, Ba, Nb, P, Zr, Ti and Y in comparison with N-MORB. However different magma types can be discriminated on the basis on their high field strength interelement ratios.

(v) On the basis of Sr isotopic data, and MORB normalised trace element data, negligible crustal contamination has occurred to the Gannakouriep magmas; suggesting the observed enrichment of the elements in (iii) are attributable to mantle source characteristics.

(vi) The degree of partial melting predicted by the REEs (3-6%) of a mantle source which the Nd isotopic data suggests may be chondritic, would derrive a primary alkali-basalt magma.

(vii) An earlier phase of high pressure fractionation of essentially olivine and plagioclase at the base of the crust (10-12 kb) may have occurred (Yoder and Tilley, 1962), permitting the tholeiites to be derived from an alkali-basalt parent. Subsequently limited tholeiitic basalt fractionation of olivine + clinopyroxene + plagioclase + Fe-Ti oxides at low pressures occurred.

(viii) The degree of mantle lithospheric interaction remains unconstrained, although low E_{Sr} and E_{Nd} values (4.17 and 0.17 respectively) suggest that it may have been limited.

8 SYNTHESIS

8.1 Introduction

In this chapter various aspects of the Gannakouriep dyke swarm are synthesised in an attempt to unify structural, tectonic and geochemical parameters which have been previously described. Parts of the ensuing discussion remain poorly constrained at present. It by no means purports to provide a definitive answer to the mega-tectonics involved in late Proterozoic break-up of the region under discussion.

8.2 Discussion

8.2.1 Crustal kinematics

A study of the intrusion mechanics of the Gannakouriep dyke swarm has highlighted the intimate structural relationship between dykes comprising discrete complexes. The dominance of lateral propagation of these dykes over vertical propagation, from a low-level crustal magma chamber, is a complex problem to quantify within the context of a continuum mechanics model. Ultimately mathematical modelling of intrusion mechanics has to consider simultaneously factors such as the variability in tensile strength of the host rock, differential remote stresses through the crust undergoing extension, and variations in vertical compressive stresses ($\sigma 2$) due to decreasing lithostatic loading, countered by decreasing effective vertical magma pressure caused by isostatic loading of the magma column itself. More complex modelling would further incorporate thermal controls imposed on basaltic fissure eruptions (Bruce and Huppert, 1989).

The crustal kinematic response to the initiation of discrete low level magma chambers is qualified here by using two approaches;

(i) By calculating excess magma pressure due to density contrasts, and

(ii) Idealising stress distribution around a low-level magma chamber due to its intrusion geometry.

Quasi-equilibrium calculations of excess magma intrusive pressures beneath continental crust using the parameters;

Average density of continental crust = 2.68 Mgm^{-3} upto 6 km depth.

Average density of continental crust = 2.80 Mgm^{-3} for 6-30 km depth.

Average density of continental crust = 3.30 Mgm^{-3} below 30 km depth.

and

Partial magmatic melt density M1 = 3.0 Mgm^{-3}

Partial magmatic melt density M2 = 3.1 Mgm^{-3}

are shown in Figure 8.1 (Bhattacharji and Koide, 1987).

A partial melt with a density 3.0 Mgm^{-3} is in quasi-equilibrium with lithostatic pressure at a depth around 50 km (Point E in Figure 8.1) and may approach close to the surface along ascent line M1, where excess pressure is assumed to approach zero. However if the magma generated by partial melting yields a higher magma density, either due to the nature of partial melting or subsequent high pressure fractionation processes such that its density becomes 3.1 Mgm^{-3}, the intrusive pressure cannot exceed the lithostatic pressure above the M2 ascent line, reaching a maximum depth of 17 km from the surface of the crust. Conversely if a felsic magma fraction

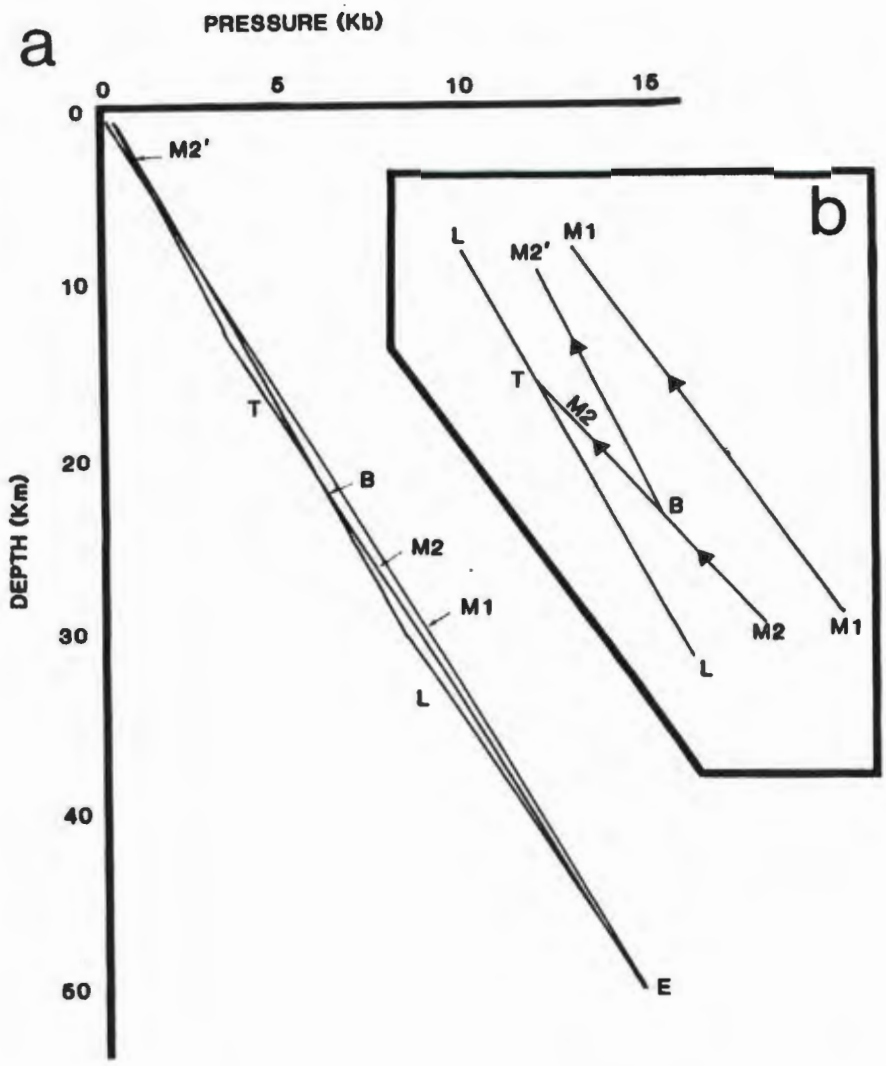

Figure 8.1. *Relationship between lithostatic pressure (L) and excess intrusive pressure (M1, M2 etc.) of a partial melt initiated at E under continental conditions (a). Inset (b), expanded section of the vectors between 5 and 10 kb. After Bhattachrji and Koide, (1987).*

(M2') separates from a high density magma (M2) during ascent of the diapir, its inherent lower density permits further upward ascent of that evolved magma from the ascent line M2 of a hypothetical point B (Figure 8.1). Thus magma density is a crucial factor in comprehending the limiting parameters to vertical propagation of dykes in the Gannakouriep dyke swarm. The lack of flood basalt associated with the intrusion of the Gannakouriep dyke swarm and predominance of lateral propagation of dykes is regarded as a direct result of the high density of the Gannakouriep magmas. In the latter, their density has been enhanced by high pressure gabbroic fractionation evolving them towards ferro-tholeiites at a crustal/lithosphere interface.

The problem as to whether lateral dyke propagation from a low level magma chamber is a low or high level crustal phenomena partially rests with the previous arguments, but may also be addressed by considering idealised geometries and the stresses they may exert on the surrounding country host rock. Stress distributions around oblate low-level magma chambers with aspect ratios of 1:10 and 1:100 calculated by Koide and Bhattacharji (1975a; 1975b) (using Poisson ratio = 0.25, delta p = -1kb) are shown in Figure 8.2 All stresses

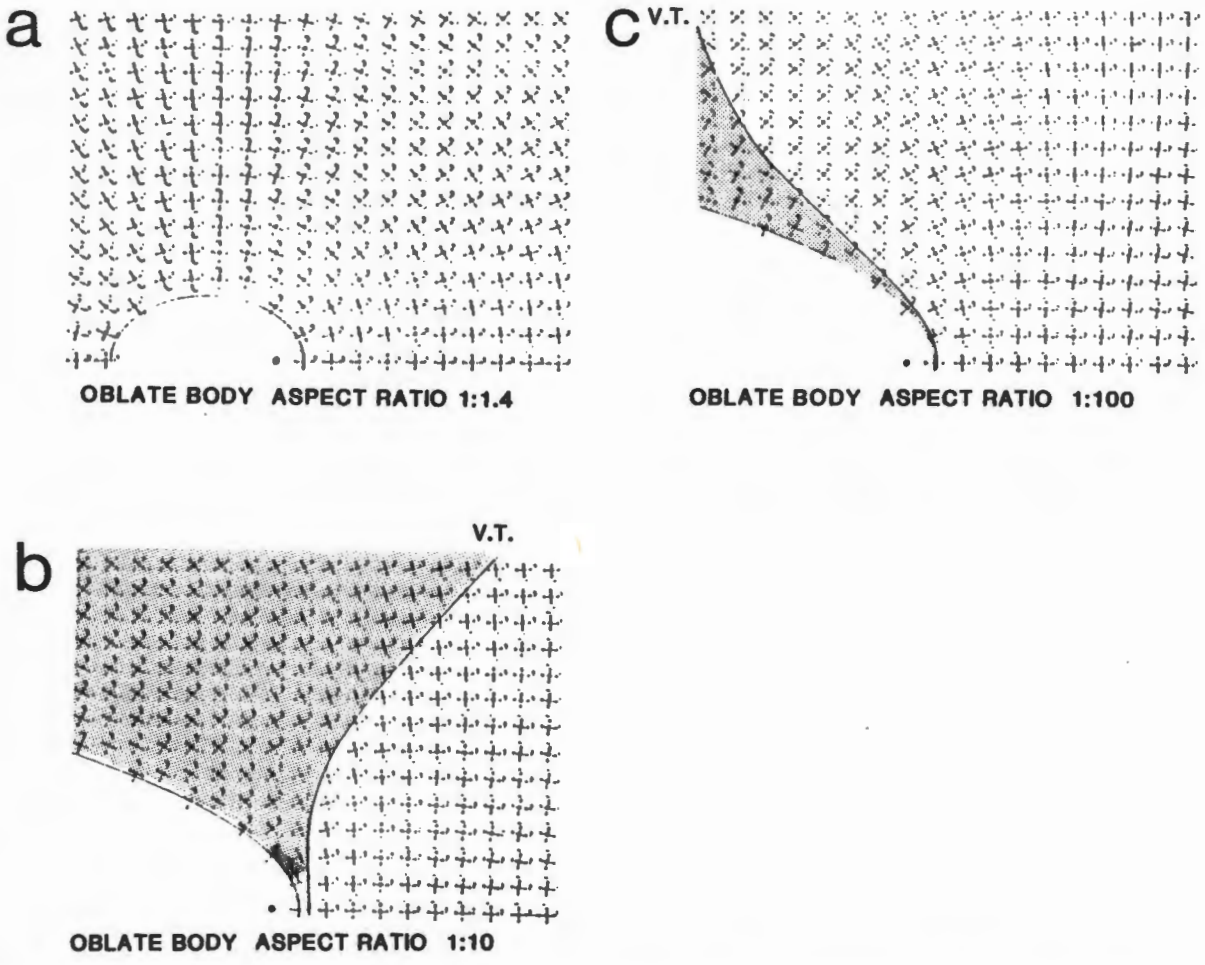

Figure 8.2. *Three dimensional stress distribution around oblate spheroidal (a) and elliptical (b) and (c) magma chambers of differing aspect ratios due to its wedging action. Maximum (1), intermediate (2), and minimum (3) (poles to page) stress directions indicated. Shaded areas inside the envelope V.T. are vertically tensile. After Bhattacharji and Koide, (1987).*

within the envelope defined by the lines VT are tensile in three dimensions. Analysis of these stress distributions clearly indicate that low level crustal magma chambers with high aspect ratios tend to produce three dimensional tensile envelopes in the shape of an inverted funnel. In this scenario, assuming all other factors are negligible, lateral propagation of dyke from a nucleation point would predominate in lower crustal regions, whilst vertical propagation would proceed in upper crustal levels. By contrast where low level magma chambers nucleated with relatively low aspect ratios (1:10), the three dimensional tensile stress fields are funnel shaped, suggesting lateral propagation would be enhanced in upper crustal levels away from a low level crustal nucleation point.

This second scenario would appear applicable to the Gannakouriep dyke swarm since lateral propagation of the dykes can be clearly demonstrated in upper crustal levels, and furthermore would explain the continuity of strike and geochemistry of dyke complexes over long distances (-100 km). Thus the nucleation zones (or low level crustal magma chambers) which served as feeders to the propagating dyke complexes may well have comprised low aspect ratios. In reality the problem is clearly far more complex in so much that variability of magma pressure, tensile host rock strength, and style of deformation in differing crustal levels all comprise major factors influencing the mode of dyke propagation.

The nature of interaction between these low-level crustal feeder magma chambers and dyke propagation is

partially elucidated by the study of intradyke geochemistry. In Chapter 6 the problems of obtaining the observed geochemical patterns across the dykes by readily understandable in situ processes has been highlighted, suggesting that the recorded geochemistry is a product of magmatic processes occurring within the magma chamber itself, rather than a product of dyke flow and crystallisation dynamics. The residence time of these magma chambers in the lower crust is regarded as small since limited assimilation and crustal contamination is implied by existing trace element and isotope data. However, it is sufficiently long for the magmas to undergo some limited fractionation and zonation as indicated by the geochemistry and the presence of cumulate plagioclase allochtholiths in high level dyke exposures. The span in Nb normalised Zr/Y ratios recorded in dyke complex GDC-4 may also suggest that the dynamics of major dyke complexes were partially controlled by periodic or finite continuous recharge from the underlying mantle fractionating reservoir.

8.2.2 Continental mantle/crust interface kinematics

The occurrence of structurally isolated dyke complexes separated by large geographical distances with identical geochemical characteristics has been used to infer the presence of a gabbroic fractionating magma reservoir along the crustal lithosphere/mantle lithosphere interface (from here on referred to as the CL/ML interface) beneath the Richtersveld igneous sub-province. The kinematic interaction between a rising diapir and the CL/ML interface is a complex problem to solve, partially due to the different Youngs' moduli of the material being intruded/displaced by the diapir. However such a process may be qualitively envisaged using a photoelastic model (Richards and Marks, 1966) treating the crustal lithosphere and underlying mantle lithosphere as separate entities along which a mechanical discontinuity may be manifest due to chemical, density and/or viscosity contrasts (i.e. quartz rather than olivine becomes the main stress bearing phase). The effect of a mechanical discontinuity (ignoring contrasting rheological properties between the crust and mantle lithospheric components) is to lower the tensile strength and shear strength along that discontinuity surface. Compressive normal strength will be transmitted across a closed discontinuity, but it cannot support the same tensile strength as the surrounding material. The amount of shear strength supported by the discontinuity is proportional to the amount of friction resistance occurring along it.

The possible effect of a CL/ML discontinuity is shown in Figure 8.3 from experimental data derived by Pollard (1973b) using grease intruded into gelatine with a lubricated discontinuity. Note that if the grease (or intruding magmatic diapir) is intruded perpendicularly to the discontinuity, the former spreads symmetrically on either side of the intruding stock. By contrast, intrusion oblique to the discontinuity (Figure 8.3) results in asymmetric lateral propagation. The degree of lateral spreading beneath the CL/ML interface of the Richtersveld Igneous sub-province by an ascending diapir remains speculative, since many of the parameters governing rheological behaviour at the base of the crust are not known. Intuitively, some lateral spreading may occur since the overlying crust has a greater Young's modulus than the mantle lithosphere, permitting greater elastic dilation of the intruding body within the mantle lithospheric domain. Ultimately the geometry of that intruding body may be partially controlled by the angle of a mechanical discontinuity at the CL/ML interface; however, the major influencing factor defining the geometry of a mantle diapir would be the partitioning of remote stresses acting on the crust and mantle lithosphere during extension. The latter is a geodynamics problem which is discussed in the subsequent section.

The kinematics of nucleation of discrete magma chambers at the base of the crust from the mantle diapir at the CL/ML interface may be addressed invoking a mechanism similar to the Heleshaw effect. Idealising a lithospheric plate and derivation of magma by partial melting in terms of contrasting high viscosity Newtonian fluids, the criteria to initiate instabilities along the interface between a rising magma diapir and crust defined by the equation

$$\frac{(U2 - U1)}{Kz2\ \ Kz1} W + (P2-P1)\, g < 0 \qquad (1)$$

(Elder, 1975)

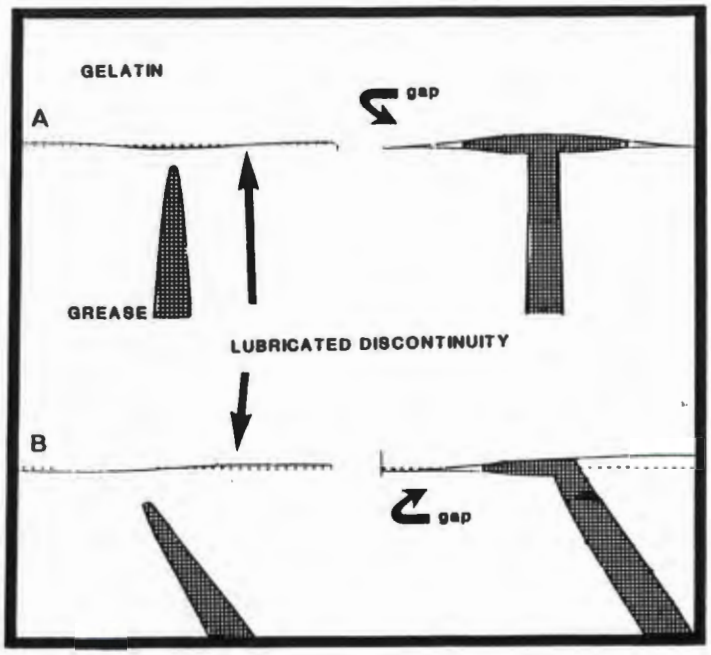

Figure 8.3. *Grease gun experiment of Pollard, (1973). In A the grease is injected in a gelatin medium perpendicularly to a lubricated discontinuity, resulting in symmetrical sill formation along the discontinuity. Whilst in B injection of grease oblique to the discontinuity results in asymmetrical sill formation.*

Where U,P,Kz refer to viscosity, density and permeability of the rock matricies (1 and 2), which will be optimised when both viscosities and density contrast between the parental melt and lithospheric plate is at a maximum.

Using the same criteria derived for the reduction in effective magma driving pressure due to density contrasts between a lithospheric plate and an ascending magmatic body (section 8.2.1), the density and viscosity contrast between a partial melt derived at 50-60 km depth may be relatively similar to that of its source region in comparison to higher mantle lithospheric levels. Thus at the generation and initial rise of a magmatic diapir the tendency for Heleshaw instabilities to generate at the interface between the diapir and overlying lithosphere may be limited. However continued ascent of the magmatic diapir would bring it into direct contact with mantle and crustal lithosphere of progressively decreasing density and increasing viscosity , promoting the nucleation of Heleshaw instabilities (equation 1). In the case of the Gannakouriep magmas density and viscosity contrasts between the latter and the lithospheric plate, may well have been enhanced at the CL/ML interface (at 10-12 kb) by the high pressure fractionation of olivine and plagioclase, evolving the magmas towards ferro-tholeiites and, as a consequence, magmas of a high density than the original parental melt. The degree to which mid and upper crustal domains can be regarded as constituting an idealised Newtonian fluid is debateable, thus the extent to which such a process is operative at higher crustal levels is subjective, however within the mantle lithosphere/lower crustal domains such a process in plausible.

The differences in Nb normalised Zr/Y ratios of various dyke complexes (ie. low level crustal magma chambers) has been broached in the previous chapter. However, to reiterate, differences between the high field strength interelement ratios cannot be explained solely by geographically distributed chemical inhomogeneities in the immediately underlying source area, since some dyke complexes (which are structurally unrelated in their crustal domain) have similar high field strength interelement ratios across the dyke swarm. Rather, these slight chemical inhomogeneities may be ascribed to the dynamics of the mantle diapir at the CL/ML interface. Periodic or partially continuous replenishment to the mantle diapir during on going gabbroic fractionation, dyke complex

nucleation and recharge of existing magma chambers in the base of the crust may account for subtle variations observed in the high field strength interelement ratios. That replenishment is caused by adiabatic partial melting of the surrounding lithosphere is a possibility; however, the lack of corrobative incompatible element variation associated with changes in high field strength element ratios may tend to negate such a hypothesis. Alternatively, replenishment and changes in high field strength interelement ratios could conceivably be caused by the late arrival of the base of the ascending diapir at the CL/ML interface during ponding of the melt beneath an extended lithospheric plate.

8.2.3 Geodynamics

Consideration of any geodynamic models proposed to account for rifting and intrusion of the Gannakouriep dyke swarm in the Gariep Arc must be able to satisfy the following criteria;

(i) Rifting in the Gariep Arc was generated by asymmetric extension, resulting in the formation of a half graben (Kroner, 1972).

(ii) A pseudo-palinspastic reconstruction of the Gariep Arc and Gannakouriep dyke swarm prior to late Proterozoic - early Cambrian deformation (Figure 2.18) suggests that the latter comprises an off-rift dyke swarm, emplaced close to a site of differential uplift (Kroner, op. cit.).

(iii) Dyke intensity of the Gannakouriep dyke swarm is asymmetrically distributed across strike, increasing westwards toward the Gariep rift basin.

(iv) No continental flood basalts associated with rifting are observed in the Gariep Arc.

(v) The continuity of basement north of the Gariep Arc suggest the presence of step overs (Aydin and Nur, 1985) during the initiation and development of the rifting phase.

White and McKenzie (1989) have suggested that the generation of continental flood basalts accompanying rifting of Gondwana during the Mesozoic originates from decompressive melting of the asthenosphere and overlying mantle lithosphere as the Earth's lithosphere is extended above a plume source. Geochemical and physical considerations (Erlank et al., 1987) have been used to infer a fertile mantle source region for at least some of these flood basalts. In high Raleigh number systems such as the mantle (McKenzie et al., 1983) these plumes advect in narrow columns (100 km wide), which upon reaching the lithospheric carapace develop wide mushroom tops several hundred degrees above normal mantle temperatures. The latter has the effect of heating the lithosphere above solidus temperatures permitting lateral flow over a domical region several thousand kilometres in diameter. In their model, rifting and extension is caused ostensibly by lithospheric/crustal doming above such a plume, where uplift in the order of 2 km has been postulated (White and McKenzie, 1989). Active rifting as this model has been termed is accompanied by the extrusion of significant continental flood basalts during deflation, and development of rift/drift unconformities with the rift margin sediments. Conversely passive rifting (McKenzie, 1978) involving crustal and mantle lithosphere extension is unaccompanied by a break-up unconformity and significant voluminous outpourings of continental flood basalts.

The first model essentially invokes a mantle weakness resulting from a plume source, and the second, a crustal weakness caused by lithotypes or pre-existing crustal flaws. Both models ostensibly result in symmetric rifting. Clearly neither case is directly applicable to the formation of the Gariep Arc or emplacement of the Gannakouriep dyke swarm.

Two other criteria are important to consider in formulating a geodynamic model for rifting in the Gariep Arc;

(i) Jackson and Zelt (1984) have delineated a zone of late Namaquan extensional tectonics (Dn4) along the western coastal zone of the Namaqua Metamorphic Province. The latter represents the first phase of deformation

to cut the regionally dominant E-W trending basement fabric, and parallels the strike of proposed late Proterozoic Gariepian extensional tectonics (Kroner, 1972);

(ii) The Richtersveld igneous sub-province comprises an island arc suite of batholithic proportions with supra-crustal volcanics (Reid, 1977) which has been accreted and thrust onto the Bushmanland sub-province along the Groothoek thrust during Namaquan orogenesis (1200-1000 Ma) (Hartnady et al., 1985). In accordance with the principle of isostasy (Bott, 1982) crustal thickening caused by thrusting of the Richtersveld igneous sub-province would be accompanied by a concomitant rise of the low velocity zone. The latter has the effect of creating a mantle weakness in the lithospheric plate since the integrated strength of olivine as the main stress bearing phase in the lithosphere is reduced. Evidence of a pre-existing mantle weakness under the Richtersveld igneous sub-province prior to the development of the Gariep Arc may also be manifest by the emplacement of the alkaline to peralkaline Richtersveld Intrusive Complex (920 Ma; Allsopp et al., 1979).

The dynamics of extensional tectonics and emplacement of the Gannakouriep dyke swarm are modelled here using the data set of Dunbar and Sawyer (1989). The latter authors idealise deformation of a composite strength lithospheric plate as a plastic continuum mechanics problem, to which mantle and/or crustal weaknesses have been included. The results of their calculations are summarised in Figure 8.4. From the foregoing discussion neither extension under crustal weakness or mantle weakness satisfy the observed criteria for extension in the Gariep Arc, since in both cases extension is symmetrical. Further complications arise with extension under mantle weakness conditions, since basalt production rates are predicted to be high, producing continental flood basalts during the initiation of rifting. A more suitable model may be included by invoking a case for both mantle and crustal weaknesses controlling the mode of extension in the Gariep Arc (Figure 8.4 (3)). In this case crustal weaknesses in the lithospheric plate model may be focused along late Namaquan Dn4 extensional faults, whilst a mantle lithospheric weakness beneath the Richtersveld igneous sub-province may have been inherent in the sub-crustal lithospheric architecture due to isostatic readjustments following Namaquan orogensis. The net result is extension under simple shear, or a combination of simple and pure shear.

The advantages of a model requiring both crustal and mantle weaknesses in the lithospheric plate for rifting and intrusion of the Gannakouriep dyke swarm are several fold;

(i) Initiation of the Gannakouriep dyke swarm from the ascending mantle diapir (Figure 8.4 (3)) is offset with regards to the main rift axis, where failure and continental separation occurs within the crustal weakness zone, offering an explanation why rifting and emplacement of the Gannakouriep Dyke swarm are non-coincidental.

(ii) The ascending mantle diapir has an asymmetric geometry, with the greatest ascent rate and overlying crustal attenuation occurring towards the rift axis. The latter could account for the observed increase in dyke intrusion intensity towards the axis of rifting in the Gariep Arc.

(iii) Interaction between the crustal and mantle weaknesses (Figure 8.4(3)) at 75 km extension has the effect of developing a sinistral vertical shear component between them. The latter effectively permits the development of a low angle detachment shear between them during further extension, producing a half graben similar to that observed in the Red Sea Rift (Coleman and McGuire, 1988) (Figure 8.5).

A further advantage of this geodynamic model is that it satisfies the following;

The ascent rate of the mantle diapir depicted in Figure 8.4 (3) would decrease as extension is transferred to the site of crustal weakness where continental separation occurs, permitting high degrees of fractionation of a partial melt prior to intrusion into the overlying crust. The latter may account for the fact that no primitive members of the Gannakouriep suite are present in upper-crustal exposures. Some of the trace element geochemistry of the Gannakouriep dyke swarm may be inherited by decompressive melting of the surrounding mantle lithosphere during retention of the diapir within the latter. However the degree of trace element enrichment with respect to MORB by partial melting of the mantle lithosphere or other such processes such as zone refining remains

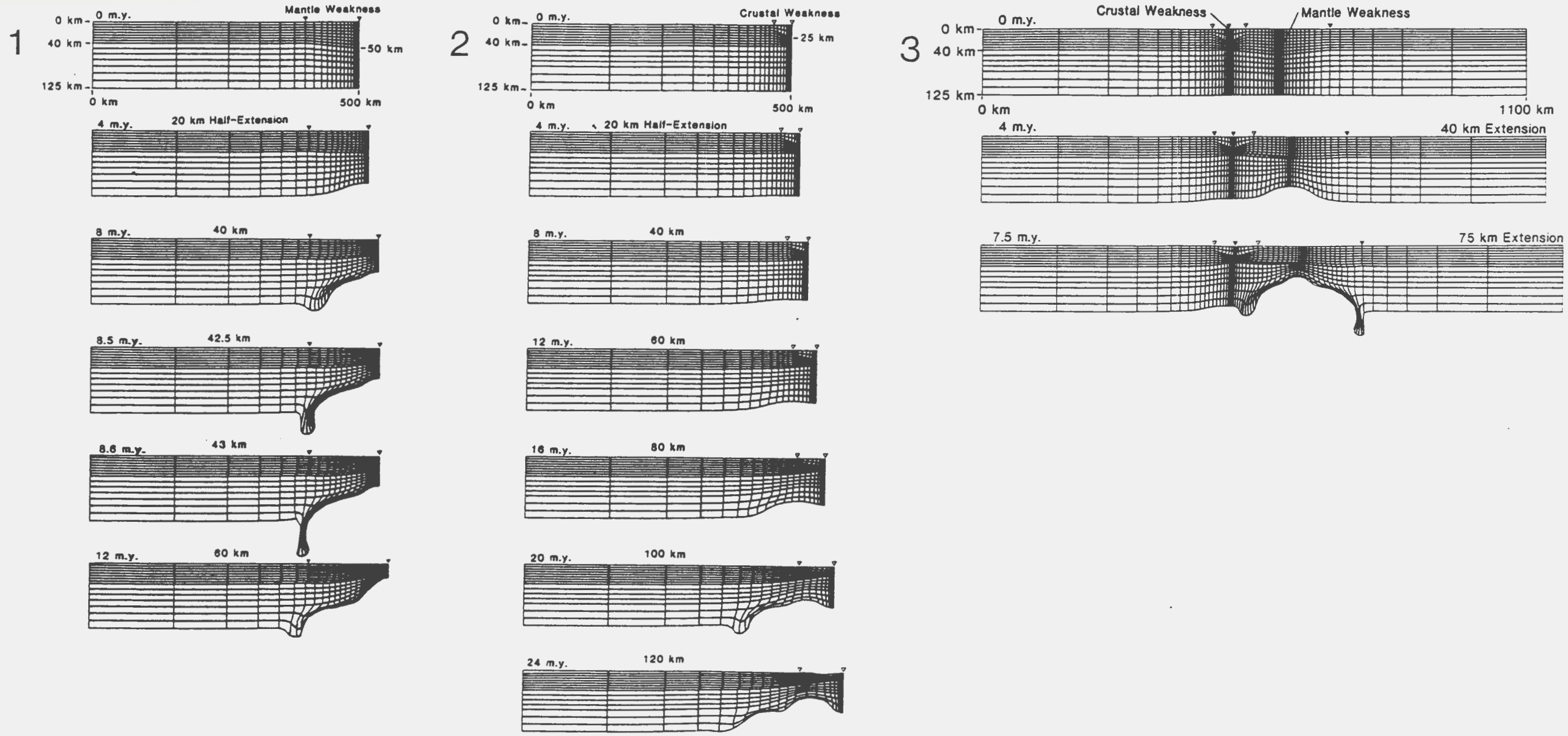

Figure 8.4. ***Case 1****: Deformation history of a half model of a lithospheric section containing an isolated weakness in the mantle strong zone. The initially 125 Km thick lithospheric section is composed of a crust with the rheology of quartz diorite overlying a mantle with the rheology of olivine. The continental lithosphere is viewed as a composite material composed of two strong layers, one in the upper mantle, and one in the middle crust. A local weakness in the mantle strong zone, located between the solid triangle symbols, is associated with an increase in crustal thickness from its nominal value of 40-50 Km, over a distance of 100 Km. Continuum modelling is for constant half extension rate of 0.5 cm/yr with left hand side fixed.*

Case 2*: Half model containing an isolated weakness in the crustal strong zone. The crustal weakness located between open triangle symbols is associated with a granitic body having a maximum thickness of 25 Km embedded within a quartz diorite crust.*

Case 3*: Full model containing horizontally offset crustal and mantle weaknesses in the crustal and mantle strong zones. The crustal weakness located between open triangle symbols is associated with a granitic body having a maximum thickness of 25 Km embedded with a quartz diorite crust. The mantle weakness located between the two solid triangle symbols is associated with a local increase in crustal thickness from 40 to 50 km. The centre of the two weaknesses are separated by a distance of 100 Km. Both weaknesses represent 30% reductions in the total strength of the lithosphere. After Dunbar and Sawyer, (1989).*

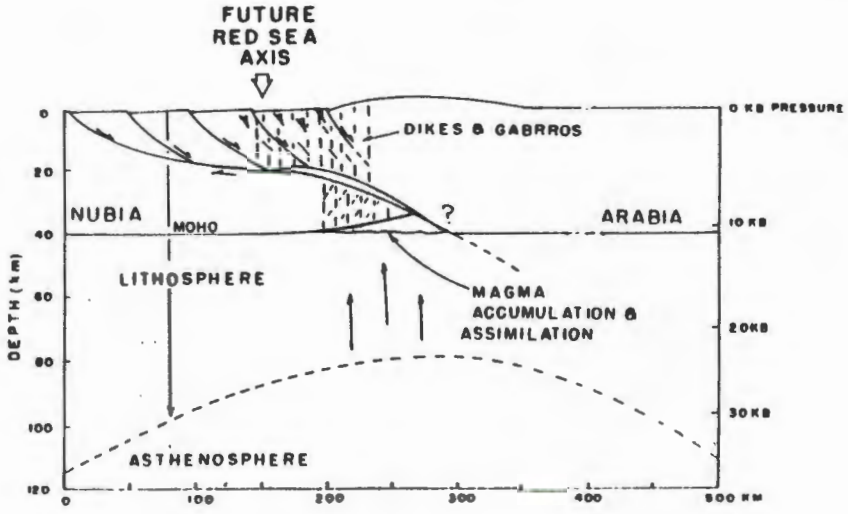

Figure 8.5. *Diagrammatic cross section for the Red Sea for the period 20-30 Ma from Coleman and McGuire, 1988. Note the asymmetrical graben formation and associated mantle diapirism non co-incidental with crustal rifting.*

unconstrained, except that such processes occurred within one lithospheric domain.

8.3 Conclusion

The Gannakouriep dyke swarm can be modelled by adiabatic upwelling of the asthenosphere associated with composite rifting involving both crustal and mantle weaknesses in a lithospheric plate model. Decompressive melting and/or zone refinement within the overlying lithosphere is regarded as limited due to low E_{Sr} and E_{Nd} values obtained from the Gannakouriep dyke swarm. However, if interaction with the mantle lithosphere occurred, the similarity in MORB normalised elemental patterns across the swarm suggest it was concentrated within a relatively homogeneous lithospheric domain, possibly of the Richtersveld igneous sub-province. Lateral spreading of the ascending diapir beneath the CL/ML interface may have been partially caused by a structural/rheological discontinuity between these two domains. The asymmetric distribution of the Gannakouriep dyke swarm is thought to be fundamentally controlled by the interaction of both mantle and crustal weaknesses under extension, producing asymmetric adiabatic upwelling of the asthenosphere and differential tension in the overlying crust. Extensive fractionation of essentially olivine and plagioclase accompanied by periodic replenishment preceeded intrusion of the evolving ferro-tholeiite Gannakouriep magmas into the lower crustal domain as a series of discrete low aspect ratio magma chambers. The latter may have resulted from Heleshaw instabilities generated between the contrasting visco-fluid properties of the mantle diapir and the lower crust.

Propagation of dykes from these discrete magma chambers during continued extension subsequently gave rise to dyke complexes related to these magma chambers at depth. The decreased pressure and thermal regimes associated with these crustal magma chambers permitted low-pressure fractionation and the progressive importance of ilmenite and Ti-magnetite during fractionation. Residence of the Gannakouriep magmas within these low-level crustal magma chambers was short lived, as inferred from the apparent lack of crustal contamination, but sufficient enough to form partially zoned magma chambers which were subsequently tapped during dyke propagation and dilation. The mode and mechanics of dyke propagation were probably fundamentally controlled by the relatively high density of the Gannakouriep magmas, such that they underwent extensive lateral propagation at higher crustal levels, but never formed continental flood basalts.

The age of intrusion of the Gannakouriep dyke swarm obtained during this study of 717 +/- 11 Ma by an internal

Rb-Sr mineral errorchron (chapter 5) is the best constraint to date for rifting along the proposed southern seaborne arm of the Damaran orogen and the formation of the alleged Admaster Ocean. Although continental rifting is clearly a diachronous event, the 717 Ma date correlates well with the age of proposed rifting in the Damaran belt (650-750 Ma; Miller, 1983).

REFERENCES

Allegre, C.J., Treuill, M., Minster, J.F., and Albarede, F., 1977. Systematic use of trace elements in igneous processes. Part 1: Fractional crystallisation in volcanic suites. *Contr. Mineral. Petrol., 60, 57-76.*

Allsopp, H.L., Kostlin, E.O., Welke, H.J., Burger, A.J., Kroner, A., and Blignault, H.J., 1979. Rb-Sr and U-Pb geochronology of late Precambrian - early Palaeozoic igneous activity in the Richtersveld (South Africa) and southern South West Africa. *Trans. Geol. Soc. S. Afr. 82, 185-204.*

Anderson, E.M., 1938. The dynamics of sheet intrusions. *Proc. R. Soc. Edinb., B, 58 (Part 3), 242-251.*

Armstrong, R.A., Bristow, J.W., Cox, K.G., 1984. The Rooi Rand dyke swarm, southern Lebombo. *Spec. Publ. Geol. Soc. S. Afr. 13, 77-86.*

Aydin, A.,and Nur, A., 1985. The types and role of stepovers in strike slip tectonics. *J. Soc. Econ. Palaeo. and Mineralogist Spec. Publ. 13, 35-44.*

Bence, A.E., and Albee, A.L., 1968. Empirical correction factors for the electron microanalysis of silicates and oxides. *J. Geol., 76, 382-403.*

Bhattacharji, S., Koide, H., 1987. Theoretical and experimental studies of mantle upwelling, penetrative magmatism, and development of rifts in continental and oceanic crust. *Tectonophysics, 143, 13-30.*

Blignault, H.J., 1977. Structural-metamorphic imprint on part of the Namaqua Mobile belt in S.W.A.. *Bull. Precambrian Res. Unit Univ. Cape Town, 23, 197pp.*

Booth, P., 1988. Calculation of displacements on some Pan African shears: the Riethoek Shear. *S. Afr. J. Geol., 91, 417-419.*

Bott, M.H.P., 1982. Origin of lithospheric tension causing basin formation. *Trans. R. Soc. London, Sec A., 305, 319-324.*

Breitkopf, J.H., 1989. Geochemical evidence for magma souce heterogenetity and activity of a mantle plume during advanced rifting in the southern Damara Orogen, Namibia. *Lithos, 23, 115-122.*

Broek, D., 1978. Elementary Engineering Fracture Mechanics. *Sigthoff and Noordhoff, Alphen aan den Rijn, the Netherlands, 437pp.*

Bruce, P.M., Huppert, H.E., 1989. Thermal controls of basaltic fissure erruptions. *Nature, 342, 665-667.*

Bussell, M.A., 1989. A simple method for the determination of the dilation direction of intrusive sheets. *J. Struct. Geol., 11, 679-687.*

Coleman, R.G., McGuire, A.V., 1988. Magma systems related to the Red Sea opening. *Tectonophysics, 150, 77-100.*

Cox, K.G., 1980. A model for flood basalt volcanism. *J. Petrology, 21, 629-650.*

Cox, K.G., Bell, J.D., and Pankhurst, R.J., 1979. The Interpretation of Igneous Rocks. *George Allen and Unwin Publishers Ltd., London, 450pp.*

Cox, K.G., Hawkesworth, C.J., 1985. Geochemical stratigraphy of the Deccan Traps at Mahabalesher, Western Ghats, India, with implications for open system magmatic processes. *J. Petrology, 26, 355-377.*

Currie, K.L., Ferguson, J., 1980. The mechanism of intrusion of lamprophyre dykes indicated by "offsetting" of dikes. *Tectonophysics, 9, 525-535.*

Davis, B.I.C., Boyd, M.E. jr, 1980. The join $Mg_2Si_2O_6$ - $CaMgSi_2O_6$ and its application to pyroxene from kimberlites. *J. Geophys. Res., 71, 3507-3576.*

Deer, F.R.S , Howie R.A., and Zussman J., 1966. An Introduction to the Rock Forming Minerals. 528pp Longman, London.

Delaney, P.T., Pollard, D.D., Ziony, J.I., and McKee, E.H., 1986. Field relations between dykes and joints: emplacement processes and palaeostress analysis. *J. Geophys. Res., 91, 4920-4938.*

De Villiers, J., and Söhnge, P.G., 1959. The Geology of the Richtersveld. *Mem. Geol. Surv. Un. S. Afr., 48, 295pp.*

Dunbar, J.A., Sawyer, D.S., 1989. How pre-existing weaknesses control the style of continental breakup. *J. Geophys. Res., 94, B6, 7278-7292.*

Duncan, A.R., Erlank, A.J., and Betton, P.J., 1984. Appendix 1 - Analytical Techniques and Database Description. *Spec. Publ. Geol. S. Afr. 13, 389-395.*

Elder, J., 1975. The Bowels of the Earth. *Ox. Uni. Press. 438pp.*

Elliot, R.B., 1973. The chemistry of gabbro/amhibolite transitions in south Norway. *Contrib. Mineral. Petrol., 47, 63-76.*

Erlank, A.J., Waters, F.J., Hawkesworth, C.J., Haggerty, S.E., Allsop, H.L., Richard, R.S., Menzies, M.A., 1987. Evidence for mantle metasomatism in peridotite nodules from the Kimberley pipes, South Africa. *221-311 In: C.J. Hawkesworth and M.A. Menzies (Eds.), Mantle Metasomatism, Academic Press, 472pp.*

Erlank, A.J., Marsh, J.S., Duncan, A.R., Miller, R.McG., Hawkesworth, C.J., Betton, P.J., and Rex, D.C., 1984. Geochemistry and Petrogenesis of the Etendeka volcanic rocks from S.W.A/Namibia. *Spec. Publ. Geol. Soc. S. Afr., 13, 195-245.*

Evans, M.E., 1987. Palaeomagnetism in dykes: can we beleive it? *In: Halls, H.C., and Farhig, W.F., (Eds.), Mafic dyke swarms. Geol. Ass. Can. Spec. Paper, 34, 195-199.*

Field, D., and Elliot, R.B., 1974. 'Residence' contamination of K, Rb, Li, and Ti in dibase dykes. *Can. J. Earth Sci., 11, 422-429.*

Gast, P.W., 1960. Limitations on the composition of the upper mantle. *J. Geophys. Res., 65, 1287-1296.*

Germs, G.J.B., 1972. The stratigraphy and palaeontology of the lower Nama Group, South West Africa. Bull. *Precambrian Res. Unit, Univ. Cape Town, 12, 250pp.*

Germs, G.J.B., 1983. Implication of sedimentary facies and depositional enviroment analysis of the Nama Group in S.W.A./Namibia. *Spec. Publ. Geol. Soc. S. Afr., 11, 409-429.*

Germs, G.J.B., Knoll, A.H., and Vida, G., 1986. Late Proterozoic microfossils of the Nama Group, Namibia (S.W.A.). *Precambrian. Res., 32, 45-62.*

Gibson, I.L., and Jagam, P., 1980. Instrumental neutron activation analysis of rocks and minerals. *In: Mueke, G.K., (Ed.), Short course in Neutron Activation Analysis in the Geosciences. Mineral. Assoc. Can., Ottawa, Ont., 109-131.*

Gibson, I.L., Sinah, M.N., and Fahrig, W.F., 1987. The Geochemistry of the Mackenzie dyke swarm, Canada. *In: Mafic Dyke Swarms, Editors Halls H.C. and Fahrig, W.F.. Geol. Ass. Canada Spec. Paper 34, 109-121.*

Griffith, A.A., 1924. Theory of rupture. *Proc. Int. Congr. Appl. Mech. 1st, Deflt, 1924, 53-63.*

Haggerty, S.E., 1976. Oxidation of opaque mineral oxides in basalts. *In: Rumble, D. III, Ed., Oxide Minerals. Mineral. Soc. Amer.. Reviews in Mineralogy 3, Hg1-Hg98.*

Hageskov, B., 1987. Tholeiitic dykes and their chemical alteration during amphibolite facies metamorphism. The Kattsung - Koster dyke swarm S.E. Norway - W. Sweden. *Sveriges Geologiska Undersokning, Ser. C, No. 817, Uppsala, 61pp.*

Harland, W.B., 1983. Proterozoic glacial record. *In: Medaris, L.G., Byers, M.W., Michelson, D.M., and Shanks, W.C., (Eds.), Proterozoic Geology. Bull. Geol. Soc. Am. Mem., 161, 279-288.*

Harper, C.T., 1970. Graphical solution to the problem of radiogenic ^{40}Ar loss from metamorphic minerals. *Eclogae Geol. Helv., 63, 119-140.*

Harrison, T.M., and McDougall, I., 1981. Excess ^{40}Ar in metamorphic rocks from Broken Hill, New South Wales: Implications for $^{40}Ar/^{39}Ar$ age spectra and the thermal history of the region. *Earth and Plan. Sci. Letts., 55, 123-149.*

Hart, S.R,, and Brookes, C., 1977. The geochemistry and evolution of early Precambrian Mantle. *Contrib. Mineral. Pet., 61, 109-128.*

Hartnady, C.J., Joubert, P., and Stowe, C.W., 1985. Proterozoic crustal evolution in southwestern Africa. *Episodes, 8, 236-244.*

Horstman, U.E., 1987. Die metamorphische entwicklung in Damara Orogen, Sudwest Afrika/Namibia, a begeleitet ans K/Ar Datierungen an detritisschen Hellglimmeren ans Molassesedimenten der Nama Group. *Gottinger Arb. Geol. Palaeont., 3, 78-86.*

Huppert, H.E. and Sparks, R.S.J., 1985. Cooling and contamination of mafic and ultramafic magmas during ascent through continental crust. *Earth and Planet. Sci. Letts., 74, 371-386.*

Irwin, G.R., 1957. Analysis of stresses and strains near the edge of a crack traversing a plate. *J. Appl. Mechn., 24, 361-364.*

Jackson, M.P.A., and Zelt, G.A.D., 1984. Proterozoic crustal reworking and superposed deformation of metabasite dykes, layered intrusions and lavas in Namaqualand, South Africa. *In: Kroner, A., and Greiling, R., (Eds.), Precambrian Tectonics Illustrated. E Schweizersartsche Verlassbuchhandlung, Stuttgart, Germany.*

Jaeger, J.C., and Cook, N.E.W., 1969. Fundamentals of Rock Mechanics. *Methuen, London, 513pp.*

Jordan, T.H., 1978. Composition and development of continental lithosphere. *Nature, 274, 544-548.*

Joubert, P., 1971. The regional tectonism of the gneisses of part of Namaqualand. *Bull. Precambrian Res. Unit, Univ. Cape Town, 10, 220pp.*

Kalsbeck, F., Bridgewater, D., and Zeck, M.P., 1978. A 1950 +/- 60 Ma Rb-Sr whole rock isochron age from two Kangamiut dykes and the timing of the Nagssugtoquidian (Hudsonian) orogeny in West Greenland. *Can. J. Earth Sci., 5, 1122-1128.*

Kennedy, Q.A., 1964. The differentiation of Africa in the Pan-African (+/-500 Ma) tectonic episode. *Res. Inst. Afr. Geol., 8th Ann. Rep., Univ. Leeds, 48-49.*

Knoper, M.W., 1988. Geochemistry of Early Proterozoic supracrustal rocks, west-central Colarado: evidence for their petrogenesis and tectonic setting. *PhD dissertation, New Mexico Institute of Minning and Technology.*

Koide, H., and Bhattacharji, S., 1975a. Mechanistic interpretation of rift valley formation. *Science, 189, 791-793.*

Koide, H., and Bhattacharji, S., 1975b. Formation of fractures around magmatic intrusions and their role in ore localisation. *Econ. Geol., 70, 781-799.*

Kretz, R., Hartree, R., Ganet, D., and Cermignani, C., 1985. Petrology of the Grenville swarm of gabbroic dykes, Canadian Precambrian shield. *Can. J. Earth Sci., 22, 53-71.*

Kroner, A., 1977. Preliminary resume of the geology of the Gariep geosyncline in the Orange River area. *In: De Villiers, J., (Ed.), A. Rep. Precambrian Res. Unit, Univ. Cape Town, 7-9, 51-57.*

Kushiro, I., 1980. Viscosity, density and structure of silicate melt at high pressures, and their petrological applications. *In: Hagreaves, R.B., (Ed.), Physics of magmatic processes. Princeton Univ. Press, Princeton, N.J., 93-120.*

Lanphere, M.A., and Dalrymple, E.B., 1977. Identification of excess $^{40}Ar/^{39}Ar$ age spectra technique. *Earth and Plan. Sci. Letts., 32, 141-148.*

Lawn, B.R., and Wilshaw, T.R., 1975. Fracture of Brittle Solids. *Camb. Univ. Press, 204pp.*

Le Roex, A.P., and Reid, D.L., 1978. Geochemistry of Karoo dolerite sills in the Calvinia district, Western Cape Province, South Africa. *Contrib. Mineral. Petrol., 351-360.*

Le Roex, A.P., and Watkins, R.T., 1990. Analysis of REE in geological samples by gradient ionchromatography: an alternative to ICP and INAA. *Chem. Geol., 86, In press.*

Lindsley, D.M., 1983. Pyroxene thermometry. *Am. Mineral., 68, 477-493.*

Marsh, J.S., and Eales H.V., 1984. The geochemistry and petrogenesis of igneous rocks of the central Karroo area. *Spec. Publ. Geol. Soc. A. Afr., 13, 27-68.*

Marsh, J.S., Bowen, M.P., Bowen, T.P., and Rogers, N.W., 1989. Volcanic rocks of the Witswatersrand triad, South Africa. II: Petrogenesis of Mafic and Felsic rocks of the Dominion Group. *Precambrian Res., 44, 39-66.*

MacDonald, G.A., and Katsura, T., 1964. Chemical composition of Hawaiian lavas. J. Petrol. 5, 82-133.

McKenzie, D.P., 1978. Some remarks on the development of some sedimentary basins. *Earth and Plan. Sci. Letts., 40, 25-32.*

McKenzie, D.P., 1984. The generation and compaction of partially molten rock. *J. Petrol., 25, 713-765.*

McKenzie, D.P., Roberts, J.M., and Weiss, W., 1973. Numerical models of convection in the Earth's mantle. *Tectonophysics, 19, 89-103.*

McMillan, M., 1968. The geology of the Witputs - Sendlingsdrif area. *Bull. Precambrian Res. Unit, 4, Univ. Cape Town.*

Middlemost, E.A.K., 1964. Petrology of the plutonic and dyke rocks of the southeastern Richtersveld. *Trans. Geol. Soc. S. Afr., 67, 227-261.*

Miller, R. McG., 1983. The Pan-African Damara Orogen in South West Africa/Namibia. *Spec. Publ. Geol. Soc. S. Afr., 11, 431-515.*

Morthurst, J.R., Zeck, M.P., and Lundegardh, P.H., 1983. The Proterozoic hyperites in southern Varmland,

Western Sweden. *Sver. Geol. Under., Ba 30, 1-104.*

Muecke, G.K., Pride, C., and Sarker, P., 1979. Rare Earth Element geochemistry of regional metamorphic rocks. *Phys. Chem. Earth, 11, 449-464.*

Nakamura, E., 1978. Determination of REE, Ba, Fe, Mg, Na, and K in carbonaceous and ordinary chondrites. *Geochim. Cosmochim. Acta., 38, 757-775.*

Nesbitt, H.W., and Young, E.M., 1982. Early Proterozoic climates and plate motions inferred from major element chemistry of lutites. *Nature, 299, 715-717.*

Nicholson, R., and Pollard, D.D., 1985. The dilation and linkage of echelon cracks. *J. Struct. Geol., 7, 583-590.*

Norrish, K., and Hutton, J.T., 1969. An accurate X-ray spectrographic method for the analysis of a wide range of geological samples. *Geochim. Cosmochim. Acta., 35, 431-453.*

O'Hara, M.J., 1965. Primary magmas and the origin of basalts. *Scott. J. Geol., 1, 19-40.*

O'Hara, M.J., 1968. The bearing of phase equilibria studies in synthetic and natural systems on the evolution of basic and ultrabasic rocks. *Earth Sci. Rev., 4, 69-133.*

O'Hara, M.J., 1977. Geochemical evolution during fractional crystallisation of a periodically refilled magama chamber. *Nature, 266, 503-507.*

Onstott, T.C., Hargraves, R.B., and Reid, D.L., 1986. Constraints on the tectonic evolution of the Namaqua Province III: Palaeomagnetic and $^{40}Ar/^{39}Ar$ results from the Gannakouriep dyke swarm. *Trans. Geol. Soc. S. Afr., 89, 171-183.*

Patchett, P.J., 1980. Thermal effects of basalt on continental crust and crustal contamination of magmas. *Nature, 238, 559-561.*

Piper, J.D.A., 1975. The palaeomagnetism of Precambrian igneous and sedimentary rocks of the Orange River belt in South Africa and S.W.A.. *Geophys. J. R. Astr. Soc., 40, 313-344.*

Pearce, J.A., 1983. Role of sub-continental lithosphere in magma genesis at active continental margins. *In: Hawkesworth, C.J., and Norry, M.J., (Eds.), Continental Basalts and Mantle Xenoliths. Nantwich, Shiva, 230-249.*

Pearce, J.A., and Cann, J.R., 1973. Tectonic setting of basic volcanic rocks determined using trace element analyses. *Earth Plan. Sci. Letts, 19, 290-300.*

Pearce, J.A., and Norry, M.J., 1979. Petrogenetic implications of Ti, Zr, Y and Nb in volcanic rocks. *Contrib. Mineral. Petrol., 69, 33-47.*

Pollard, D.D., 1973a. Derivation and evaluation of a mechanical model for sheet intrusions. *Tectonophysics, 19, 233-269.*

Pollard, D.D., 1973b. Equations for stress displacement fields around pressurised elliptical holes in elastic solids. *J. Int. Assoc. Math. Geol., 5 (1), 1-25.*

Pollard, D.D., 1987. Elementary fracture mechanics applied to the structural interpretation of dykes. *In: Halls, H.C., and Farhig, W.F., (Eds), Mafic Dyke Swarms. Geol. Assoc. of Can. Spec. Paper, 34, 5-24.*

Pollard, D.D., and Muller, O.H., 1976. The effect of regional gradients in stress and magma pressure on the formation of sheet intrusions in cross-section. *J. Geophys. Res., 18, 975-984.*

Pollard, D.D., Segall, P., and Delaney, P.T., 1982. Formation and interpretation of dilation echelon cracks. *Geol. Soc. Am. Bull., 93, 1291-1303.*

Porada, H., 1989. Pan-African rifting and orogenesis in southern equitorial Afica and eastern Brasil. *Precambrian Res., 44, 103-136.*

Presnall, D.C., Dixon, S.A., O'Donnell, T.H., Brenner, N.L., Schrock, R.L., and Dycus, D.W., 1978. Liquidus phase relations on the join Diopside - Fosterite - Anorthite from 1 atms to 20 Kbars: their bearing on the generation and crystallisation of basaltic magma. *Contrib. Mineral. Petrol., 66, 203-220.*

Reid, D.L., 1977. Geochemistry of Precambrian igneous rocks in the lower Orange River region. *Precambrian Res. Unit, Bull. 22, Univ. Cape Town, 394pp.*

Reid, D.L., Welke, H.J., Erlank, A.J., and Betton, P.J., 1987. Composition, age and tectonic setting of amphibolites in the central Bushmanland Group, Western Namaqua Province, Southern Africa. *Precamb. Res., 36, 99-126.*

Richards, P., and Marks, R., 1966. Gelatin models for photoelastic analysis of gravity structures. *Exp. Mech., 6, 30-38.*

Richardson, S.H., 1979. Chemical variation induced by flow differentiation in an extensive Karoo dolerite

sheet, southern Namibia. *Geochim. Cosmochim. Acta, 43, 1433-1441.*
Richardson, S.H., 1984. Sr, Nd and O isotope variation in an extensive Karoo dolerite sheet, southern Namibia. *Spec. Publ. Geol. Soc. S. Afr., 13, 289-293.*
Ringwood, A.E., 1985. Mantle dynamics and basalt petrogenesis. *Tectonophysics, 112, 17-34.*
Ritter, U., 1980. The Precambrian evolution of the eastern Richtersveld. *Precambrian Res. Unit, Bull., 26, Univ. Cape Town, 276pp.*
Robson, E.R., and Barr, K.G., 1964. The effect of shear stress on faulting and minor intrusions in the vicinity of a magma body. *Bull. Volcanol., 27 (Part 1), 325-330.*
Roeder, P., and Emslie, R.F., 1970. Olivine - liquid equilibrium. *Contrib. Mineral. Petrol., 29, 275-289.*
Shafiquillah, M., and Damon, P.E., 1974. Evaluation of K-Ar isochron methods. *Geochim. et Cosmochim. Acta, 38, 1341-1358.*
Shimron, A.E., and Von Veh, M.W., 1987. Proterozoic orogenesis and crustal evolution in the Richtersveld sub-province. *Ann. Rep. Precambrian Res. Unit, Univ. Cape Town, 21 - 23, 58-66.*
Springer N., Mills, E.F., and Rodrick, R.T. , 1983. Sr diffusion rates across a geiss/metagabbro boundary within the Coastal Dyke Swarm, Brithish Columbia. J. Can. Earth Sci., 14, 67-82.
Sweeney, R.J., 1989. Geochemistry of the Sabie River basalt formation in the Central Lebombo, Karoo Igneous Province. *pp387 Unpubl. PhD thesis, Univ. Cape Town.*
Taylor, H.P., 1968. The oxygen isotope chemistry of igneous rocks. Contrib. Mineral Petrol., 19, 1-71.
Taylor, H.P., 1980. The effects of assimulation of country rocks by magmas on $^{18}O/^{16}O$ and $^{87}Sr/^{86}Sr$ systematics in igneous rocks. *Earth Plan. Sci. Letts., 47, 243-254.*
Thompson, R.N., 1982. Magmatism of the British Tertiary volcanic province. *Scott. J. Geol., 18, 49-107.*
Thompson, R.N., Morrison, M.A., Dickin, A.P., and Hendry, G.L., 1983. Continental flood basalts....Arachnids rule OK? *In: Hawkesworth, C.J., and Norry, M.J., (Eds.), Continental Basalts and Mantle Xenoliths. Shiva, Cheshire, 158-185.*
Timoshenko, G., and Goodier, J.N., 1951. Theory of Elasticity. *McGraw-Hill, New York, N.Y., 506pp.*
Turcotte, D.L., and Schubert, G., 1982. Geodynamic Applications of Continuum Physics to Geological Problems. *John Wiley, New York, 450pp.*
Van der Merwe, S.W., and Botha, B.J.V., 1988. The structural development of part of the Namaqua Mobile belt in an area between Springbok and Vioolsdrif: the result of thrust tectonics. *Ext. Abs. 22nd Earth Sci. Congr. Geol. Soc. S. Afr., 657-659.*
Venneman, T., and Smith, H.S., 1990. The rate and temperature of reaction of ClF_3 on silicate minerals, and their relevance to oxygen isotope analysis. *Chem. Geol., 86, In press.*
Von Veh, M.W., 1988. The stratigraphy and structural evolution of the late Proterozoic Gariep belt in the Sendlingsdrif - Annisfontein area, N.W. Cape province. *pp233 Unpubl. PhD thesis, Univ. Cape Town.*
Walker, F., 1957. Ophitic textures and basalt crystallisation. *J. Geol., 65, 1-14.*
Wang, A.J., 1953. Plastic flow in a deeply notched bar with a semi-circular root. *Q. Appl. Math., 11, 427-438.*
Weaver, B.L., and Tarney, J., 1984. Estimating the composition of continental crust: an empirical approach. *Nature, 310, 575-577.*
Weaver, B.L., and Tarney, J., 1985. Major and trace element composition of the continental lithosphere. *In: Pollack, H.N., and Morthy, V.R., (Eds.), Structure and Evolution of Continental Lithosphere. Physics and chemistry of the earth, 15, 39-68.*
White, R.S., 1988. The earths crust and lithosphere. *J. Petrol. Spec. Lithosphere Issue, 1-10.*
White, R.S., and McKenzie, D., 1989. Magmatism at Rift zones: the generation of volcanic continental margins and flood basalts. *J. Geophys. Res., 94, 7685-7729.*
Winkler, H.G.F., 1967. Petrogenesis of metamorphic rocks. *Springer-Verlag, New York, 348pp.*
Yoder, H.S. Jr, and Tilley, C.E., 1962. Origin of basalt magmas: an experimental study of natural and synthetic rock systems. *J. Petrol., 3, 342-532.*
Zeck, H.P., and Kalsbeck, F., 1981. Geochemistry of amphibolite metamorphism of a suite of basic dykes, Precambrian basement, Greenland. *Chem. Erde., 40, 1-22.*

Table of Contents

Appendix 1. Mineral Chemistry *111*
1.1 Analytical Technique and Precision *111*
1.2 Data *112*
Appendix 2. Geochronology *123*
2.1 Sample Preparation *123*
2.1.1 Whole Rock *123*
2.1.2 Mineral Separates *123*
2.2 Analytical Techniques and Precision *123*
2.3 Data *124*
Appendix 3. Intra-dyke Chemistry *126*
3.1 XRF *126*
3.1.1 Sample Preparation *126*
3.1.2 Analytical Technique and Precision *126*
3.1.3 Data *127*
3.2 REE *131*
3.2.1 Sample Preparation *131*
3.2.2 Analytical Technique and Precision *131*
3.2.3 Data *131*
3.3 Isotopes *132*
3.3.1 Sample Preparation *132*
3.3.2 Analytical Techniques and Precision *132*
3.3.3 Data *133*
Appendix 4. Inter-dyke Chemistry *134*
4.1 XRF *134*
4.1.1 Sample Preparation *134*
4.1.2 Analytical Techniques and Precision *134*
4.1.3 Data *135*
4.2 REE *172*
4.2.1 Sample Preparation *172*
4.2.2 Analytical Techniques and Precision *172*
4.2.3 Data *173*
Appendix 5. Sample Locations *178*
5.1 Collated database grid references *178*
5.2 Samples collected in this thesis *180*
5.3 Sample location map *End Cover*

Appendix 1 Mineral Chemistry

1.1 Analytical Technique and Precision

Mineral chemical analyses were undertaken at the University of Cape Town using a Cameca-Camebax Electron Microprobe with samples prepared as double polished thin sections on a glass slide.

The following operating conditions were used:

Beam current:	40 nA
Accelerating voltage:	15 Kv
Analyte line:	K_α
Analysing crystals:	TLAP for Na, Mg, Si, and Al
	LiF(200) for Fe, Mg and Ni
	PET for Ca, K, Ti, Cr and P
Detectors:	Flow counters with Ar/CO_2 gas mixture

Beam: 2 - 4 um for olivines, pyroxenes and oxides
8 - 12 um for feldspars and biotite

A full list of standards used for calibration are given in Sweeney, 1988. Background and dead time corrected raw data was reduced for all minerals used the method developed by Bence and Albee (1968).

Typical precisions (2 s.d.) and lower limits of detection at 99% confidence level are as follows:

Clinopyroxene - DRD-151

Oxide	Concentration	Precision	LLD
SiO_2	50.21	0.24	0.04
TiO_2	1.15	0.06	0.04
Al_2O_3	2.47	0.05	0.03
FeO	11.94	0.27	0.08
MnO	.38	0.05	0.07
MgO	13.73	0.16	0.04
CaO	19.98	0.17	0.04
Na_2O	.40	0.04	0.03
K_2O	ND	0.03	0.03
Cr_2O_3	ND	-	0.03*
NiO	ND	-	0.04*

* LLD derrived from data from Fe-Ti oxides.

1.2 Data

Olivine

	1	2	3	4	5	6
SIO2	32.79	33.64	33.97	33.12	33.12	32.87
TIO2	.05	.05	.05	.03	.04	.03
AL2O3	ND	-	ND	-	.02	.03
CR2O3	.02	ND	ND	ND	-	.02
FEO	42.50	40.61	41.46	39.86	40.11	40.93
MNO	.65	.64	.68	.71	.65	.64
MGO	24.08	24.91	24.85	26.11	26.06	25.28
CAO	.04	-	ND	.07	.07	.08
NA2O	-	-	-	-	-	-
K2O	-	-	-	-	-	-
NIO	.07	-	-	.06	.06	.04
TOTAL	100.21	99.86	101.04	99.97	100.13	99.92
** ATOMIC PROPORTIONS BASED ON SELECTED NO. OF OXYGENS **						
OXYGEN	4	4	4	4	4	4
SI	.952	.968	.968	.951	.950	.950
TI	.001	.001	.001	.001	.001	.001
AL	-	-	-	-	.001	.001
CR	.000	-	-	-	-	.000
FE2+	1.032	.977	.988	.957	.963	.989
MN	.016	.016	.016	.017	.016	.016
MG	1.042	1.068	1.056	1.118	1.114	1.089
CA	.001	-	-	.002	.002	.002
NA	-	-	-	-	-	-
K	-	-	-	-	-	-
NI	.002	-	-	.001	.001	.001
SUM	3.047	3.031	3.030	3.048	3.048	3.049

	7	8	9	10	11	12
SIO2	32.53	32.26	32.99	32.81	32.96	33.01
TIO2	.06	.05	.04	.04	.04	.04
AL2O3	ND	-	ND	-	.03	-
CR2O3	-	ND	-	-	.02	-
FEO	40.88	42.50	41.16	40.66	40.95	39.53
MNO	.66	.80	.66	.54	.60	.62
MGO	25.19	23.54	25.02	25.23	24.65	25.90
CAO	.05	ND	.02	.20	.06	.08
NA2O	-	-	-	-	-	-
K2O	-	-	-	-	-	-
NIO	.02	.03	.06	.02	.04	.06
TOTAL	99.40	99.20	99.96	99.37	99.49	99.22
** ATOMIC PROPORTIONS BASED ON SELECTED NO. OF OXYGENS **						
OXYGEN	4	4	4	4	4	4
SI	.946	.949	.953	.952	.957	.954
TI	.001	.001	.001	.001	.001	.001
AL	-	-	-	-	.001	-
CR	-	-	-	-	.000	-
FE2+	.994	1.046	.995	.987	.994	.956
MN	.016	.020	.013	.015	.015	.015
MG	1.092	1.032	1.078	1.091	1.066	1.116
CA	.002	-	.001	.002	.006	.002
NA	-	-	-	-	-	-
K	-	-	-	-	-	-
NI	.000	.001	.001	.000	.001	.001
SUM	3.052	3.050	3.045	3.047	3.042	3.045

Sample Description:

1. DRD-151	**2. DRD-151**	**3. DRD-151**	**4. DRD-151**	**5.DRD-151**	**6. DRD-151**
7. DRD-151	**8. DRD-151**	**9. DRD-151**	**10. DRD-151**	**11.DRD-151**	**12. DRD-151**

Pyroxene

	1		2		3		4		5		6		7		8
SIO2	49.46	SIO2	50.47	SIO2	50.21	SIO2	50.23	SIO2	51.17	SIO2	51.37	SIO2	48.92	SIO2	50.04
TIO2	1.82	TIO2	.95	TIO2	1.15	TIO2	1.09	TIO2	.70	TIO2	.62	TIO2	1.77	TIO2	1.20
AL2O3	3.58	AL2O3	1.87	AL2O3	2.47	AL2O3	2.42	AL2O3	1.67	AL2O3	1.45	AL2O3	3.96	AL2O3	2.44
CR2O3	ND	CR2O3	ND	CR2O3	ND	CR2O3	ND	CR2O3	ND	CR2O3	ND	CR2O3	ND	CR2O3	ND
FEO	10.12	FEO	11.32	FEO	11.94	FEO	11.61	FEO	11.66	FEO	11.70	FEO	10.07	FEO	9.73
MNO	.24	MNO	.30	MNO	.38	MNO	.35	MNO	.35	MNO	.29	MNO	.30	MNO	.30
MGO	14.24	MGO	14.21	MGO	13.73	MGO	13.68	MGO	14.11	MGO	14.04	MGO	14.25	MGO	15.12
CAO	20.65	CAO	20.31	CAO	19.98	CAO	19.88	CAO	20.65	CAO	20.67	CAO	20.56	CAO	20.47
NA2O	.44	NA2O	.38	NA2O	.40	NA2O	.37	NA2O	.36	NA2O	.40	NA2O	.43	NA2O	.37
K2O	ND	K2O	ND	K2O	ND	K2O	ND	K2O	ND	K2O	ND	K2O	ND	K2O	ND
TOTAL	100.55	TOTAL	99.81	TOTAL	100.26	TOTAL	99.63	TOTAL	100.67	TOTAL	100.54	TOTAL	100.26	TOTAL	99.67

* * ATOMIC PROPORTIONS BASED ON SELECTED NO. OF OXYGENS * *

OXYGEN	6		6		6		6		6		6		6		6
SI	1.850	SI	1.909	SI	1.894	SI	1.902	SI	1.920	SI	1.930	SI	1.836	SI	1.884
TI	.051	TI	.027	TI	.033	TI	.031	TI	.020	TI	.018	TI	.050	TI	.034
AL	.158	AL	.083	AL	.110	AL	.108	AL	.074	AL	.064	AL	.175	AL	.108
CR	-	CR	-	CR	-	CR	-	CR	-	CR	-	CR	-	CR	-
FE	.317	FE	.358	FE	.377	FE	.368	FE	.366	FE	.368	FE	.316	FE	.306
MN	.008	MN	.010	MN	.012	MN	.011	MN	.011	MN	.009	MN	.009	MN	.009
MG	.794	MG	.801	MG	.772	MG	.772	MG	.789	MG	.786	MG	.797	MG	.848
CA	.828	CA	.823	CA	.807	CA	.806	CA	.830	CA	.832	CA	.827	CA	.825
NA	.032	NA	.028	NA	.030	NA	.027	NA	.026	NA	.029	NA	.031	NA	.027
K	-	K	-	K	-	K	-	K	-	K	-	K	-	K	-
SUM	4.038	SUM	4.039	SUM	4.035	SUM	4.025	SUM	4.036	SUM	4.036	SUM	4.041	SUM	4.041
WO	42.54	WO	41.32	WO	41.02	WO	41.20	WO	41.59	WO	41.71	WO	42.41	WO	41.49
EN	40.81	EN	40.23	EN	39.21	EN	39.45	EN	39.53	EN	39.41	EN	40.89	EN	42.64
FS	16.66	FS	18.45	FS	19.76	FS	19.35	FS	18.88	FS	18.88	FS	16.70	FS	15.88

	9		10		11		12		13
SIO2	51.51	SIO2	49.85	SIO2	50.80	SIO2	50.93	SIO2	51.49
TIO2	.62	TIO2	1.38	TIO2	1.07	TIO2	1.08	TIO2	.62
AL2O3	1.36	AL2O3	3.02	AL2O3	2.24	AL2O3	2.20	AL2O3	1.34
CR2O3	ND	CR2O3	ND	CR2O3	ND	CR2O3	ND	CR2O3	ND
FEO	11.23	FEO	10.34	FEO	10.56	FEO	10.07	FEO	11.65
MNO	.33	MNO	.29	MNO	.27	MNO	.23	MNO	.32
MGO	14.02	MGO	14.42	MGO	14.77	MGO	15.01	MGO	13.90
CAO	20.48	CAO	20.32	CAO	20.20	CAO	20.37	CAO	20.58
NA2O	.38	NA2O	.37	NA2O	.37	NA2O	.36	NA2O	.43
K2O	ND	K2O	ND	K2O	ND	K2O	ND	K2O	ND
TOTAL	99.93	TOTAL	99.99	TOTAL	100.28	TOTAL	100.25	TOTAL	100.33

* * ATOMIC PROPORTIONS BASED ON SELECTED NO. OF OXYGENS * *

OXYGEN	6		6		6		6		6
SI	1.941	SI	1.875	SI	1.903	SI	1.904	SI	1.937
TI	.018	TI	.039	TI	.030	TI	.030	TI	.018
AL	.060	AL	.134	AL	.099	AL	.097	AL	.060
CR	-	CR	-	CR	-	CR	-	CR	-
FE	.354	FE	.325	FE	.331	FE	.315	FE	.366
MN	.011	MN	.009	MN	.009	MN	.007	MN	.010
MG	.788	MG	.808	MG	.825	MG	.837	MG	.780
CA	.827	CA	.819	CA	.811	CA	.816	CA	.829
NA	.028	NA	.027	NA	.027	NA	.026	NA	.032
K	-	K	-	K	-	K	-	K	-
SUM	4.027	SUM	4.036	SUM	4.035	SUM	4.032	SUM	4.032
WO	41.78	WO	41.73	WO	41.05	WO	41.32	WO	41.77
EN	39.80	EN	41.21	EN	41.77	EN	42.37	EN	39.26
FS	18.42	FS	17.05	FS	17.18	FS	16.31	FS	18.97

Sample Description:

1. DRD-151 2. DRD-151 3. DRD-151 4. DRD-151 5. DRD-151 6. DRD-151
7. DRD-151 8. DRD-151 9. DRD-72 10. DRD-72 11. DRD-72 12. DRD-72
13. DRD-72

Plagioclase

	1		2		3		4		5		6		7		8
NA2O	4.29	NA2O	4.40	NA2O	5.34	NA2O	4.33	NA2O	5.35	NA2O	4.09	NA2O	4.27	NA2O	5.39
K2O	.38	K2O	.44	K2O	.29	K2O	.15	K2O	.44	K2O	.36	K2O	.18	K2O	.41
SIO2	54.24	SIO2	54.42	SIO2	56.37	SIO2	53.88	SIO2	56.21	SIO2	53.40	SIO2	53.54	SIO2	56.95
AL2O3	28.23	AL2O3	28.55	AL2O3	27.09	AL2O3	28.55	AL2O3	26.82	AL2O3	28.84	AL2O3	28.57	AL2O3	26.72
FEO	.33	FEO	.26	FEO	.31	FEO	.55	FEO	.44	FEO	.39	FEO	.30	FEO	.27
MGO	ND	MGO	ND	MGO	ND	MGO	.11	MGO	.05	MGO	ND	MGO	ND	MGO	ND
CAO	12.22	CAO	11.93	CAO	10.61	CAO	12.18	GAO	10.34	CAO	12.42	CAO	12.42	CAO	10.04
TOTAL	99.69	TOTAL	100.00	TOTAL	100.01	TOTAL	99.75	TOTAL	99.65	TOTAL	99.50	TOTAL	99.28	TOTAL	99.78

* * ATOMIC PROPORTIONS BASED ON SELECTED NO. OF OXYGENS * *

OXYGEN	8		8		8		8		8		8		8		8
NA	.378	NA	.386	NA	.466	NA	.381	NA	.469	NA	.362	NA	.378	NA	.471
K	.022	K	.026	K	.016	K	.008	K	.025	K	.021	K	.010	K	.024
SI	2.464	SI	2.462	SI	2.540	SI	2.446	SI	2.543	SI	2.434	SI	2.443	SI	2.566
AL	1.512	AL	1.523	AL	1.438	AL	1.528	AL	1.430	AL	1.549	AL	1.536	AL	1.419
FE	.013	FE	.010	FE	.012	FE	.021	FE	.017	FE	.015	FE	.011	FE	.010
MG	-	MG	-	MG	-	MG	.007	MG	.004	MG	-	MG	-	MG	-
CA	.595	CA	.578	CA	.512	CA	.592	CA	.501	CA	.607	CA	.607	CA	.485
SUM	4.984	SUM	4.985	SUM	4.984	SUM	4.983	SUM	4.989	SUM	4.988	SUM	4.985	SUM	4.975
AB	37.99	AB	38.98	AB	46.86	AB	38.83	AB	47.11	AB	36.56	AB	37.98	AB	48.07
OR	2.22	OR	2.59	OR	1.66	OR	.86	OR	2.55	OR	2.14	OR	1.03	OR	2.43
AN	59.79	AN	58.42	AN	51.48	AN	60.31	AN	50.34	AN	61.30	AN	60.99	AN	49.49

9		10		11		12		13		14		15	
NA2O	5.26	NA2O	5.62	NA2O	5.32	NA2O	5.51	NA2O	4.32	NA2O	4.19	NA2O	4.17
K2O	.34	K2O	.32	K2O	.54	K2O	.25	K2O	.43	K2O	.36	K2O	.40
SIO2	56.62	SIO2	56.98	SIO2	56.11	SIO2	56.68	SIO2	54.13	SIO2	53.97	SIO2	53.99
AL2O3	27.20	AL2O3	26.66	AL2O3	27.06	AL2O3	26.95	AL2O3	27.99	AL2O3	28.58	AL2O3	28.70
FEO	.27	FEO	.34	FEO	.33	FEO	.39	FEO	.31	FEO	.41	FEO	.36
MGO	ND	MGO	ND	MGO	ND	MGO	ND	MGO	ND	MGO	ND	MGO	ND
CAO	10.51	CAO	9.92	CAO	10.36	CAO	10.21	CAO	12.15	CAO	12.37	CAO	12.40
TOTAL	100.20	TOTAL	99.84	TOTAL	99.72	TOTAL	99.99	TOTAL	99.33	TOTAL	99.88	TOTAL	100.02

* * ATOMIC PROPORTIONS BASED ON SELECTED NO. OF OXYGENS * *

OXYGEN	8		8		8		8		8		8		8
NA	.458	NA	.490	NA	.466	NA	.481	NA	.382	NA	.369	NA	.366
K	.020	K	.019	K	.031	K	.014	K	.025	K	.021	K	.023
SI	2.543	SI	2.566	SI	2.538	SI	2.552	SI	2.469	SI	2.449	SI	2.447
AL	1.440	AL	1.415	AL	1.442	AL	1.430	AL	1.505	AL	1.529	AL	1.533
FE	.010	FE	.013	FE	.012	FE	.015	FE	.012	FE	.016	FE	.014
MG	-	MG	-	MG	-	MG	-	MG	-	MG	-	MG	-
CA	.506	CA	.479	CA	.502	CA	.493	CA	.594	CA	.602	CA	.602
SUM	4.977	SUM	4.982	SUM	4.991	SUM	4.985	SUM	4.987	SUM	4.986	SUM	4.985
AB	46.59	AB	49.64	AB	46.65	AB	48.69	AB	38.18	AB	37.21	AB	36.95
OR	1.99	OR	1.88	OR	3.10	OR	1.43	OR	2.51	OR	2.08	OR	2.33
AN	51.42	AN	48.47	AN	50.25	AN	49.89	AN	59.31	AN	60.72	AN	60.73

Sample Description:

1. DRD-151 2. DRD-151 3. DRD-151 4. DRD-151 5. DRD-151 6. DRD-151
7. DRD-151 8. DRD-151 9. DRD-151 10. DRD-151 11. DRD-151 12. DRD-151
13. DRD-151 14. DRD-151 15. DRD-151

Ti-Magnetite

	1		2		3		4
SIO2	ND	SIO2	ND	SIO2	ND	SIO2	ND
TIO2	8.68	TIO2	9.58	TIO2	10.28	TIO2	9.92
AL2O3	3.86	AL2O3	4.79	AL2O3	3.91	AL2O3	2.49
CR2O3	.84	CR2O3	.73	CR2O3	.67	CR2O3	.65
FEO	81.08	FEO	79.54	FEO	79.48	FEO	82.16
MNO	.19	MNO	.24	MNO	.24	MNO	.20
MGO	.91	MGO	1.18	MGO	1.06	MGO	.30
TOTAL	95.56	TOTAL	96.06	TOTAL	95.64	TOTAL	95.72

* * ATOMIC PROPORTIONS BASED ON SELECTED NO. OF OXYGENS * *

OXYGEN	4		4		4		4
SI	-	SI	-	SI	-	SI	-
TI	.290	TI	.313	TI	.338	TI	.334
AL	.202	AL	.245	AL	.202	AL	.131
CR	.030	CR	.025	CR	.023	CR	.023
FE	3.009	FE	2.887	FE	2.909	FE	3.076
MN	.007	MN	.009	MN	.009	MN	.008
MG	.060	MG	.076	MG	.069	MG	.020
SUM	3.598	SUM	3.555	SUM	3.550	SUM	3.592

Sample Description:
1. DRD-151 2. DRD-151 3. DRD-151 4. DRD-151

Ilmenite

	1		2		3		4		5		6		7		8
SIO2	ND	SIO2	ND	SIO2	ND	SIO2	ND	SIO2	ND	SIO2	ND	SIO2	ND	SIO2	ND
TIO2	52.55	TIO2	47.03	TIO2	48.09	TIO2	53.35	TIO2	49.97	TIO2	53.53	TIO2	53.59	TIO2	51.99
AL2O3	.78	AL2O3	ND	AL2O3	.08	AL2O3	ND	AL2O3	ND	AL2O3	ND	AL2O3	ND	AL2O3	ND
CR2O3	ND	CR2O3	ND	CR2O3	.13	CR2O3	ND	CR2O3	.14	CR2O3	ND	CR2O3	ND	CR2O3	ND
FEO	45.22	FEO	51.71	FEO	50.43	FEO	45.50	FEO	49.19	FEO	45.53	FEO	44.82	FEO	47.66
MNO	.54	MNO	.63	MNO	.82	MNO	.84	MNO	.87	MNO	.71	MNO	.65	MNO	.96
MGO	2.03	MGO	.61	MGO	.85	MGO	1.43	MGO	.53	MGO	1.32	MGO	1.33	MGO	.41
TOTAL	101.12	TOTAL	99.98	TOTAL	100.40	TOTAL	101.12	TOTAL	100.70	TOTAL	101.09	TOTAL	100.39	TOTAL	101.02

* * ATOMIC PROPORTIONS BASED ON SELECTED NO. OF OXYGENS * *

OXYGEN	3		4		4		3		3		3		3		3
SI	-	SI	-	SI	-	SI	-	SI	-	SI	-	SI	-	SI	-
TI	.976	TI	1.229	TI	1.239	TI	.995	TI	.956	TI	.997	TI	1.005	TI	.983
AL	.023	AL	-	AL	.003	AL	-	AL	-	AL	-	AL	-	AL	-
CR	-	CR	-	CR	.003	CR	-	CR	.003	CR	-	CR	-	CR	-
FE	.934	FE	1.502	FE	1.445	FE	.944	FE	1.047	FE	.943	FE	.935	FE	1.003
MN	.011	MN	.019	MN	.024	MN	.018	MN	.019	MN	.015	MN	.014	MN	.020
MG	.075	MG	.031	MG	.044	MG	.053	MG	.020	MG	.049	MG	.049	MG	.015
SUM	2.019	SUM	2.781	SUM	2.758	SUM	2.010	SUM	2.045	SUM	2.004	SUM	2.003	SUM	2.021

	9		10		11		12		13		14		15		16
SIO2	ND	SIO2	6.70	SIO2	.21	SIO2	ND	SIO2	ND	SIO2	ND	SIO2	.38	SIO2	ND
TIO2	52.40	TIO2	42.88	TIO2	50.46	TIO2	50.40	TIO2	50.31	TIO2	50.34	TIO2	50.07	TIO2	50.37
AL2O3	ND	AL2O3	1.44	AL2O3	ND	AL2O3	ND	AL2O3	ND	AL2O3	ND	AL2O3	ND	AL2O3	ND
CR2O3	ND	CR2O3	.91	CR2O3	ND	CR2O3	ND	CR2O3	ND	CR2O3	ND	CR2O3	ND	CR2O3	ND
FEO	47.57	FEO	40.02	FEO	47.07	FEO	48.07	FEO	47.37	FEO	47.96	FEO	47.01	FEO	47.59
MNO	1.21	MNO	1.54	MNO	1.97	MNO	1.79	MNO	2.01	MNO	1.94	MNO	2.04	MNO	2.02
MGO	.14	MGO	.84	MGO	ND	MGO	ND	MGO	ND	MGO	ND	MGO	.09	MGO	.07
		CAO	4.51												
		NB2O5	ND												
		ZRO2	ND												
TOTAL	101.32	TOTAL	98.84	TOTAL	99.71	TOTAL	100.26	TOTAL	99.69	TOTAL	100.24	TOTAL	99.59	TOTAL	100.05

* * ATOMIC PROPORTIONS BASED ON SELECTED NO. OF OXYGENS * *

OXYGEN	3		3		3		3		3		3		3		3
SI	-	SI	.164	SI	.005	SI	-	SI	-	SI	-	SI	.010	SI	-
TI	.988	TI	.791	TI	.973	TI	.970	TI	.973	TI	.969	TI	.965	TI	.970
AL	-	AL	.041	AL	-	AL	-	AL	-	AL	-	AL	-	AL	-
CR	-	CR	.018	CR	-	CR	-	CR	-	CR	-	CR	-	CR	-
FE	.998	FE	.821	FE	1.010	FE	1.029	FE	1.018	FE	1.026	FE	1.008	FE	1.020
MN	.026	MN	.032	MN	.043	MN	.039	MN	.044	MN	.042	MN	.044	MN	.044
MG	.005	MG	.031	MG	-	MG	-	MG	-	MG	-	MG	.003	MG	.003
		CA	.119												
		NB	-												
		ZR	-												
SUM	2.017	SUM	2.017	SUM	2.031	SUM	2.038	SUM	2.035	SUM	2.037	SUM	2.030	SUM	2.037

	17		18		19		20		21
SIO2	ND	SIO2	.26	SIO2	ND	SIO2	ND	SIO2	2.56
TIO2	50.37	TIO2	50.77	TIO2	50.30	TIO2	50.29	TIO2	46.36
AL2O3	.10	AL2O3	ND	AL2O3	.08	AL2O3	ND	AL2O3	1.80
CR2O3	ND	CR2O3	ND	CR2O3	ND	CR2O3	ND	CR2O3	ND
FEO	47.02	FEO	46.64	FEO	46.92	FEO	47.61	FEO	45.00
MNO	1.84	MNO	1.88	MNO	2.02	MNO	1.97	MNO	1.88
MGO	ND	MGO	.06	MGO	ND	MGO	.06	MGO	1.25
TOTAL	99.33	TOTAL	99.61	TOTAL	99.32	TOTAL	99.93	TOTAL	98.85

* * ATOMIC PROPORTIONS BASED ON SELECTED NO. OF OXYGENS * *

OXYGEN	3		3		3		3		3
SI	-	SI	.007	SI	-	SI	-	SI	.065
TI	.974	TI	.976	TI	.974	TI	.969	TI	.879
AL	.003	AL	-	AL	.003	AL	-	AL	.054
CR	-	CR	-	CR	-	CR	-	CR	-
FE	1.011	FE	.997	FE	1.010	FE	1.020	FE	.949
MN	.040	MN	.041	MN	.044	MN	.043	MN	.040
MG	-	MG	.002	MG	-	MG	.002	MG	.047
SUM	2.028	SUM	2.023	SUM	2.031	SUM	2.034	SUM	2.034

Sample Description:

1. DRD-151	2. DRD-151	3. DRD-151	4. DRD-151	5. DRD-151	6. DRD-151
7. DRD-151	8. DRD-72	9. DRD-72	10. DRD-72	11. DRD-72	12. DRD-72
13. DRD-72	14. DRD-72	15. DRD-55	16. DRD-55	17. DRD-55	18. DRD-55
19. DRD-55	20. DRD-55	21. DRD-55			

Mica

	1		2
F	.30	F	.34
CL	.10	CL	.14
NA2O	.30	NA2O	.20
K2O	9.21	K2O	9.41
SIO2	38.15	SIO2	37.46
TIO2	4.14	TIO2	5.73
AL2O3	14.53	AL2O3	14.45
CR2O3	ND	CR2O3	ND
FEO	18.44	FEO	18.41
MNO	ND	MNO	ND
MGO	13.94	MGO	12.90
CAO	ND	CAO	ND
TOTAL	99.11	TOTAL	99.04

* * ATOMIC PROPORTIONS BASED ON SELECTED NO. OF OXYGENS * *

OXYGEN	22		22
F	.137	F	.160
CL	.026	CL	.035
NA	.086	NA	.058
K	1.717	K	1.766
SI	5.577	SI	5.508
TI	.456	TI	.633
AL	2.504	AL	2.504
CR	-	CR	-
FE	2.254	FE	2.264
MN	-	MN	-
MG	3.037	MG	2.828
CA	-	CA	-
SUM	15.794	SUM	15.756
MF	7.40	MF	5.54

Sample Description:
1. DRD-151 2. DRD-151

Appendix 2 Geochronology

2.1 Sample Preparation

2.1.1 Whole rock

Whole rock samples were obtained from, (i) a sieb rock powder (-200 mesh) of sample DRD-151, ground in a tungsten carbide swing mill (WRa, DRD-53); and (ii) a fraction < 120 mesh obtained from a mineral separate crush (WRb).

2.1.2 Mineral separates

Two size fractions, 40-60 mesh and 60-90 mesh were sieved from a whole rock crush (DRD-151), and washed in distilled H_2O. Initial mineral separation was performed on a Frantz magnetic separator. The 40-60 mesh fraction was used to collect biotite and plagioclase mineral separates, whilst the 60-90 mesh fraction was used to obtain a clinopyroxene separate. Both the clinopyroxene and plagioclase separates were picked and sorted by hand in alcohol with the aid of a binocular microscope. The biotite fraction Mica separate A was also picked in alcohol, whilst the subsequent two mica separates B and C were sorted in air.

Mineral separate descriptions are as follows:

Clinopyroxene - 10 mg of purple-brown augite cores were collected to avoid minor incipient chloritisation, and the subophitic incorporation of apatite needles.

Plagioclase - 20 mg of plagioclase laths were collected, having been visually screened for any minor serricisation. Typically these exhibit a light blue colouration under reflected light.

Biotite - three mineral separates each comprising 10 mg were collected. The dark ox blood red-brown mineral separates typically comprise a psuedohexagonal habit, occuring in 'book' form, which were prised apart under the microscope to ensure mineral separate purity.

2.2 Analytical techniques and precision

Sr isotope analyses were carried out at the Bernard Price Institute of Geophysical Research, Johannesberg using the methods described by Allsopp et al. (1979) and Hart and Brookes, (1977). All Rb and Sr (ppm) was measured by isotope dilution. Nd-Sm whole rock analysis was performed by Reid, D.L. at New Mexico Tech, using the method outlined by Allsopp et al. (1979).

Precision, accuracy and lower limits of detection for both Sr and Nd isotope analyses are to be found in Allsopp et al., (op. cit.).

2.3 Data

Rb/Sr

Sample	Rb	Sr	$^{87}Rb/^{86}Sr$	$^{87}Sr/^{86}Sr$	
DRD-151/WRA	6.80?	475.9	0.041	.706225 ± 52	
DRD-151/WRB	20.87	485.5	0.124	.706387 ± 18	
DRD-151 seive	21.35	479.0	0.129	.706265 ± 39	
DRD-151 carb.	-	-	-	.706846 ± 62	
DRD-151 cpx.	0.31	49.95	0.0180	.705265 ± 62	Rb is blank correct
DRD-151 mica A	283.7	58.76	14.12	.819432 ± 36	mica leached
DRD-151 mica B	300.2	33.84	26.35	.980363 ± 66	mica leached
DRD-151 mica C	355.6	24.77	43.28	1.138344 ± 52	mica leached

Errors on $^{87}Sr/^{86}Sr$ are 2 in-run std.error.

Model Ages for DRD151 Micas (Ma)

	Ro		
	.705	.710	.730
A	568	544	445
B	732	719	666
C	702	694	661

Opinion: 702 Ma is best model age because mica has highest Rb/Sr, $^{87}Sr/^{86}Sr$. This is a function of not leaching in addition to more experience in mica preparation by Joe Aphane.

Sample #	Rb	Sr	$^{87}Sr/^{86}Sr$	$^{87}Rb/^{86}Sr$
DRD-50	29.6	250	.713364+/-88	.341
DRD-50A	23.7	345	.71290+/-14	.199
DRD-51	43.4	520	.713871+/-36	.241
DRD-52	40.7	472	.71224+/-14	.249
DRD-53	64.8	436	.71093+/-17	.430
DRD-54	44.6	405	.709068+/-32	.313
DRD-55	36.3	339	.709569+/-46	.309
DRD-60	47.3	395	.710861+/-56	.346
DRD-56	34.5	267	.7714134+/-38	.373
DRD-57	76.0	277	.72061+/-11	.792
DRD-58	38.8	241	.71444+/-15	.465
DRD-59	34.1	280	.710966+/-14	.352

Notes: - not determined

Sample	Rb	Sr	$^{87}Rb/^{86}Sr$	$^{87}Sr/^{86}Sr$	
DRD-66 Wr	28.09	350.2	0.232	.716232 ± 16	
DRD-67 WR	31.96	313.5	0.295	.715193 ± 26	
DRD-68 WR	45.64	355.3	0.372	.716672 ± 20	
DRD-69 WR	57.92	478.2	0.351	.713958 ± 20	
DRD-70 WR	58.27	466.3	0.362	.712283 ± 18	
DRD-71 WR	67.35	414.8	0.470	.712016 ± 18	
DRD-72 WR	75.18	430.4	0.506	.713780 ± 38	Sr poor
duplicate	77.19	420.9	0.531	.713308 ± 24	
duplicate	76.87	-	-	.713369 ± 18	
DRD-73 WR	59.38	339.5	0.506	.713685 ± 30	Sr poor
duplicate	56.53	339.0	0.483	.713549 ± 20	
DRD-73 Ac	-	-	-	.713544 ± 18	
duplicate	64.94	419.00	0.449	.71334 ± 8	Sr poor
DRD-74 WR	59.71	362.8	0.476	.712111 ± 30	Sr poor
duplicate	57.45	363.5	0.457	.712081 ± 18	
DRD-74A WR	70.38	412.5	0.494	.715715 ± 26	
DRD-75 WR	61.47	367.9	0.484	.717534 ± 32	
DRD-76 WR	34.39	353.4	0.282	.715998 ± 28	
DRD-77 WR	26.77	403.5	0.182	.717669 ± 38	
duplicate	26.89	-	-	-	
duplicate	-	423.4	-	.717826 ± 22	
DRD-170 plag.	1.17	826.9	0.004	.704965 ± 20	
DRD-170 ep.	-	-	-	.715362 ± 42	
DRD-170 c	-	-	-	.717848 ± 18	

Errors on $^{87}Sr/^{86}Sr$ are 2 in-run std.error.

Sm/Nd

Sample DRD-53

Sample	Sm(ppm)	Nd(ppm)	$^{143}Nd/^{144}Nd$	$^{147}Nd/^{144}Nd$
DRD-53	6.633	30.42	0.512342 +/- 38	0.1317

THCUR age = 696 Ma

Appendix 3 Intra-dyke Chemistry

3.1 XRF

3.1.1 Sample preparation

Samples were prepared at UCT by splitting in a hydraulic splitter, crushing in a jaw crusher with Mn-steel jaws, and grinding in a tungsten-carbide Siebtechnik swing mill to -300#.

3.1.2 Analytical technique

Major Oxides

Major oxide analyses were performed using the technique of Norrish and Hutton (1969) to produce glass disks. Na_2O was analysed from a 6g pressed powder briquette. Data compiliation, calibration, reduction and correction used the methods described by Duncan et al., (1984).

Trace Elements

Trace element analyses were performed on 6g pressed powder briquettes using the techniques described by Duncan et al., (op. cit.).

Analytical precision for both major and trace element analyses are taken from Duncan et al., (op. cit) and shown below.

Major Oxide Analysis by XRF

Oxide	% Concentration	Precision	"Accuracy"	L.L.D.
SiO_2	50.0	0.140	0.264	0.04
TiO_2	1.0	0.008	0.008	0.005
Al_2O_3	15.0	0.080	0.079	0.02
Fe_2O_3	9.0	0.038	0.064	0.014
MnO	0.15	0.008	0.003	0.008
MgO	8.0	0.148	0.086	0.07
CaO	12.0	0.028	0.030	0.008
Na_2O	2.5	0.032	0.067	0.08
K_2O	0.20	0.002	0.022	0.002
P_2O_5	0.20	0.012	0.018	0.011

Precision is expressed as an absolute error in % oxide (2 sigma counting error) on the given concentration. "Accuracy" is the average absolute difference (in % oxide) between the recommended values for standards on the calibration line and their calculated values. L.L.D. is the lower limit of detection (in % oxide) at the 99 % confidence level.

Trace Element Analysis by XRF

Element	Concentration Range (ppm)	Precision	L.L.D.
Nb	4*–150	1.6–1.2	1.8
Zr	40–400	0.9–1.4	1.4
Y	20–40	0.8–1.0	1.3
Rb	3*–90	0.8–1.1	1.5
U	4–10	2.0–2.5	3.5
Sr	80–800	1.0–1.7	1.5
Th	5–30	2.3–3.1	4.0
Pb	5–100	2.3–3.2	4.5
Zn	8–150	0.9–1.7	1.4
Cu	5–90	1.8–2.1	2.9
Ni	10–210	0.7–1.0	1.2
Ga	15–20	0.38–0.46	0.45
Ba	10–800	2.1–6.0	3.7
Sc	25–40	1.0–1.2	1.2
Co	15–100	1.9–2.5	4.5
Cr	25–350	1.5–2.1	2.2
V	50–350	2.4–3.7	5.5
S	20–5000	10–40	20

Precision is expressed as an absolute error in ppm (2 sigma counting error) in the given concentration range. L.L.D. is the lower limit of detection (in ppm) at the 99 % confidence level.

* For many samples at or approaching the detection limit for Nb and Rb, samples were re-analysed using longer counting times in order to attain lower detection limits and better precision.

3.1.3 Data

Profile GD-I

	DRD-66	DRD-67	DRD-68	DRD-69	DRD-70	DRD-71
SIO2	45.36	46.18	45.58	45.67	47.41	48.19
TIO2	3.28	3.08	3.23	3.24	3.10	3.13
AL2O3	15.08	14.76	15.01	16.06	16.96	15.96
FE2O3	15.78	15.13	15.66	14.56	12.87	13.17
FEO						
MNO	.22	.22	.22	.20	.19	.21
MGO	5.67	5.96	5.35	4.67	4.14	4.07
CAO	8.47	8.73	8.18	8.94	8.38	8.36
NA2O	2.88	2.58	3.19	2.42	3.30	2.94
K2O	.74	.71	.94	1.32	1.49	1.69
P2O5	.50	.46	.51	.40	.44	.51
Total	100.00	100.00	100.00	100.00	100.00	100.00
H2O-	.03	.03	.04	.07	.03	.05
H2O+	3.5	3.3	3.2	3.3	2.9	2.5
CO2	.2	.5	.6	.8	.2	.7
LOI						
MO						
NB	30	27	28	20	24	31
ZR	272	258	285	211	223	274
Y	38	36	39	31	32	40
SR	355	319	365	484	475	427
U						
RB	28	32	47	60	60	70
TH						
PB						
ZN	152	158	153	143	128	128
CU	57	24	26	31	27	22
NI	66	73	67	53	31	30
CO	60	62	61	53	47	40
MN						
CR	65	65	62	46	29	29
V	295	278	276	299	266	246
BA	406	312	271	471	463	479
SC	27	24	26	25	26	24

	DRD-72	DRD-73	DRD-74	DRD-75	DRD-76	DRD-77
SIO2	49.20	46.63	46.90	46.63	46.54	44.71
TIO2	2.77	2.78	2.95	3.30	3.11	3.22
AL2O3	16.63	15.48	14.99	14.94	14.93	14.89
FE2O3	12.56	13.64	15.31	15.44	15.47	16.11
FEO						
MNO	.25	.24	.22	.21	.20	.20
MGO	4.05	4.63	5.57	5.30	5.70	5.86
CAO	7.03	7.55	8.56	8.10	8.11	9.16
NA2O	3.04	2.45	2.21	2.66	2.94	2.17
K2O	2.00	1.65	1.41	1.24	.64	.76
P2O5	.63	.54	.50	.53	.50	.50
Total	100.00	100.00	100.00	100.00	100.00	100.00
H2O-	.09	.34	.07	.04	.03	.10
H2O+	2.9	3.1	2.7	2.9	3.2	3.2
CO2	.2	2.7	.2	.4	.3	.3
LOI						
MO						
NB	30	27	17	26	27	26
ZR	305	267	264	242	276	282
Y	43	38	38	37	39	41
SR	432	348	383	365	356	403
U						
RB	80	58	61	63	36	26
TH						
PB						
ZN	167	183	155	150	162	152
CU	12	32	20	26	28	56
NI	13	38	54	57	61	65
CO	35	50	54	59	58	61
MN						
CR	17	32	42	57	56	63
V	169	278	263	282	262	296
BA	580	417	477	424	284	450
SC	22	32	24	25	24	28

Profile GD-II

	DRD-50	DRD-50A	DRD-51	DRD-52	DRD-53	DRD-54
SIO2	45.25	48.78	46.36	48.09	46.70	46.62
TIO2	3.33	3.34	2.82	2.83	2.73	3.34
AL2O3	15.07	14.06	15.56	15.02	17.01	16.19
FE2O3	15.84	14.44	14.33	14.20	13.73	13.80
FEO						
MNO	.23	.26	.22	.21	.17	.19
MGO	7.07	6.24	6.74	5.31	4.81	4.58
CAO	6.51	5.86	6.97	7.69	8.66	9.44
NA2O	2.78	3.25	2.55	2.38	2.38	2.53
K2O	.71	.70	1.28	1.26	1.41	1.20
P2O5	.52	.56	.41	.44	.39	.40
Total	100.00	100.00	100.00	100.00	100.00	100.00
H2O-	.21	.20	.09	.09	.10	.06
H2O+	4.1	3.2	3.8	3.4	3.3	3.0
CO2	.2	.7	.5	.7	.1	.1
LOI						
MO						
NB	31	29	24	23	19	21
ZR	291	263	237	241	203	206
Y	38	38	31	35	29	32
SR	250	345	520	472	436	405
U	<2.8					
RB	30	24	43	41	65	45
TH	<3.3					
PB						
ZN	182	162	160	133	130	135
CU	52	51	14	27	42	29
NI	66	56	81	67	66	41
CO	62	58	63	59	59	53
MN						
CR	67	62	54	63	53	40
V	309	276	229	238	295	300
BA	284	272	272	382	415	366
SC	27	28	28	25	21	27

	DRD-55	DRD-60	DRD-56	DRD-57	DRD-58	DRD-59
SIO2	46.04	45.60	47.42	47.84	46.61	45.58
TIO2	3.18	3.01	3.26	2.94	3.23	3.31
AL2O3	14.13	15.92	14.49	14.83	14.87	14.98
FE2O3	15.57	15.17	15.85	14.59	15.43	15.95
FEO						
MNO	.22	.22	.20	.21	.28	.25
MGO	6.31	5.32	6.63	6.87	5.88	5.71
CAO	9.64	7.90	4.13	4.21	5.82	7.98
NA2O	1.47	2.49	2.57	2.60	3.17	3.13
K2O	.89	1.32	1.04	1.90	.68	.70
P2O5	.37	.36	.60	.47	.51	.51
Total	100.00	100.00	100.00	100.00	100.00	100.00
H2O-	.07	.18	.12	.10	.73	.09
H2O+	3.4	3.8	4.7	4.2	3.9	3.0
CO2	.3	.4	.9	1.0	.8	.5
LOI						
MO						
NB	19	19	24	27	32	30
ZR	202	190	237	254	293	287
Y	30	29	36	36	39	38
SR	339	395	267	277	241	280
U						
RB	36	47	35	76	39	34
TH						
PB						
ZN	154	145	191	172	153	155
CU	40	40	8.1	26	25	26
NI	79	78	67	62	61	65
CO	67	69	59	59	58	56
MN						
CR	89	79	53	48	59	64
V	328	294	271	251	296	300
BA	297	468	472	691	191	295
SC	28	21	30	28	29	28

3.2 REE

3.2.1 Sample preparation

Sample analysed for whole rock REE content were prepared from whole rock siebed powders used for XRF analyses (see section 3.1.1).

3.2.1 Analytical technique

Whole rock REE analyses were measured at New Mexico Tech by Dave Reid using the INAA technique described by Gibson and Jagam (1980). Precision, accuracy and detection limits are described in Knoper, 1988.

3.2.3 Data

	DRD-50	DRD-55	DRD-59	DRD-60	DRD-72	DRD-77
LA	30.9	25.6	31.4	24.7	39.0	31.9
CE	73.2	60.1	71.5	55.7	88.2	71.9
ND	44.2	36.6	42.4	32.8	47.3	35.6
SM	9.5	7.7	10.0	7.3	11.7	9.6
EU	2.6	2.2	2.7	2.1	3.1	2.7
GD	9.0	7.7	9.1	6.6	11.0	9.2
TB	1.4	1.3	1.4	1.0	1.7	1.5
YB	3.7	3.1	3.8	2.8	4.6	3.8
LU	.6	.5	.6	.4	.7	.6
LAc	98.0	81.2	99.7	78.4	123.8	101.2
CEc	90.0	73.9	87.9	68.5	108.5	88.4
NDc	74.0	61.3	71.0	54.9	79.2	59.6
SMc	49.4	40.1	52.0	37.8	61.0	49.7
EUc	35.9	30.2	37.3	29.2	43.4	37.3
GDc	34.9	29.6	35.2	25.4	42.4	35.5
TBc	29.4	25.5	29.0	20.8	35.3	30.0
YBc	18.0	15.0	18.5	13.3	22.0	18.2
LUc	18.8	15.3	17.8	13.8	22.2	18.8
EU*	41.5	34.5	42.8	31.0	50.8	42.0

*** ALL ZERO VALUES PRINTED AS BLANKS ***

3.3 Isotopes

3.3.1 Sample preparation

Whole Rock Samples

Whole rock Sr and O isotope samples were taken directly from a -#300 whole rock sieb used for XRF analyses.

Mineral Separates

Mineral separates acquired for Sr and O isotope analyses were initially separated from a 60-90# mesh sieve using a Frantz magnetic separator. Subsequently these crude separates were washed in distilled H_2O, prior to being sorted by hand under binocular microscope.

Mineral separate descriptions are as follows;

Clinopyroxene: 25 mg of cores from subophitic augites were separated for O isotope analyses. Difficulty in obtaining 100% pure clean minerals was experienced due to the advanced state of chloritisation encountered.

Epidote: 20 mg of epidote formed from the advanced uralisation of plagioclase was separated for Sr isotopic analysis. Difficulty in obtaining 100% pure epidote was experienced due to incomplete pseudomorphing of plagioclase, however sample purity is estimated to lie in the range 85-90% pure epidote.

Chlorite: 20 mg of chlorite was separated by hand from large chlorite bundles (2 cm) present in sample DRD-170 for O isotopic analysis. Purity is estimated at around 95% chlorite.

Calcite: 8 g of pure calcite was separated by hand from sample DRD-170 from calcite viens associated with greenschist facies metamorphism. The latter sample was analysed for Sr content by XRF, and for Sr isotopes.

Quartz: 20 mg of pure quartz was separated from sample DRD-170 for O isotope analysis. The latter comprises part of the greenschist metamorphic mineralogy, containing minor fluid inclusions.

3.3.2 Analytical techniques

Sr Isotopes

Sr isotope analyses were carried out at the Bernard Price Institute of Geophysical Research using the techniques described by AllsopP et al., (1979) and Hart and Brookes, (1977). Sr and Rb were mearured by isotope dilution for profile GD-I, and by XRF for profile GD-II. Analytical precison, accuracy and detection limits are to be found in Allsopp et al., (1979).

Oxygen Isotopes

O isotope analyses were carried out at the University of Cape Town using the methods described by Venneman and Smith, (1990). Accuracy, precison and detection limits of the technique are to be found in Venneman and Smith (op. cit.).

3.3.3 Data

Sample	Rb	Sr	$^{87}Rb/^{86}Sr$	$^{87}Sr/^{86}Sr$	
DRD-66 Wr	28.09	350.2	0.232	.716232 ± 16	
DRD-67 WR	31.96	313.5	0.295	.715193 ± 26	
DRD-68 WR	45.64	355.3	0.372	.716672 ± 20	
DRD-69 WR	57.92	478.2	0.351	.713958 ± 20	
DRD-70 WR	58.27	466.3	0.362	.712283 ± 18	
DRD-71 WR	67.35	414.8	0.470	.712016 ± 18	
DRD-72 WR	75.18	430.4	0.506	.713780 ± 38	Sr poor
duplicate	77.19	420.9	0.531	.713308 ± 24	
duplicate	76.87	–	–	.713369 ± 18	
DRD-73 WR	59.38	339.5	0.506	.713685 ± 30	Sr poor
duplicate	56.53	339.0	0.483	.713549 ± 20	
DRD-73 Ac	–	–	–	.713544 ± 18	
duplicate	64.94	419.00	0.449	.71334 ± 8	Sr poor
DRD-74 WR	59.71	362.8	0.476	.712111 ± 30	Sr poor
duplicate	57.45	363.5	0.457	.712081 ± 18	
DRD-74A WR	70.38	412.5	0.494	.715715 ± 26	
DRD-75 WR	61.47	367.9	0.484	.717534 ± 32	
DRD-76 WR	34.39	353.4	0.282	.715998 ± 28	
DRD-77 WR	26.77	403.5	0.182	.717669 ± 38	
duplicate	26.89	–	–	–	
duplicate	–	423.4	–	.717826 ± 22	
DRD-170 plag.	1.17	826.9	0.004	.704965 ± 20	
DRD-170 ep.	–	–	–	.715362 ± 42	
DRD-170 c	–	–	–	.717848 ± 18	

Errors on $^{87}Sr/^{86}Sr$ are 2 in-run std.error.

Sample #	Rb	Sr	$^{87}Sr/^{86}Sr$	$^{87}Rb/^{86}Sr$	$^{87}Sr/^{86}Sr$ @ 717 Ma	$d^{18}O$
DRD-50	29.6	250	.713364+/-88	.341	.7095	4.91
DRD-50A	23.7	345	.71290+/-14	.199	.7106	5.47
DRD-51	43.4	520	.713871+/-36	.241	.7111	5.27
DRD-52	40.7	472	.71224+/-14	.249	.7090	5.58
DRD-53	64.8	436	.71093+/-17	.430	.7060	5.01
DRD-54	44.6	405	.709068+/-32	.313	.7054	5.45
DRD-55	36.3	339	.709569+/-46	.309	.7060	5.53
DRD-60	47.3	395	.710861+/-56	.346	.7069	5.38
DRD-56	34.5	267	.7714134+/-38	.373	.7099	5.46
DRD-57	76.0	277	.72061+/-11	.792	.7116	5.93
DRD-58	38.8	241	.71444+/-15	.465	.7091	5.38
DRD-59	34.1	280	.710966+/-14	.352	.7069	5.18

Notes: - not determined

Appendix 4 Inter-dyke Chemistry

4.1 XRF

4.1.1 Sample Preparation

Sample preparation was carried out at the University of Cape Town by initially splitting samples with a hydraulic splitter. Subsequently the raw material was crushed in a Mn-Fe jaw crusher, prior to being siebed to -#300 in a Siebtechinks tungsten carbide swingmill.

4.1.2 Analytical technique and Precision.

Major Oxides

Major oxide analyses were performed using the technique of Norrish and Hutton (1969) to produce glass disks. Na_2O was analysed from a 6g pressed powder briquette. Data compiliation, calibration, reduction and correction used the methods described by Duncan et al., (1984).

Trace Elements

Trace element analyses were performed on 6g pressed powder briquettes using the techniques described by Duncan et al, (op. cit.), except in some samples where no major element data was available for the computation of absorption co-efficents, a calculated average value was used.

Analytical precision for both major and trace element analyses are taken from Duncan et al. (op. cit) and shown in section 3.1.2.

4.1.3 Data

Sector 1 Dykes

Dyke Complex GDC-1

	GKR-109	GKR-103	GKR-97	GKR-101	GKR-74	GKR-40
SIO2	46.41					
TIO2	2.80					
AL2O3	14.40					
FE2O3	13.92					
FEO						
MNO	.19					
MGO	5.08					
CAO	8.37					
NA2O	2.71					
K2O	1.82					
P2O5	.47					
CR2O3						
NIO						
H2O-	.14					
H2O+						
CO2						
LOI	3.25					
TOTAL	99.55					
MO	.8	1.4	1.2	1.3	.8	1.1
NB	25	22	22	22	21	23
ZR	284	316	312	314	312	324
Y	48	53	53	54	54	58
SR	198	202	225	292	272	174
U	2.8	3.1	2.1	3.1	2.3	<1.8
RB	58	58	106	36	63	74
TH	2.9	3.3	5.0	2.7	3.7	4.6
PB	5.6	5.7	8.1	5.7	11	13
ZN	156	159	139	139	135	215
CU	7.9	7.9	14	13	18	212
NI	43	33	33	34	31	34
CO	56	49	48	53	50	63
MN	1793.1	1379.1	1623.2	1453.4	1529.4	1942.0
CR	75	45	39	42	37	46
V	290	305	282	303	268	340
BA	457	409	471	443	515	679
SC	23	31	26	28	29	33

*** ALL ZERO VALUES PRINTED AS BLANKS ***

Dyke Complex GDC-2

	GKR-78	GKR-69	GKR-102	GKR-49	GKR-83	GKR-100
SIO2	45.65	46.52	46.99	47.32		
TIO2	3.39	3.42	3.34	2.87		
AL2O3	15.25	15.13	14.90	14.73		
FE2O3	14.94	14.78	14.31	14.49		
FEO						
MNO	.22	.25	.19	.20		
MGO	4.88	5.00	4.25	5.18		
CAO	8.68	7.39	6.98	8.56		
NA2O	2.30	2.98	3.11	2.44		
K2O	1.80	1.47	2.49	1.86		
P2O5	.61	.64	.69	.49		
CR2O3						
NIO						
H2O-	.07	.15	.25	.13		
H2O+						
CO2						
LOI	2.99	2.63	2.45	1.69		
TOTAL	100.78	100.36	99.96	99.94		
MO	1.3	1.9	1.1	1.2	.9	1.8
NB	29	30	32	26	17	25
ZR	311	318	343	293	194	285
Y	49	50	54	48	35	48
SR	333	302	397	199	328	267
U	<1.9	2.4	1.9	<1.9	1.7	2.0
RB	72	91	121	33	119	61
TH	2.7	4.7	3.2	<2.6	2.5	3.6
PB	7.4	10	4.6	6.2	38	8.2
ZN	141	150	116	144	129	145
CU	22	21	21	16	21	17
NI	35	30	21	47	46	46
CO	45	50	43	65	68	61
MN	1501.1	1816.6	1383.9	1709.5	1602.4	1744.6
CR	33	27	16	55	82	62
V	245	259	235	264	306	259
BA	338	224	916	424	789	581
SC	26	26	25	27	23	23

*** ALL ZERO VALUES PRINTED AS BLANKS ***

	GKR-93	GKR-63	GKR-47	GKR-76	GKR-81	GKR-82
SIO2						
TIO2						
AL2O3						
FE2O3						
FEO						
MNO						
MGO						
CAO						
NA2O						
K2O						
P2O5						
CR2O3						
NIO						
H2O-						
H2O+						
CO2						
LOI						
TOTAL						
MO	1.0	1.3	<.7	.8	.8	1.4
NB	25	29	31	18	18	30
ZR	285	306	320	196	206	314
Y	47	48	51	35	37	49
SR	258	375	412	234	239	233
U	<1.8	<1.9	<1.8	1.9	<1.8	3.3
RB	39	61	53	44	46	107
TH	4.0	3.5	4.4	3.1	<2.5	4.3
PB	9.4	13	10.0	6.6	5.7	7.6
ZN	150	138	143	116	113	135
CU	18	21	8.9	14	24	21
NI	41	43	24	35	42	31
CO	55	54	47	55	57	46
MN	1941.4	1491.0	1720.4	1579.3	1644.6	1519.6
CR	66	46	17	89	72	22
V	285	247	233	231	269	237
BA	528	443	644	687	481	634
SC	26	21	26	25	23	31

*** ALL ZERO VALUES PRINTED AS BLANKS ***

	GKR-105
SIO2	
TIO2	
AL2O3	
FE2O3	
FEO	
MNO	
MGO	
CAO	
NA2O	
K2O	
P2O5	
CR2O3	
NIO	
H2O-	
H2O+	
CO2	
LOI	
TOTAL	
MO	.9
NB	17
ZR	188
Y	33
SR	302
U	2.2
RB	51
TH	<2.5
PB	6.5
ZN	143
CU	17
NI	40
CO	59
MN	2034.1
CR	80
V	238
BA	206
SC	29

*** ALL ZERO VALUES PRINTED AS BLANKS ***

Dyke Complex GDC-3

	GKR-89	GKR-106	GKR-99	GKR-111	GKR-80	GKR-59
SIO2	48.62	46.74	44.97	47.94	46.19	47.16
TIO2	3.55	3.42	3.58	3.30	3.09	3.43
AL2O3	14.04	13.95	14.78	13.76	14.85	13.86
FE2O3	15.98	15.63	15.71	15.07	14.82	15.30
FEO						
MNO	.27	.25	.25	.22	.19	.23
MGO	5.72	5.03	4.76	5.22	5.26	4.68
CAO	5.90	7.70	7.35	7.00	8.17	8.06
NA2O	3.43	2.85	2.23	2.77	2.70	2.44
K2O	.45	1.65	1.01	1.44	1.19	1.63
P2O5	.67	.58	.62	.56	.52	.63
CR2O3						
NIO						
H2O-	.14	.19	.14	.18	.13	.15
H2O+						
CO2						
LOI	1.95	2.68	3.08	2.04	2.95	3.25
TOTAL	100.74	100.66	98.48	99.48	100.07	100.81
MO	1.3	1.4	1.5	1.0	1.2	1.4
NB	23	21	22	21	22	22
ZR	336	293	302	292	314	315
Y	56	51	52	50	55	54
SR	206	266	183	320	316	265
U	<1.8	2.4	<1.8	<1.8	2.5	<1.9
RB	34	82	34	94	59	88
TH	2.9	3.3	2.6	3.4	4.3	4.4
PB	15	13	13	7.3	8.4	8.9
ZN	148	144	143	144	138	138
CU	25	18	15	14	18	19
NI	36	36	31	32	29	32
CO	56	56	61	53	50	55
MN	2171.3	1748.2	1753.5	1724.3	1535.1	1736.7
CR	42	43	45	45	33	42
V	317	303	314	293	293	299
BA	187	587	316	302	246	425
SC	34	26	35	28	26	30

*** ALL ZERO VALUES PRINTED AS BLANKS ***

	GKR-64	GKR-42	GKR-61	GKR-41	GKR-39	GKR-29
SIO2						
TIO2						
AL2O3						
FE2O3						
FEO						
MNO						
MGO						
CAO						
NA2O						
K2O						
P2O5						
CR2O3						
NIO						
H2O-						
H2O+						
CO2						
LOI						
TOTAL						
MO	<.7	1.5	.7	1.4	1.4	1.2
NB	22	25	24	22	22	22
ZR	294	369	361	291	316	312
Y	50	58	59	51	55	52
SR	350	135	307	252	178	323
U	2.8	<1.9	1.9	<1.9	2.6	2.4
RB	123	69	106	99	22	18
TH	3.3	4.7	<2.6	2.6	3.4	<2.6
PB	13	47	8.7	15	5.3	7.6
ZN	130	193	149	161	141	146
CU	48	17	17	19	16	18
NI	36	29	33	35	34	35
CO	52	58	53	55	49	55
MN	1417.7	2098.7	1664.2	1751.1	1626.8	1655.3
CR	41	27	29	41	43	46
V	284	316	300	303	308	293
BA	527	290	422	179	603	423
SC	29	30	32	31	33	28

*** ALL ZERO VALUES PRINTED AS BLANKS ***

	GKR-113	GKR-66	GKR-55	GKR-73	GKR-88	GKR-56
SIO2						
TIO2						
AL2O3						
FE2O3						
FEO						
MNO						
MGO						
CAO						
NA2O						
K2O						
P2O5						
CR2O3						
NIO						
H2O-						
H2O+						
CO2						
LOI						
TOTAL						
MO	1.4	1.3	.9	1.3	.8	.8
NB	22	21	21	22	23	23
ZR	306	290	280	300	333	330
Y	52	51	49	51	56	55
SR	275	281	184	192	235	204
U	<1.9	2.5	<1.8	<1.8	<1.9	<1.8
RB	101	40	73	29	82	22
TH	3.4	4.5	<2.5	2.8	3.7	3.2
PB	7.4	19	18	30	9.4	111
ZN	148	131	143	176	152	179
CU	20	18	14	16	18	73
NI	42	34	39	40	36	37
CO	54	53	63	58	54	54
MN	1447.4	1684.0	2064.4	2069.7	1031.3	1615.5
CR	42	47	44	45	39	41
V	291	299	316	334	291	314
BA	553	273	454	340	654	276
SC	26	26	31	22	31	34

*** ALL ZERO VALUES PRINTED AS BLANKS ***

	GKR-62	GKR-50	GKR-31	GKR-48
SIO2				
TIO2				
AL2O3				
FE2O3				
FEO				
MNO				
MGO				
CAO				
NA2O				
K2O				
P2O5				
CR2O3				
NIO				
H2O-				
H2O+				
CO2				
LOI				
TOTAL				
MO	.8	<.7	1.5	1.6
NB	22	22	23	24
ZR	313	296	334	326
Y	54	52	56	57
SR	267	170	242	137
U	<1.9	2.3	<1.9	<1.9
RB	16	26	111	20
TH	3.0	<2.5	3.4	2.8
PB	13	21	9.1	31
ZN	143	161	151	321
CU	16	7.9	16	31
NI	35	32	33	36
CO	52	59	55	58
MN	1639.6	2179.3	1673.8	1921.3
CR	41	44	39	42
V	288	277	288	336
BA	833	249	369	108
SC	20	34	30	34

*** ALL ZERO VALUES PRINTED AS BLANKS ***

Dyke Complex GDC-4

	GKR-94	GKR-92	GKR-85	GKR-77	GKR-38	GKR-98
SIO2	44.48	46.12	46.03	44.45	44.38	45.68
TIO2	2.71	3.45	3.09	3.23	2.88	3.37
AL2O3	16.19	16.13	14.89	15.45	15.90	16.32
FE2O3	15.62	16.31	14.77	15.13	13.49	13.90
FEO						
MNO	.18	.20	.20	.25	.23	.29
MGO	6.72	6.76	5.27	5.98	6.94	5.49
CAO	6.25	4.73	8.16	8.40	9.11	6.83
NA2O	3.08	2.54	2.61	1.62	2.50	3.05
K2O	.52	.37	1.20	1.73	.81	1.83
P2O5	.38	.58	.52	.53	.43	.59
CR2O3						
NIO						
H2O-	.13	.14	.13	.12	.13	.10
H2O+						
CO2						
LOI	2.93	3.04	2.99	2.66	3.02	2.43
TOTAL	99.19	100.37	99.87	99.56	99.84	99.89
MO	1.1	3.0	1.5	1.2	1.4	.8
NB	19	28	27	28	23	26
ZR	199	284	276	280	265	271
Y	37	45	45	42	45	42
SR	320	180	299	367	246	306
U	<1.8	<1.8	1.9	<1.8	1.8	2.5
RB	19	15	50	59	81	90
TH	<2.5	<2.5	5.5	3.4	3.3	<2.6
PB	4.2	174	13	7.7	20	6.5
ZN	169	244	132	128	146	144
CU	16	24	19	20	18	21
NI	37	59	51	56	26	62
CO	61	69	59	58	53	59
MN	1553.4	1716.4	1533.7	2030.2	1581.5	1651.7
CR	66	66	52	55	38	55
V	280	323	249	254	245	259
BA	150	105	1602	198	467	368
SC	29	29	34	34	24	25

*** ALL ZERO VALUES PRINTED AS BLANKS ***

	GKR-104	GKR-90	GKR-51	GKR-32	GKR-45	DRD-63
SIO2	45.67	45.16	44.27	45.44	47.32	48.95
TIO2	3.23	3.01	3.08	3.27	2.85	3.41
AL2O3	15.25	15.47	14.57	13.91	14.48	13.65
FE2O3	15.53	14.90	15.09	15.09	14.71	14.96
FEO						
MNO	.22	.19	.21	.24	.25	.22
MGO	5.83	5.40	5.81	6.50	5.01	4.73
CAO	8.31	9.71	9.00	6.40	9.32	8.27
NA2O	2.63	1.56	2.62	2.15	1.59	2.87
K2O	1.22	1.89	.85	1.48	1.13	1.40
P2O5	.52	.48	.51	.56	.48	.54
CR2O3						
NIO						
H2O-	.10		.17	.29	.13	.06
H2O+						2.4
CO2						.2
LOI	1.91	1.50	3.93	3.99	2.69	
TOTAL	100.43	99.27	100.10	99.33	99.95	101.66
MO	1.4	.9	1.4	1.4	1.2	
NB	29	24	26	21	22	32
ZR	296	232	269	225	259	304
Y	51	37	43	43	46	43
SR	205	252	366	267	366	360
U	<1.8	<1.8	2.3	2.3	<1.8	
RB	64	140	66	59	72	40
TH	3.0	3.3	3.9	3.1	2.8	
PB	21	7.9	9.3	456	8.0	
ZN	232	122	133	335	134	140
CU	68	21	22	24	16	21
NI	31	77	59	42	29	38
CO	52	60	55	68	54	49
MN	2441.3	1461.4	1572.3	1939.6	2022.7	
CR	22	59	54	75	38	38
V	274	235	259	260	248	272
BA	379	369	232	141	560	479
SC	25	20	24	27	25	29

*** ALL ZERO VALUES PRINTED AS BLANKS ***

	DRD-123	DRD-124	GKR-79	GKR-75	GKR-87	GKR-72
SIO2	46.24	44.72				
TIO2	3.24	2.98				
AL2O3	14.73	15.53				
FE2O3	14.84	14.94				
FEO						
MNO	.21	.20				
MGO	5.14	6.42				
CAO	8.11	8.95				
NA2O	2.56	2.28				
K2O	1.09	.53				
P2O5	.52	.48				
CR2O3						
NIO						
H2O-	.15	.14				
H2O+	2.5	2.9				
CO2						
LOI						
TOTAL	99.33	100.00				
MO	4.2	3.5	1.3	1.4	1.1	1.5
NB	29	22	27	19	22	26
ZR	298	232	274	201	265	267
Y	46	42	44	35	45	43
SR	326	354	285	276	249	356
U	<6.6	<6.7	<1.9	<1.8	<1.8	1.9
RB	31	42	43	25	72	14
TH	<8.2	<8.2	2.8	<2.5	4.9	<2.6
PB	<9.2	<9.3	5.4	4.2	8.9	8.0
ZN	138	136	135	147	135	134
CU	21	20	21	33	17	64
NI	50	81	56	43	25	61
CO	55	66	56	59	53	62
MN			1564.2	1863.7	1490.5	1565.2
CR	41	65	58	62	41	62
V	267	278	269	255	257	273
BA	506	183	427	408	414	475
SC	27	23	23	30	26	20

*** ALL ZERO VALUES PRINTED AS BLANKS ***

	GKR-114	GKR-107	GKR-54	GKR-84	GKR-91	GKR-52
SIO2						
TIO2						
AL2O3						
FE2O3						
FEO						
MNO						
MGO						
CAO						
NA2O						
K2O						
P2O5						
CR2O3						
NIO						
H2O-						
H2O+						
CO2						
LOI						
TOTAL						
MO	<.7	1.3	1.4	1.0	1.8	1.0
NB	18	23	25	18	26	26
ZR	192	334	258	194	253	256
Y	36	55	42	35	41	42
SR	313	240	344	271	281	209
U	2.0	2.3	2.7	2.5	<1.8	<1.8
RB	54	275	23	83	77	47
TH	<2.5	4.0	4.5	<2.5	<2.6	3.0
PB	3.4	8.8	7.2	6.7	26	5.2
ZN	122	147	138	117	142	133
CU	17	17	35	14	27	21
NI	46	36	59	40	66	61
CO	59	52	58	52	65	61
MN	1558.6	1603.7	1500.0	1599.3	1735.3	1637.9
CR	58	35	59	69	52	58
V	231	291	267	251	259	264
BA	309	480	228	590	413	420
SC	23	29	26	27	24	25

*** ALL ZERO VALUES PRINTED AS BLANKS ***

	GKR-53	GKR-67	GKR-44	GKR-43	GKR-58	GKR-30
SIO2						
TIO2						
AL2O3						
FE2O3						
FEO						
MNO						
MGO						
CAO						
NA2O						
K2O						
P2O5						
CR2O3						
NIO						
H2O-						
H2O+						
CO2						
LOI						
TOTAL						
MO	1.0	<.7	.8	1.4	.9	1.0
NB	19	21	19	19	19	22
ZR	210	233	215	198	206	274
Y	38	39	40	35	33	45
SR	257	127	226	296	205	250
U	<1.8	11	<1.8	<1.8	<1.7	2.4
RB	112	138	94	34	5.8	60
TH	<2.6	3.5	2.5	<2.5	<2.3	2.8
PB	5.9	17	7.8	5.6	13	7.2
ZN	120	85	106	114	128	116
CU	17	96	25	13	14	18
NI	44	34	37	39	38	28
CO	57	18	54	54	62	57
MN	1580.3	854.1	1653.4	1506.9	3464.3	1473.3
CR	71	85	72	68	81	42
V	253	230	268	258	315	256
BA	398	374	538	320	76	713
SC	25	30	32	29	33	30

*** ALL ZERO VALUES PRINTED AS BLANKS ***

	GKR-35	GKR-46	DRD-61	DRD-64	DRD-65	DRD-121
SIO2			46.31	46.24	47.01	46.57
TIO2			3.43	3.30	3.32	3.16
AL2O3			15.50	16.28	15.80	14.61
FE2O3			14.84	14.19	13.93	14.63
FEO						
MNO			.18	.19	.20	.19
MGO			4.93	5.08	4.49	5.07
CAO			8.92	9.50	9.42	8.34
NA2O			2.58	2.51	2.65	2.48
K2O			1.38	1.00	1.33	1.19
P2O5			.41	.34	.45	.52
CR2O3						
NIO						
H2O-			.06	.04	.06	.16
H2O+			2.9	2.8	2.7	2.4
CO2			.2	.1	.1	
LOI						
TOTAL			101.64	101.57	101.46	99.32
MO	1.0	1.1				3.5
NB	25	19	20	19	24	25
ZR	245	215	209	188	235	265
Y	40	40	32	29	35	43
SR	320	302	464	417	422	399
U	2.2	2.3				<6.6
RB	127	34	61	47	47	35
TH	3.3	<2.5				<8.2
PB	7.0	9.7				<9.2
ZN	128	118	139	129	141	138
CU	22	20	19	34	37	21
NI	66	37	50	52	36	52
CO	57	60	57	57	47	53
MN	2119.4	1740.3				
CR	55	84	48	49	32	42
V	244	279	314	338	289	264
BA	405	315	414	303	425	507
SC	22	28	31	28	29	26
				16	22	24
				48	71	72
				32	42	49

*** ALL ZERO VALUES PRINTED AS BLANKS ***

	DRD-122	DRD-125	DRD-129	DRD-50A	DRD-51	DRD-52
SIO2	48.88	42.99	45.72	48.78	46.36	48.09
TIO2	2.84	3.24	2.83	3.34	2.82	2.83
AL2O3	16.38	15.24	14.55	14.06	15.56	15.02
FE2O3	12.09	14.83	15.14	14.44	14.33	14.20
FEO						
MNO	.71	.29	.23	.26	.22	.21
MGO	3.29	5.63	5.48	6.24	6.74	5.31
CAO	7.91	9.13	8.98	5.86	6.97	7.69
NA2O	3.66	1.54	1.90	3.25	2.55	2.38
K2O	1.66	1.95	1.32	.70	1.28	1.26
P2O5	.42	.48	.38	.56	.41	.44
CR2O3						
NIO						
H2O-	.16	.13	.11	.20	.09	.09
H2O+	1.8	5.1	3.3	3.2	3.8	3.4
CO2				.7	.5	.7
LOI						
TOTAL	99.80	100.55	99.94	101.59	101.63	101.62
MO	5.6	5.1	5.7			
NB	33	23	20	29	24	23
ZR	316	231	215	263	237	241
Y	49	34	39	38	31	35
SR	442	339	359	345	520	472
U	<6.2	<6.5	7.4			
RB	38	114	38	24	43	41
TH	<7.7	<8.0	<5.9			
PB	<8.6	<9.0	7.2			
ZN	119	144	128	162	160	133
CU	5.6	21	23	51	14	27
NI	10	80	40	56	81	67
CO	35	59	54	58	63	59
MN						
CR	7.7	59	65	62	54	63
V	171	282	291	276	229	238
BA	538	473	322	272	272	382
SC	23	24	32	28	28	25

*** ALL ZERO VALUES PRINTED AS BLANKS ***

	DRD-53	DRD-54	DRD-55	DRD-56	DRD-57	DRD-58
SIO2	46.70	46.62	46.04	47.42	47.84	46.61
TIO2	2.73	3.34	3.18	3.26	2.94	3.23
AL2O3	17.01	16.19	14.13	14.49	14.83	14.87
FE2O3	13.73	13.80	15.57	15.85	14.59	15.43
FEO						
MNO	.17	.19	.22	.20	.21	.28
MGO	4.81	4.58	6.31	6.63	6.87	5.88
CAO	8.66	9.44	9.64	4.13	4.21	5.82
NA2O	2.38	2.53	1.47	2.57	2.60	3.17
K2O	1.41	1.20	.89	1.04	1.90	.68
P2O5	.39	.40	.37	.60	.47	.51
CR2O3						
NIO						
H2O-	.10	.06	.07	.12	.10	.73
H2O+	3.3	3.0	3.4	4.7	4.2	3.9
CO2	.1	.1	.3	.9	1.0	.8
LOI						
TOTAL	101.49	101.45	101.59	101.91	101.76	101.91
MO						
NB	19	21	19	24	27	32
ZR	203	206	202	237	254	293
Y	29	32	30	36	36	39
SR	436	405	339	267	277	241
U						
RB	65	45	36	35	76	39
TH						
PB						
ZN	130	135	154	191	172	153
CU	42	29	40	8.1	26	25
NI	66	41	79	67	62	61
CO	59	53	67	59	59	58
MN						
CR	53	40	99	53	48	59
V	295	300	308	271	251	296
BA	415	366	307	472	691	191
SC	21	27	28	30	28	29

*** ALL ZERO VALUES PRINTED AS BLANKS ***

	DRD-60	DRD-67	DRD-68	DRD-69	DRD-70	DRD-71
SIO2	45.60	46.18	45.58	45.67	47.41	48.19
TIO2	3.01	3.08	3.23	3.24	3.10	3.13
AL2O3	15.92	14.76	15.01	16.06	16.96	15.96
FE2O3	15.17	15.13	15.66	14.56	12.87	13.17
FEO						
MNO	.22	.22	.22	.20	.19	.21
MGO	5.32	5.96	5.35	4.67	4.14	4.07
CAO	7.90	8.73	8.18	8.94	8.38	8.36
NA2O	2.49	2.58	3.19	2.42	3.30	2.94
K2O	1.32	.71	.94	1.32	1.49	1.69
P2O5	.36	.46	.51	.40	.44	.51
CR2O3						
NIO						
H2O-	.18	.03	.04	.07	.03	.05
H2O+	3.8	3.3	3.2	3.3	2.9	2.5
CO2	.4	.5	.6	.8	.2	.7
LOI						
TOTAL	101.69	101.64	101.71	98.65	101.32	101.48
MO						
NB	19	27	28	20	24	31
ZR	190	258	285	211	223	274
Y	29	36	39	31	32	40
SR	395	319	365	484	475	427
U						
RB	47	32	47	60	60	70
TH						
PB						
ZN	145	158	153	143	128	128
CU	40	24	26	31	27	22
NI	78	73	67	53	31	30
CO	69	62	61	53	47	40
MN						
CR	79	65	62	46	29	29
V	294	278	276	299	266	246
BA	468	312	271	471	463	479
SC	21	24	26	25	26	24

*** ALL ZERO VALUES PRINTED AS BLANKS ***

	DRD-72	DRD-73	DRD-74	DRD-75	DRD-76	DRD-77
SIO2	49.20	46.63	46.90	46.63	46.54	44.71
TIO2	2.77	2.78	2.95	3.30	3.11	3.22
AL2O3	16.63	15.48	14.99	14.94	14.93	14.89
FE2O3	12.56	13.64	15.31	15.44	15.47	16.11
FEO						
MNO	.25	.24	.22	.21	.20	.20
MGO	4.05	4.63	5.57	5.30	5.70	5.86
CAO	7.03	7.55	8.56	8.10	8.11	9.16
NA2O	3.04	2.45	2.21	2.66	2.94	2.17
K2O	2.00	1.65	1.41	1.24	.64	.76
P2O5	.63	.54	.50	.53	.50	.50
CR2O3						
NIO						
H2O-	.09	.34	.07	.04	.03	.10
H2O+	2.9	3.1	2.7	2.9	3.2	3.2
CO2	.2	2.7	.2	.4	.3	.3
LOI						
TOTAL	101.35	101.73	101.59	101.69	101.67	101.18
MO						
NB	30	27	17	26	27	26
ZR	305	267	264	242	276	282
Y	43	38	38	37	39	41
SR	432	348	383	365	356	403
U						
RB	80	58	61	63	36	26
TH						
PB						
ZN	167	183	155	150	162	152
CU	12	32	20	26	28	56
NI	13	38	54	57	61	65
CO	35	50	54	59	58	61
MN						
CR	17	32	42	57	56	63
V	169	278	263	282	262	296
BA	580	417	477	424	284	450
SC	22	32	24	25	24	28

*** ALL ZERO VALUES PRINTED AS BLANKS ***

	DRD-59	DRD-66	DRD-50
SIO2	45.58	45.36	45.25
TIO2	3.31	3.28	3.33
AL2O3	14.98	15.08	15.07
FE2O3	15.95	15.78	15.84
FEO			
MNO	.25	.22	.23
MGO	5.71	5.67	7.07
CAO	7.98	8.47	6.51
NA2O	3.13	2.88	2.78
K2O	.70	.74	.71
P2O5	.51	.50	.52
CR2O3			
NIO			
H2O-	.09	.03	.21
H2O+	3.0	3.5	4.1
CO2	.5	.2	.2
LOI			
TOTAL	101.69	101.71	101.82
MO			
NB	30	30	31
ZR	287	272	291
Y	38	38	38
SR	280	355	250
U			<2.8
RB	34	28	30
TH			<3.3
PB			
ZN	155	152	182
CU	26	57	52
NI	65	66	66
CO	56	60	62
MN			
CR	64	65	67
V	300	295	309
BA	295	406	284
SC	28	27	27

*** ALL ZERO VALUES PRINTED AS BLANKS ***

Dyke Complex GDC-5

	GKR-140	GKR-147	DRD-12	DRD-15	DRD-30	DRD-31
SIO2			47.05	46.26	46.67	47.60
TIO2			3.16	2.84	3.71	3.57
AL2O3			15.13	15.15	14.42	15.13
FE2O3			16.47	14.79	16.27	15.73
FEO						
MNO			.23	.22	.24	.21
MGO			6.10	6.37	5.25	5.11
CAO			8.86	7.19	8.31	8.02
NA2O			1.89	2.37	2.44	2.28
K2O			1.28	2.00	.87	1.60
P2O5			.50	.39	.84	.83
CR2O3						
NIO						
H2O-						
H2O+			2.4	3.2	2.2	1.8
CO2						
LOI						
TOTAL			103.07	100.78	101.22	101.88
MO	1.6	1.2				
NB	26	19	18	19	26	26
ZR	361	262	251	216	354	346
Y	58	43	39	37	52	51
SR	319	317	336	207	306	351
U	<1.9	<1.9				
RB	32	53	48	107	35	53
TH	<2.5	4.1				
PB	33	4.7				
ZN	154	150	161	162	174	154
CU	19	22	23	25	17	13
NI	33	50	61	48	38	41
CO			56	59	45	54
MN						
CR			45	72	51	43
V			281	304	305	241
BA			456	481	356	603
SC			26	35	30	24

*** ALL ZERO VALUES PRINTED AS BLANKS ***

	DRD-D	GKR-119	GKR-120	GKR-121	GKR-122	GKR-123
SIO2	48.08					
TIO2	3.73					
AL2O3	14.87					
FE2O3	15.78					
FEO						
MNO	.22					
MGO	4.33					
CAO	8.79					
NA2O	2.16					
K2O	1.72					
P2O5	.87					
CR2O3						
NIO						
H2O-						
H2O+	1.8					
CO2						
LOI						
TOTAL	102.35					
MO		1.5	1.7	1.7	1.7	1.5
NB	30	25	27	28	23	26
ZR	370	339	355	367	314	356
Y	56	52	53	57	49	56
SR	342	267	309	338	307	339
U		<1.8	3.4	<1.9	2.5	2.3
RB	107	62	81	104	74	114
TH		3.1	4.1	<2.6	3.7	4.4
PB		6.2	15	4.9	7.0	5.8
ZN	161	148	138	149	143	137
CU	13	14	15	13	14	11
NI	28	33	31	31	36	27
CO	52	56	58	46	49	43
MN		1854.9	1642.8	1528.3	1607.8	1372.2
CR	27	52	45	35	44	30
V	273	267	278	253	258	244
BA	613	354	502	587	452	507
SC	26	25	24	23	22	22

*** ALL ZERO VALUES PRINTED AS BLANKS ***

	GKR-28	GKR-36	GKR-37
SIO2	46.47	44.03	
TIO2	3.55	2.88	
AL2O3	14.17	15.81	
FE2O3	15.53	13.47	
FEO			
MNO	.22	.23	
MGO	4.60	6.92	
CAO	8.34	9.05	
NA2O	2.41	2.43	
K2O	1.62	.79	
P2O5	.84	.43	
CR2O3			
NIO			
H2O-	.13	.25	
H2O+			
CO2			
LOI	2.83	3.18	
TOTAL	100.68	99.47	
MO	2.0	1.3	1.0
NB	28	21	20
ZR	376	280	253
Y	59	45	41
SR	354	333	306
U	1.9	2.7	<1.9
RB	108	29	173
TH	4.4	3.4	3.6
PB	7.3	7.3	7.7
ZN	148	145	141
CU	12	19	20
NI	25	42	50
CO	44	54	57
MN	1505.3	1744.7	3063.8
CR	26	48	49
V	241	277	284
BA	597	413	271
SC	24	28	29

*** ALL ZERO VALUES PRINTED AS BLANKS ***

Haib Area, Sector I

	DRD-160	DRD-161	DRD-162	DRD-163	DRD-165	DRD-166
SIO2	45.74	45.92	46.60	45.67	46.18	49.06
TIO2	3.25	3.31	2.92	2.97	2.58	2.92
AL2O3	14.25	13.82	16.66	17.32	14.68	15.69
FE2O3	16.38	15.61	13.54	13.48	14.03	13.29
FEO						
MNO	.22	.19	.18	.17	.21	.21
MGO	5.14	6.03	4.59	4.61	6.07	3.25
CAO	7.21	6.52	8.45	8.80	7.71	7.17
NA2O	1.83	1.98	2.98	2.63	2.17	3.63
K2O	2.40	2.98	1.36	1.47	1.26	1.48
P2O5	.44	.46	.47	.39	.35	.59
CR2O3						
NIO						
H2O-	.29	.45	.21	.25	.18	.27
H2O+						
CO2						
LOI	2.16	2.51	1.90	1.95	3.92	1.80
TOTAL	99.31	99.77	99.88	99.71	99.35	99.37
MO	1.3	1.3	1.7	.7	1.5	2.1
NB	23	24	23	19	17	25
ZR	258	265	238	194	185	282
Y	45	45	39	32	35	50
SR	309	192	489	511	353	441
U	2.0	<1.9	<1.8	<1.8	<1.8	<1.8
RB	105	117	68	109	73	47
TH	6.6	6.8	<2.4	2.7	<2.3	3.2
PB	7.4	4.0	7.0	4.7	4.3	7.1
ZN	137	129	129	106	118	133
CU	35	21	24	30	20	16
NI	39	38	43	43	35	3.4
CO	59	54	47	47	49	35
MN	1602.8	1447.8	1242.9	1161.1	1414.7	1498.8
CR	28	34	50	40	55	10
V	286	302	239	254	275	181
BA	555	684	428	384	301	402
SC	26	29	21	20	34	23

*** ALL ZERO VALUES PRINTED AS BLANKS ***

	DRD-167	DRD-168	DRD-169	DRD-171	DRD-172	DRD-173
SIO2	45.96	46.03	48.99	45.77	47.33	48.03
TIO2	3.13	3.30	2.73	3.61	3.52	3.18
AL2O3	16.81	16.33	16.99	15.64	13.44	14.15
FE2O3	13.65	12.84	11.60	14.38	15.52	14.78
FEO						
MNO	.17	.33	.18	.19	.21	.20
MGO	4.79	4.16	3.28	4.85	4.89	4.70
CAO	9.05	7.95	7.39	8.38	7.30	7.73
NA2O	2.67	2.30	3.20	2.68	2.57	2.32
K2O	1.39	1.35	1.98	1.57	2.07	1.92
P2O5	.39	.34	.61	.52	.64	.64
CR2O3						
NIO						
H2O-	.21	.16	.30	.26	.29	.23
H2O+						
CO2						
LOI	1.76	3.74	2.26	2.07	1.57	1.88
TOTAL	99.98	98.85	99.51	99.91	99.34	99.76
MO	1.5	1.8	1.6	1.8	1.9	2.0
NB	20	23	32	25	22	23
ZR	200	231	334	260	328	314
Y	34	37	52	42	56	55
SR	437	439	444	427	382	301
U	<1.8	<1.8	<1.7	<1.8	<1.9	1.9
RB	42	41	57	68	79	69
TH	<2.4	4.7	5.8	<2.4	3.3	4.8
PB	4.5	46	7.5	6.2	7.4	9.5
ZN	115	125	124	134	149	147
CU	33	19	12	27	21	18
NI	43	28	9.6	43	38	32
CO	50	44	29	51	52	47
MN	1167.8	2156.0	1368.2	1294.3	1443.3	1416.5
CR	38	20	10.0	35	37	36
V	288	241	154	278	291	249
BA	501	433	723	532	663	537
SC	23	29	18	23	28	24

*** ALL ZERO VALUES PRINTED AS BLANKS ***

	DRD-175	DRD-176	DRD-177E	DRD-178	DRD-179	DRD-180
SIO2	45.82	45.45	46.80	45.28	33.69	44.96
TIO2	3.54	3.47	3.05	3.31	4.54	3.78
AL2O3	13.87	13.85	14.54	14.02	11.14	14.40
FE2O3	15.44	15.14	13.14	15.12	13.88	14.52
FEO						
MNO	.29	.41	.16	.24	.31	.22
MGO	5.98	5.28	1.89	5.90	7.48	5.78
CAO	6.48	7.57	18.14	6.19	12.10	6.33
NA2O	2.59	1.52	.05	2.54	.55	1.73
K2O	1.70	1.42	.13	2.03	2.63	1.52
P2O5	.58	.63	.52	.58	.90	.62
CR2O3						
NIO						
H2O-	.26	.22	.16	.24	.30	.22
H2O+						
CO2						
LOI	2.89	4.47	.72	3.27	11.95	4.98
TOTAL	99.46	99.43	99.30	98.72	99.46	99.07
MO	1.5	1.5	2.5	1.3	<.7	2.9
NB	25	26	24	25	137	27
ZR	287	302	263	290	441	308
Y	48	51	45	48	36	48
SR	320	252	1771	377	707	217
U	<1.8	<1.8	<2.0	1.8	3.4	<1.8
RB	106	71	6.0	146	96	52
TH	3.8	4.6	<2.6	3.2	12	<2.3
PB	10	9.9	97	18	31	29
ZN	178	254	34	131	218	194
CU	25	20	10	24	43	22
NI	45	41	21	49	140	41
CO	51	51	21	50	55	53
MN	1992.2	2864.1	1175.9	1873.5	2553.5	1745.7
CR	45	42	73	62	308	57
V	285	268	284	292	367	310
BA	629	521	46	632	477	396
SC	26	28	31	29	31	30

*** ALL ZERO VALUES PRINTED AS BLANKS ***

Sector 2 Dykes

Fish River / AiAis Area

	GKR-300	GKR-301	GKR-302	GKR-304	GKR-305	GKR-306
SIO2	44.69	45.98	44.75	42.95	45.37	45.40
TIO2	3.60	2.77	1.67	3.61	3.58	2.66
AL2O3	14.56	15.37	16.07	14.49	14.43	14.98
FE2O3	15.80	14.23	11.76	15.57	15.54	14.34
FEO						
MNO	.21	.19	.19	.18	.22	.19
MGO	5.54	6.69	6.86	5.40	5.60	5.94
CAO	7.51	9.14	10.87	5.52	8.44	8.81
NA2O	2.93	1.79	2.14	2.01	2.13	2.51
K2O	1.16	.94	.73	1.89	1.46	.70
P2O5	.64	.41	.39	.77	.65	.37
CR2O3						
NIO						
H2O-	.09	.05	.07	.12	.12	.02
H2O+						
CO2						
LOI	2.39	1.97	4.38	6.03	1.90	3.32
TOTAL	99.12	99.52	99.88	98.55	99.43	99.23
MO	.8	1.4	.9	1.1	1.6	1.1
NB	22	17	26	24	27	17
ZR	290	208	134	327	304	204
Y	49	36	27	49	47	36
SR	450	341	620	217	359	432
U	<1.9	2.0	<1.7	<1.8	<1.8	<1.8
RB	50	44	35	92	45	34
TH	4.1	<2.3	2.6	4.3	4.6	<2.3
PB	5.1	3.8	<2.5	18	6.5	7.2
ZN	150	110	77	219	152	125
CU	28	30	52	37	20	26
NI	61	97	66	48	48	63
CO	57	58	51	53	55	59
MN	1444.7	1267.7	1445.5	1558.4	1462.3	1433.6
CR	64	94	34	46	47	62
V	284	237	185	279	270	257
BA	476	323	395	588	521	207
SC	25	22	23	30	22	26

*** ALL ZERO VALUES PRINTED AS BLANKS ***

	GKR-307	GKR-308	GKR-311	GKR-312	GKR-315	GKR-316
SIO2	45.42	45.57	46.41	50.70	53.46	45.14
TIO2	3.29	3.12	3.18	1.36	.98	3.76
AL2O3	14.36	15.38	14.99	15.97	16.12	14.41
FE2O3	14.94	15.55	14.75	9.50	9.90	16.37
FEO						
MNO	.21	.21	.20	.14	.15	.21
MGO	5.95	5.80	5.09	4.82	5.98	5.28
CAO	7.75	8.72	8.34	7.96	7.97	7.48
NA2O	1.89	2.44	2.34	1.85	1.94	1.32
K2O	1.59	1.05	1.68	1.62	2.11	.90
P2O5	.54	.45	.58	.29	.35	.63
CR2O3						
NIO						
H2O-	.05	.03	.10	.17	.07	.08
H2O+						
CO2						
LOI	3.25	1.64	1.72	4.85	.94	3.82
TOTAL	99.25	99.95	99.39	99.22	99.98	99.38
MO	1.3	1.1	1.4	1.5	.9	2.2
NB	20	20	22	22	11	31
ZR	259	222	271	207	214	318
Y	44	39	44	37	33	49
SR	314	358	376	335	369	364
U	<1.8	<1.8	<1.8	<1.6	2.5	<1.8
RB	71	32	66	48	69	23
TH	<2.4	3.6	4.5	9.3	11	5.0
PB	10	4.6	4.8	8.7	18	14
ZN	140	129	134	68	90	159
CU	26	19	22	29	39	29
NI	66	57	44	53	112	65
CO	53	60	54	41	42	62
MN	1338.7	1392.3	1383.3	1032.3	1192.3	1504.0
CR	46	39	43	92	124	28
V	261	252	256	150	155	273
BA	406	338	531	408	842	353
SC	26	21	24	28	30	26

*** ALL ZERO VALUES PRINTED AS BLANKS ***

	GKR-317	GKR-318	GKR-319	DRD-137	DRD-136
SIO2	45.95	46.20	46.68	44.91	44.61
TIO2	3.56	2.90	2.20	3.22	3.43
AL2O3	14.02	14.77	15.11	14.92	14.35
FE2O3	16.51	15.37	12.65	15.15	15.46
FEO					
MNO	.23	.22	.20	.20	.20
MGO	5.20	5.41	5.27	6.14	5.64
CAO	6.54	7.66	9.08	8.22	8.06
NA2O	2.54	2.42	1.55	1.92	2.23
K2O	1.67	1.55	.83	1.15	1.32
P2O5	.61	.66	.64	.50	.61
CR2O3					
NIO					
H2O-	.12	.07	.12	.23	.25
H2O+				2.5	2.4
CO2					
LOI	2.34	2.05	4.67		
TOTAL	99.29	99.29	98.99	99.07	98.55
MO	1.4	1.9	1.9	5.0	6.1
NB	22	24	54	19	28
ZR	289	321	258	239	312
Y	50	51	54	44	49
SR	280	482	574	356	380
U	<1.9	<1.8	<1.7	<6.2	<6.3
RB	63	52	13	77	58
TH	<2.4	4.4	8.7	<6.1	<6.1
PB	7.1	6.0	11	<6.7	<6.7
ZN	166	155	107	118	155
CU	19	12	26	28	18
NI	41	52	48	79	50
CO	56	50	27	57	56
MN	1670.7	1594.6	801.8		
CR	41	61	30	60	41
V	300	223	117	269	257
BA	409	564	403	470	690
SC	26	20	32	27	22

*** ALL ZERO VALUES PRINTED AS BLANKS ***

Klein Karas Area

	GD-1	GD-2	GD-3	GD-4	847	848
SIO2	47.32	47.93	46.04	45.52	44.39	46.25
TIO2	3.47	3.18	3.41	3.02	4.10	3.42
AL2O3	15.95	16.97	16.40	16.08	14.43	16.53
FE2O3	15.87	14.75	15.16	14.57	18.47	15.73
FEO						
MNO	.21	.20	.21	.19	.29	.27
MGO	5.48	5.07	5.38	4.98	5.61	4.72
CAO	8.91	8.42	9.52	8.07	7.87	9.41
NA2O	2.35	2.51	2.35	2.46	2.25	2.52
K2O	.90	1.80	.89	1.72	1.66	1.23
P2O5	.59	.48	.43	.45	.88	.73
CR2O3						
NIO						
H2O-						
H2O+	2.0	2.1	1.6	2.2	2.5	1.6
CO2						
LOI						
TOTAL	103.05	103.41	101.39	99.26	102.45	102.41
MO						
NB	23	23	22	22	23	12
ZR	274	253	220	248	325	243
Y	56	41	37	42	47	39
SR	374	443	384	453	311	383
U						
RB	47	88	36	95	54	48
TH					5.0	
PB						
ZN	141	113	115	121	169	116
CU	19	24	26	23	18	25
NI	54	54	58	57	59	45
CO	62	55	53	52	69	55
MN						
CR	43	29	35	37	70	46
V	271	235	267	239	285	266
BA	420	593	386	596	574	433
SC	24	23	28	24	22	26

*** ALL ZERO VALUES PRINTED AS BLANKS ***

	DRD-138	DRD-139	DRD-142	DRD-143
SIO2	44.53	44.67	44.85	45.74
TIO2	2.86	3.51	3.13	3.37
AL2O3	14.80	13.61	14.95	14.29
FE2O3	15.17	15.85	15.40	15.29
FEO				
MNO	.20	.24	.21	.17
MGO	6.34	4.55	6.09	5.17
CAO	8.55	6.22	8.88	8.21
NA2O	2.44	1.98	2.31	2.24
K2O	1.10	2.98	.82	.99
P2O5	.44	2.36	.47	.56
CR2O3				
NIO				
H2O-	.29	.25	.26	.26
H2O+	2.8	2.7	2.5	1.9
CO2				
LOI				
TOTAL	99.52	98.92	99.87	98.19
MO	6.9	6.7	4.6	6.7
NB	18	44	21	24
ZR	208	359	240	282
Y	39	44	43	46
SR	355	830	359	312
U	<6.1	<6.3	<6.2	<6.1
RB	67	109	45	38
TH	<5.9	<6.1	<6.0	8.4
PB	<6.5	11	<6.6	8.8
ZN	138	174	144	132
CU	20	13	26	17
NI	52	23	73	48
CO	61	40	59	56
MN				
CR	45	19	57	40
V	276	155	291	268
BA	436	1636	288	549
SC	26	8.6	26	25

*** ALL ZERO VALUES PRINTED AS BLANKS ***

Sector 3 Dykes

	K588	K589	156/1	DRD-96	DRD-97	DRD-98
SIO2	44.18	45.93	47.86	50.62	54.85	45.69
TIO2	4.48	4.43	3.60	3.30	2.70	3.24
AL2O3	17.55	14.41	18.42	14.79	14.39	14.60
FE2O3	17.53	17.63	13.23	14.56	12.11	15.41
FEO						
MNO	.22	.26	.18	.20	.18	.22
MGO	4.19	4.39	3.37	3.21	3.18	6.03
CAO	7.19	9.01	9.40	6.75	5.34	7.75
NA2O	2.81	2.93	3.25	2.69	2.41	3.40
K2O	1.01	1.27	1.00	2.27	2.87	.70
P2O5	.45	.67	.31	.67	.56	.53
CR2O3						
NIO						
H2O-				.23	.17	.13
H2O+	2.4	1.2	1.2	1.7	1.7	2.6
CO2				.1	.1	.1
LOI						
TOTAL	102.01	100.93	101.82	101.09	100.56	101.57
MO				6.3	4.9	4.4
NB	17	20	14	41	37	22
ZR	195	270	159	380	300	202
Y	25	39	21	58	45	37
SR	457	362	549	348	343	452
U				<6.6	<6.3	<6.4
RB	29	39	28	90	109	33
TH	4.1	5.0	3.0	11	10	<7.9
PB	15	13	12	15	17	22
ZN	148	162		150	111	106
CU	69	108		37	29	29
NI	277	250	17	19	17	30
CO	69	60	50	44	38	47
MN						
CR	59	60	18	4.0	5.0	18
V	320	370	309	192	167	261
BA	580	485	303	652	676	298
SC	20	38	28	25	21	24

*** ALL ZERO VALUES PRINTED AS BLANKS ***

	DRD-99	DRD-101	DRD-102	DRD-103	DRD-104	DRD-105
SIO2	48.02	47.29		44.76	43.56	40.83
TIO2	3.53	3.94		3.05	4.16	5.48
AL2O3	15.93	15.49		16.67	15.95	15.15
FE2O3	14.45	15.13		15.68	18.24	18.78
FEO						
MNO	.19	.20		.19	.19	.20
MGO	3.50	4.22		6.27	5.72	7.27
CAO	7.37	7.85		8.28	8.04	7.15
NA2O	3.28	2.83		2.76	2.37	1.99
K2O	1.77	1.77		.43	.89	.76
P2O5	.56	.46		.26	.35	.34
CR2O3						
NIO						
H2O-	.12	.12		.13	.08	.11
H2O+	1.4	.4		1.6	.6	1.5
CO2	.1					
LOI						
TOTAL	100.22	99.71		100.10	100.15	99.56
MO	6.1	6.2	5.1	5.9	7.4	4.1
NB	33	30	15	11	22	17
ZR	292	244	148	135	180	141
Y	47	42	31	20	30	22
SR	430	440	479	555	450	448
U	<6.6	<7.2	<6.6	<7.1	<7.6	<7.6
RB	59	72	37	10	24	21
TH	<8.1	<8.9	<8.2	<8.8	<9.4	<9.4
PB	14	9.9	11	<9.8	<10.0	11
ZN	141	184	140	148	168	173
CU	52	49	12	2.8	128	154
NI	19	23	139	104	116	131
CO	46	46		69	72	89
MN						
CR	<3.0	<3.0		242	<4.0	23
V	230	277		302	470	411
BA	604	631	304	120	343	249
SC	24	30	15	17	22	20

*** ALL ZERO VALUES PRINTED AS BLANKS ***

	DRD-110	DRD-111	DRD-112	DRD-89	DRD-90	DRD-91
SIO2	45.10	45.56		44.91	45.11	47.40
TIO2	3.94	3.91		3.50	3.63	3.11
AL2O3	14.32	14.24		13.88	14.43	15.93
FE2O3	16.56	16.90		15.43	14.79	14.10
FEO						
MNO	.21	.23		.22	.18	.21
MGO	5.59	5.43		5.38	6.27	4.41
CAO	5.07	4.44		7.62	5.13	7.31
NA2O	2.17	2.67		1.03	1.99	3.65
K2O	1.00	1.24		4.13	5.29	.78
P2O5	.78	.87		.65	.69	.64
CR2O3						
NIO						
H2O-	<.01	.09		.08	.07	.08
H2O+	4.8	3.7		2.8	2.4	2.6
CO2				1.3	.9	.2
LOI						
TOTAL	99.53	99.29		100.93	100.88	100.42
MO	6.1	4.9	5.0	6.1	4.6	4.6
NB	31	32	37	27	28	25
ZR	420	438	530	303	319	298
Y	64	70	77	43	45	46
SR	275	226	213	352	118	359
U	<7.0	<7.2	<6.2	<6.7	<6.6	<6.4
RB	42	57	64	164	243	28
TH	<8.8	<8.9	14	<8.2	<8.2	<7.9
PB	13	12	13	<9.1	<9.1	17
ZN	165	189	121	148	165	144
CU	20	27	26	19	85	19
NI	58	50	26	47	46	39
CO	55	54		55	54	52
MN						
CR	36	29		44	43	28
V	273	253		293	307	254
BA	592	555	1043	647	615	363
SC	28	30	22	24	23	27

*** ALL ZERO VALUES PRINTED AS BLANKS ***

	DRD-92	DRD-93	DRD-94	DRD-95	DRD-80	DRD-81
SIO2	45.29	45.78	45.24	51.49	58.78	53.72
TIO2	3.52	3.23	2.68	2.06	1.33	1.84
AL2O3	14.82	14.62	15.14	18.14	16.18	16.47
FE2O3	17.11	15.41	14.90	10.05	9.10	10.55
FEO						
MNO	.19	.22	.20	.16	.16	.17
MGO	6.29	6.08	6.06	2.58	1.30	2.44
CAO	3.42	7.75	9.58	7.42	4.29	6.01
NA2O	1.72	2.56	2.19	4.33	4.91	6.09
K2O	2.37	.70	.80	1.58	2.58	.62
P2O5	.63	.54	.37	.60	.42	.56
CR2O3						
NIO						
H2O-	.07	.12	.04	.17	.12	.10
H2O+	4.2	3.8	3.3	1.9	1.2	1.6
CO2	.3	.1	.1	.1	.4	1.2
LOI						
TOTAL	99.93	100.91	100.60	100.58	100.77	101.37
MO	2.6	3.9	3.8	4.8	4.2	2.8
NB	26	25	20	29	53	41
ZR	286	266	216	360	562	495
Y	45	47	38	54	83	66
SR	84	294	337	447	317	352
U	<6.5	<6.7	<6.7	5.9	6.1	<5.8
RB	141	30	30	25	77	16
TH	<8.1	<8.3	<8.2	7.5	11	8.3
PB	30	<9.2	<9.1	11	23	15
ZN	197	153	134	114	140	86
CU	53	22	38	7.0	7.0	3.0
NI	47	47	57	8.0		10
CO	61	54	63	28	17	29
MN						
CR	17	53	60	4.0	<2.0	9.0
V	262	285	281	109	34	87
BA	565	492	362	881	966	266
SC	33	31	31	22	13	19

*** ALL ZERO VALUES PRINTED AS BLANKS ***

	DRD-82	DRD-84	DRD-85	DRD-86	DRD-87	DRD-88
SIO2	52.73	44.89	45.72	48.60	43.45	43.54
TIO2	1.78	3.41	3.42	2.93	3.12	4.06
AL2O3	17.13	14.66	14.69	14.80	14.17	15.43
FE2O3	10.36	15.81	15.91	14.66	14.89	16.95
FEO						
MNO	.18	.24	.21	.22	.19	.24
MGO	2.22	5.40	5.45	4.33	5.57	6.38
CAO	5.52	7.31	7.79	7.18	5.69	2.92
NA2O	4.87	2.25	2.92	3.14	1.56	1.68
K2O	2.02	2.11	1.03	1.82	5.73	3.03
P2O5	.58	.59	.57	.81	.55	.69
CR2O3						
NIO						
H2O-	.11	.18	.07	.09	.08	.05
H2O+	1.6	3.0	2.8	2.0	1.9	4.4
CO2	1.0	.7	.3	.1	3.5	1.5
LOI						
TOTAL	101.10	100.55	100.88	100.62	100.40	100.87
MO	3.7	5.1	5.5	4.9	5.7	6.2
NB	39	25	27	35	26	34
ZR	519	294	293	418	291	365
Y	64	45	44	59	39	53
SR	372	316	375	348	230	63
U	<5.9	<6.7	<6.6	<6.5	<6.7	<6.6
RB	51	86	32	51	204	360
TH	8.8	<8.3	<8.2	<8.1	<8.3	<8.2
PB	18	15	27	<8.9	<9.2	11
ZN	105	186	134	175	133	212
CU	13	21	20	9.0	38	134
NI	7.0	55	45	26	48	64
CO	24	55	55	43	55	62
MN						
CR	5.0	55	37	22	42	28
V	74	300	307	211	296	347
BA	775	462	285	673	1360	288
SC	15	29	30	27	30	32

*** ALL ZERO VALUES PRINTED AS BLANKS ***

	K580	K581	K582	DRD-145	gkr-126	gkr-130
SIO2	44.75	46.15	45.92	46.21	60.73	64.27
TIO2	2.83	2.77	2.85	2.83	1.17	1.32
AL2O3	15.98	16.01	15.92	15.27	14.82	14.52
FE2O3	17.84	11.78	12.34	14.69	10.63	11.32
FEO						
MNO	.27	.19	.24	.18	.13	.04
MGO	5.83	5.16	4.98	5.27	1.33	.94
CAO	8.00	8.86	8.64	8.69	2.41	1.06
NA2O	2.25	2.83	2.64	2.13	4.16	8.28
K2O	1.38	2.40	2.78	.68	4.34	.24
P2O5	.72	1.96	2.01	.48	.32	.44
CR2O3						
NIO						
H2O-				.18	.14	.19
H2O+	2.6	3.3	3.2	2.9		
CO2						
LOI					1.49	.43
TOTAL	102.45	101.41	101.52	99.51	101.68	103.06
MO				3.8	2.4	.9
NB	19	39	40	20	69	52
ZR	282	256	256	224	653	677
Y	36	33	35	42	90	80
SR	356	1610	1520	423	132	34
U				<5.2	2.9	2.9
RB	38	73	84	41	141	7.5
TH	3.0			<6.6	14	15
PB	17	7.9	13	7.6	44	8.4
ZN	161	88	87	138	110	16
CU	22	13	14	23	7.6	14
NI	247	15	14	63	<2.0	<1.8
CO	61	35	35	62		
MN						
CR	79	21	19	49		
V	332	204	202	265		
BA	634	1160	1615	201		
SC	23	20	21	31		

*** ALL ZERO VALUES PRINTED AS BLANKS ***

	DRD-151
SIO2	46.46
TIO2	2.52
AL2O3	17.93
FE2O3	14.22
FEO	
MNO	.17
MGO	6.08
CAO	8.77
NA2O	2.95
K2O	.90
P2O5	.36
CR2O3	
NIO	
H2O-	.10
H2O+	
CO2	
LOI	
TOTAL	100.46
MO	.9
NB	17
ZR	163
Y	27
SR	495
U	<1.8
RB	21
TH	3.3
PB	5.1
ZN	106
CU	22
NI	98
CO	59
MN	1244.1
CR	170
V	221
BA	315
SC	16

*** ALL ZERO VALUES PRINTED AS BLANKS ***

4.2 REE

4.2.1 Sample Preparation

Sample analysed for whole rock REE content were prepared from whole rock siebed powders used for XRF analyses (see section 4.1.1).

4.2.2 Analytical Techniques and Precision

REE analyses were performed by a variety of techniques. Initial REE analyses were performed at New Mexico Tech by Dave Reid using the INAA technique described by Gibson and Jagam (1980), whilst the majority of samples were analysed at the University of Cape Town by ion chromatography using the techniques described by le Roex and Watkins, (1990).

Analytical precision, accuracy and detection limits for both techniques are to be found in Knopper, (1988) and Le Roux and Watkins, (1990) respectively.

4.2.3 Data

Sector 1 Dykes by IC.

	GKR-100	GKR-55	GKR-74	GKR-40	GKR-105	GKR-102
LA	33.5	35.4	32.7	35.3	20.5	40.0
CE	75.3	82.1	81.6	81.9	45.9	95.4
PR	10.1	11.3	11.1	9.1	6.3	12.2
ND	44.3	50.3	49.8	50.3	24.2	52.0
SM	10.3	11.6	11.2	12.5	6.5	11.6
EU	2.9	3.2	2.6	2.5	2.2	3.1
GD	9.7	11.4	10.6	9.9	6.7	10.9
TB	1.5	1.7	1.7	1.5	1.0	1.7
DY	8.7	10.1	10.0	9.4	6.4	9.8
ER	4.6	5.1	4.9	5.1	3.3	5.4
YB	3.9	4.0	3.8	4.2	2.5	4.3

*** ALL ZERO VALUES PRINTED AS BLANKS ***

REE data from Sector 1 dykes by IC

Filename : sector1_ree

	GKR-59	GKR-111	GKR-74b	GKR-84	GKR-90	GKR-37
LA	33.1	31.9	32.7	19.4	27.7	23.6
CE	76.0	71.0	81.6	46.4	65.3	57.7
PR	10.3	9.5	11.1	5.6	8.7	7.9
ND	47.5	43.6	49.8	28.5	38.7	36.5
SM	11.1	9.8	11.2	6.7	8.3	8.5
EU	2.9	2.6	2.6	2.1	2.6	2.7
GD	10.7	9.4	10.6	6.7	7.9	8.5
TB	1.6	1.4	1.7	1.1	1.2	1.3
DY	9.6	8.5	10.0	6.4	6.9	7.6
ER	5.1	4.3	4.9	3.3	3.5	3.9
YB	4.2	3.6	3.8	2.7	3.0	3.3

*** ALL ZERO VALUES PRINTED AS BLANKS ***

	GKR-69	GKR-106	GKR-83	GKR-48	GKR-103	GKR-78
LA	37.2	32.0	21.4	35.3	31.4	38.2
CE	87.6	72.7	50.5	82.2	79.4	87.2
PR	11.3	9.8	7.0	11.5	11.1	11.2
ND	48.6	42.6	30.7	51.9	47.5	48.4
SM	11.0	9.8	7.1	12.1	11.2	10.6
EU	3.0	2.7	2.2	3.0	2.7	3.0
GD	10.3	9.8	7.4	11.5	11.5	10.1
TB	1.5	1.5	1.2	1.8	1.8	1.5
DY	9.1	9.0	7.2	10.4	10.3	8.7
ER	4.8	4.9	3.8	5.1	5.4	4.7
YB	4.3	4.4	3.3	4.1	4.4	4.1

*** ALL ZERO VALUES PRINTED AS BLANKS ***

REE data from Sector 1 dykes by IC

Filename : sector1_ree

	GKR-104	GKR-72
LA	36.6	30.2
CE	85.6	73.7
PR	10.8	9.8
ND	46.2	42.2
SM	10.5	9.7
EU	3.1	3.0
GD	10.2	9.3
TB	1.6	1.4
DY	9.1	7.8
ER	4.7	4.2
YB	3.9	3.6

*** ALL ZERO VALUES PRINTED AS BLANKS ***

Sector 2 Dykes by IC.

	DRD-136	DRD-137
LA	39.0	22.7
CE	94.8	52.7
PR	11.8	7.6
ND	51.1	31.5
SM	11.2	6.8
EU	9.1	2.4
GD	12.6	7.7
TB	2.1	1.1
DY	12.3	7.6
HO		
ER	4.8	3.3
TM		
YB	4.4	3.3
LU		
LAc	123.8	72.1
CEc	116.6	64.9
PRc	102.1	65.1
NDc	85.5	52.8
SMc	58.3	35.6
EUc	126.3	33.2
GDc	48.8	29.6
TBc	43.5	23.3
DYc	37.7	23.5
HOc		
ERc	22.8	15.7
TMc		
YBc	21.2	15.8
LUc		

*** ALL ZERO VALUES PRINTED AS BLANKS ***

Sector 3 Dykes by IC.

	DRD-80	DRD-81	DRD-82	DRD-95	DRD-98	DRD-99
LA	74.1	50.6	52.4	40.8	27.5	38.7
CE	167.5	117.2	133.0	95.7	64.8	88.8
ND	94.4	65.9	65.9	54.3	37.7	48.1
SM	17.4	13.9	14.1	11.6	7.9	10.4
EU	4.2	3.8	3.9	3.4	2.4	2.9
GD	16.7	14.4	14.0	11.3	7.6	10.1
TB	2.7	2.4	2.3	1.8	1.2	1.6
YB	7.6	5.8	5.8	4.9	2.9	4.4
LU	1.2	.9	1.0	.8	.5	3.8
LAc	235.4	160.6	166.3	129.5	87.2	122.9
CEc	206.0	144.2	163.6	117.7	79.7	109.2
NDc	158.1	110.4	110.4	91.0	63.1	80.6
SMc	90.6	72.2	73.6	60.3	41.3	54.0
EUc	58.4	52.4	53.6	46.7	33.7	40.7
GDc	64.4	55.6	53.9	43.6	29.5	38.9
TBc	54.3	48.8	46.1	37.1	24.9	33.1
YBc	36.6	27.9	27.7	23.4	14.0	21.3
LUc	37.2	29.7	30.3	24.1	15.0	118.4
EU*	76.4	63.3	63.0	51.3	34.9	45.9

*** ALL ZERO VALUES PRINTED AS BLANKS ***

	DRD-88	DRD-97	DRD-98	DRD-105	DRD-122
LA	45.9	42.5	27.8	15.8	39.8
CE	97.5	88.4	60.9	31.1	84.9
PR	11.7	10.2	8.4	4.4	10.7
ND	52.8	45.6	32.5	17.3	45.2
SM	10.3	9.7	7.3	3.9	9.0
EU	2.8	3.2	2.1	1.9	2.9
GD	11.6	9.7	7.4	4.0	9.6
TB	1.8	1.5	1.2	.6	1.5
DY	10.5	9.3	6.2	4.0	9.5
HO					
ER	4.3	4.1	3.0	1.7	4.1
TM					
YB	4.6	4.3	2.7	1.5	3.9
LU					
LAc	145.7	134.8	88.3	50.0	126.3
CEc	119.9	108.8	74.9	38.3	104.4
PRc	100.5	87.8	72.2	37.8	92.3
NDc	88.5	76.4	54.4	29.0	75.7
SMc	53.8	50.5	38.1	20.2	46.8
EUc	38.9	43.9	29.6	26.0	40.7
GDc	44.8	37.4	28.5	15.5	37.1
TBc	36.3	31.0	24.5	13.3	30.4
DYc	32.3	28.7	19.0	12.2	29.1
HOc					
ERc	20.4	19.1	14.1	8.1	19.1
TMc					
YBc	22.2	20.8	12.9	7.3	18.9
LUc					

*** ALL ZERO VALUES PRINTED AS BLANKS ***

Appendix 5 Sample locations

5.1.1 DRD samples collated by Reid, D.L..

Positions expressed in degrees, and decimal fraction there of.

Sample #	Logitude (SXX.XXX)	Latitude (EXX.XXX)	Loc.#
DRD-50	17.708	28.837	1
DRD-50A	17.708	28.837	2
DRD-51	17.708	28.837	3
DRD-52	17.708	28.837	4
DRD-53	17.708	28.837	5
DRD-54	17.708	28.837	6
DRD-55	17.708	28.837	7
DRD-60	17.708	28.837	8
DRD-56	17.708	28.837	9
DRD-57	17.708	28.837	10
DRD-58	17.708	28.837	11
DRD-59	17.708	28.837	12
DRD-66	17.662	28.940	13
DRD-67	17.662	28.940	14
DRD-68	17.662	28.940	15
DRD-69	17.662	28.940	16
DRD-70	17.662	28.940	17
DRD-71	17.662	28.940	18
DRD-72	17.662	28.940	19
DRD-73	17.662	28.940	20
DRD-74	17.662	28.940	21
DRD-75	17.662	28.940	22
DRD-76	17.662	28.940	23
DRD-77	17.662	28.940	24
DRD-61	17.716	28.809	25
DRD-63	17.672	28.906	26
DRD-64	17.672	28.906	27
DRD-65	17.672	28.906	28
K588	17.048	28.335	29
K589	17.048	28.335	30
156/1	17.048	28.335	31
DRD-96	17.054	28.316	32
DRD-97	17.054	28.316	33
DRD-98	17.054	28.316	34
DRD-99	17.054	28.316	35
DRD-101	17.048	28.335	36
DRD-102	17.048	28.335	37
DRD-103	17.082	28.444	38
DRD-104	17.082	28.444	39
DRD-105	17.082	28.444	40
DRD-110	17.075	28.175	41
DRD-111	17.075	28.175	42
DRD-112	17.075	28.175	43

DRD-106A	17.082	28.444	44
DRD-106B	17.082	28.444	45
DRD-106C	17.082	28.444	46
DRD-108	17.027	28.188	47
DRD-01	17.686	28.821	48
DRD-02	17.686	28.821	49
DRD-04	17.686	28.821	50
DRD-05	17.686	28.821	51
DRD-06	17.686	28.821	52
DRD-07	17.686	28.821	53
DRD-10	17.686	28.821	54
DRD-10A	17.686	28.821	55
DRD-12	17.686	28.821	56
DRD-15	17.686	28.821	57
DRD-30	17.997	28.871	58
DRD-31	17.997	28.871	59
DRD-D	17.733	28.945	60
GD-1	18.101	27.571	61
GD-2	18.101	27.571	62
GD-3	18.101	27.571	63
GD-4	18.101	27.571	64
847	18.101	27.571	65
848	18.101	27.571	66
K580	17.184	28.841	67
K581	17.184	28.841	68
K582	17.184	28.841	69
K590	17.013	28.283	70
D11	17.222	28.350	71
DRD-80	16.944	28.279	72
DRD-81	16.964	28.285	73
DRD-82	16.964	28.285	74
DRD-84	17.000	28.293	75
DRD-85	17.013	28.283	76
DRD-86	17.013	28.283	77
DRD-87	17.013	28.283	78
DRD-88	17.006	28.317	79
DRD-89	17.222	28.387	80
DRD-90	17.222	28.387	81
DRD-91	17.222	28.387	82
DRD-92	17.222	28.387	83
DRD-93	17.222	28.387	84
DRD-94	17.222	28.387	85
DRD-95	17.222	28.387	86
HJ308	17.463	29.260	87
DRD-121	17.605	29.014	88
DRD-122	17.605	29.014	89
DRD-123	17.605	29.014	90
DRD-124	17.605	29.014	91
DRD-125	17.605	29.014	92
DRD-129	17.605	29.014	93
DRD-131	17.605	29.014	94
DRD-132	17.605	29.014	95

DRD-136	17.703	27.841	96
DRD-137	17.726	27.672	97
DRD-138	18.058	27.564	98
DRD-139	18.058	27.564	99
DRD-140	18.101	27.571	100
DRD-141	18.101	27.571	101
DRD-142	18.101	27.571	102
DRD-143	18.116	27.576	103
DRD-144	18.138	27.592	104
DRD-145	17.206	28.960	105
DRD-151	17.086	28.464	106
DRD-162	17.852	28.629	107
DRD-163	17.852	28.629	108
DRD-165	17.871	28.631	109
DRD-167	17.808	28.680	110
DRD-168	17.808	28.680	111
DRD-169	17.808	28.662	112
DRD-171	17.810	28.638	113
DRD-172	17.801	28.625	114
DRD-173	17.783	28.619	115
DRD-175	17.766	28.663	116
DRD-182	17.811	28.604	117
DRD-183	17.827	28.607	118
DRD-184	17.827	28.697	119

Appendix 5.1.2 Samples collected by the author.

Sample locations expressed in degrees, minutes, and seconds.

Sample #	**Location** *(Latitude and Longitude)*		*Loc.#*
	SXX°XX'XX''	EXX°XX'XX''	
GKR-28	29 01 52	17 50 10	120
GKR-29	28 59 36	17 37 20	121
GKR-30	29 02 04	17 37 50	122
GKR-31	29 01 11	17 39 00	123
GKR-32	28 59 31	17 40 40	124
GKR-33	28 59 33	17 41 42	125
GKR-36	29 02 12	17 45 41	126
GKR-37	29 02 36	17 44 52	127
GKR-38	29 02 04	17 39 00	128
GKR-39	28 59 28	17 37 38	129
GKR-40	28 53 38	17 38 55	130
GKR-41	28 59 29	17 38 00	131
GKR-42	28 58 03	17 40 19	132
GKR-43	28 59 30	17 39 41	133
GKR-44	28 59 29	17 41 10	134
GKR-45	28 59 33	17 38 29	135
GKR-46	28 57 40	17 42 56	136
GKR-47	28 53 51	17 39 41	137
GKR-48	29 02 08	17 38 32	138

GKR-49	28 59 31	17 36 27	139
GKR-50	29 01 53	17 37 08	140
GKR-51	28 59 31	17 40 45	141
GKR-52	28 58 05	17 41 21	142
GKR-53	28 58 01	17 41 33	143
GKR-54	28 57 08	17 41 46	144
GKR-55	28 53 59	17 40 58	145
GKR-56	28 49 31	17 42 59	146
GKR-57	28 58 00	17 40 37	147
GKR-58	29 01 02	17 38 31	148
GKR-59	29 01 49	17 36 43	149
GKR-60	28 58 01	17 41 34	150
GKR-61	28 59 32	17 38 31	151
GKR-62	29 00 43	17 37 11	152
GKR-63	28 52 30	17 40 58	153
GKR-64	28 56 41	17 40 08	154
GKR-65	28 57 08	17 42 00	155
GKR-66	28 52 41	17 41 27	156
GKR-67	28 58 02	17 41 51	157
GKR-68	28 59 33	17 41 40	158
GKR-69	28 49 47	17 42 51	159
GKR-70	28 58 00	17 40 35	160
GKR-72	28 55 49	17 41 59	161
GKR-73	28 55 12	17 40 03	162
GKR-74	28 52 17	17 40 01	163
GKR-75	28 51 57	17 44 08	164
GKR-76	28 55 11	17 38 51	165
GKR-77	28 52 23	17 44 53	166
GKR-78	28 54 41	17 42 03	167
GKR-79	28 52 31	17 45 00	168
GKR-80	28 58 01	17 39 02	169
GKR-81	28 57 51	17 37 20	170
GKR-82	28 57 58	17 37 55	171
GKR-83	28 49 17	17 42 43	172
GKR-84	28 58 01	17 40 39	173
GKR-85	28 52 12	17 44 49	174
GKR-87	28 55 41	17 41 54	175
GKR-88	28 55 18	17 41 11	176
GKR-89	28 49 37	17 44 09	177
GKR-90	28 57 07	17 41 28	178
GKR-91	28 58 00	17 40 51	179
GKR-92	28 50 53	17 45 07	180
GKR-93	28 52 19	17 40 07	181
GKR-94	28 49 31	17 45 43	182
GKR-95	28 52 09	17 44 35	182
GKR-97	28 49 53	17 41 07	184
GKR-98	28 57 00	17 41 09	185
GKR-99	28 51 31	17 42 07	186
GKR-100	28 51 07	17 40 57	187
GKR-101	28 51 11	17 40 31	188
GKR-102	28 51 00	17 41 28	189
GKR-103	28 49 21	17 40 09	190

GKR-104	28 58 03	17 41 07	191
GKR-105	28 59 28	17 36 15	192
GKR-106	28 49 21	17 43 07	193
GKR-107	28 57 07	17 41 20	194
GKR-109	28 48 58	17 41 27	195
GKR-110	28 49 41	17 44 00	196
GKR-111	28 55 41	17 40 03	197
GKR-113	28 49 51	17 44 17	198
GKR-114	28 57 05	17 41 09	199
GKR-119	29 01 52	17 50 16	200
GKR-120	29 01 52	17 50 16	201
GKR-121	28 51 49	18 01 07	202
GKR-122	28 51 47	18 01 11	203
GKR-123	28 51 44	18 01 04	204
GKR-126	28 03 41	17 03 11	205
GKR-130	28 29 11	17 14 43	206
GKR-140	29 08 15	17 47 58	207
GKR-147	29 08 13	17 48 03	208
GKR-300	27 56 30	17 30 30	209
GKR-301	27 56 31	17 30 31	210
GKR-302	27 56 31	17 30 32	211
GKR-304	27 56 31	17 30 33	212
GKR-305	27 56 47	17 31 03	213
GKR-306	27 56 48	17 31 02	214
GKR-307	27 56 33	17 30 34	215
GKR-308	27 56 30	17 30 29	216
GKR-311	27 56 11	17 30 33	217
GKR-312	27 56 12	17 30 34	218
GKR-315	27 56 18	17 30 29	219
GKR-316	27 56 18	17 30 32	220
GKR-317	27 56 21	17 30 33	221
GKR-318	27 55 41	17 29 42	222

Appendix 5.2 Sample location Map

SEE POCKET IN REAR COVER

APPENDIX 5.2

THE GANNAKOURIEP DYKE SWARM OF THE LOWER ORANGE RIVER REGION, SOUTHERN AFRICA.